EINDHOVEN UNIVERSITY OF TECHNOLOGY

Department of the Built Environment
Unit of Structural Engineering and Design

Exploratory research into the integration of Vibro-Acoustical resilient behaviour CLT-Concrete Composite floors

Master thesis (7K45M0) 2023-2024

E.C.L. (Edwin) van Houte (1374176)

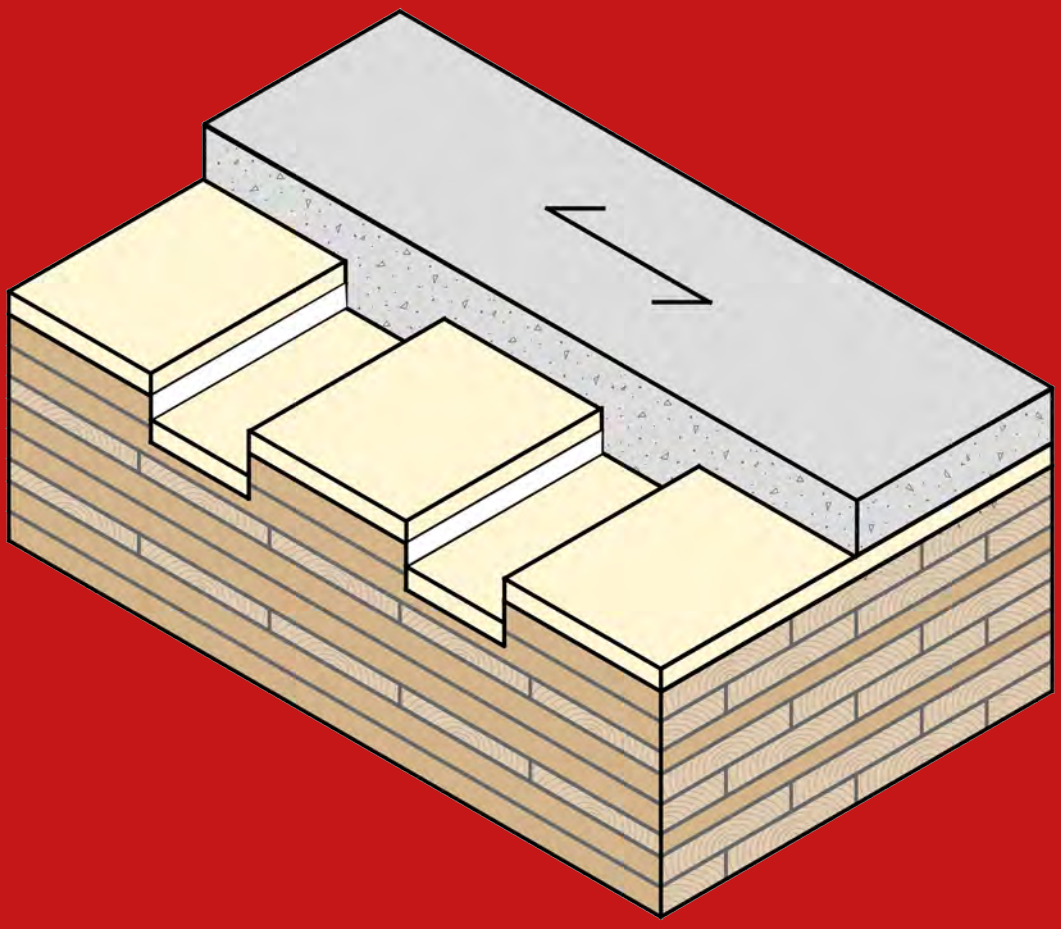

Exploratory research into the integration of Vibro-Acoustical resilient behaviour in CLT-Concrete Composite floors

Thesis for the final graduation project of the Master track Structural Engineering and Design of the master 'Architecture, Building and Planning' at Eindhoven University of Technology.
November 4, 2024

By
E.C.L. (Edwin) van Houte (1374176)

Graduation supervising committee

- Dr. ir. S.P.G. (Faas) Moonen
  Associate Professor in the chair of Innovative Structural Design, TU/e.
- Ir. A.P.H.W. (Arjan) Habraken
  Assistant Professor in the chair of Innovative Structural Design, TU/e.
- Dr. ir. G.S. (Susanne) Bron-van der Jagt
  Managing director and consultant, Level Acoustics & Vibrations B.V.

Abstract

This master's thesis explores an innovative approach to enhance the vibro-acoustical performance of CLT–Concrete Composite (CCC) floors by integrating a resilient layer between the CLT and concrete. While CCC have caught the eye of researches and the industry due to its structural efficiency, transverse stiffness and favorable vibro-acoustical properties compared to timber floor and reduced environmental impact relative to concrete floors, it cross-section often still needs to be increased or an floating floor added to reach the desirable criteria for tactile structural vibrations and sound transmission, especially in long-span residential context.

The research aims to improve vibro-acoustic performance while maintaining structural integrity through the integration of a resilient interlayerlayer between that adds damping and decouples the system acoustically. A comparative study of various connection types, including steel mesh, screw fasteners, and notches, and their improved versions was conducted, with resilient notch connections showing the most promise. This study further investigated the floor performance by evaluating and comparing three types of floors: traditional, decoupled, and a conceptual floor featuring the resilient notch connectors.

Results indicate that altough a significant reduction in connection stiffness for the conceptual floor was found, the bending stiffness was only reduced by approximately 10% relative to the traditional floor. While for the vibration performance there were positive indications for an improvement, such as an increase in damping ratio of 4.2% compared to 2.9% in traditional floors, further investigations are required to show the significance of the improvement. The acoustic results indicate that the conceptual CCC floors provide improved potential acoustic performance, particularly in mid to high-frequency ranges, due to effective decoupling and increased damping. However, further research is required in the critical low-frequency range to provide further improvements.

In conclusion, resilient notch connections can significantly improve the governing acoustic insulation of CCC floors without increasing floor height, but reaching the criteria remains a challenge. The findings offer potential for reduced material use and enhanced sustainability in multi-residential buildings, though further investigations are necessary to address dynamic issues fully.

Keywords: *Timber-Concrete composite, TCC, CLT-Concrete Composite, CCC, notches, acoustics, vibrations, damping, decoupling, resilience, floating floor, sound transmission, acoustic insulation.*

Acknowledgements

Before you dive into my master thesis I would like to say my word of thanks to several people for their support over the last year.

First of all, I would like to thank Arjan Habraken for his supervision throughout the project. His combined academic knowledge and practical experience in innovative structures, along with his critical perspective on how I communicated my story were very valuable to me. I would also like to thank Susanne Bron-van der Jagt for her supervision, enthusiasm, positivity and the time she made available to me help me fully grasp the dynamic design aspects and methods. Furthermore, I would like to thank Faas Moonen for his inspiration and many great advises throughout my studies.

Furthermore, I would also like to thank Jelle Langedijk of Level Acoustics & Vibrations B.V. for his time-investment and collaboration in the execution, processing and conclusion formation of the experimental vibration data, along with his general advises and review of the thesis. Besides, I would also like to thank Vincent Staat of MDLX for our great contact about the (experimental) structural performance of the CCC floors.

Additionally, I thank Geelen Beton, Verhoeven Timmerfabriek and the personnel of the Structures Laboratory of the TU/e for their collaboration in the fabrication of the test specimens and the execution of the experimental tests.

At last, I thank my family for their constant confidence in me, my study & football friends for their many great advises, critical reviews, 'gezelligheid' and distractions, and especially my girlfriend for her unconditional support.

Contents

1 Introduction

In the last century, Europe featured many damaged or demolished buildings and large shortages of steel caused by the two world wars on the continent. To rebuild or reinforce these buildings, a solution was found in Timber Concrete Composite (TCC) floor systems [57]. As shown in Figure 1.1a, the initial systems featured a timber joist layer and a coupled concrete top layer. The coupling of the two layers constraints the horizontal slip of the concrete and therefore forces the two layers to collaborate together. This collaboration is called 'composite interaction'. It indicates the cooperation between concrete, with its favorable compressive strength, and timber, which performs significantly well concerning its tensile-flexural properties relative to its weight. It results in the ability to reach long spans between 7 and 15 meter, which made it a good alternative for floor systems using steel. Furthermore, covering timber, a combustible material, with concrete increases the fire resistance properties of the composite. Besides, it can not only be used in new constructed building but also proved to be a good solution to easily reinforce existing timber floors.

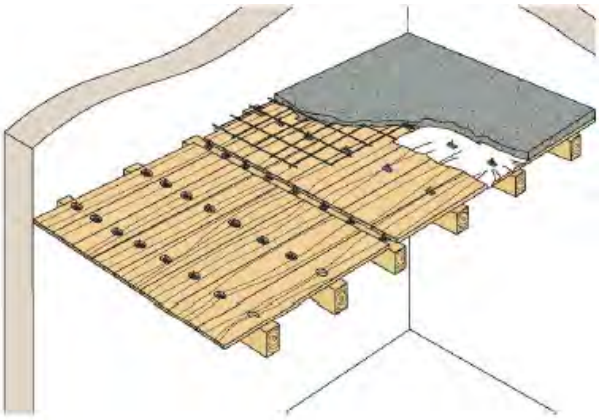

(a) TCC joist floor, studded dowel-type connectors (Tecnaria dowels) [50].

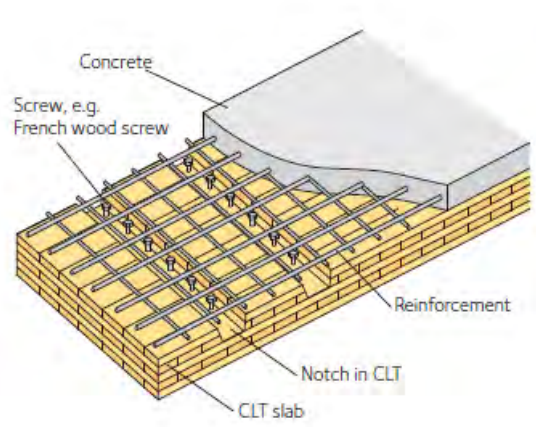

(b) CCC floor, notch connector system [24].

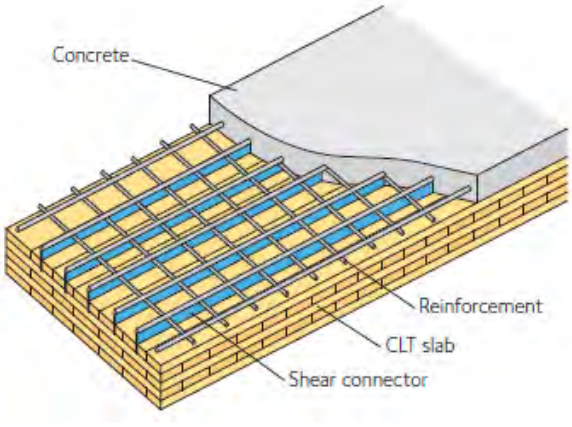

(c) CCC floor, HBV connector system [24].

Figure 1.1: Possible designs of TCC and specifically CCC floor systems.

Next to the development of TCC floors, engineers and researchers have put their attention back on the general usage of timber for structural design of buildings and infrastructure due to low environmental impact of the material [33]. This results in many developments and innovations over the last decades. One of these developments is Cross-laminated Timber (CLT). In this type of engineered timber, also referred to as mass timber, a series of often pine or spruce lamellae are perpendicularly stacked and glued upon each other This creates a massive timber slab element. One of the main advantages of CLT comes from its decrease of anisotropic properties naturally present in the timber. Therefore, CLT contains both longitudinal and transverse stiffness of significant magnitude, allowing for a larger geometrical freedom. Furthermore, due to its configuration as massive slab it features a high bending stiffness resulting in decreased floor heights compared to other timber floor types such as cassette floors. This is especially governing in high-rise buildings where a decrease in floor height results in significant gains over all the floors.

As mentioned in previous paragraph, this effect can be even further enhanced when the timber is combined with a coupled concrete top layer. When using CLT as base layer, a CLT-Concrete Composite (CCC) floor is formed. Due to the combination of decent transverse stiffness of the CLT and the isotropic stiffness of the concrete, the floors can also be used in lateral bracing systems [55] or possibly even 2-direction spanning systems [39]. Similar to joist TCC-floor, the composite interaction can be ensured by several types of shear connectors, such as screws, longitudinal glued-in steel meshes and (perpendicular) notches in the timber. An example of the implementation of the latter two is shown in Figures 1.1b and 1.1c. A great recent example of the usage of CCC floors with notches as shear connector is the in Amsterdam built 73 meter high (21 levels) residential tower HAUT. The construction finished in 2021 and featured a BREEAM outstanding classification for sustainability parlty due to the use of CCC floors [1], [55].

However, there is also another reason CCC floors were used in the HAUT building: mass. Although the lightweight of timber is one of its main benefits, its low mass makes it also susceptible to vibrations. Especially in longer spans, this can cause major comfort problems in two dynamic aspects shown in Chapter 1. The first one is in the form of human-induced tactile structural vibrations perceived by users on the same floor, e.g. the vibrations a person working at its desk feels and when somebody is walking in the room. Although very generalized, in the field of light-weight structures, this is often referred to as 'vibrations' in short. This criteria often becomes governing after a span of 7.5 meters for pure CLT floors [45]. The second aspect is acoustic performance in the form of sound transmission to the unit underneath the source. The lack of mass in pure timber floors therefore often needs additional measures, such as extra structural height for increased stiffness, additional loose mass and resilient insulation layers. Due to the contribution of concrete, TCC structures already feature this required additional mass and an increased stiffness to improve dynamic performance. This is especially important since the ratio between these two influences the natural frequency, which is one of the main parameters of dynamic response and is most commonly kept above approximately 8 Hz [21], [45], [53], [58]. While an increase of stiffness increases the natural frequency, an increase in mass and span lowers it. Beneficially, the transformation the CLT floor into a CCC floor generally results in a higher increase of bending stiffness relative to the increase of mass, thus increasing its natural frequency [45], [53], [58]. AT last, CCC floors feature an additional increased dynamic performance due to the relative high mass of CLT compared to other timber floor types and featuring beneficial transverse stiffness.

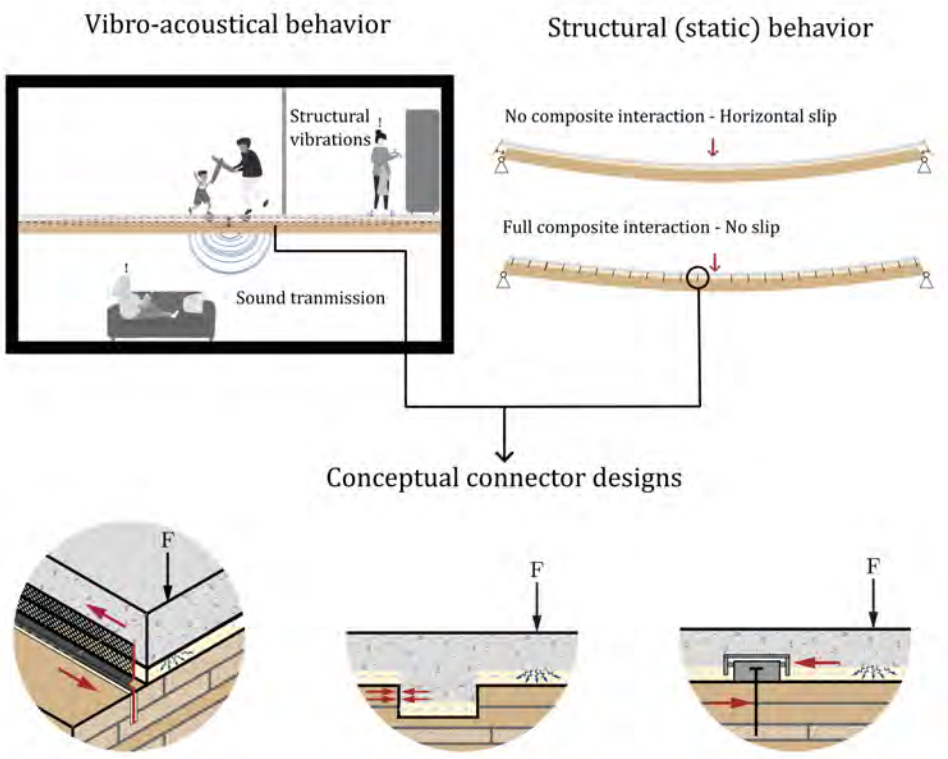

Figure 1.2: Overview of the three considered performance aspects and possible connector designs to achieve dynamic resilient behavior while maintaining structural composite interaction.

Although these properties are beneficial for its dynamic performance, a long-span CCC floor purely designed for static structural criteria will not satisfy tactile vibration and acoustic criteria. The vibration criteria can often be reached by the addition of dead mass and increase of dimensions. While the acoustic performance could benefit from these measures, it still often requires the addition of decoupled elements such as (heavy) floating floors or suspended ceilings. This results in a much higher material usage and total floor height than required for the static requirements. In residential context, floating floors are often used due to its increased damping, which especially improves the vibration performance, and decoupling, which mainly improves the acoustic performance. However, the extra material used in floating floors is not used for the structural gain due to their decoupled nature. Therefore, the focus of this study is to integrate a resilient layer in between the CLT and concrete layers to add damping and the decoupling effect in the structural composite system aiming to reduce the need for additional measures, material reduction and total floor height. Since the structural coupling and acoustic decoupling feature contradicting natures, special focus should be placed on the shear connector detail to ensure acoustic decoupling in the form of free vertical movement while constraining horizontal slip to maintain the composite interaction as shown in Figure 1.2.

1.1 Research objective and outline

As introduced in previous section this thesis will focus on increasing the damping and decoupling in a CLT-Concrete composite floor to improve its vibration and acoustic performance while maintaining its structural performance. This will be done by the integration of a resilient insulation layer in between the structural CLT and concrete layers. The study will focus the design of floors for multi-floor residential buildings due to their increased usage of long-span systems for flexibility and its high impact on vibration performance and the high requirements for acoustic sound transmission between separate units. However, due the novelty of the principle, the contradicting nature of the principle and many influencing parameters, this study will only explore the potential of vibro-acoustical improvement. This objective can be summarized in the following main research question:

Can a composite connector detail of a simply supported long-span CLT-Concrete Composite floor, spanning a single direction over a single floor field, be designed to improve vibro-acoustical performance while maintaining its structural composite interaction?

The main research questions will be answered by the use of the following sub-questions:

1. *What is the structural and vibro-acoustical performance of CLT floors using a concrete layer without composite interaction?*
2. *What is the structural and vibro-acoustical performance of CLT-Concrete composite floors using commonly used connection types?*
3. *Which commonly-used or conceptual composite connection type shows the most potential for improved vibro-acoustical performance of CLT-concrete composite floors?*
4. *What is the structural performance of floors using the designed composite connector detail?*
5. *What is the vibration performance of floors using the designed composite connector detail?*
6. *What is the acoustical performance of floors using the designed composite connector detail?*
7. *Does the designed composite connector detail feature improved vibro-acoustical performance while maintaining composite interaction?*

The first, second and third sub-question will be answered in the first part of the thesis. This part will cover a literature review, a multi-criteria analysis and detailed assessment of the connector design to answers these questions and are described in Chapters 2 and 3.

The fourth to seventh sub-question will be answered in the second part of the thesis consisting out of Chapters 4 to 7. For this part the four floor types shown in Figure 1.3 will be considered. The traditional floor-type refers to standard CLT-Concrete-Composite floors as introduced in previous section. It features satisfactory structural performance, but poor vibration and acoustic performance due to its lack of damping and decoupling. In contrast, the decoupled floor-type, features poor structural and vibration performance due to the lack of composite action. However, due to the presence of decoupling, the acoustic performance is expected to be satisfactory. The conceptual floor type is based the main focus of this study and integrates the principles of the

traditional and decoupled floor-types. While it maintains its composite action, it theoretically also features increased damping and decoupling. At last, another way to combine the traditional and decoupled floor is by the addition of a floating floor on top of the traditional CCC floor, as is common practice at the moment. It features the same combination effects as the conceptual floor, but differs from it by its considerably increased cross-section and weight. The latter also further increases its theoretical acoustic performance. Due to this inherent difference compared to the other floor-types it is difficult to compare and will therefore not feature extensive investigations.

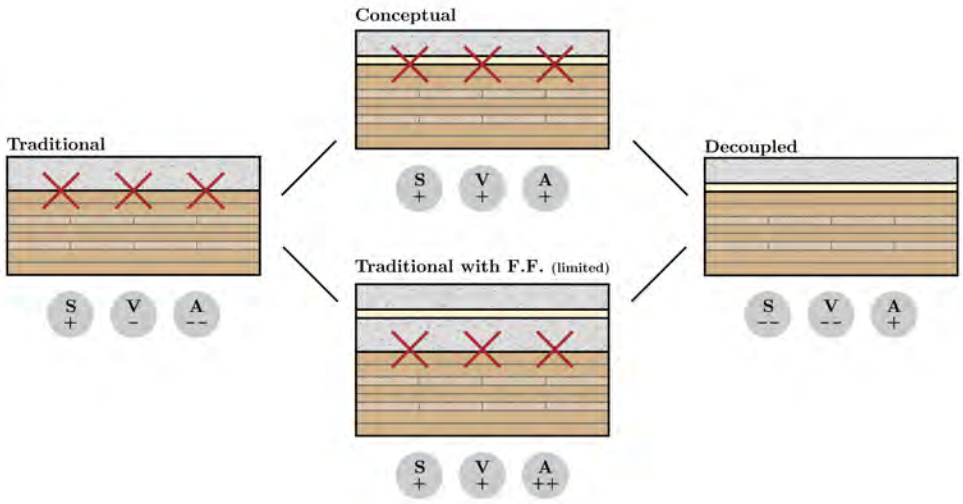

Figure 1.3: Schematic of the four considered floor types, including their theoretical structural (S), vibration (V) and Acoustic (A) performances.

These floor types will be further dimensioned in accordance to three design categories, as described in Chapter 4. It will result in nine extensively investigated floors and three limited investigated floors in part 2. Chapter 5 will focus on the evaluation of the structural performance of these floors, using numerical push-out tests to determine the connection stiffness, cross-section analysis through the separated and extended γ-method, notch failure analysis through the Boccadoro-model and experimental 6-point bending tests. Chapter 6 will describe the vibration performance of these floors based on the results of the re-EC5 method, numerical vibration analysis using time-dependent and frequency-dependent analysis types and experimental vibration ball-fall tests. Chapter 7 will provide an indication of the acoustic performance of the considered floor based on the analytical calculation software Bassist, the numerical vibration analysis and the experimental vibration ball-fall tests.

In Chapter 8 the conclusions of the three performance aspects will be brought together and the last sub-question and main research question will be answered. Chapter 9 will outline recommendations for further research based on the results and gained experience during this thesis.

1.2 Project scope

Due to the large amount of parameters involved into the design of TCC structures, and especially when extending it with vibrational and acoustical performance, it is crucial to set boundaries to the research.

As mentioned in previous section, the study will be in the context of multi-level residential buildings. The reason is the application of these floor types in residential high rise, due to the long span situation and the slim dimensions compared to other mass timber(-composite) floors. Furthermore, often floating floors are using in residential buildings instead of suspended ceilings to allow for an exposed timber ceiling, thus fitting the study.

A corresponding structural schematic of a simply supported 8.7 m span will be considered. Although the systems features a significant transverse, only a single floor direction will be considered.

For the vibrational context only the perception of the floor within the same single room apartment will be considered. The floors are therefore assumed to be fully dilated from their neighbors.

For the acoustic performance, the sound transmission through the floor to another residential unit directly underneath will be assessed. Hereby, the flanking transmission is outside the scope for the project and thus only the direct transmission will be evaluated. However, even though the floor system will be put and compared into an residential context, the aim of the study is to gain improved vibro-acoustical performance and thus not specifically satisfy the associated requirements.

Beside the environmental limitations, there are also some design limitations. First of all, only CLT fully using C24 timber according to EN 338:1996 will be used. For the CLT configurations 5s-, 7s-, 7ss- and 8ss-ply are considered. Secondly, the concrete will be limited to a minimum thickness of 60 mm based on standard practice for concrete structural floors and a maximum of 100 mm. For the concrete grade only the commonly available C20/25 to C50/60 grades will be considered. Besides, due to the limitation to only standard available concrete, the density of the limited to the standard $\rho = 2400 kg/m^2$. Besides, to prevent moisture problems, a moisture retaining foil should always be present between the concrete and CLT or insulation. At last, the insulation layer is limited to the usage of Rockfloor Base mineral wool with a constant thickness of 20 mm on the surface and in the notch.

2 Literature review

This chapter will review essential background info in the design and performance of timber, TCC and CCC structures. Firstly, the fundamental connection systems and the impact of the composite actions will be discussed in Sections 2.1 and 2.2. Secondly, the leading principles for dynamic performance, conventional methodology and common floor performances will be described in Section 2.3.

2.1 Connection systems

The collaboration causing the structural benefits between the timber and concrete is called composite (inter)action and is achieved by the constraining the longitudinal slip between the two materials. This is reached by implementing a connection system transferring forces from one element to the other. As shown in Figure 2.1a there is a large variety in connection systems with each its own behavior. The amount of composite interaction is mainly determined by its stiffness of this connection, which relates to the slope of the load-slip diagram shown in Figure 2.1. The higher the stiffness, the higher the composite interaction. Other important factors are the ultimate failure load and the ductility of the system. All these factors can be seen in Figure 2.1 by respectively the slope, the ending of a line and the continuation of the line after the peak in the load slip diagram.

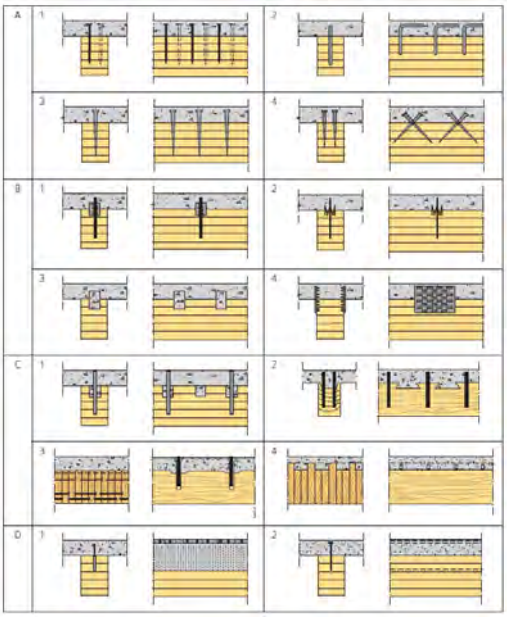

(a) Overview of commonly used connection systems [31], [38].

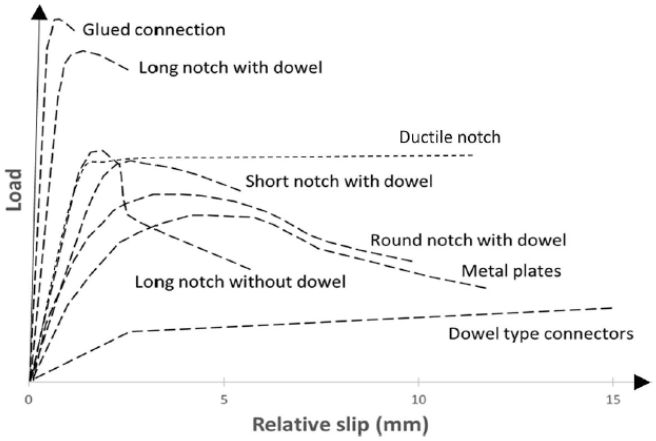

(b) Load slip diagram of different connection systems [33].

Figure 2.1: Overview of TCC connection systems.

It can for example be observed that glued connections feature a very high stiffness and strength, while featuring a very low ductility, causing undesired brittle failures. Next to that it is

difficult to control the quality of glued connections [14], [21]. In contrast, dowel type connectors, shown in group A of Figure 2.1a, feature low stiffness and strength but feature high ductility and are very easy and fast to manually install (for low amounts). Especially (inclined) screws are one of the most used connection types together with two other connection types: Notch connections and metal mesh systems.

The former, shown in group C of Figure 2.1a and Figure 1.1b, is created by making a indent in the timber which is filled up by the concrete during pouring and therefore creates a direct mechanical interlock between the two elements. It strongly advised to add fasteners, for example in the form of self-tapping screws, in the notch to increase the post-peak ductility and act as vertical reinforcement to prevent the almost impossible to predict brittle concrete notch shear failure [4]. Furthermore, the fasteners are also critical in their role to prevent separation, also referred to as gap opening, between the timber and concrete. This is caused by the eccentricity between the notch and the axial forces in the two layers, difference in shear deflection of the two materials and if compressive plasticity in the timber at the contact area is reached due to the volumetric vertical expansion of the timber, and can cause a preliminary sudden and quick progressive collapse of the system [4]. It was even advised in to add additional surface fasteners at the center if there are no notches present [29]. Since notches work with the interlock of the timber and concrete in the primary span-direction of the floor (and preferably in the longitudinal direction of the timber), continuous notch grooves will be made in the transverse direction of the floor. However, also discrete notches could be used, for example for better control of the connection stiffness relative to the shear distribution over the span [3]. Besides, discrete notches feature a higher stiffness per mm notch width due to loaded timber not only being supported from its bottom plane but also from its sides. They are however more difficult to construct. Furthermore, although an increase of notch depth increases the stiffness, it is advised to limit it too allow for the governing of the Notch Timber Compression failure of the system, since it is the only available ductile failure mechanism in TCC structures with notch connections [4], [33]. This is especially the case for most types of CLT where the penetration of the notch depth into the second perpendicular layer lowers the connection stiffness and strength considerably due to low perpendicular shear strength and stiffness [34], [39]. This can however be tackled by the usage of double longitudinal layers in the CLT, as used in 7ss- and 8ss-ply, and accepting a lower transverse stiffness. Additionally, due to improvements into in Computer Numerical Control (CNC)-milling, notches become more and more easy to install, especially in larger production scales.

The metal mesh systems, shown in group D of Figure 2.1a and Figure 1.1c and for which the Holz-Beton-Verbund (HBV) system is the most common, are inserted in a slender cut made in the timber and fixed by resin. Secondly, the wet concrete will go in between the mesh openings. Due to this increased bond, the mesh systems feature increased stiffness in relation to similar massive metal plate systems. The mesh systems are always placed in longitudinal direction of the floor span to transfer the shear load over the stiff plane of the mesh. These systems can reach very high connection stiffness's and features a ductile failure mechanism in the form of yielding of the steel [21]. Its largest downsides are the high labour effort and costs, and concerns about quality control [53].

It results in screws, notches and steel meshes being the most promising connection types for wide application in the building industry. An overview of in literature described connection types is shown in Table 2.1. Firstly, it important to note the large variety stiffness values, even in similar connection types, due to the many influencing parameters, such as timber type and

density, concrete grade, presence and thickness of an interlayer, presence of moisture retaining foil, notch depth, notch length, notch pre-timber length, notch edge angle and type-, diameter-, length-, embedment length-, angle- of (notch) fastener. Besides, there is a wide variety of set-up parameters influencing the results of the common used push-out tests [48]. Overall, it is most important to note that all the systems can reach high composite interaction ,between 70% and 85% [24], depending on how densely the connectors are spaced. Even the individually low stiffness screws can reach high composite interaction due to their low spacing requirements. This is especially the case since the shown values for K_s are on the top side of investigated screws [2], [33], [53]. However, the result is a significant increase of, at the moment most common, manual labor, especially in large multi-floor buildings. Besides, there its also results in a significant steel usage in these systems. For the notches it can be observed that mainly continuous notches are beneficial, especially taking into account the longitudinal spacing can still approximately be halved if required. For the discrete notches, this can also be done in even larger amount in lateral direction. Furthermore, its good to note that discrete notches feature an increased stiffness per notch width compared to the continuous notch since the directly loaded timber is not only constraint at its bottom but also its sides. However, discrete notches are also more difficult to produce.

Table 2.1: Overview of steel mesh-, notch- and screw connection systems for TCC floors including a connection stiffness indication.

#	Connection type	Slip modulus K_s [kN/mm]	Connector width [mm]	Lateral spacing [mm]	Longi--tudinal spacing s [mm]	Number of connectors per m^2 [-]	Effective connection stiffness C [kN/mm/m^2]	Ref.
1	Continuous **steel mesh** in CLT (GM4)	890	-	400	-	2,5 m	2193	[21]
2	Continuous **steel mesh** in CLT with insulation interlayer (GM7)	640	-	400	0	2,5 m	1600	[21]
3	Discrete triangular **notches** in glulam with Ultra High Performance Fiber Reinforced Concrete (GLT-UHPFRC2-35-2)	566	300	800[1]	650[1]	1,9	1088	[33]
4	Discrete triangular **notches** in glulam with High Performance Concrete (GLT-HPC-20-4)	488	300	800[1]	650[1]	2,1	938	[33]
5	Discrete triangular **notches** in glulam with High Performance Concrete and insulation (GLT-HPC-20-4-I)	387.9	300	800[1]	650[1]	2.1	746	[33]
6	Discrete triangular **notches** in CLT with High Performance Concrete (CLT-HPC-20-4)	312	300	800[1]	650[1]	2.1	600	[33]
7	Discrete rectangular **notches** in CLT (Series I)	242	200	800[2]	650[3]	2,1	465	[53]
8	Continuous rectangular **notches** in CLT (N180-2)	411	450	-	650[4]	1,53	1405	[29]
9	90 deg **screws** (SFC-100-90)	3.29	-	220	150	30,3	100	[40]
10	45 deg inclined (single) **screws** in CLT (SFC-100-45)	44,59	-	220	150	30,3	1351	[40]
11	45 deg inclined **screw**-pairs in CLT (10x240 ASSY VG @45 - VG 14)	67,5[5]	-	200	150	33,33	2250	[21]
12	45 deg inclined **screw**-pairs with 25 mm insulation interlayer (10x240 ASSY VG @30 - VG17)	42[5]	-	200	150	33,33	1403	[21]
13	30 deg inclined **screws** in CLT (10x240 ASSY VG @30 - VG10)	71,9	-	200	150	33,33	2396	[21]

[1] No full scale set-up, but assumed as common spacing in [33]. Lateral spacing can be signicantly decreased if wanted, s can be lowered up $12{,}5h_n$ [6], resulting in s_{min}=250-365 mm for h_n=25-30 mm.
[2] Kept constant with connection type 3., 725 mm in experiment of source
[3] Kept constant with connection type 3., in experiment of source 1000 mm (low-level composite, combined with [2]: C_{exp}=338 kN/mm/m^2) or 330 mm (high level composite, combined with [2]: C_{exp}=1011 kN/mm/m^2).
[4] kept constant with connection type 3., 700 mm in experiment of source (C_{exp}=1305 kN/mm/m^2).
[5] Value given for the pair.

At last, several studies have been done investigating the effect of an assumed non-load bearing interlayer. The addition of an interlayer is either interesting in the form of stiff material to function as formwork for the concrete or as insulation material for acoustic or thermal improvements. For steel plate meshes an addition of formwork generally decreased the connection

stiffness and strength by approximately -30%, due to local buckling effect over the unrestrained insulation height [21]. For screws with an added interlayer, a decrease of connection stiffness was observed from ranging from -25% to -81% and a decrease of strength ranging from -3% to -32%, due to the increased eccentricity and thus lever arm in the screw [15]. For triangular notches featured the lowest observed decrease of connection stiffness with a range of -9,56% to -20,97% [33]. Finally, it should be noted that in most of the approaches the specimen with additional interlayer, feature the same geometry for its timber and concrete layer. While this results in comparable results on small-scale it should be noted that the increased total height and eccentricity between the two layers increases its bending stiffness.

2.2 Composite interaction and calculation methods

The earlier explained composite interaction comes into three states: No interaction or collaboration, incomplete or partial interaction and complete, composite or rigid interaction, as shown in Figure 2.2. Although complete interaction is not achievable, high interaction can increase the stiffness of the structure significantly. Secondly, due to partial interaction, it should always be taken into account that in most cases there will be tensile stress in the concrete. If the tensile stresses are high enough and cause flexural cracks, the cracked part of the concrete should be seen as a non-load bearing layer in the cross-section analysis [6] due to its lost ability to transfer forces. However, next to the fact that valuable concrete is not used, the cracks can also lower the strength and stiffness of the connection. It is therefore strongly advised to design the build-up element such that the neutral axis is either very close to or far into the timber part and/or significant normal stresses are present in the structure which compensate for the tensile stresses [57]. The maximum ratio of the concrete is therefore 40% of the full height [24], while for the Thomas Clarkson Community College this ratio was even only 25% [45].

One of the main methods to calculate the amount of collaboration, effective stiffness EI_{eff}, stresses and strains is the γ-method by Mohler, implemented in Eurocode 5 by Kreuzinger [32]. It features a γ-value between 0 and 1, relating to no and full interaction respectively. This value is then multiplied by a second factor taking into account the stiffness and lever arm of the parts next to the standard sum of the stiffness of each individual part. The γ-value itself is based on the stiffness of the connector and the spacing between each connector. Due to its integration in Eurocode 5 and its due to its easy to use method it is the most common used method [8]. The major downside is however its limited applicability range: it can only be used for flat beams, single spanning systems, structural determined structures, systems with a maximum of 3 layers and only allows minimal changes over its span. However, several other methods are available.

The γ-method is spin-off from the differential equation method, where for certain parameters certain conditions were assumed, such as sinusoidal load distribution and a simply supported beam configuration. The differential equation method itself can also be used for many composite elements featuring 2 elements and provide exact results. However, the effort required for the method will increase significantly by adding extra parameters. It is therefore rarely applied in practice.

Furthermore, there is the Jorissen method. Although it looks quite similar to the γ-method, since it uses a γ-value with a similar equation for the effective stiffness, strains and stresses, there is a fundamental difference. The Jorissen-method is based on the Euler beam theory and uses a different approach on the γ-value. In the γ-method the bending stresses are calculated as

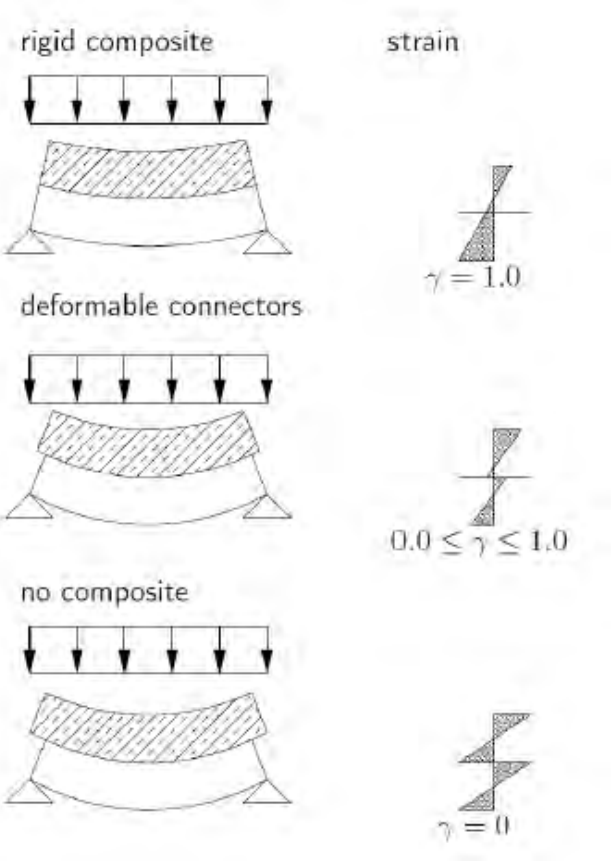

Figure 2.2: Qualitative strain diagram of TCC floor, caused by pure bending, with varying degree of interaction following the γ-method [8].

without any cooperation and normal stresses are calculated using the γ-value. In the latter, the γ-value functions as a value determining the cooperation of the secondary elements in regards to the main element. The γ-value of the main element is therefore always 1, while for the one or two secondary elements it can be anywhere between 0 and 1. Besides, for the calculation of the cooperation-included normal stresses, it can be noticed that with an increase of the γ-value the neutral axis of the composite system moves away from centroid of the main element and that when full composite interaction is reached the neutral axis of the composite system is still within the main element. Since the lever arms a_{i} are the distance between the centroids and the neutral axis of the composite system, they will follow this movement and change in value. In contrast, in the Jorissen-method the lever arms a_{i} will be frozen but not only the γ-value of the secondary element but also the γ-value of the main element will be adjusted using a different formula. It results in different input in the similar final equations. However, as shown by Roks [50], the final results of the γ-method and the Jorissen-method are well in agreement. The major advantage of the Jorissen method is that there are equation available for elements up to five layers.

Fourthly, an approximation method for composite systems, using La Place theory, was made by Girhammar [22]. It follows a similar procedure as the γ-method, however it assumes arbitrary boundary conditions and loading configurations. For these situations it assesses the beam with a fully composite interaction. The full composite stiffness is then later replaced with the effective stiffness based on two parameters: the composite action parameter and the relative bending stiffness parameter. As said this method is an approximation, but it still agrees for

simple situations very well with the other mentioned methods. Next to that, it allows for more reliable calculation of 'non-standard' situations with varying boundary conditions and load configurations [50].

Another method is the method of shear analogy by Kreuzinger. This method does not feature the limitations of the γ-method and is unique since there are no limitations or increased efforts for the amount of layers of the system. This method is therefore especially use full in the calculation of multi-layered systems such as CCC floors, where the CLT can be modeled with individual layers. The main principle of the method is the creation and coupling of two separate system, as shown Figure 2.3. However for elements with only two layers, these systems still have to be created and therefore requires much more effort compared to the other methods [8].

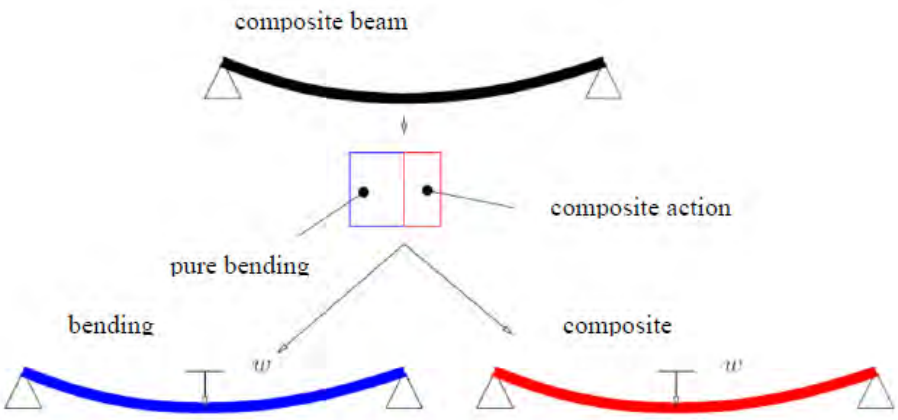

Figure 2.3: Splitting of the composite beam in two systems following the method of Shear analogy [8].

In the case of a two element system, the Strut-and-tie method, next to the γ-method, is much more practical. This method is well known in the field of structural engineering and models a two element system as two beams in their centroids with coupling elements in between representing the connections, as shown in Figure 2.4. Similar to the method of shear analogy, it does not feature the limitations of the γ-method. While it can also be calculated by hand, due to the considerable increase of effort when assessing systems with increasing amount of layers it is practically always used in combination with software.

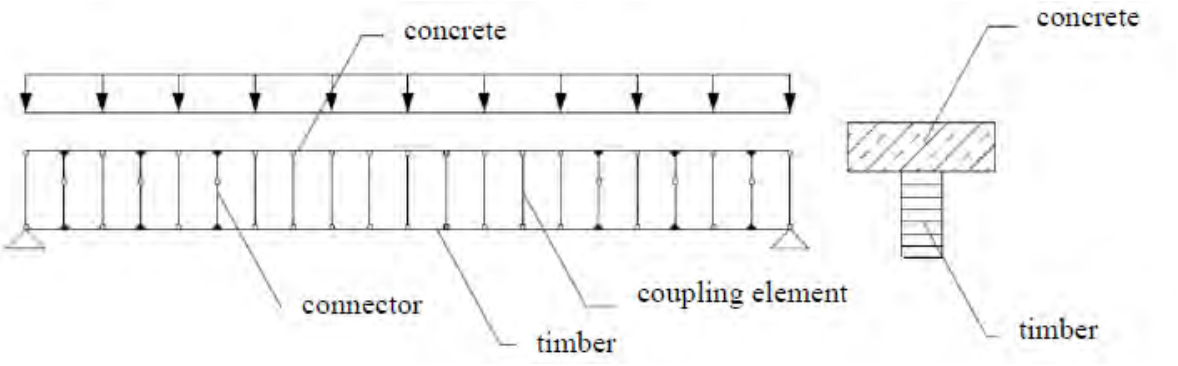

Figure 2.4: Modelling of a TCC system as a framework following the Strut-and-Tie method [8].

At last, there is the numerical method called the Finite Element Method (FEM). Due to the complexity of most space and time-dependent problems the corresponding Partial Differential Equations are approximately solved by FEM [7]. For the usage of FEM a digital model has to be made, which the software subdivides, in small finite elements. This is called the discretionary of the model. The smaller the elements, the more accurate the result but the higher the computation time of the system. Therefore a good balance between these two parameters should be found to gain reliably results while keeping the efforts low. This also applies for the complexity of the system in regards to other parameters such as boundary conditions or amount of layers. The method is therefore not often used in daily design, but is used in calculations of complex geometries and detailed research [8].

2.3 Vibration and acoustical performance

As introduced in Chapter 1, the vibration and acoustic performance is often governing for long-span Timber, TCC and CCC floors. The field of dynamics considers the effect of motion on a body. When the body is elastic, a cyclic motion will occur. This cyclic motion is called a vibration [53]. For floors this is usually started by a periodic vertical load, causing an up and down motion in its natural frequency. Alignment of the cyclic loading with the eigenfrequencies, for which the first one is often the strongest and also referred to as the natural frequency, can cause a significant buildup of the response called resonance. While there can be many sources of vibrations with different energy levels, such as sound, human activity, machinery, traffic and earthquakes, pedestrian traffic is the most usual source for floors. While the dynamic behavior is not critical due to safety aspects, it can be governing for comfort requirements. The comfort regarding vibrations of the floor can be split into two main branches. Firstly, the tactile structural vibrations are perceived by directly standing on top of the floor. The governing frequencies are in the range of 0 and 20 Hz. Secondly, there is acoustics which is the perception of sound waves through the air, caused by a vibrating element. For floors the sound waves can be caused due to longitudinal, or compression, waves trough the floor or structural, or bending, waves of the floor. While the former is especially governing in the high hearable frequency range up to 5000 Hz, the latter features similarities with the tactile vibration and is governing in the low frequency ranges down to 25 Hz.

2.3.1 Basics and parameters of tactile vibrations

Tactile structural vibrations of the floors, also often referred to as human induced vibrations in the context of this main source, can be directly described as mentioned in the previous paragraph. When walking a person want to set off its foot, it creates contact and puts a downward force on the floor causing a deflection. While taking the next step, the force is (partly) relieved, lowering the deflection and causing an upward motion. With the next steps this process is repeated, causing the up and down motion of the floor shown in Figure 2.5. These vibrations can then be felt by the walking person itself or another person present on the floor.

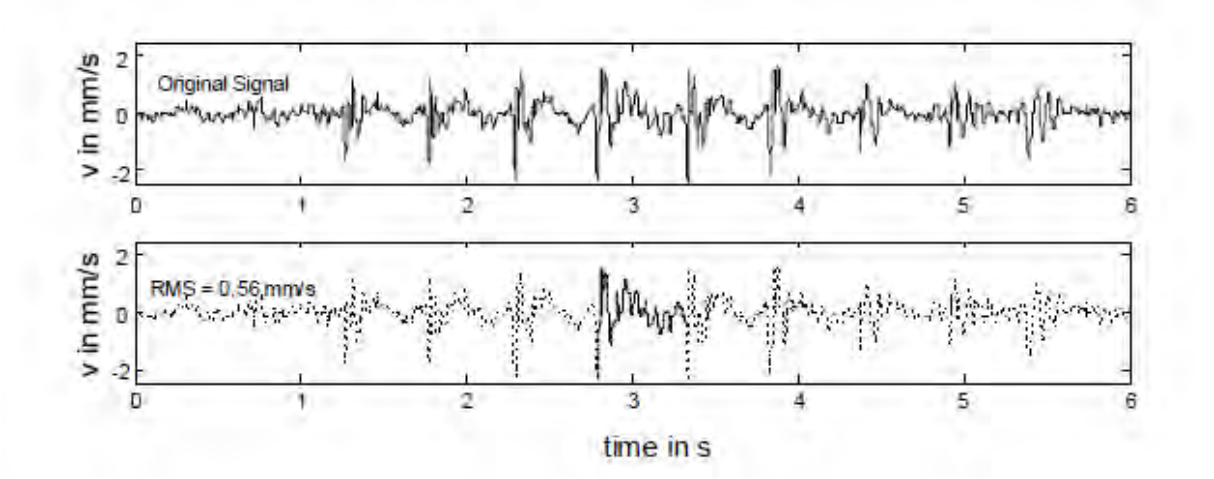

Figure 2.5: Top graph: Typical velocity response cycles of a floor due to walking loads. Bottom graph: The selection of the time frame for a single step. [20].

The response of the floor can be characterized by four main properties; the eigenfrequencies of the floor, its modal shapes, its modal mass and its modal damping. The eigenfrequencies, or natural frequencies, are the specific amounts of oscillations per second, on which an element is much more susceptible to vibrations. When the external force is relieved, the free response of the element is mainly formed by the linear superimposed eigenfrequencies. The lowest frequency is called the first eigenmode, which needs the lowest amount of energy to be excited and often follows a half cycle sinusoidal shape. Following eigenmodes often become weaker and can either be a multiplication of the original shape or become very complex shapes, for example due to a combination of modes in two directions. In theory, a continuous system like a beam or a slab can have an infinite amount of eigenshapes. However, luckily only the first few have significant impact on the response caused by walking. As described, if the load cycle aligns with one of the eigenfrequencies, by exactly exciting the floor while it reaches a peak amplitude in its free state, the magnitude of the response can be significantly amplified.

Another parameter significantly impacting the magnitude of the response is the modal mass of the floor. The modal mass is the mass activated by the a specific mode shape. In general, it can be said that an increased amount of activated mass, lowers the response magnitude.

The last of the main properties is modal damping, which can be described as the dissipation of energy in to a form which does not impact vibrations. It lowers the response magnitude under excitement and determines the rate of decay of vibration amplitudes under free vibrations [27]. Sadly, it is also the most complex property, effected by each small detail of the full structure, e.g. the stiffness and friction of each material, each connector, each joint and each contact.

Although these properties are clearly defined and described, it is hard for designers to control them. They try to mainly control them through three parameters: Stiffness, mass and, due to its complexity only limited, damping.

Overall an increased stiffness of the structure lowers the deflection (under static and dynamic loads), and therefore also create a lower response magnitude. Furthermore, an increase in stiffness also increases the natural frequencies, which is a positive effect as explained below. Next to the material and element type, the stiffness of the structure is determined by its boundary conditions. While the determination of these aspects under static conditions are common practice for structural designers, to accurately determine the dynamic stiffness S_d of the structure some key differences between static and dynamic conditions should be taken into account. For example many supports are seen as fully hinged under static conditions, while they behave much more rigid under dynamic conditions due to the relatively small forces and deflections. Besides, even though the floor is only one-way spanning, the transversal stiffness of the element should also be taken into account since it influences the mode shapes and the amount of activated mass in this direction.

Secondly, the mass of the floor, in the form of kilogram per square meter, is the most straight forward parameter. An increase floor mass, the more kilograms will be activated, thus increasing the modal mass and lowering the response magnitude. There is however one downside, an increase of mass lowers the eigenfrequency of the structure.

Third and lastly, as made clear earlier it is difficult for designers to increase the damping inside of the element. They can however also apply a floating floor principle or tuned mass dampers. The ideas of these systems is that the resonance magnitudes are decreased by absorbing the energy. They both are however still hard to design, and if wrongly designed can even negatively increase the response of the floor. Besides, the usage of tuned mass dampers is very costly.

2.3.2 Design criteria for Structural vibrations in timber and TCC floors

As said, human-induced vibrations are a comfort and thus an perception issue. Since each individual differently perceives vibrations in different situations, it is difficult to come up with simple and clear criteria. For example people are often more annoyed by vibrations while doing activities requiring high concentration, like working or performing surgery, than by activities requiring low concentration. Besides, the annoyance is also based on how active the person itself is at the moment of perception, a person running or walking perceives vibrations not as strong than a person standing still or sitting at a desk. It was found that the general walking frequency of people is around 2 Hz [27] and that humans are most sensitive to vibrations between 4 and 8 Hz [51].

Ohlsson therefore proposed to split timber floors into low frequency and high frequency floors. The low frequency floors feature a natural frequency up to 8 Hz. For these frequencies resonance is governing due to the high likeliness and impact of the response amplitudes coinciding with the walking frequency. For high frequency floors with a natural frequency above 8 Hz, this effect and the often response magnitude limiting mass is much smaller and are therefore governed by the transient response directly caused by excitement from the footfall. He therefore proposed three main criteria; the natural frequency of the floor should be higher than 8 Hz, the static deflection under a 1 kN force on the floor should be below 1.5 millimeters, and the peak

velocity due to a unit impulse should be limited. The design process following this method is shown in Figure 2.6. The first and second criteria make sure that problems due to resonance are prevented since low frequency floors are excluded and the low frequency resonance, which is seen as semi-static, is limited. The third criteria is an addition to the second to control the magnitude response of the higher frequency components.

This approach is also adopted in the Eurocode 5, which focuses on timber structures and was published in 2004. However, since this method is very conservative regarding low frequency floors, only considers a overgeneralized modal damping ratio of 1%, uses a hard to calculate and only mathematical unit impulse instead of a physical property, it includes every property of eigenmodes up until 40 Hz, it is difficult to use and accurately verify [27]. Therefore several other methods are proposed.

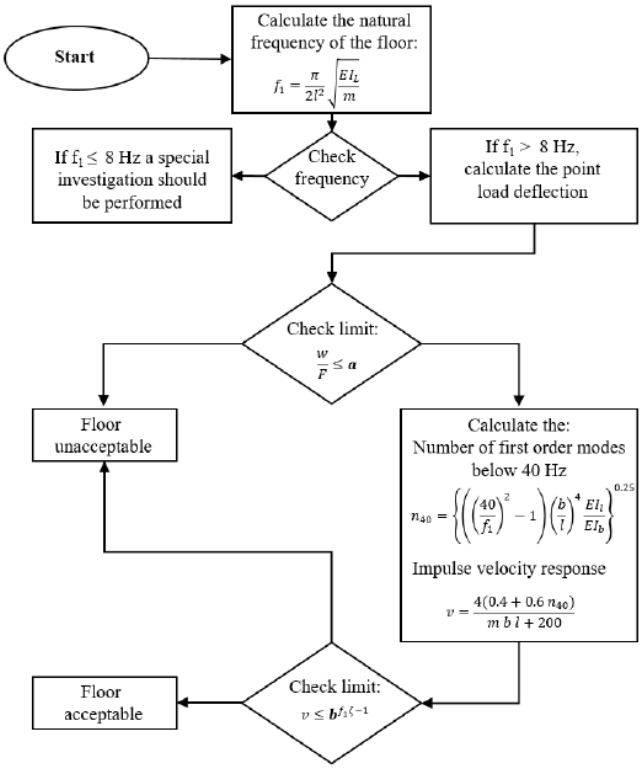

Figure 2.6: Schematic of the design process following the Ohlsson method adopted in Eurocode 5 [51].

The in 2021 published technical specification for the design of timber concrete composite structures, CEN/TS 19103, specifies the use of the vibration requirements mentioned in Eurocode 1 instead of the method mentioned in Eurocode 5 [18]. This is due to the natural frequency of TCC floors often being lower than 8 Hz. Eurocode 1 only uses a frequency and deflection criteria based on two function categories [17]. For floors with mainly pedestrian traffic, the natural frequency should be above 3 Hz and the static deflection due to the quasi-static load combination not greater than 34 millimeter. For floors with a lot of jumping and/or dancing, this is respectively 5 Hz and 12 millimeter. The British annex to Eurocode 1 increases the natural frequency requirements to respectively 5 and 8.4 Hz [45]. Overall, these criteria are not strict in

comparison to the other method and mostly focus around preventing resonance and not transient responses.

Another of the main recurring methods is to use the ratio of natural frequency in regard to the static deflection, first mentioned in 2002 by Hu et al [27]. Overall it allows a lower frequency if the static deflection is also decreased. The parameters of this ratio are over time further optimized and validated for timber joist, CLT and CCC floors [53]. The latest criteria for CCC floors mentioned in the Canadian design guide of 2020 for TCC floors is shown in Equation (2.1) [11], where f_1 is the natural frequency of the first eigenmode and deflection due to a 1 kN force at mid span.

$$\frac{f_1}{d_{1\text{kN}}^{0.14}} \geq 5.75 \tag{2.1}$$

An additional analytical method is to calculate and evaluate vibrations in timber floors is the usage of the OS-RMS value. This method is based on the Human Induced Vibrations in Steel Structures (HIVOSS) publication [16] and the follow-up 2009 JRC joint report [20] for its implementation into building codes, which do not focus themselves on timber floors but on similar light-weight steel floors. The OS-RMS value stands for the one step-root mean square value and is named after the method to create an effective response value by evaluating the acceleration over the time frame of a single step as shown in Figure 2.5. Based on the evaluation of many experimental results, graphs for each specific damping ratio were made. One of those graphs is shown in Figure 2.7. The input of the eigenfrequency and modal mass of the floor can be calculated through supplied formulas and guidelines described in the report for many situations, such as a variety of boundary conditions and orthography of floors. From the graphs the OS-RMS-value can be determined and the class the floor is in. To integrate the earlier described variety in perception based on activity, different functions allow a different range of classes, as shown in Table 2.2.

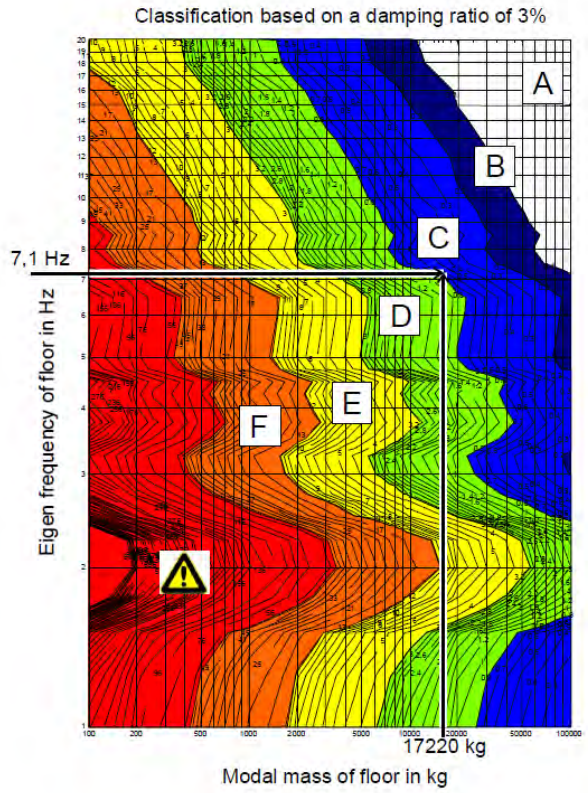

Figure 2.7: Example of the use of a design chart of the $OS - RMS_{90}$ for floors with a damping ratio of 3% [20].

Table 2.2: Allocation of classes of perception A to F to threshold values of $OS - RMS_{90}$-values and relation of occupancy's of floors to comfort limits [20].

Class	$OS\text{-}RMS_{90}$ Lower limit	$OS\text{-}RMS_{90}$ Upper limit	Usage of the floor structure: Critical areas	Hospitals, surgeries	Schools, training centers	Residential buildings	Office buildings	Meeting rooms	Senior citizens' Residential building	Hotels	Industrial Workshops	Sports facilities
A	0.0	0.1										
B	0.1	0.2										
C	0.2	0.8										
D	0.8	3.2										
E	3.2	12.8										
F	12.8	51.2										

Recommended
Critical
Not recommended

The last main analytical method is mentioned in the draft of the revision of Eurocode

5, planned to be published in the coming years. This revision is not only needed tackle the mentioned problems the currently adopted Ohlsson method has, but to also provide guidelines for low frequency floors below the 8 Hz boundary. This is more often the case with the increased usage of TCC joist floors, CLT-floors and CCC floors. The method, for which the design process is shown in Figure 2.8, is next to the point load deflection focused around the Response factor. This factor can be calculated through a simplified formula for the RMS-acceleration for floors with a natural frequency between 4.5 and 8 Hz and through the RMS-velocity response for floors with a natural frequency above 8 Hz. The method only features low-frequency floors until a natural frequency of 4.5 Hz since lower frequencies are increasingly harder to model due to resonance and even heavier timber and composite floor variants will not reach such a low natural frequency. Furthermore, similar to the JRC report, the method features extra guidelines to more accurately calculate parameters like frequency, damping and modal mass. Besides, Table 2.3 shows that the response factor or stiffness criteria determines floor performance level of the floor, while Table 2.3 shows the recommended floor performance level per function. Here it can be seen that in contrast with the JRC report, office buildings require stricter criteria than residential buildings. At last, from a comparison study between the current and revised Eurocode 5, it was found that there are significant changes between the two methods, but in general the revised version is more strict [51].

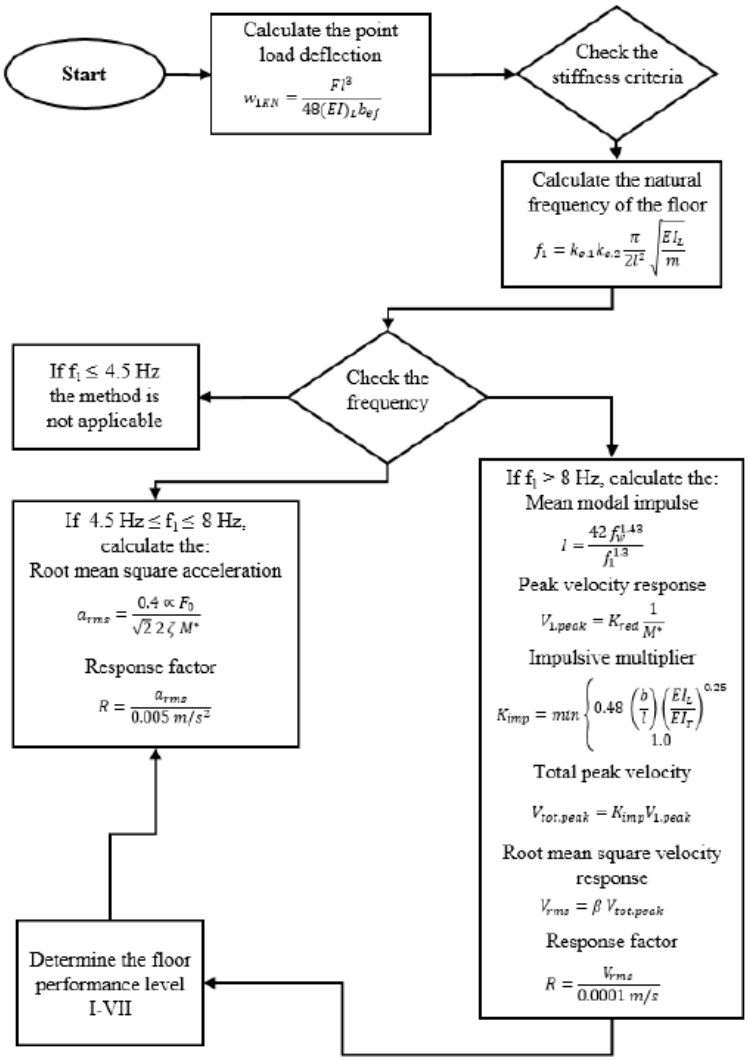

Figure 2.8: Schematic of the design process following the method described in the revised Eurocode 5 [51].

Table 2.3: Floor vibration criteria of the classification system in the revised EC 5 [51].

	Floor performance levels						
Criteria	**I**	**II**	**III**	**IV**	**V**	**VI**	**VII**
Frequency f_1 [Hz] $\geq$	4.5						
Stiffness criteria w_{1kN} [mm] $\leq$	0.25		0.5	0.8	1.2	1.6	Unacceptable
Response factor R	4	8	12	16	24	32	Unacceptable
Acceleration criteria when $f_1 < 8$ [Hz] a_{rms}[m/s^2] $\leq$	R$\times$ 0.005						
Velocity criteria when $f_1 \geq 8$ [Hz] v_{rms} [m/s] $\leq$	R$\times$ 0.0001						

Table 2.4: Recommended selection of floor performance levels based on function [51].

Use category	Quality choice	Base choice	Economy choice
A (residential)			
multi-storey	level I, II, III	level IV	level V
Single house	level I, II, III, IV	level V	level VI
B (office)	level I, II	level III	level IV

In addition to the analytical methods, FEM models can be used to simulate dynamic behavior of floors. These models could estimate the eigenfrequencies of complex structures, it has for example already been accurately applied to light weight steel-concrete composite floors, TCC joist floors and CCC floors. An example of the latter is shown in Figure 2.9. The results of this models can be compared to the above described criteria to determine the vibration performance.

Furthermore, vibrations can also be experimentally tested in a similar way as with FEM modeling. These often use a tapping machine **VanThai2022EvaluationFloors** or heel drop plate [30] as an exciter and several accelerators as transducers. This can be done in the laboratory or on-site.

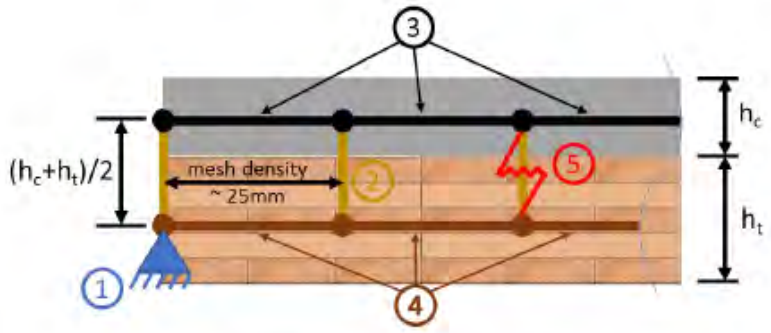

Figure 3.5. Composite beam FEM model

Figure 2.9: Schematic of an CCC beam FEM model [53], where (1) the support, (2) The rigid vertical struts, (3) The concrete elements, (4) The timber elements (5) The horizontal connector elements defined as spring elements with a horizontal stiffness.

To conclude, there are several main methods to evaluate the vibrational performance of floors. The current Eurocode 5 features Ohlsson's method, which limits the frequency to high frequency floors, static deflection and difficult to use unit impulse based on velocity. The code for TCC structures refers to Eurocode 1, where only frequency and static deflection are loosely restricted. In Canada it is more common to use the ratio between natural frequency and static deflection, allowing low frequency under high restrictions. For which the ratios are tuned to the specific timber or TCC floor type. Fourthly, JRC research based on similar light-weight steel structures proposes the extensive evaluation based on OS-RMS values, which can be determined through design charts. At last, the draft for the revised Eurocode 5 proposes the use of the response factor, which uses a similar acceleration approach as the JRC for low-frequency floors while using a velocity approach for high frequency floors. Overall, the latter is the most extensive and accurate however there are still some debatable aspects in the method. These aspects could possibly be filled up by taking carefully picked guidelines of the other methods, like from the

JRC report, FEM modeling, or experimental tests. As extra control function, the Canadian guidelines can be used due to their extensive validation for each floor type.

2.3.3 Structural vibrations in timber and TCC floors

In general, timber floors are characterized by their lightweight. It results in high frequency floors, sensitive to transient responses. However, due the wide variety of parameters influencing the vibrations behavior, the design for structural vibrations in timber floors is different for every situation.

One of the examples is the earlier introduced CCC floor in the Thomas Clarkson Community College. The design process initially started with the use of regular CLT floors, however in these floors vibrations become critical from a span of 7.5 meter. Due the increase span of 10 meters the CLT floors would only feature a natural frequency of 5.7 Hz [45]. Therefore, the design did not meet the minimal 8.4 Hz requirement of the used British annex of Eurocode 1. By replacing the floor with the TimCrete CCC floor the stiffness improved by 3.5 times and the mass was more than doubled. Although the increased mass lowered the natural frequency, the larger increase in stiffness made sure it increased above the regulation threshold. However, through on site Frequency Response Function (FRF) modal testing of both floor situations (before and after pouring of the concrete, it was found that the first natural frequency was actually above the threshold as shown in Table 2.5. It should however be noted that the full mass on the floor, from for example partitioning walls and finished which was used in calculation, was not fully present. This would lower the natural frequency, however the designer believe it would still be above the threshold. They believe its results from a combination of three aspects; The end conditions behaved more rigid in dynamics than the assumed hinges, the degree of two way spanning instead of the one way spanning used in calculation and a higher stiffness in dynamic situations compared to static situations. Besides, even though it was not checked since it was not required by the used standard, the response magnitude would be decreased by the mass. Since the natural frequency in the on-site testing does not differ much for both floor types, the increase in mass would be the main factor for improved vibration performance, while the increase of stiffness made sure the natural frequency would stay similar.

Table 2.5: Results of on-site vibration testing at the Thomas Clarkson Community college [45].

Mode number	Bare CLT floor	TimCrete floor
1	10·7 Hz	11·7 Hz
2	12·2 Hz	12·4 Hz
3	12·6 Hz	14·9 Hz
4	15·6 Hz	18·4 Hz

In an experimental study by Thai, vibration performance of CCC floors was also compared with bare CLT floors. The experiment used 175 mm thick 5-ply CLT specimens with a simply supported span of 8.7 meters and width of 1 meter. For the CCC beams, the CLT was topped of with 80 mm of C35 concrete. In contrast to the Timcrete CCC floors which used HBV steel mesh connectors, in this study notch connections were used to create composite interaction.

These notches were both present in the bare CLT and CCC specimens in three levels of surface density and thus three levels of composite interaction. The experiment consisted out a deflection test with a 1 kN load at mid span and a vibration test using an impact hammer on varying location as exciter, low frequency accelerators as transducers and Experimental modal analsysis (EMA) software. From the static deflection test, from which the results are shown in Table 2.6, it logically proved that CCC beams feature a much higher stiffness and thus a lower static deflection. Furthermore it was concluded that the amount of notches influenced the effective stiffness of the bare CLT and it should be taken into account for the CLT stiffness used for calculations of the effective stiffness of CCC floors if the notches cover more than 5% of the surface area. Next to that it was found that for low deflections in slender CLT and CCC beams, like in vibrations, the influence of shear deformation is negligible. Since the gamma method and method of Shear analogy already underestimated the static stiffness, it was advised to not use their extensions which include additional shear deformation in their results since it would create an even greater underestimation.

Table 2.6: Results of static deflection test in the research by Thai [53].

	d_{m-1kN} $[mm]$		EI_{app} $[MNm^2/m]$		EI_{eff} $[MNm^2/m]$
Beam	Bare CLT	CCC 28 days	Bare CLT	CCC 28 days	Bare CLT
1	3.41	2.50	4.02	5.50	4.25
2	3.62	0.81	3.79	16.83	3.99
3	3.73	0.75	3.68	18.15	3.87

From the results of the vibration test, shown in Table 2.7, it was concluded that an increase in composite interaction lowered the amount of damping. This is because a lower composite interaction allows the timber and concrete to move over each other and dissipate energy through friction. The natural frequencies on the other hand only increased slightly due to the increased stiffness of the higher composite beams. Overall, the tested specimens featured a much lower, than in the Thomas Clarkson Community college, and not representative natural frequency since the used CLT and CCC is much thinner and would for example only fulfill to SLS deflection check with a total maximum load of 1.1 kN/m^2. Overall it is interesting to note that an increase in composite interaction on one hand increase vibration performance due to an increase in stiffness, while on the other hand decreases vibration performance due to decrease in damping.

The study also compared the results to the Ohlsson/Eurocode 5 and the Canadian criteria. None of the floors satisfied either the 8 Hz threshold or frequency deflection ratio. Only beam 2 and 3 would satisfy the frequency deflection ratio if the span would be decreased to 8 meter. However, the author also mentions that the current set-up features the worst case scenario due to its 1 meter strip. In this case the transversal stiffness and boundaries conditions, and therefore also an increase of modal mass, are not contributing to the results. In addition to the likeliness of usage of thicker floor systems, the CCC floors feature potential to fulfill the criteria. It would therefore be interesting how these specimens would compare to the criteria of the revised Eurocode 5. At last, the author mentions two additional conclusions. Firstly, it is concluded that the gamma method for estimation of first natural frequency is sufficient, while the in the study mentioned more complex Wu et al. method would be a better alternative for the determination of higher mode frequencies. Secondly, it was concluded that the proposed simplified FEM model, shown in Figure 2.9 could be used to quickly evaluate natural frequencies, especially for complex structures like CCC floor systems. The only disadvantage is that it only

uses the connection stiffness as a constant and does not describe the notch connector influence locally, like notch depth, notch length and spacing.

Table 2.7: Results of vibration test in the research by Van Thai [53].

Mode	Beam 1		Beam 2		Beam 3	
	Freq.	Damping	Freq.	Damping	Freq.	Damping
Bare CLT beams						
1	4.30 Hz	0.6 %	4.26 Hz	0.5 %	4.17 Hz	0.6 %
2	16.49 Hz	1.0 %	15.70 Hz	0.2 %	15.50 Hz	0.9 %
3	34.62 Hz	1.5 %	32.29 Hz	2.5 %	32.68 Hz	1.3 %
4	58.75 Hz	1.3 %	59.08 Hz	0.9 %	56.93 Hz	1.4 %
CCC beams at 28 days						
1	4.95 Hz	2.1 %	5.27 Hz	1.2 %	5.35 Hz	0.6 %
2	16.02 Hz	2.9 %	18.11 Hz	1.9 %	18.52 Hz	1.6 %
3	28.77 Hz	4.8 %	33.53 Hz	3.8 %	35.62 Hz	2.8 %
4	44.63 Hz	4.6 %	49.70 Hz	3.5 %	52.09 Hz	3.3 %

The last interesting aspect to note is the common implementation of floating floors on top of timber or TCC floors to increase vibration performance. Floating floors can be described as applying a stiff cover floor on top of a resilient layer. The function of the cover layer is to add mass to the system and distribute the impact over a larger area to distribute the force and prevent the feeling of sinking in the floor with your step. On the other hand, the function of the resilient layer is to dampen the vibration. Where for the more effective heavy floating floors the cover layer is made from concrete or screed, while lighter versions consist of a top layer of sheeting like gypsum boards. The resilient layer can consist for example out of a continuous layer of (soft) insulation material, linear strips or by spaced springs. However, improving the vibrational performance by implementation a floating floor is not as simple. If the resilient layer is too soft, the cover floor will start vibrating on its own. The vibration might not reach the structural layer and not transmit it to other building elements, but it can still be felt for persons present on the same floor. The floating floor therefore has to be carefully tuned, or 'afveren' in dutch. An lower tune-frequency, also known as resonance frequency, can be reached by using a stiffer resilient layer. The formula used to determine the tune-frequency is shown in Equation (2.2), for which s' is the dynamic stiffness of the resilient layer and m' is the mass of the floating cover floor [52]. To prevent acoustic resonance in the hearable frequency domain, and thus cause high sound transmission, it is advised that floating floors are tuned to have a resonance frequency below 20 Hz [44]. However, for tactile vibrations the same research by TNO in lightweight structures mentioned that floating floors should be tuned for a resonance frequency as low as 1 Hz. It also mentioned that this is however not practically feasible. It therefore advises that to improve vibration performance, no floating floor should be applied so the stiffness of the structural layer is fully effective instead of partially applied, an resilient layer would only cause resonance. This is however different to the methods mentioned in the JRC report and the revised Eurocode 5 which both only feature an positive increased modal damping ratio if a floating floor is applied without it affecting the stiffness and thus taking into account this resonance effect. It is therefore less clear what the exact effect of floating floors is. Besides, this contrast is similar to consideration between floors with lower and higher composite floors mentioned earlier.

$$f_o = 160 \cdot \sqrt{\frac{s'}{m'}} \tag{2.2}$$

2.3.4 Basics and parameters of floor acoustics

As explained at the beginning of this section, the acoustics of a floor involves the production of sound waves due to propagation of longitudinal waves through the floor and bending waves due to vibration of the floor. When the sound waves can be heard in one room through activity in the other, it is called sound transmission. The source of the initial vibration of the floor distinguish two transmission categories. The first one is airborne sound (transmission), where by the floor is excited by sound waves through for example speech, television or music. The second one is impact sound (transmission), which is when the floor is excited by impacts such as footfall, moving furniture or machinery. As shown in Figure 2.10, there is a second distinction which describe the sound paths. The direct, or structure borne, sound path is formed by the source exciting the element, which directly creates the hearable sound wave. In contrast, indirect, or flanking, sounds are when the first element excites a second element which thus creates the sound wave after an additional step. This one is thus not only governed by the properties of the first element, but also by the second and the node in between the elements.

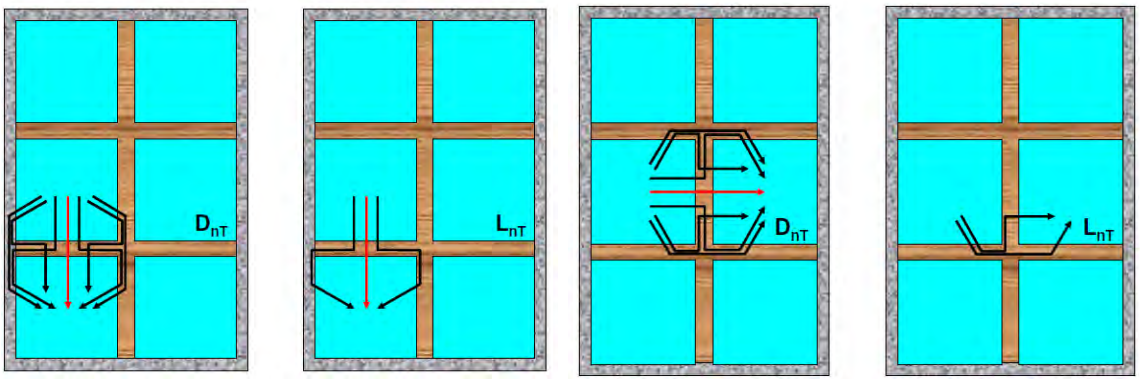

(a) Vertical sound transmission. (b) Horizontal sound transmission.

Figure 2.10: Schematics of sound paths from one room to another, where the left sections show the sound paths from airborne sound and the rights sections from impact sound on the floor. The direct sound transmittance is shown in red, while the indirect flanking sound is shown in black [43].

The sound transmission performance, in this thesis also referred to as acoustical performance, is governed by a combination of insulation, which focuses around the absorption of sound energy in the element, and isolation, which focuses around using the air in between elements [12]. This can be explained when looking back at the definition of sound. Where vibrations focus around the motion of an solid body, sound is the vibration of individual molecules. When a sound wave travels through air, the molecules itself are not actively following the wave but start vibration back and forth in its direction. By doings so it excites the next air molecules in the direction of the wave and gives it its energy. These molecules then also start vibrating in the same direction and transfer its energy to the next set of molecules. This is called a longitudinal, or compression, waves. Since air is a gas where the molecules are far apart from each other, it is a relatively poor

sound conductor. The speed of sound in water is for example almost 3 times larger than the speed of sound in air [42]. However, due to the low density of molecules in air it is also easier to excite air in comparison to a high density solids where each molecule is kept in place by its close surrounding molecules. The property of the amount of force or pressure is required to give a molecule or object a specific velocity is called impedance [54]. The frequency of the vibration and amount of molecules vibrating can be combined in the sound energy of a wave, which is logically affected by similar parameters as structural vibrations. The sound energy determines the level of the sound through the height of the amplitude of the wave. A higher sound energy, and thus am increased amplitude, results in a higher sound pressure level.

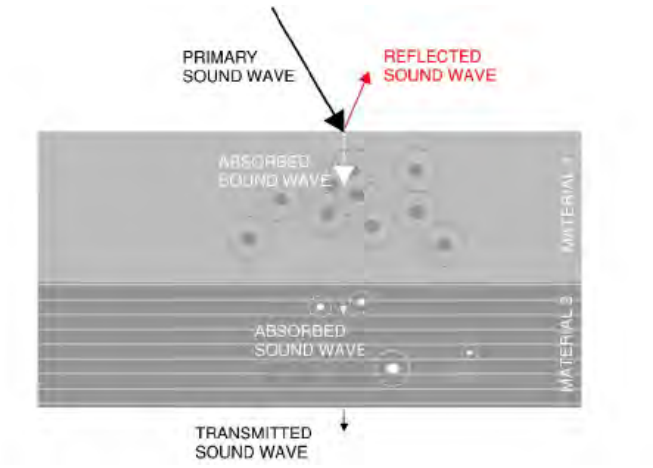

Figure 2.11: Schematic of an sound wave energy passing through an assembly [12].

The longitudinal wave in the air can continue propagating through the floor, which can in this scenario be seen as a stationary stiff material. The main parameter for its sound insulation is mass. Due to the high density, most of the hit molecules do not start vibrating and therefore most of the sound energy is reflected, as shown in Figure 2.11. The sudden higher requirement of energy to start excitement of the molecules, which thus results in high reflection, is also called a jump in impendence, or in Dutch 'Impendantie-sprong'. The influence of mass is described in the Theoretical mass-law, which states that the sound reduction index R is increased with 6 dB by doubling the mass and by doubling the frequency [5]. The same effect of reflectivity is present for stiff materials, where the molecules are tightly bonded to each other. In general, the increase in mass has a higher influence on the reflectivity off the material for low frequency sounds, while stiffness has a higher effect on high frequency sound. Furthermore, the amount of energy which is absorbed into the material is not entirely transmitted to the second layer, but also spread out through the material forming a transverse wave, or bending wave. Furthermore, at each contact with another molecule a little bit of energy is transformed into heat. Therefore, increased mass and thickness of the material helps increasing the energy dissipation, for which the latter is especially only accurate for low frequency sounds [36]. In contrast with the sound reflection, a lower material stiffness, and thus higher softness, has a positive effect on the absorption since it traps energy by conducting it on random paths. Therefore, foam materials and insulation wool, with a relatively low ratio of stiffness over mass, are great sound insulators. When applied into a construction assembly, they are often called damping or resilient layers and are applied between two massive layers. For absorption it can again be said that in general an increase in mass and

thickness has mainly positive effects for low frequency sound, while the use of soft materials help with high frequency sound. At last, closely related to its own natural frequency and impedance, each layer has its own critical frequency. Due to the combination of the above mentioned parameters, this is the frequency where it features the lowest sound insulation. This effect can be seen at f_0 in Figure 2.12. Overall, combining several layers with different materials, thickness, stiffness and mass can therefore introduce jumps in impedance, spread critical frequencies and feature damping and thus result in good acoustical insulation.

When introducing an air layer in between the assembly, it allows the two parts of the structure to vibrate individually and utilizes the poor conductive properties of air in combination with its scattering of the sound. This is therefore an isolation strategy, significantly lowering the sound transmission. However, it should be noted that a layer of air, or damping material, can sustain standing sound waves, or resonance waves, in the layer. If the frequency of the standing wave aligns with one of the natural frequencies of the surrounding layers they will start to resonate, decreasing the total sound insulation significantly as shown in Figure 2.12. This strategy therefore has to be combined with partially filling the cavity or the strategy of using jumps in impedance. Another noteworthy aspect, similar to heat transmission, air gaps should be prevented since the air does not feature dissipative properties and could also move the sound wave into the room due to the flow of air itself. At last, when required the two parts can be connected using resilient elements such as clips, springs and damping blocks. The use of resilient elements is crucial since it can be generalized that the acoustical performance of an assembly is as good as its weakest link. If there is one rigid element penetrating the damping layer and reaching another rigid element, most of the damping in between is lost.

However, as mentioned in the previous paragraph, longitudinal air waves can also cause transverse waves in the element. These transverse waves are also known as structural or bending waves and are the same type of waves as tactile structural vibrations. They therefore also feature the same impact of from bending stiffness, mass and damping. The main difference is in the perception higher perception range starting from 25 Hz, while tactile structural vibration are most perceived in the 0-20 Hz range. An important difference with the longitudinal sound transmission is also that it does not benefits as much from decoupling.

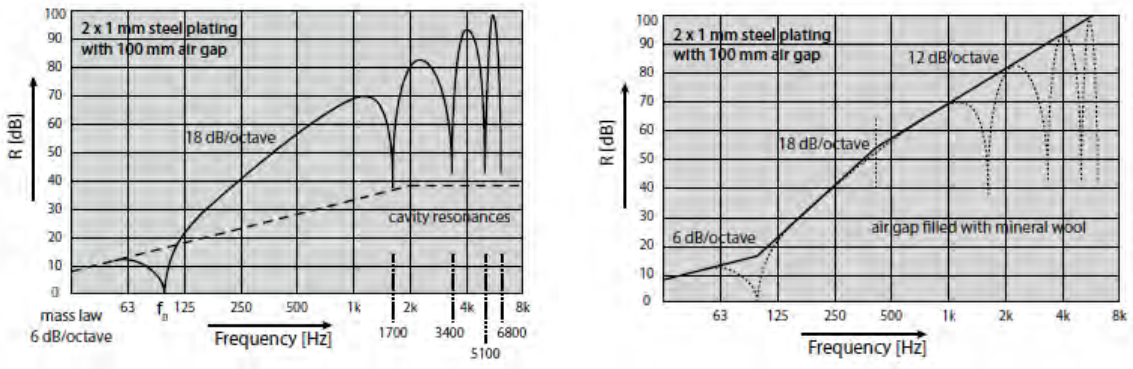

(a) Assembly with an air cavity. (b) Assembly with a mineral wool filled cavity.

Figure 2.12: Schematised airborne sound reduction curves for constructions with and without a filled cavity [5]

2.3.5 Design criteria for floor acoustics

As a result of research by the European Union supported COST Action TU0901 work group, there is since the last decade a harmonized approach regarding sound insulation, calculation methods and criteria [9].

The work group proposed to describe the airborne sound insulation by the Weighted Standardized Airborne Sound Level Difference $D_{\mathrm{nT,w}}$ or $D_{\mathrm{nT,A}}$ as its main quantity. It consists of the addition of the Standardized Airborne Sound Level Difference D_{nT} plus the the spectrum adaptation term for pink noise C or traffic noise C_{tr} described in ISO 717-1:2020. These spectrum adaptation terms are meant to tune our hearing to the actual sound pressures per frequency and follow the A-weighting curve. To calculate D_{nT}, the sound reduction indexes for direct transmission R_{Dd} and flanking transmission R_{ij}, based on experimental values, should be combined [43]. Besides, the working group proposed to use a frequency range for airborne sound evaluation of 100-3150 Hz for heavy buildings and a frequency range of 50-3150 Hz for lightweight buildings. This is due to the lack of mass and increase in complexity in lightweight construction. In a study by Öqvist [47], it was even proposed to evaluate lightweight buildings down to 25 Hz, since using the same sound insulation values determined with the frequency range down to 50 Hz still provided a significantly higher annoyance due to walking for lightweight construction than for heavy construction and there was a large variation in sound insulation values between identical construction. However, if the range was extended to 25 Hz, the sound insulation values correlated better with the annoyance of each construction type. Combining this with a decrease in variance of sound insulation values, the safety margins can be decreased and light weight construction have to be less 'over-dimensioned'.

For impact sounds the main quantity is the Weighted Standardised Impact Sound Pressure Level $L'_{\mathrm{nT,w}}$ or $L'_{\mathrm{nT,A}}$, which similarly consists out of the addition of the Standardised Impact Sound Pressure Level L'_{nT} and the spectrum adaptation term for a tapping machine C_{I} or $C_{\mathrm{I},50-2500}$ described in ISO 717-2:2020. However, if the value for C_{I} is negative, it can be ignored. Opposite from airborne sound calculations, the L'_{nT} can be calculated by its own components for direct sound transmission $L'_{\mathrm{n,Dd}}$ and flanking transmission $L'_{\mathrm{n,ij}}$, which are both based on experimental values, in addition to a factor taking into account the volume and absorption of the other walls of the receiving room. For airborne sound this is already included in R_{Dd} and R_{ij}. For impact sounds the working group proposed a frequency range from 50 or 100 Hz to 2500 Hz, for which it is similarly beneficial to extend down to 25 Hz according to Öqvist.

In the Netherlands the requirements for airborne and impact sounds are regulated in the building code and shown in Table 2.8. It distinguishes two receiving area types, residing and closed residential areas. It is logical that residing residential have stricter requirements since these are areas where people normally reside for longer times like a living room, bed room and kitchen. Closed rooms are rooms where inhabitants normally do not, or only temporarily, visit that room, like bathrooms, technical rooms, storage's and hallways. Increased sound levels over a longer period of time, in combination with specific activities, increases annoyance. For sounds coming from other rooms in the same residence, the least sound insulation is required. It is however interesting to note that these regulations are lower than proposed by the COST working group shown in Table 2.9. For airborne sound insulation criteria would conform to the class E of the working group, in a range from A to F.For impact sound insulation the Dutch criteria would fit in Class C for the same range. At last, it should also be noted that since $D_{\mathrm{nT,A}}$ is a sound level difference, it has a minimum value and increasing it increases comfort. While on the other hand, $L'_{\mathrm{nT,A}}$ indicates the sound level in a receiving room based on the sound of tapping

machine, it therefore features a maximum and decreasing it increases comfort.

Table 2.8: Dutch requirements for sound insulation in residential buildings according to Bouwbesluit 2012 - Section 3.4 Sound insulation between rooms for new construction [46].

Situation	$D_{\mathrm{nT,A}}$ [dB]	$L'_{\mathrm{nT,A}}$ [dB]
Producing room to an residing area of another residence	≥ 52	≤ 54
Producing room to an closed area of another residence	≥ 47	≤ 59
Producing room to an residing area of the same residence	≥ 32	≤ 79

Table 2.9: Description of sound insulation classes described by COST Action TU0901 [9].

Class	General	Sound insulation judged poor
A	A quiet atmosphere with a high level of protection against sound	less than 5%
B	Under normal circumstances a good protection without too much restriction to the behaviour of the occupants	around 5%
C	Protection against unbearable disturbance under normal behaviour of the occupants, bearing in mind their neighbours	around 10%
D	Regularly disturbance by noise, even in case of comparable behaviour of occupants, adjusted to neighbours	around 20%
E	Hardly any protection is offered against intruding sounds	around 35%
F	No protection is offered against intruding sounds	50% or more

2.3.6 Acoustics in timber and TCC floors

Similar to structural vibrations, the lightweight and elasticity of timber constructions create challenges to reach desirable acoustical performance. This is especially the case for flanking transmission and low frequency impact sounds. To comply with current regulations for residential homes, timber floors always have to be either fitted with acoustical measures such as a suspended ceiling or a floating floor, or transformed into an TCC floor, which increases its mass and stiffness. As indicated in Table 2.10, this is also still the case for the heavier and stiffer massive timber floors like CLT. The most common used heavy floating floors are often executed with a cover layer of 50 mm anhydrite or up to 80 mm cement based materials layer [52]. The thickness of the resilient layer is often between 30 mm and up to 90 mm.

Table 2.10: Examples of CLT floor build ups and their respective acoustical performance [24].

Floor structure type	Material (mm)	Total height (mm)	Weight (kg)	Impact sound $L_{n,w}$ ($C_{I,50-2500}$) (dB)	Airborne sound D_w ($C_{50-3150}$) (dB)
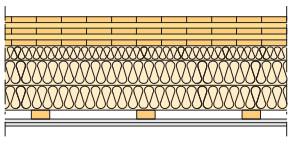	**Floor type 1** 140 CLT slab 70 insulation 45 × 220 studs, self-supporting 2 × 95 insulation 28 battens 2 × 13 gypsum plasterboard	449	130	≤ 54	≥ 56
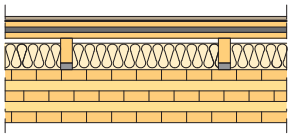	**Floor type 2** 14 wood flooring 3 foam underlay 22 fibreboard 20 acoustic matting 22 fibreboard 95 floor joists 95 insulation 25 Sylodyn 220 CLT slab	421	155	≤ 54 (+6)	≥ 52 (–4)
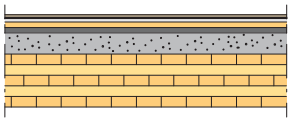	**Floor type 3** 14 wood flooring 3 foam underlay 13 plasterboard 22 fibreboard 20 acoustic matting 80 washed gravel 220 CLT slab	372	245	≤ 44 (+6)	≥ 63 (-1)
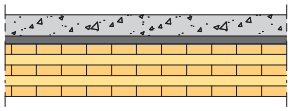	**Floor type 4** 80 concrete 30 acoustic matting dynamic stiffness ≤: 9 MN/m³ 200 CLT slab	310	270	52 (+5)	63 (–8)
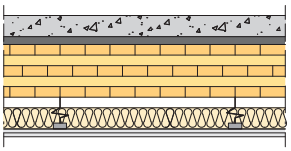	**Floor type 5** 80 concrete 30 acoustic matting dynamic stiffness ≤: 9 MN/m³ 200 CLT slab 120 suspended ceiling joists 80 insulation 2 × 15 gypsum plasterboard	460	310	33 (+17)	79 (–14)
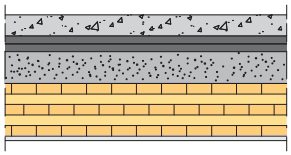	**Floor type 6** 80 concrete 2 × 20 acoustic matting, dynamic stiffness ≤: 12 MN/m³ 120 washed gravel 200 CLT slab 13 plasterboard	453	460	40 (+4)	75 (–7)

The design and evaluation of timber floors has been extensively investigated in the European wide and commercially supported Silent Timber Build project. The project consisted out of three work packages (WP). In WP 1 the goal was to create prediction tools for low, medium and high frequencies. This was especially important since the labor intensive experimental testing was the main working method in the field of (floor) acoustics. Combined with complexity and

wide variety of parameters in lightweight timber structures it haltered progress and innovation. For higher frequencies, between 100 and 3150 Hz, Statistical Energy Analysis (SEA) was used and found effective. With SEA all the the vibrating sub-systems can be coupled together and solve the resulting matrix of energy balance equations. To accurately determine the subsystems and SEA parameters of each structure, the method is coupled to FEM modeling. Even small details of the geometry are therefore captured in its parameters. For low frequencies, between 20 Hz and 200 Hz, FEM modeling itself was used to capture the dynamic behavior. It was found to be sufficiently accurate for frequencies down to 31.5 Hz. Below that frequency, simple boundary conditions were found to be lowering the accuracy of the method and extensive research needs to be done to get more accurate boundary conditions.

The goal of WP 2 was to collect data of several different timber and TCC floor types and to validate the in WP 1 proposed models. As a result it provided a clear comparison and state of the art of acoustical performance of this floor types. One of the main studies contributing to WP 2 was performed by Homb et al. in 2016 and focused on impact insulation of massive floors [26]. The study distinguished three types of floor:

- Type 1 - Basic floor structures without a floating floor:
  Massive wood floor or CCC elements.
- Type 2 - Light floor assemblies with a floating floor:
  Massive wood floor with additional lightweight elements above the element.
- Type 3 - Heavy floor assemblies with a floating floor:
  Massive wood floors with either gravel or concrete on top of below the resilient layer.

From evaluation of Type 1 timber floors it was found that there were many similarities between the 100 Hz and 2500 Hz domain, even though it consisted of CLT, joist of stack beam floors. These floors performed in a $L'_{\mathrm{nT,w}}$ range of 83 to 87 dB. Interestingly, for these floors the mass per unit area (mpua) in kg/m^2 was not significant. The results of Type 1 CCC floors are shown in Figure 2.13a and Table 2.11 and indicated by a red square. The trend of both floors shows similarities, but a difference in performance. This difference was not further investigated, but could be explained by difference in mass and height. The trend shows similarities with traditional concrete floors by featuring increasing L'_{n} over frequency. The performance for high frequencies is governed by the trivial surface softness of the floor, which in this case resulted into a significant increase in L'_{n} due to the lack of floor covering. This effect is not taken into account with the determination of the $L'_{\mathrm{nT,w}}$, which performs similar to the non-composite floors. However, based on the increased performance at low and mid frequency, the CCC are expected to be better performing, but still far from the $L'_{\mathrm{nT,w}} \leq 54$ dB threshold, than the non-composite floors with floor covering present.

For Type 2 floors the evaluation was mainly focused on the difference in type of resilient layer. The worst performance came from CLT floors with the simplest resilient layer, a continuous elastic layer with high S_ds. It should however be mentioned that this expected to be mainly due the continuous elastic layer having a high S_d instead of a low S_d. It was followed up by floors with an elevated covering floor on point elastic supports, often seen in office floors. The best performing, and only criteria fulfilling, resilient layer was with optimized line elastic supports, for which Floor 2 of Table 2.10 is an example. The overall $L'_{\mathrm{nT,w}}$ range of these floors was between

55 and 68 dB

From analysis of Floor type 3 floors with gravel directly on top of the CLT and a light floating floor above, for which Floor 3 of Table 2.10 is an example, the performance increased considerably due to the increased mass to a $L'_{\mathrm{nT,w}}$ range of 57 dB and 50 dB compared to Type 2 floors. Besides, it was found that a resilient layer with lower S_d performs better since it reaches the same performance levels as floors with increased mass and S_d.

Furthermore, two categories of Floor type 3 using concrete are compared and the results shown in Figure 2.13b and Figure 2.13. The first category are floors consisting of a heavy concrete floating floor, for which Floor 4 of Table 2.10 is an example, are compared. These floors are in the results indicated with a blue border. The most interesting aspect from comparing these two floors is again in the S_d of the resilient layer. Even though the CH floor with a high dynamic features increased mass and therefore a better performance in low frequencies, the DE floor with low S_d significantly outperforms it. Both of the floors were not fitted with a covering floor, explain the poor performance in high frequency. The second category consists of CCC floors with 60 mm of concrete and equipped with a light floating floor, for which examples are shown in Figures 1.1b and 1.1c. These are indicated in the results with a orange border. The difference between the, in low frequency, better performing NO floor with a mpau of 265 kg/m^2 and a optimized line elastic resilient layer, which is often heavier, is mainly credited due to the increase in mass. The application of a low S_d continuous elastic layer for the NO floor with a mpau of 241 kg/m^2 features no significant improvement to compensate for the lower mass. Although these floor categories are hard to be compared due to the difference in mass and surface softness, for CLT with floating concrete floors it is hard to reach desirable performance and an extra gravel layer to increase mass or a suspended ceiling needs to be applied. However for CCC floors, heavier variants can reach desirable performance. Besides, for CLT floor with floating concrete floors, the impact of the S_d is much more significant which could be explained by the higher ratio of mass being applied above the resilient layer. This creates a more significant mass-spring-mass system.

Overall, it was concluded that for Floor type 2 floors there is a high correlation between mass and acoustical performance and that floors without a suspended ceiling only reaches the requirement threshold if on the higher end of the mass spectrum and featuring a low S_d. For floor type 3 floors the correlation between mass and performance was still present but weaker. Besides, the scatter was larger, this showed that more factors played a role. This could for example be research parameters, such as the limited amount of tested floors and impact of floor covering. Similarly, the correlation between a lower S_d and increased acoustical performance is also weaker.

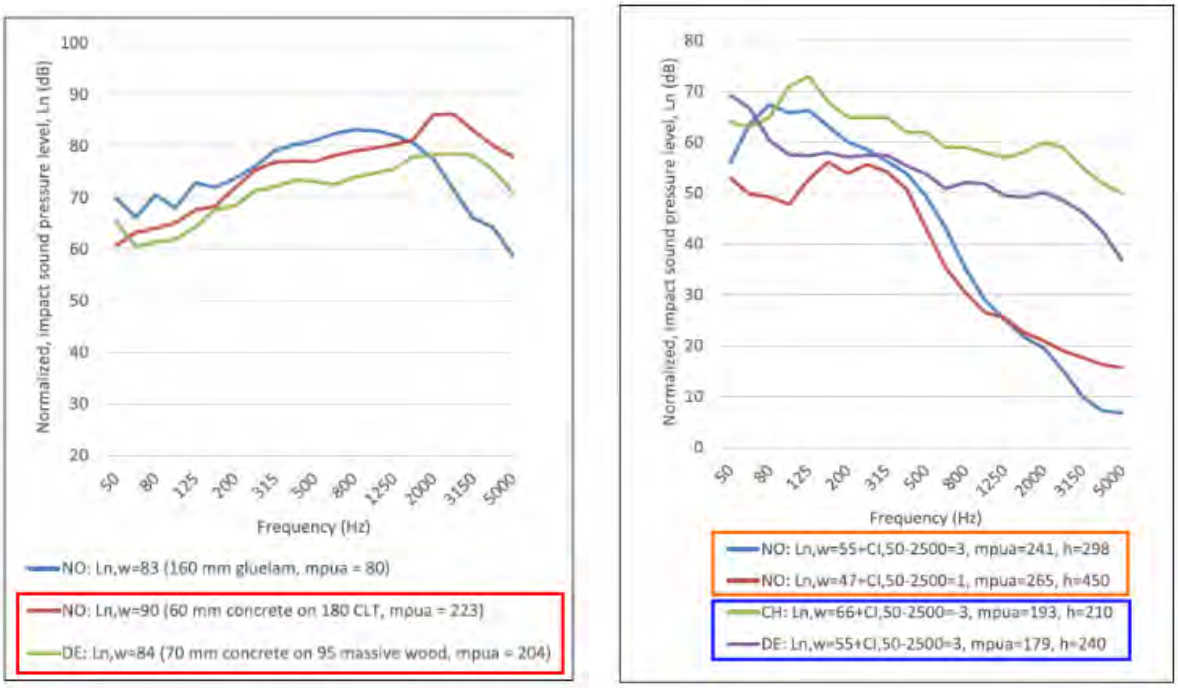

(a) Type 1, including a joist floor as reference.

(b) Type 3

Figure 2.13: Acoustical performance of hybrid floor assemblies [26].

Table 2.11: Overview of the results for type 1 and type 3 floors [26].

Type I and III	$L_{n,w}$ (dB)	$C_{I,50-2500}$ (dB)	SUM[a] (dB)	Mass per unit area (kg/m^2)	Dynamic stiffness (MN/m^3)	Source
Single	84	−12	84	204	–	DE
Single	90	−13	90	223	–	NO
FR	55	3	58	179	6	DE
FR	66	−3	66	193	20	CH
FR	56[b]	1	57	235	>20	NO
FR	55[b]	3	58	241	<10	NO
FR	44[b]	6	50	245	<10	NO
FR	47[b]	1	48	265	Line elastic	NO
FR	40	7	47	269	6	DE
FR	47	3	50	282	40	DE
FR	47	1	48	298	6	DE
FR	46	6	52	345	20	CH
FR-CR	46	10	56	182	<15	AU

[a]Negative values of $C_{I,50-2500}$ neglected in the sum according to NS 8175:2012.[21]
[b]Measurement object with some type of floor covering.

The project was concluded by the design process chart shown in Figure 2.14. Its main features are the creation of a SEA and FEM model and validating it through the given equations for $L'_{\mathrm{nT,w}}$ based on mpau. Timber floors were divided into four groups; Group A features timber

joist floors, Group B features hybrid timber joist floors, Group C features massive wood floors and Group D features hybrid massive floors. These floors are further divided based on the application of a floating floor and suspended ceiling. The code FS stands for a stiff connection of the cover floor to the structural floor, while the code FR stands for a resilient connection and thus described a floating floor. The codes CS, CR and CN described a suspended ceiling with respectively a stiff, resilient or no connection to the structural floor. The latter is for example a wall mounted suspended ceiling. Based on these equations, CCC floors will reach a sufficient acoustical performance if it features a mpau over 250 kg/m^2. Furthermore, due to WP 3, the design could also be started or validated by the digital data base accessible, from the site of Lignumdata.

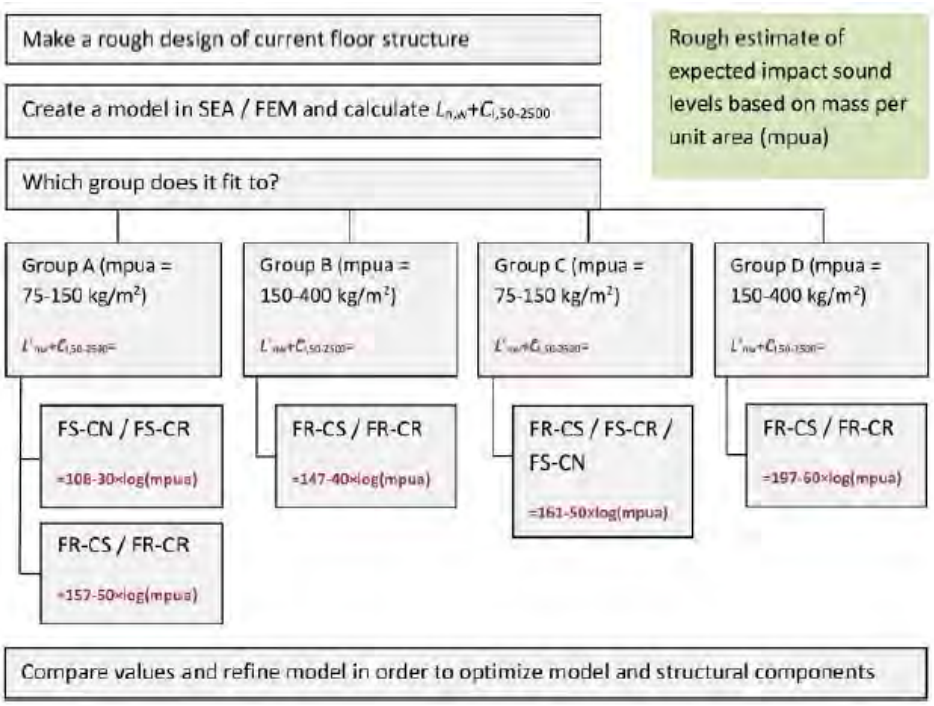

Figure 2.14: Design process chart according to the Silent timber built project [25].

At last, in 2023 an interesting research has been conducted into an innovative way to improve bare CLT floors [37]. It featured a combination of two improvements. The first one is the use densified wood for its lamellae and the second one is the integration of a resilient layer as the center layer of the build-up. The study indicated a potential performance increase of 7 dB in airborne sound insulation and 7 dB decrease in impact sound insulation. It however also mentions that further research should be done in the critical low frequency range.

2.3.7 Conclusion

To conclude, Structural vibrations and acoustics are both dynamic aspects of floor behavior. They therefore feature similar parameters and aspects. The most significant is the positive increase of mass, followed by the positive increase of stiffness and damping. The largest difference in the design of both aspects is however in the scale and the tuning. Where structural vibrations are not only governed by the properties of the floor itself but also by its boundary conditions and especially span, this is not the case for acoustics. It is therefore for acoustics easier the

case to compare a small scale specimen to a whole floor situation. Furthermore, there is a big difference in desirable tuning of the damping layers. Generally said, for acoustics it is preferred to decouple the structure as much as possible. Therefore resilient layers with a tuned frequency below 20 Hz, and therefore with a low dynamic stiffness, are preferred. However for structural vibrations this is the exact range resonance in the cover floor can occur. For structural vibrations it is ideal to tune the floating floor to below 1 Hz, however this is practically not feasible. It is therefore preferred to use stiffer resilient layer which tunes it above 20 Hz, which also cause a more effective use of the stiffness of the structural layer. Overall, it is a careful balance between the two aspects.

3 Preliminary connection design

This chapter will focus on the preliminary design of the connection detail. Firstly, Section 3.1 will describe the considered improved commonly-used and conceptual connection types. It will describe their expected performance based on the knowledge gained from the literature review discussed in Chapter 2. Section 3.2 will describe the considered steps for further development of the connection detail.

3.1 Variant study

As introduced in previous paragraph this section will describe and evaluate several variants for the connection detail based on the commonly used connection types consisting of steel mesh connectors, screw fasteners and notch connections, or new conceptual connection types. The variant with the highest potential is then chosen based on a relative multi-criteria analysis. The considered criteria and the chosen weighting are described as follows:

- **Structural performance - 30%**
  The structural performance takes into account how easy it is for the system to reach high composite interaction, if it features high shear strength to remain the composite interaction, if the governing failure mechanism is ductile and if there are other potentially problematic phenomena. Due to it being a safety criteria, it features the highest weighting of the criteria.

- **Vibration performance - 25%**
  The vibration criteria of the connection detail mainly takes into account the introduced extra damping in the system. Additionally, due to the large influence of bending stiffness on the vibration performance of the floor, also the connection stiffness is taken into account.

- **Acoustic performance - 25%**
  Similar to the vibration criteria, the acoustic criteria focused on increased damping. However, it does not focus on the connection stiffness but on the improved decoupling of the system based on the theoretical allowed vertical movement.

- **Buildability - 20%**
  The buildability of the connection type takes into account the easy of large scale manufacturing and floor construction of floors systems using the connection type. This includes the quality to make the intended detail such that it properly functions, an negative example is for example the ability of concrete to easy fill up cavities its not meant to fill restraining intended free movement. Due to this being a practical reason, with more easily further development in a later stage this criteria features the lowest.

3.1.1 Variant 1: Steel mesh connections

The first variant is based on the improvement of the steel mesh connectors as introduced in Section 2.1. It features five versions shown in Figure 3.1.

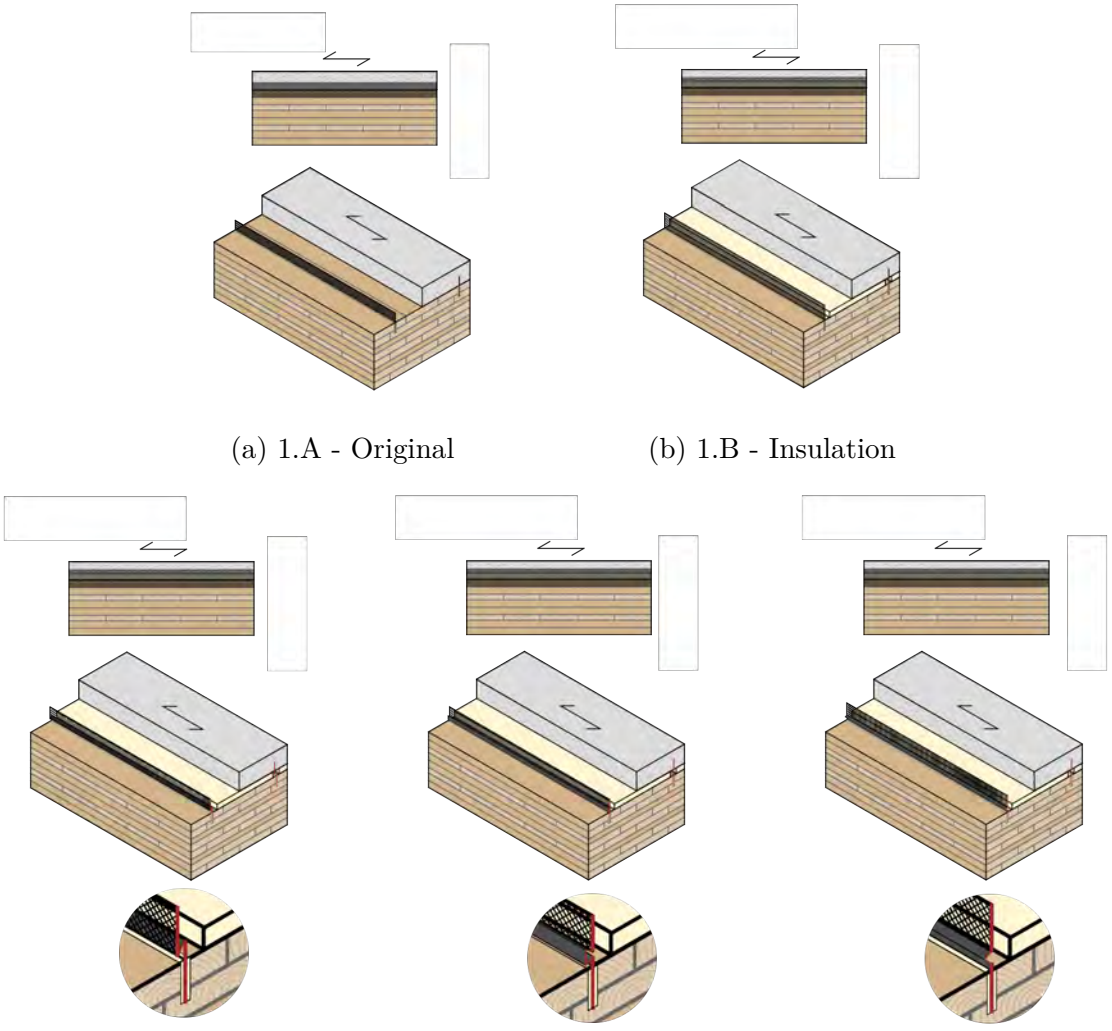

(a) 1.A - Original (b) 1.B - Insulation

(c) 1.C - Z-profile (d) 1.D - Dovetail-profile (e) 1.E - V-profile

Figure 3.1: Versions of Variant 1: Steel mesh connections

Variant 1.A features the standard steel mesh connector. It features stiffness and can easily reach full composite action. Besides, it is an high capacity connector with a ductile failure mode. Although no damping is present in the system, its high connection stiffness allows for increased natural frequencies. However, due to its lack of decoupling, it performs poorly for acoustics. Furthermore, the construction process requires additional steps such as making the the incisions in the timber and applying the resin in a controlled environment. Variant 1.B is based on the in practice applied version with insulation. The interlayer decreases the connection stiffness due to local buckling of the mesh over the unrestrained interlayer, but is still in the higher end relative to other connection types. The combination of the good connection stiffness and increased damping, also increases the vibration performance. Although the connection still couples the concrete and timber, the low amount of total transmission area and small amount of allowed buckling increases its acoustic performance. This is effect is even more enhanced for versions 1.C-1.E, which feature indentations to create compliant mechanisms. While not expected to be detrimental, the indentations can create local weakness points and the compliant mechanism can results in fatigue problems over time. Furthermore, it also creates an additional

steps for the creation of the mesh and the proper installation, e.g. due to the asymmetric profiles its advised to mirror the adjacent mesh plates to each other. Furthermore, the indentation can cause weakness points which can get easily damaged in construction and transport. This is less the case for Variant 1.E due to its simplicity. Table 3.1 shows an overview of the allocated values per criteria and its weighted score.

Table 3.1: Results of the multi-criteria analysis for Variant 1: Steel mesh connectors.

Criteria	Structure	Vibrations	Acoustics	Buildability	Score
Weighting	30%	25%	25%	20%	
1.A	9	6	3	5	5,95
1.B	8	7	6	5	6,65
1.C	7	7	7	3	6,20
1.D	7	7	7	3	6,20
1.E	7	7	7	4	6,40

3.1.2 Variant 2: Screw fasteners

The second variant is focused on the usage of screws as main shear load transferring system. The main considered connection versions are shown in Figure 3.2.

Variant 2.A1 is the base variant using perpendicular fasteners screws. However, as show in Section 2.1, the stiffness of perpendicular screw fasteners is only very small compared to the other connection types. This also results in a poor vibration performance. The reason the vibration performance is not lower rated is due to the observation that lower composite interaction beams also feature increased damping due to small movements and friction between the elements [53]. From a acoustic perspective the floor is still fully coupled. While the screws are easy to individually install, the high required amounts often installed in manually limit its buildability score. Variant 2.B1 uses inclined screws, significantly improving the connection stiffness of the system. It thus also results in an improved vibration performance. The buildability is however lowered due to the requirement of an screw place holder to drill the inclined screw. Its insulation version 2.B2 however loses its improved connection stiffness again. Its damping is increased due to the springiness of the screw for vertical loads, increasing its vibration and acoustic performance. Lastly, a deflection screw was considered, due to its allowance of vertical movements and increased damping, thus improving its acoustic and vibration performance. However, to make this work the screw should be also in its weaker perpendicular configuration. Besides, these screws are currently only used in non-load bearing situations thus have to be further developed into stronger and stiffer version. The higher complexity of the screw will increase the material cost. Table 3.2 shows an overview of the allocated values per criteria and its weighted score.

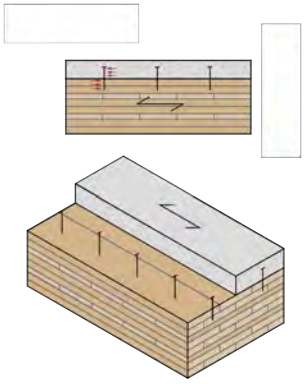

(a) 2.A1 - Perpendicular screws

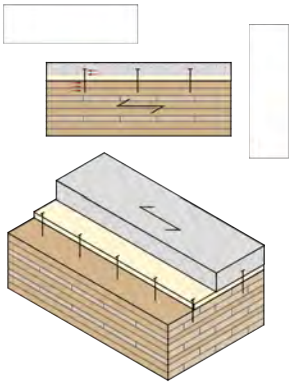

(b) 2.A2 - Perpendicular screws with insulation

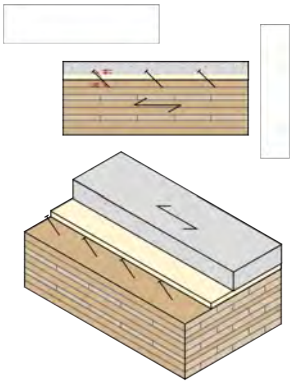

(c) 2.B2 - Inclined screws with insulation

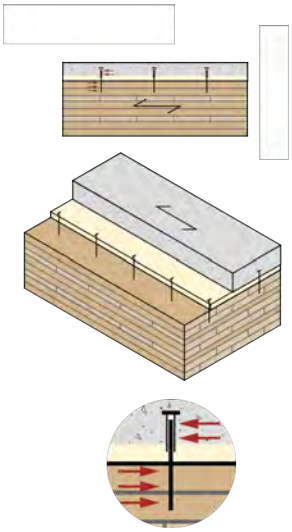

(d) 1.C - Perpendicular deflector screws with insulation

Figure 3.2: Versions of Variant 2: Screw fasteners

Table 3.2: Results of the multi-criteria analysis for Variant 2: Screw fasteners.

Criteria	Structure	Vibrations	Acoustics	Buildability	Score
Weighting	30%	25%	25%	20%	
2.A1	3	4	3	7	4,05
2.A2	2	5	4	7	4,25
2.B1	6	5	4	6	5,25
2.B2	5	6	5	6	5,45
1.E	3	8	8	5	5,90

3.1.3 Variant 3: Notch connection

The third variant uses notch connections and their resulting interlock as main load bearing system. The considered versions are shown in Figure 3.3.

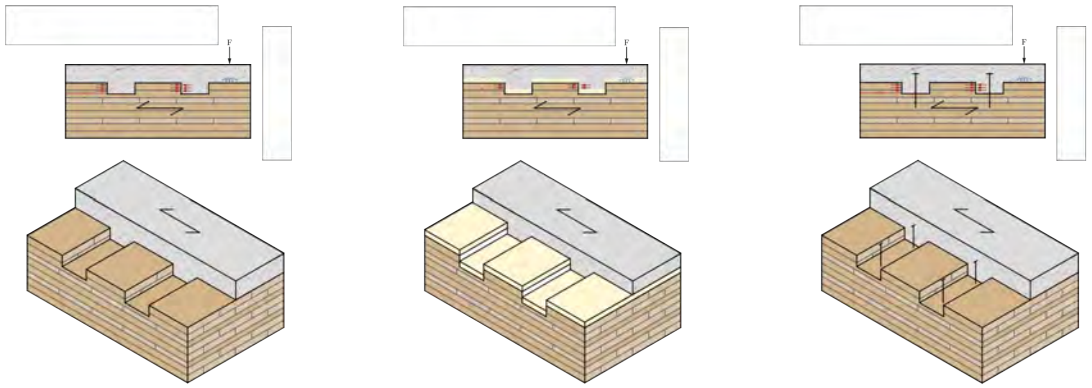

(a) 3.A1 - Rectangular notches (b) 3.A2 - Rectangular notches with insulation and PTFE (c) 3.B1 - Rectangular notches with fasteners.

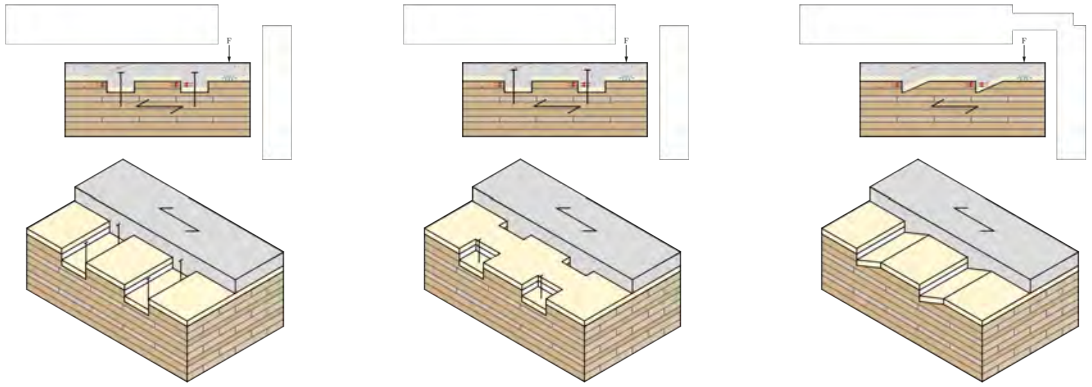

(d) 3.B2 - Rectangular notches with fasteners and insulation (e) 3.C2 - Discrete rectangular notches with insulation and fasteners (f) 3.D2 - Triangular notches with insulation

Figure 3.3: Versions of Variant 3: Notch connections

The first version features a continuous rectangular notches transverse to the floor direction. As introduced in Section 2.1, it features a great connection stiffness but its structural integrity is limited due the lack of a fasteners for reinforcement of the concrete and to prevent separation. While the connection stiffness ensures a decent vibration performance, the lack of damping and decoupling results in a poor acoustic performance. Due to the rise of CNC milling, its fabrication becomes more and more easy. The major downside is its high material waste. Version 3.A2 introduces an insulation in between the timber and concrete, while also covering the notch sides with PTFE, also widely known under the brand name Teflon, to ensure minimum friction for vertical movements. Its connection stiffness and strength is only slightly reduced, while the damping and decoupling are significantly improved. For the buildability it requires one extra step of placement of the insulation and PTFE in the production process. Version 3.B1 is again a version without insulation, but with a fasteners to ensure the structural integrity. It also reduced to an decrease in decoupling. Due to the presence of the fasteners, its counter part with insulation 3.B2 does not feature similar vibration and acoustic performance as the Version 3.B1. A possibility is also to use discrete notches as shown in version 3.C2. While it features improved

dynamic performance due to the decreased contact area between the timber and concrete, it therefore also features a lower connection stiffness. However, most importantly is its increased complexity in the manufacturing process. Version 3.D2 uses right-angled triangular notches. Its main benefit compared to 3.A2 is its lack of a second side with possible contact and thus acoustic improvement. While under load loads the concrete and timber on these sides comes loose due to the horizontal slip in the system, in the elastic domain this effect is minimal. It is thus, although unloaded, another contact area. However, to create consistent angles the large scale manufacturing is more difficult. Table 3.3 shows an overview of the allocated values for the different versions of Variant 3 per criteria and its weighted score.

Table 3.3: Results of the multi-criteria analysis for Variant 3: Notch connections.

Criteria	Structure	Vibrations	Acoustics	Buildability	Score
Weighting	30%	25%	25%	20%	
3.A1	7	6	4	8	6,20
3.A2	6	8	8	7	7,20
3.B1	9	7	3	7	6,60
3.B2	8	7	5	6	6,60
3.C	6	8	7	4	6,35
3.D	6	8	9	4	6,85

3.1.4 Variant 4: Conceptual connectors

The first variant consists of several conceptual connectors. These either consists of add-on 'boxes' or U-profiles in the notch featuring a spring, compliant mechanisms or rollers, as shown in Figure 3.4.

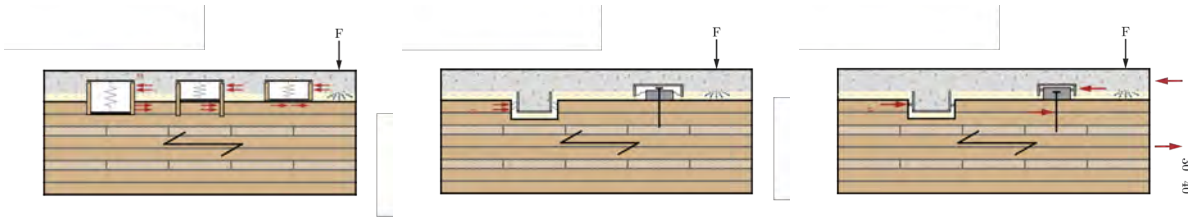

(a) 4.A - Spring box connectors (b) 4.B - Compliant connectors (c) 4.C - Roller connectors

Figure 3.4: Versions of Variant 4: Conceptual connections

As introduced, the first version focuses on the creation of a stiff box which included a vertical spring to provide similar freedom of vertical movement as the insulation layer. The first option to implement this idea is to glue the box in a notch of the timber. This does however not feature the same stiffness as for a notch, since the box is not solid and the sides can bend due to the shear force transfer. Furthermore, next to fabrication of the box,due to the requirement of its placement in notches it results in high labor requirements. The second way of implementing this box is by only penetrating its load bearing sides into the timber, creating support for to transfer the shear force. This actual stiffness is however still expected to be limited. The option is to only place the box above surface, significantly reducing the required labor. It main downside is however its usage of an adhesive bond as main system to transfer the shear load. While extremely stiffness, it is also very brittle and difficult to product. The quality and structural integrity is

therefore difficult to ensure.

The second versions uses compliant connectors in the form of waves plates which allow transverse movement but no horizontal movement. However, generally the horizontal stiffness of these plates is regarded as very poor. Besides, the first option of inserting a 'decoupled' U-profile in the notch is very difficult to construct while properly ensuring the correct placement and attachment of the fragile small plates. Besides, while an moisture retaining foil should be placed between the concrete and other elements, a possible small leak could quickly disrupt the compliant mechanism. While this expected to be less the case for the add-on box option, it features an extra element reducing the total connection stiffness of the system, its screw. The low connection stiffness of individual screws especially impact the connection stiffness since the boxes are not expected to be able to be spaced as densely as standard screw configurations, to ensure the structural integrity or due to an increase in costs. The third version is similar to the second one, but uses a roller instead of a wave plate to transfer the load while allowing vertical movement. While the roller features increased stiffness in the element itself, for the inserted U-profile it also creates large local stresses in the timber. Due to the weakness of the timber perpendicular to its fiber directions, it features poor performances onl local scale. Furthermore, a possible indentation of the roller into the timber due to the pressure could constrain the free vertical movement. The box option does not feature these problems due to the ability to use rigid materials, but it still features its low connection stiffness due to the usage of a screw.

Table 3.4 shows an overview of the allocated values for the different versions of Variant 4 per criteria and its weighted score.

Table 3.4: Results of the multi-criteria analysis for Variant 4: Conceptual connections.

Criteria	Structure	Vibrations	Acoustics	Buildability	Score
Weighting	30%	25%	25%	20%	
4.A1	4	7	8	3	5,55
4.A2	5	8	8	5	6,50
4.A3	3	7	8	8	6,25
4.B1	3	7	9	4	5,7
4.B2	3	7	9	6	6,10
4.C1	3	7	9	4	5,70
4.C2	3	7	9	6	6,10

3.1.5 Conclusion

Comparing the scores of the Multi-Criteria Analysis taking into account structural-, vibration-, acoustic performance and buildability Variant 3: Notch connections clearly featured the most promising connector designs. Especially version 3.A2 consisting of a continuous rectangular notch with insulation and PTFE at the notch sides, and without fasteners proved most promising and therefore be further developed. It major challenge will be its lack of vertical reinforcement and prevention of separation.

3.2 Variant development

This section will focus on the further development and details of the continuous rectangular notch connection with an insulation layer, as was concluded as the most promising connection

type described in Section 3.1.

As introduced the connection type is characterized by two main features. The first one is the presence of the surface insulation and notch insulation. Especially the latter of interest. To remain an equal effective notch height $h_{n,eff}$ between the timber and concrete, since it is one of the main influencing parameters regarding the connection stiffness of the notch, it was decided to deepen to notch to make space for the notch insulation. While this does not directly influence the notch stiffness due to it keeping the same contact area, it disrupts a larger part of the timber cross-section. One of the possible results would be a lower location of the center of axial stress in the timber, increasing the eccentricity between this force and the notch force. It was therefore considered if the notch insulation could be halved. However, this would cause an undesirable increase in dynamic stiffness s'. The insulation material would therefore have to be changed to a very soft option. However, although the concrete in stiff state can be mainly carried by the surface insulation, in can already cause compression problems in the soft insulation in its wet state. Due to the focus on this study on the main principle, this was not further considered.

The second main feature is the presence of PTFE strips on the notch sides to reduce as much friction as possible in these areas. This can be achieved by the very low friction coefficient of PTFE strips and is especially helpful in the outer notch sides where all the shear forces are transferred in the form of contact compression. Additionally, the connection detail should feature a moisture retaining foil to prevent moisture transfer from the fresh concrete and insulation and timber. This might trap the moisture, weaken the timber and possibly decrease its integrity. For traditional floors it also prevents the timber and concrete from bonding at their interface. While the interface bonding slightly increases the connection stiffness of the floor, it is often advised to not take it into account and thus better prevent it to ensure the shear transfer is fully done by the notch contact and thus can be controlled [53]. For the conceptual floor the foil should be placed over the insulation and PTFE covered notch sides. Due to the smoothness of the foil compared to the concrete, it lowers the friction with the PTFE even further.

Furthermore, an horizontal steel reinforcement mesh should be present to prevent shrinkage cracks in the concrete due to it being constrained by the timber. For the conceptual floor this is also beneficial for bending in the concrete due to its partly floating conditions, similar to standard floating floor [52].

Next to this general considerations, two specific alternatives were considered to increase it structural performance. As introduced in Sections 2.1 and 3.1, the structural integrity of the conceptual floor is negatively influenced by its lack of notch fasteners. They often feature thee main purposes. The first one is providing vertical reinforcement in the loaded notch area. This is especially important due to the presence of vertical tensile stresses perpendicular to the compression strut, shear stresses in the area and tensile stresses resulting from the eccentricity between the notch force and concrete axial force. In combination with these different but related mechanisms, the tensile and shear resistance is difficult to accurately predict due to the high variability in tensile strength and aggregate interlock [4]. This becomes even more complex when other forms of concrete (micro) cracks such as shrinkage cracks or flexural cracks are present in the area. By providing shear reinforcement, these cracks still initiate but remain thin and do not lead to failure. It is therefore generally advised to simply add vertical reinforcement in the notch [4]. Secondly, if failure occurs, the fasteners have the tendency to keep the geometry together

and redistribute the force over the other connectors [14]. It therefore improves the post-peak behavior by adding ductility. Lastly, it also makes sure that during the elastic and plastic phase no separation of the timber and concrete can occur. This is critical since the separation can result in preliminary quick progressive collapses [4].

To tackle the separation and ductility problem, in combination with keeping the improved decoupling of the system, the decoupled fastener was designed and is shown in Figure 3.5a. It was inspired by deflector screw and prevent bonding of the screw with the concrete by the addition of a plastic sleeve around the shaft of the screw. The screw length is further increased such that its head is above the concrete layer. A small space between the bottom of the head and the top of the concrete should be left free, or filled by a soft ring. The idea is that the concrete can freely move up and down when the floor is excited and lightly loaded in his serviceability limit state. When separation starts occurring, the concrete will start to make contact with the screw head which will keep it in place and retain the structural integrity of the system. Furthermore, after failure the fastener can still provide its ductility benefits. It is however not perse beneficial for the function of shear reinforcement due to the lack of bonding. This alternative was however not further pursued since even though the screw would theoretically be unboned from the concrete and the latter would theoretically be able to move up and down, this is likely not be the case in practice. There will for example also be pressure on the soft sleeve causing it to be compressed against the screw, causing it to feature a waved surface on its outside. Furthermore, bending of the screw could also significantly reduce the intended effect. Additionally, the separation of the timber and concrete might already be reduced by compression of the insulation layer due to the weight of the concrete. Due to it limiting the decoupling of the system and the still unknown magnitude of the anticipated problems with the structural integrity it was decided to not include the decoupled floor in the design.

The concrete cracking and ductility challenges could also be solved by addition of a stirrup in the loaded notch area, as shown in Figure 3.5b. Research by Jiang and Crocetti, featured additional stirrups next to their fasteners in traditional CCC floors to improve the resistance of the concrete against notch shear failure [29]. Even though this addition looks promising, it was not further considered in the study due to the provided traditional CCC specimen not featuring it and thus creating a more difficult comparison.

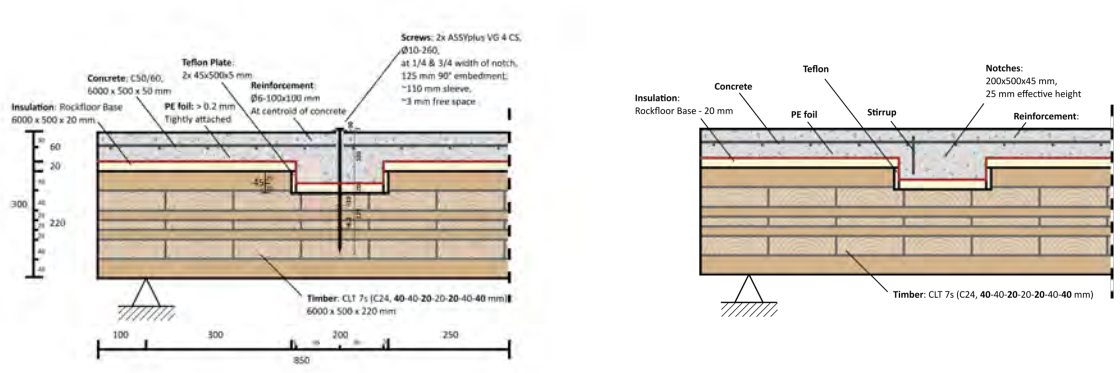

(a) Decoupled fastener (b) Stirrup

Figure 3.5: Considered connection details for the conceptual floor

Figure 3.6 shows the chosen connection detail for the conceptual floor next to the connection

detail of the provided traditional CCC floor specimen for experimental testing. These connection details will be used in the second part of this research for extensive investigations of the floor types. Next to the above mentioned considerations, the notch dimensions of the conceptual floor are based on the notch dimensions of the traditional connection details. These also align with the used notch dimensions by Thai in his large scale experiments on notched CCC beams after extensive small-scale investigations into notch parameters [53]. These dimensions will be kept constant through-out the study.

To conclude, the chosen connection details will thus consist of a notch connection with surface- and notch insulation and PTFE-covered sides to provide the system with the desired dynamic resilient behavior. Additionally, PE-foil was added to protect the insulation and timber from moisture damage and a horizontal reinforcement mesh was added to prevent shrinkage problems. Although considered, the addition of a decoupled screw or stirrup to improve the shear resistance in the concrete and ductility while also prevent critical separation were not implemented due to the desire for full decoupling and yet unknown magnitude of these challenges.

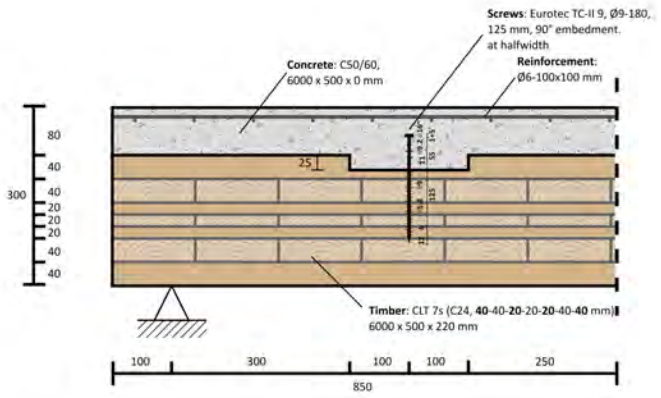

(a) Traditional

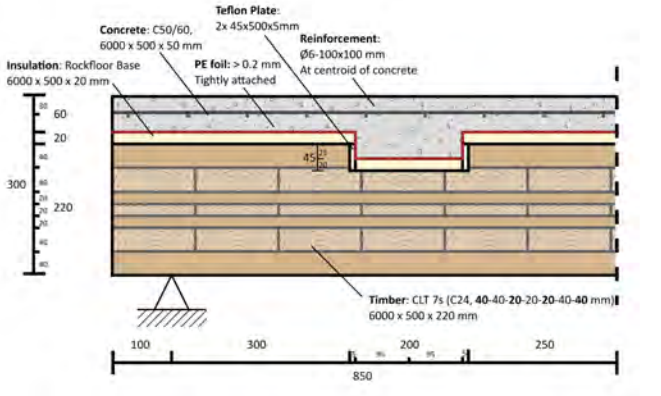

(b) Conceptual

Figure 3.6: Chosen connection details for the traditional and conceptual floor

4 Floor designs

This chapter provides an overview of the floor designs considered for the detailed analysis of this study. Next to the traditional, conceptual and decoupled floor types described in Chapter 1, this study features also three design categories; the Experimental Design, the Large Span Design and Large Span Design+ categories. This results in the detailed analysis of nine floor build-ups in total.

Next to the dimensions and approach for each design category, the following section will feature the expected performance per floor on a scale from -- to ++, as shown in Table 4.1. These expectations are based on the earlier described preliminary research and will be refined in Chapters 5, 6 and 7. The final performance levels using results from the detailed investigations, for which an overview is giving in Chapter 8, will make sure of more detailed requirements for each of three evaluated aspects, as described in Chapters 5 to 7 respectively.

Table 4.1: Considered performance level indicators for indication of the Structural, Vibration and Acoustic performance.

Performance level	Indicator
Very good performance	++
Satisfactory performance	+
Unsatisfactory performance	-
Very poor performance	--

4.1 Large Span Design category

The connection detail fo the traditional and conceptual floors in the Large Span Design (LSD) category are designed as shown in Figure 3.6, while its cross-section build-up is designed at the threshold of the structural performance for the set 8.7 meter span. As more elaborately described in Section 5.1, this has been done by numerically modeling of a push-out test to determine the connection stiffness K^*, the extended γ-method for the cross-sectional analysis and the Boccadoro-method for notch failure to ensure a ductile governing failure mode. The design limitations of the design process, such as the maximum concrete height, notch dimensions and inter layer dimensions, are mentioned in Section 1.2. The full design process is described in Appendix B. The decoupled floor functions as reference for the vibrational and acoustical performance of the floors. To keep this the best comparable, it features the same build-up as the conceptual floor but without its shear connections. The floor designs int the LSD category are shown in Figure 4.1.

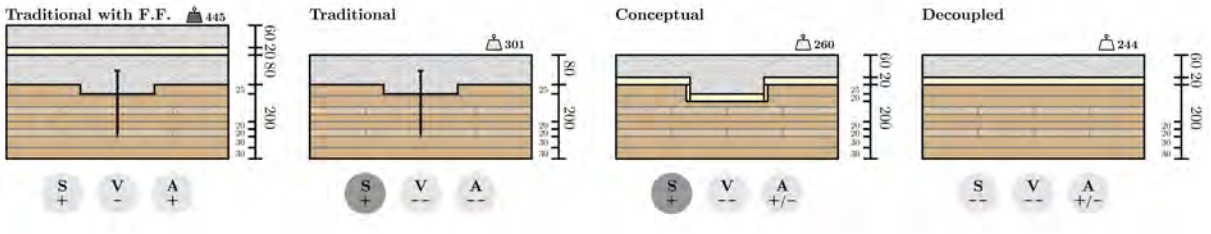

(a) Floor Build up and expectations

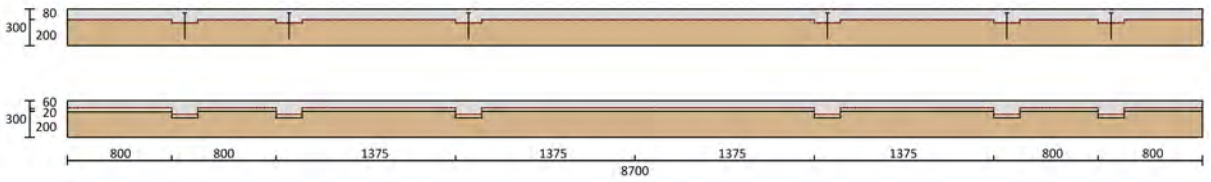

(b) Floor design

Figure 4.1: Floor design of the Large Span Design (LSD) floors, with expected Structural (S), Vibration (V), Acoustic (A) performance.

4.2 Large Span Design+ category

The build-up of the traditional and conceptual floors in the Large Span Design+ (LSD+) category are designed in such a way that they just meet the desirable vibrational performance for the set 8.7 meter span. This is done by the analytical reEC-5 method, which will be further explained in Section 6.1. Besides the method requiring some input from the structural approach to determine the stiffness of the system, the static structural requirements will also be considered. A full elaboration of the design process can be found in Appendix B. The resulting floor is shown in Figure 4.2. Instantly notable is that it features considerably increased dimensions compared to the LSD floors, which therefore meet the vibration requirements and over dimension for the structural requirements.

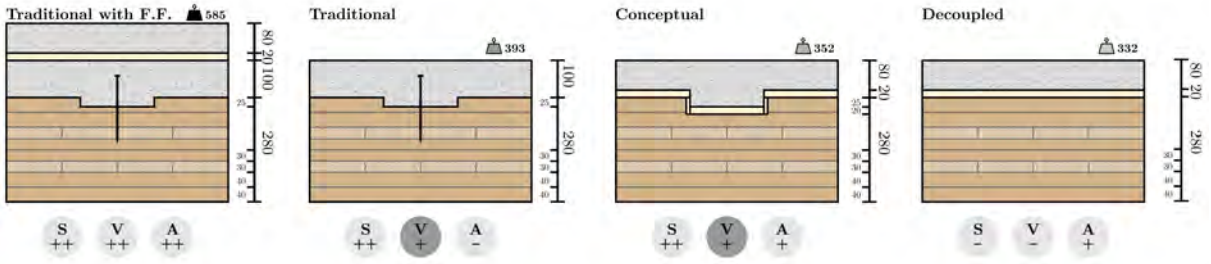

(a) Floor Build up and expectations

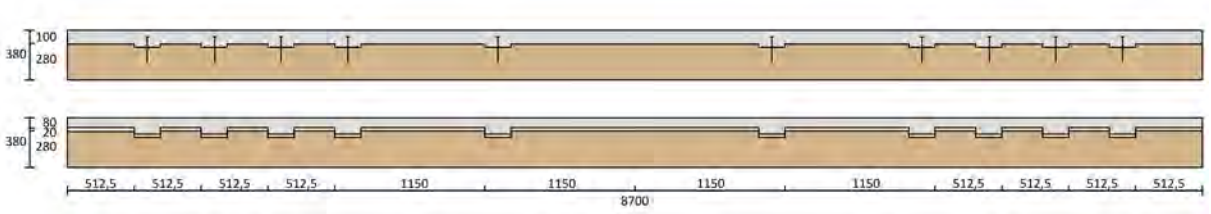

(b) Floor design

Figure 4.2: Floor design of the Large Span Design+ (LSD) floors, with expected Structural (S), Vibration (V), Acoustic (A) performance.

4.3 Experimental Design category

The design of the three floor types in the Experimental Design (ED) category are based on the traditional CCC specimen gifted by MDLX BV, which will be used for the experimental vibration and bending investigations. One of their main governing parameters for the design was the practice guideline of a minimum mass of 300 kg/m^2 of the base floor to reach a desirable vibration and acoustical performance after addition of a floating top floor. The build-up is shown in Figure 4.3. Similar to the LSD and LSD+ designs, for the conceptual floor the concrete height was reduced with the same amount as the height of the added insulation layer such that the total height of the conceptual floor is equal to the total height of the traditional floor. The most notable aspect for this design category is however its 6 meter length, while the other 2 feature the 8.7 m span of the project scope. Besides, the specimens features a 0,5 meter width. To keep the results to the other design categories, the width will be adjusted to a 1 meter width for the analytical and numerical calculations. The experimental results will also be processed such that they convey the equivalent results for a 1 meter wide specimen. The floor designs in the Experimental Design category are shown in Figure 4.3.

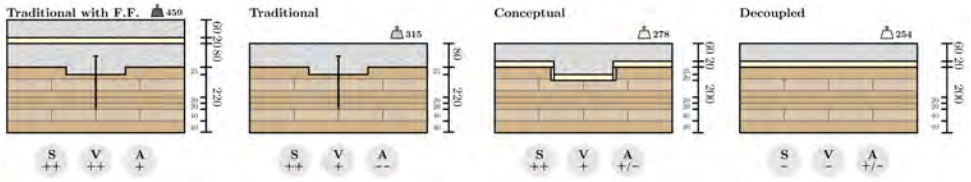

(a) Floor Build up and expectations

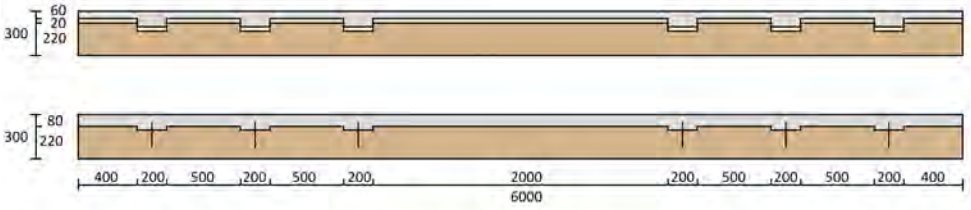

(b) Floor design

Figure 4.3: Floor design of the Experimental Design (ED) floors, with expected Structural (S), Vibration (V), Acoustic (A) performance.

5 Structural performance

In this chapter the evaluation of the static structural performance of the three floor types, for each of the three design categories is described. In Section 5.1 the set requirements for the serviceability limit state and the ultimate limit state are described. The former will focus on instantaneous and long term deformation, while the latter will focus on cross-sectional stresses, notch failure mechanisms and ductile failure. Furthermore it will describe a numerical modeling approach for the determination of the connection stiffness, an analytical approach using the separated and extended γ-method for cross-sectional analysis, an analytical calculation model for the prediction of notch failures and an experimental program using a 6 point bending test. The results of these investigations will be described in Section 5.2 and their validity in Section 5.3. In Section 5.4 the conclusions regarding the structural performance of these floors is described.

5.1 Requirements & methodology

This section describes the requirements and criteria used to determine the structural performance of each floor type.

For the floor type to reach satisfactory performance (+) it should fulfill the serviceability limit state (SLS) and ultimate limit state (ULS) requirements as described in dutch version of the Eurocode 0 - Basis of the design: NEN-EN 1990:2002 (EC1) in combination with additional guidelines from the 2019 draft of the upcoming addition to EC5: Structural Design of Timber concrete structures (EC-TCC), Eurocode 5 - Design of timber structures (EC5), Eurocode 2 - Design of concrete structures (EC2) and mentioned literature.

This study will mostly focus on the instantaneous and long term static deflection for the SLS. For the long term deflection creep will be considered in the form of reduced stiffness for the elastic moduli for the concrete, timber and the connection in accordance to the EC-TCC. Moisture effects, thermal influences, the construction phase (propping) and elastic strains due to shrinkage are not taken into account. The criteria for structural vibration performance will be tackled separately in Chapter 6.

For to satisfy for the ULS, this study will take into account the cross-sectional stresses of the layers. Due to the composite interaction, there are extra axial stresses in these layers beside the bending stresses. Therefore, for the timber layer the combined bending-compression and bending-timber stress checks will be used as stated in the TCC-EC. For the concrete checks, the axial and bending stresses will simply be added to each other. Since for concrete the element does not directly fail when the tensile strength is reached and flexural cracks start to form, the TCC-EC describes a iterative calculation progress whereby the cracked concrete height should be considered as a non-load bearing layer. However, allowing flexural cracking at the bottom of the concrete could compromise the integrity of the notch connections. The flexural cracking of the concrete top layer is therefore not allowed for the design in this study. Besides, the combined axial and bending stresses, the shear stress check of the element will also have to be satisfied. Next to the cross-sectional failures, the capacity of the notches should also be sufficient enough to resist the load due to shear stress at the interface of the two layers. At last, since these failures are themselves brittle or will cause instant progressive collapse (e.g. due to loss of composite

interaction), ductility of the floor system is difficult but important to achieve. As described by Boccadora et al., the only ductile failure mechanism of TCC systems is the timber compression failure (TCF) due to the plasticity of the timber in compression [4]. Next to satisfying all the failure mechanisms, the floors will also have to be checked if the TCF is the governing failure mode.

5.1.1 Numerical determination of connection stiffness

For the determination of the connection stiffness per meter width K^*, a numerical version of the commonly used push-out test will be used. For these tests a small TCC specimen consisting of the timber and concrete layer connected by the tested shear connector is fabricated. The specimen is then loaded in shear in such a way that the force is only transferred by the shear connector. Based on the slip between the concrete and timber, the connection stiffness of the connector type can be determined. The most straight forward is the asymmetric push-out test due to its representation of the TCC floor. However, the eccentric nature of the set-up in combination with friction can cause overestimation of the connection stiffness of up to 10% [38], [53]. To tackle this, feature increased stability and lower impact of local imperfections, also symmetric push-out tests have been conducted in which the timber is also connected to a second concrete slab on its other side, or vice versa, using a second connector. The specimens for these tests are however more difficult to fabricate. Both set-ups are shown in Figure 5.1.

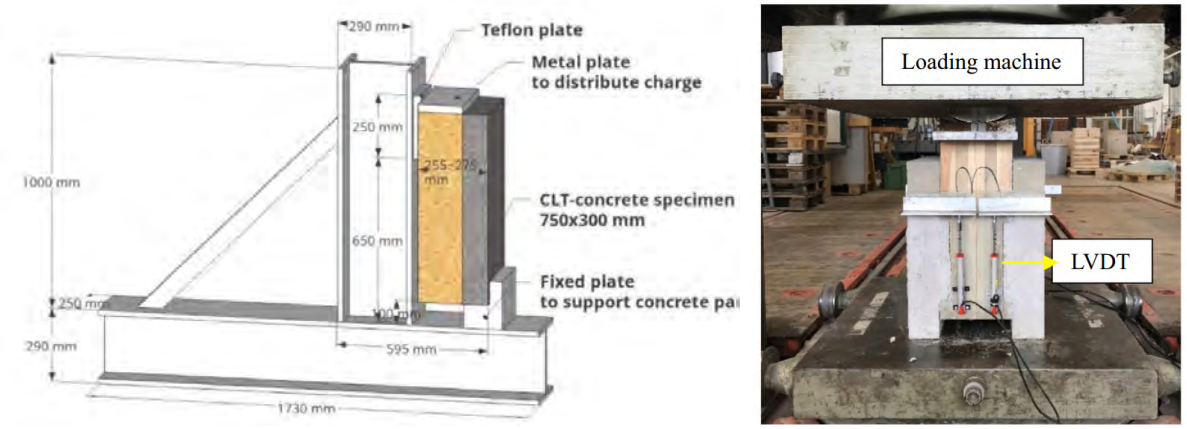

(a) Asymmetrical push-out test by Thai [53]

(b) Symmetrical push-out test by Jiang and Crocetti [29].

Figure 5.1: Asymmetrical and symmetrical push-out tests for the determination of the connection stiffness in CCC structures using notch connections.

Besides experimental investigations, these test are also replicated by numerical modeling using the Finite Element Method (FEM) to determine the connection stiffness This is especially useful due to the many parameters, such as notch dimensions, timber and concrete geometry and the presence and type of fasteners, influencing the results in combination with a complex structural mechanism. Besides, there are currently no clear and sufficiently accurate go-to analytical formulations. The results is that for almost each design (iteration) an individual push-out test should be done experimentally or thus numerically. Numerical modeling allows to do this without the need for a rigorous experimental approach. Therefore, numerical modeling of the push-out test will also be used in this study for the determination of the connection

stiffness. For this the asymmetrical push-out tests will be chosen due to its representation of actual CCC floor build-up and the nullification of the eccentricity problem due to modeling of a fully friction-less CLT-Concrete surface, resembling the advised moisture retaining foil in between the materials.

For the numerical modeling of the push-out test, the FEM software package Ansys Mechanical in the Ansys 2024 R1 environment will be used. Next to its 'static structural' analysis component, it also features different types of vibration analysis and thus allows continuity with the numerical modeling in regard to the vibrational performance described in Chapter 6.

The initial modeling approach was based on important work in the development of numerical analysis of push-out test by Dias [13], Jiang and Crocetti [29] and Thai [53]. The preliminary modeling will then be validated by replication of two experimental investigations into the connection behavior of CCC structures with rectangular notches by Jiang and Crocetti [29] and Thai [53] and by an experimental investigation of the connection behavior of triangular notches of TCC structures using CLT and glue-laminated timber (GLT) as its timber layer by Lamothe et al. [33]. Most interestingly, the latter also featured an investigation into the effect of the addition of an inter layer of insulation material on the notch behavior for the GLT specimens. Next to the replication of the experimental investigations, extra configurations and settings will be tried to find the most applicable modeling approach.

For the final modeling approach a 3D model using linear 8-node solid elements will be used. The model will feature a general mesh size of 10 mm, which is refined around the notch area to 5 mm. The timber is modeled as a elastic-perfectly plastic material using the Hill-criterion and the concrete is modeled as a tri-linear material. Further failure mechanisms, such a concrete tensile crack formations or compressive crushing, are omitted due to the scope of the study on the elastic range. The material properties for the CLT are based on the properties of the C24 timber grade according to in longitudinal and perpendicular direction according to EN 338:1996. For the concrete the corresponding properties of the concrete grade as described in EC2 will be used. Furthermore, the system is loaded by an steel loading plate covering the timber height up until the notch depth. The steel loading plate is constrained in transverse direction. The concrete is supported in longitudinal and transverse direction by a steel loading plate at the other end. Fasteners are left-out of the model due their minimal direct impact of the shear behavior. To replicate their function to prevent separation, the longitudinal surface between the CLT and concrete will be modeled using the 'no separation' contact type. While this type constrains penetration and separation, it allows free sliding (shear) of the elements and therefore represents the lack of friction due to the moisture retaining foil. The perpendicular CLT and concrete surface, also referred to as the notch sides, will be modeled as 'friction-less' and the individual CLT-layers will be glued together using the 'bonded' contact type. This is similar to the conceptual floor, which additionally feature a 'bonded' CLT-insulation contact surface and a 'rough' insulation-concrete contact surface. Since the approach of using the 'no separation' interface is not applicable, the models of the conceptual floors are stabilized by an additional added vertical roller at the unloaded concrete end. The boundary conditions are visualized in Figure 5.2, indicating the width-symmetry plane in red, the vertical support and horizontal displacement loading in yellow, the vertical and horizontal concrete support in orange and the vertical roller support for stabilization in blue. At last, only half the specimen will be modeled including a symmetry plane to get the original width to cut computational costs.

The detailed modeling process and approach can be found in Chapter A.

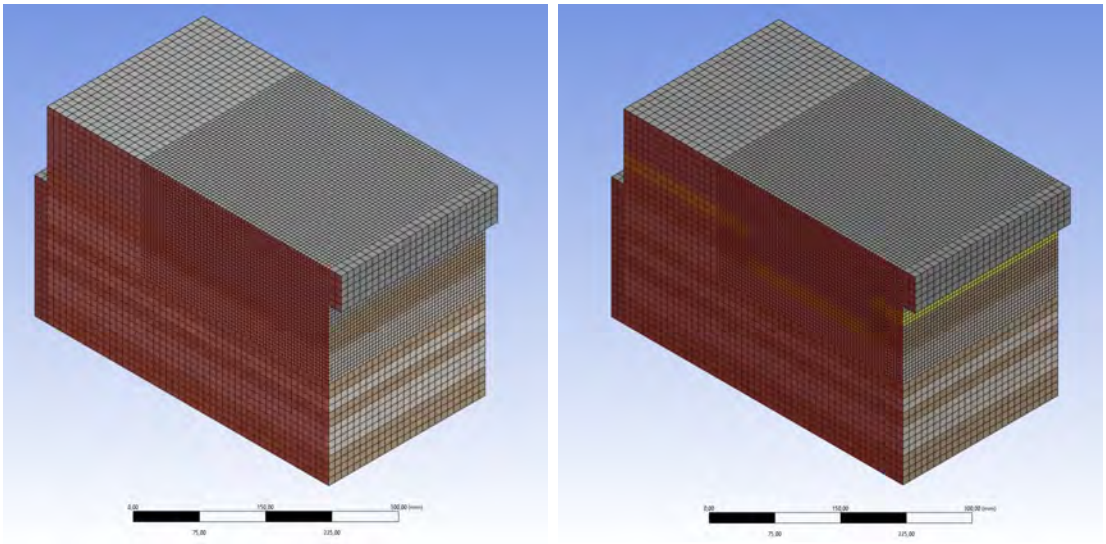

(a) 3D geometry and mesh

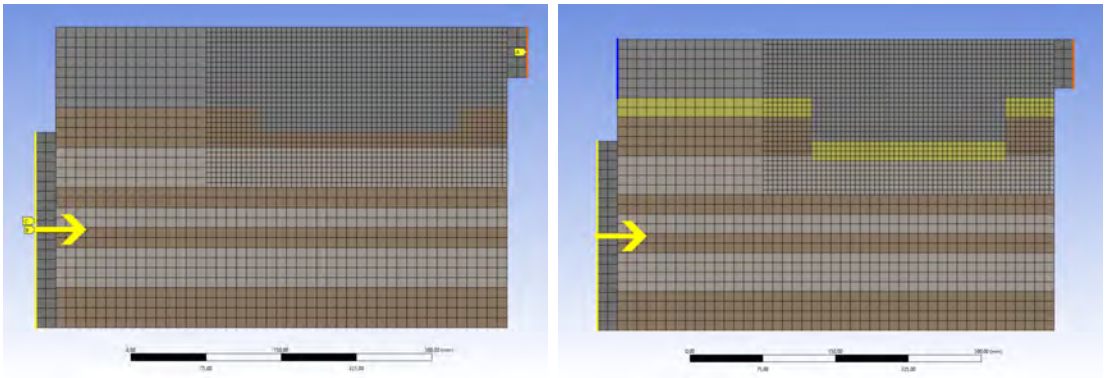

(b) Boundary conditions

Figure 5.2: Overview of the numerical modelling with the specimen of the ED-traditional floor on the left and the ED-conceptual floor on the right.

5.1.2 Analytical cross-section analysis

This section will elaborate the methodology for the determination of the elastic bending stiffness, stresses and strains in the composite cross-section. This will be done by two variations of the original gamma-method (γ-method), presented in the Annex of EC5. Central in the γ-method is the evaluation of composite interaction between the different layers by usage of a γ-value, which can be in between 0 and 1. The determined γ-value is based on the material properties, span and most importantly connection stiffness between the layers. The equations for the determination of the γ-value, distance to the effective neutral axis a_i and effective bending stiffness EI_{eff} for a two-layered system where the location of the rigid neutral axis $z_{na,rigid}$ is in element 2, are shown in Equations (5.1) to (5.5). If $z_{na,rigid}$ is located in element 1, the equations in Equations (5.2) and (5.3) are simply reversed and the parameters adapted accordingly. In these equations the thickness of the non-load bearing insulation t is already integrated. At last the effective bending stiffness of the composite system can be determined using Equation (5.6).

$$z_{(na,\text{rigid})} = \frac{ES_y}{EA} = \frac{((EA)_1 \cdot z_1) + ((EA)_2 \cdot z_2)}{((EA)_1 + (EA)_2} \tag{5.1}$$

$$\gamma_1 = \frac{1}{1 + \frac{\pi^2 \cdot (EA)_1}{L^2 \cdot C_i}} \tag{5.2}$$

$$\gamma_2 = 0 \tag{5.3}$$

$$a_1 = \frac{h_1}{2} + t + \frac{h_2}{2} - a_2 \tag{5.4}$$

$$a_2 = \frac{\gamma_1 \cdot (EA)_1 \cdot (h_1 + t + h_2)}{2 \cdot (\gamma_1 \cdot (EA)_1 + \gamma_2 (EA)_2)} \tag{5.5}$$

$$EI_{\text{eff}} = \sum_{i=1}^{2} \left(E_i \cdot I_i + \gamma_i \cdot E_i \cdot A_i \cdot a_i^2 \right) \tag{5.6}$$

When the layers of the composite system are connected by a shear connector, the distributed shear stiffness can be calculated from Equation (5.7), in which K is the connection stiffness, n is the amount of connectors in width direction and s_{eff} is the effective spacing in length direction. A 3-ply CLT element can also be calculated using the formulas for a two layer composite system by assuming the longitudinal layers as the main layers and the weak transverse layer as an imaginary shear connector. The only adjustments are the numbering of layers, the addition of the height of the non-load bearing layers similar to the integration of t and the determination of C based on the rolling shear stiffness shown in Equation (5.8).

$$C = \frac{n \cdot K}{s_{\text{eff}}} \tag{5.7}$$

$$C = \frac{G_{2,90} \cdot b}{h_2} \tag{5.8}$$

The normal strains and stresses over the cross-section can also be determined with the γ-method. This will be done by the addition of two strain and stress categories. The first category features the strains and stresses due to pure bending of each individual layer without taking into account the composite interaction, which can be determined using Equations (5.9) and (5.10).

$$\varepsilon_{b,i} = \kappa \cdot e_i = \frac{M}{EI_{\text{eff}}} \cdot \pm \frac{1}{2} h_i \tag{5.9}$$

$$\sigma_{b,i} = \varepsilon_{b,i} \cdot E_i = \frac{M \cdot E_i}{EI_{\text{eff}}} \cdot \pm \frac{1}{2} h_i \tag{5.10}$$

The second one features the uniform strains and stresses per layer due to the composite interaction. These can be determined by using Equations (5.11) and (5.12).

$$\varepsilon_{\gamma,i} = \gamma \cdot (\kappa \cdot a_i) = \frac{\gamma_i \cdot M}{EI_{\text{eff}}} \cdot a_i \tag{5.11}$$

$$\sigma_{N,i} = \varepsilon_{\gamma} \cdot E_i = \frac{\gamma_i \cdot (M \cdot E_i)}{EI_{\text{eff}}} \cdot a_i \tag{5.12}$$

For a two element composite structure the stresses in the in the top and bottom of each layer can thus be calculated using Equations (5.13) to (5.16).

$$\sigma_{1,top} = (-\frac{1}{2}h_1 + \gamma_1 \cdot a_1) \cdot \frac{M \cdot E_i}{EI_{\text{eff}}} \tag{5.13}$$

$$\sigma_{1,bot} = (\frac{1}{2}h_1 + \gamma_1 \cdot a_1) \cdot \frac{M \cdot E_i}{EI_{\text{eff}}} \tag{5.14}$$

$$\sigma_{2,top} = (-\frac{1}{2}h_2 + \gamma_2 \cdot a_2) \cdot \frac{M \cdot E_2}{EI_{\text{eff}}} \tag{5.15}$$

$$\sigma_{2,bot} = (\frac{1}{2}h_2 + \gamma_2 \cdot a_2) \cdot \frac{M \cdot E_2}{EI_{\text{eff}}} \tag{5.16}$$

Furthermore, the shear stresses in the cross-section can be determined by analysing the horizontal equilibrium between the axial stress up until the investigated location and the residual shear force F_v over an infinitesimal small change of in x-direction dx. This is visualized in Figure 5.3a for the neutral axis. The derivation of the shear stress at the neutral axis is shown below. The shear stress at the the interface, for which the equilibrium is shown in Figure 5.3b, follows a similar approach.

$$\sum H = 0 \tag{5.17}$$

$$F_{v.na} \cdot dx = \left(d\sigma_{1,bot} \cdot h_1 b + \frac{(d\sigma_{1,top} - d\sigma_{1,bot}) \cdot h_1 b}{2} \right) + \frac{d\sigma_{2,1,top} \cdot h_1 b}{2}$$

$$F_{v.na} = \frac{(d\sigma_{1,top} + d\sigma_{1,bot} + d\sigma_{2,1,top}) \cdot h_1 b}{2 \cdot dx}$$

$$F_{v.na} = \frac{\left(2 \cdot \gamma_1 \cdot a_1 \cdot E_1 + \left(\gamma_2 \cdot a_2 - \frac{1}{2} \cdot h_2\right) \cdot E_2\right) \cdot \frac{dM}{EI_{eff}} \cdot h_1 b}{2 \cdot dx}$$

$$F_{v.na} = \frac{\left(2 \cdot \gamma_1 \cdot a_1 \cdot E_1 + \left(\gamma_2 \cdot a_2 - \frac{1}{2} \cdot h_2\right) \cdot E_2\right) \cdot h_1 b}{2 \cdot EI_{eff}} \cdot \frac{dM}{dx}$$

$$F_{v.na} = \frac{\left(2 \cdot \gamma_1 \cdot a_1 \cdot E_1 + \left(\gamma_2 \cdot a_2 - \frac{1}{2} \cdot h_2\right) \cdot E_2\right) \cdot h_1 b}{2 \cdot EI_{eff}} \cdot V$$

$$\sigma_{v.na}(x) = \frac{F_{v.na}(x)}{b} = \frac{\left(2 \cdot \gamma_1 \cdot a_1 \cdot E_1 + \left(\gamma_2 \cdot a_2 - \frac{1}{2} \cdot h_2\right) \cdot E_2\right) \cdot h_1 b}{b \cdot EI_{eff}} \cdot V(x) \tag{5.18}$$

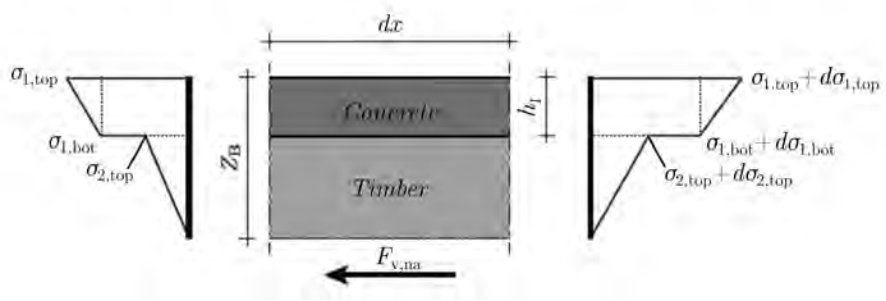

(a) Location of neutral axis in timber

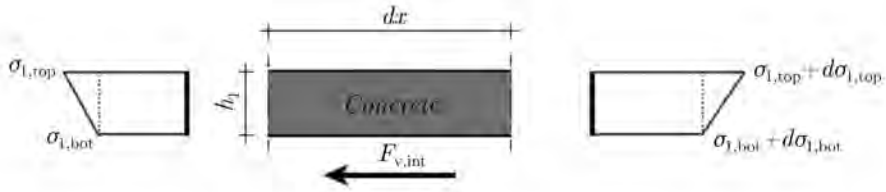

(b) Location of interface

Figure 5.3: Overview of the horizontal equilibrium to determine the shear stress at the neutral axis, assumed in the timber, and concrete-timber interface, based on [23].

At last, it is important to note that this method is a simplification from the method of differential equations based on Euler-Bernoulli beam theory in which a sinusoidal distributed load, a statically determinate structure, a constant cross-section and evenly smeared connectors are assumed [8]. Besides, the original method is limited to the evaluation of the three main layers for asymmetrical cross-sections. If used within these limitations, the γ-method is much easier to use than the method of Shear Analogy, strut-tie method or FE-modeling and can be done by hand. It is therefore the most accessible method for the evaluation of a TCC structure [8], [53]. However, due to the limitations in the amount of layers, CCC structures using 5s-, 7s-, 7ss- and 8ss-ply CLT cannot be evaluated using the base γ-method. Therefore, two variations on the base γ-method will be used; the separated γ-method and extended γ-method.

5.1.2.1 Separated Gamma-method

The idea of the separated gamma-method, described by Maanen [39] and Bao [2], is a two-step approach in which first the CLT is combined into an single effective homogeneous layer and secondly the combination of the effective CLT and concrete into the effective composite cross-section.

While a 3-ply CLT layer can use Equations (5.1) to (5.5) and (5.8) for the determination of the bending stiffness of the effective homogeneous layer, the properties of a 5-ply CLT layer can be calculated using Equations (5.19) to (5.26). By assuming the double longitudinal layers as a single layer, 7ss- and 8ss-ply CLT can also be calculated With these formulas. The effective bending stiffness of 7s-ply CLT, used in the floors of the Experimental Design category, can

however not be calculated using this approach due to the presence of five longitudinal layers in the CLT. Therefore $\gamma_1, 3, 5, 7 = 1$ is assumed. Based on the gained experienced an overestimation of up to 5% for the $EI_{eff,CLT}$ is expected for the 7s-ply CLT due to this assumption.

$$\gamma_1 = \frac{1}{1 + \frac{E_1 \cdot A_1}{C_2} \cdot \frac{\pi^2}{L^2}} \tag{5.19}$$

$$\gamma_3 = 1 \tag{5.20}$$

$$\gamma_5 = \frac{5}{1 + \frac{E_5 \cdot A_5}{C_4} \cdot \frac{\pi^2}{L^2}} \tag{5.21}$$

$$a_1 = \frac{h_1}{2} + h_2 + \frac{h_3}{2} - a_3 \tag{5.22}$$

$$a_3 = \frac{\gamma_1 \cdot E_1 \cdot b \cdot h_1 \cdot \left(\frac{h_1}{2} + h_2 + \frac{h_3}{2}\right) - \gamma_5 \cdot E_5 \cdot b \cdot h_5 \cdot \left(\frac{h_5}{2} + h_4 + \frac{h_3}{2}\right)}{\gamma_1 \cdot E_1 \cdot b \cdot h_1 + \gamma_3 \cdot E_3 \cdot b \cdot h_3 + \gamma_5 \cdot E_5 \cdot b \cdot h_5} \tag{5.23}$$

$$a_5 = \frac{h_5}{2} + h_4 + \frac{h_3}{2} - a_3 \tag{5.24}$$

$$C_2 = \frac{G_{2,90} \cdot b}{h_2} \tag{5.25}$$

$$C_4 = \frac{G_{4,90} \cdot b}{h_4} \tag{5.26}$$

Furthermore, next to the effective bending stiffness $EI_{eff,CLT}$ also the axial stiffness $EA_{eff,CLT}$ of the CLT is required for the second step. Due to the fundamentals of the γ-method in the determination of an effective cross-section, in the form of an effective second of moment of area I_{eff}, and not in the determination of an effective modulus of elasticity E_{eff}, this cannot be simply be determined from $EI_{eff,CLT}$. The net area method will therefore be used described by the The CLT Handbook [24]. The determination of $EA_{net,CLT}$ based on this method is shown in Equation (5.27).

$$EA_{\text{net,CLT}} = E_0 * \sum_{i=1}^{5} \left(\frac{E_i}{E_0} \cdot A_i\right) \tag{5.27}$$

For the second step the properties of the concrete, the determined effective properties of the CLT and the numerically found connection stiffness of the notch K^*_{FEM}, can simply be inserted into Equations (5.1) to (5.6), (5.7), (5.13) to (5.16) and (5.18), to investigate the composite structure.

5.1.2.2 Extended Gamma-method

Due to the layer limitations of the base γ-method, Schelling decided to further develop it and formulated the extended γ-method [56]. It resulted in the relation of the matrix V and γ and s shown in Equation (5.28), for which V and s are based on the connection stiffness to the adjacent layers, the distance of the element to the rigid neutral axis and the stiffness of the element and can be filled in by the usage of Equations (5.29) to (5.33). When these values are gathered, the inverse of V can be multiplied to s and the γ-values per layer can be found. At last, Equations (5.6), (5.10), (5.12) and (5.18) can be used again to further analyse the composite system. This approach thus allows the calculation of an infinite amount of layers at the cost of increased calculation complexity. Furthermore, it is important to note that the other assumptions and limitations of the base γ-method are still active.

$$V \cdot \gamma = s \tag{5.28}$$

$$\begin{bmatrix} v_{1,1} & v_{1,2} & 0 & \cdots & 0 \\ v_{2,1} & v_{2,2} & v_{2,3} & \cdots & 0 \\ 0 & v_{3,2} & v_{3,3} & \cdots & 0 \\ \vdots & \vdots & \vdots & \ddots & \vdots \\ 0 & 0 & 0 & \cdots & v_{m,m} \end{bmatrix} \cdot \begin{bmatrix} \gamma_1 \\ \gamma_2 \\ \gamma_3 \\ \vdots \\ \gamma_m \end{bmatrix} = \begin{bmatrix} s_1 \\ s_2 \\ s_3 \\ \vdots \\ s_m \end{bmatrix}$$

$$v_{i,i-1} = -C_{i,i-1} \cdot a_{i-1} \tag{5.29}$$

$$v_{i,i} = (C_{i-1,i} + C_{i,i+1} + D_i) \cdot a_i \tag{5.30}$$

$$v_{i,i+1} = -C_{i,i+1} \cdot a_{i+1} \tag{5.31}$$

$$s_i = -C_{i,i+1} \cdot (a_{i+1} - a_i) + C_{i-1,i} \cdot (a_i - a_{i-1}) \tag{5.32}$$

$$D_i = \frac{\pi^2 E_i b h_i}{L^2} \tag{5.33}$$

5.1.2.3 Connector spacing

As mentioned, the γ-method assumes a perfectly smeared out shear connection between the two materials. There are however two attention points regarding this assumption. Firstly, many TCC structures do not feature a constant spacing but adapt the spacing linearly or in two zones in accordance to the shear force distribution over the span [8]. This is due to the combination of the low impact of connectors at the center of the floor span and the reduction costs and construction efforts. Secondly, while for small spacing between the connectors the difference between the determined bending stiffness and actual bending stiffness is negligible, for spacing above 5% of the span this assumption does not accurately describe the actual bending stiffness anymore [8], [11]. This is especially often the case for notched connections. To tackle this, different sources feature their own equations for a effective spacing s_{eff} [6], [8], [11]. For this study the formulation of Michelfelder [8], shown in Equation (5.34), will be used.

$$s_{eff} = 1,14 \cdot s_{min} + 3,14 \cdot \frac{s_{max}}{L} \cdot (s_{max} - s_{min}) \tag{5.34}$$

Furthermore, in this study the two zone principle for spacing will be used in the design of the LSD and LSD+ floors. It means an outer zone at $0 \geq x \geq 1/4L$ and $3/4L \geq x \geq L$, where

the minimal spacing is based on the design criteria of the notch shown in Equation (5.35), and an inner zone at $1/4L < x < 3/4L$ which features $V_{max,z2} = 0,5V_{max,z1}$ and therefore has a maximum spacing shown in Equation (5.36).

$$s_{z1,min} = l_{v,min} + l_n = 12,5 \cdot h_{n,eff} + l_n \tag{5.35}$$

$$s_{z2,max} = 2 \cdot s_{z1} \tag{5.36}$$

5.1.3 Analytical connection failure analysis

Next to the cross-sectional failure, the failure mechanisms around the notch connection should also be checked to satisfy ULS requirements. This can be done by usage of approach regarding the minimal notch resistance given by the TCC- EC [6], as shown in Equation (5.37). Besides, the TCC-EC also mentions the checking of the tensile capacity of the fasteners based on the compression strut angle or 10% of the notch force.

$$F_{\mathrm{n,Rd}} = \min \begin{cases} f_{v,c,d}\, b_n\, l_n & \text{a) shear of concrete} \\ f_{c,d}\, b_n\, h_n & \text{b) crushing of concrete} \\ k_{cr}\, f_{v,t,d}\, b_n\, l_{\min} & \text{c) shear of timber} \\ f_{c,0,d}\, b_n\, h_n & \text{d) crushing of timber} \end{cases} \tag{5.37}$$

However, this approach is significantly oversimplified and does for example not take into account the extra tensile stresses in the timber due to eccentricity which lowers the resistance against shearing-off failure. Furthermore, the approach describes that for each zone the outer connector should be checked. The notch force used for this check should be determined from taking the shear force at its location and dividing it by the spacing in that zone. For the first notch (N1) the notch force is thus $F_{N1} = \sigma_{v.inter}(x_{N1}) * b * s_{z1}$, as visualized in Figure 5.4. Besides not capturing the shear distribution in that area, the part with the highest shear stresses between the floor end and the first notch is ignored.

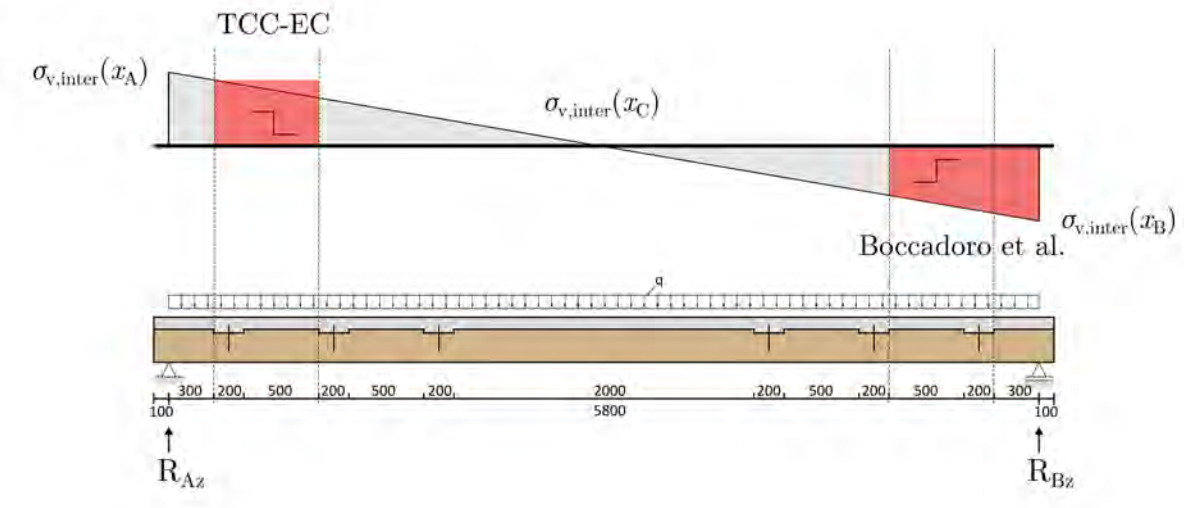

Figure 5.4: Approaches for the determination of $F_{n,N1}$ according to the TCC-EC [6] and Boccadoro et al. [4].

Therefore it was chosen to use the elaborate model for the prediction of notch failure by Boccadoro et al. [4]. This study specifically focuses on LVL-concrete composites 'thick' concrete slabs for which the neutral axis is located in the concrete layer and the concrete is thus cracked. Since this is not the case for the present study some of the equations found in the model will be adapted. Hereby also the presence of surface and notch insulation in the conceptual notch designs and the presence of the individual parameters for notch length l_n and the effective notch pre-timber length $l_{v,eff}$ has been taken into account. Furthermore, the floor will only be considered up until mid-span due to symmetry.

The equations for the determination of the notch load for N1 and the following notches are shown in Equations (5.38) and (5.39) respectively.

$$F_{v,N1,Ed} = \int_0^{x_{N2}} \sigma_{v,inter,Ed}(x)\, dx \tag{5.38}$$

$$F_{v,N_i,Ed} = \int_{x_{N_i}}^{x_{N_{i+1}}} \sigma_{v,inter,Ed}(x)\, dx \tag{5.39}$$

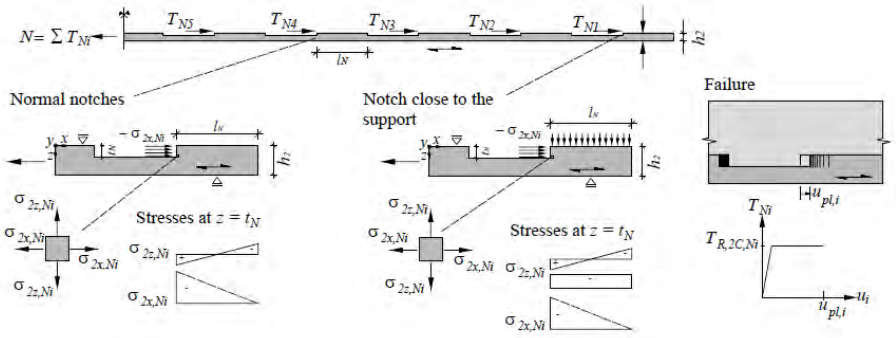

Figure 5.5: Cantilever model by Boccadoro for the prediction of Timber Compression Failure (TCF) in the notch for traditional TCC floors with a 'thick' cracked concrete slab [4].

For the calculation of the timber compression failure (TCF) a bi-axial stress state is assumed for which Equations (5.40) and (5.41) can be used for the calculation of the present horizontal and vertical stresses respectively. The first term of Equation (5.41) describes the vertical tensile stresses due to eccentricity of the notch force and the center of the axial force in the timber. Therefore, it is also chosen to use the contact height of the CLT and concrete $h_{n,eff}$ over the total notch height, including the notch insulation, h_n in this term. The latter term describes the influence of the compression strut directly to the support and is thus only applicable for the most outer notch. Equation (5.43) features the failure criterion for the bi-axial stress state based on the Tensor Polynomial theory. However, the vertical stresses should not be taken into account if they do not have a significantly negative impact compared to the horizontal stresses. In that

case the notch resistance can be calculated using Equation (5.48).

$$\sigma_{2,Ni,x,Ed} = \frac{F_{v,Ni,Ed}}{b \cdot h_{n,eff}} \tag{5.40}$$

$$\sigma_{2,Ni,z,Ed} = \frac{3 \cdot h_{n,eff} \cdot F_{v,Ni,Ed}}{b_n \cdot l_v^2} - \frac{F_{v,Ni,Ed} \cdot e_{n,2}}{2b_n \cdot l_v} \tag{5.41}$$

$$F_1\sigma_x + F_2\sigma_z + F_{11}\sigma_x^2 + 2F_{12}\sigma_x\sigma_z + F_{22}\sigma_z^2 > 1 \tag{5.42}$$

$$F_1 = \frac{1}{f_{t,0,d}} - \frac{1}{f_{c,0,d}} \tag{5.43}$$

$$F_2 = \frac{1}{f_{t,90,d}} - \frac{1}{f_{c,90,d}} \tag{5.44}$$

$$F_{11} = \frac{1}{f_{c,0,d} \cdot f_{t,0,d}} \tag{5.45}$$

$$F_{22} = \frac{1}{f_{c,90,d} \cdot f_{t,90,d}} \tag{5.46}$$

$$F_{12} = \pm\sqrt{F_{11} \cdot F_{22}} \tag{5.47}$$

$$F_{N1,TCF,Rd} = f_{c,0,d} \cdot b \cdot h_{n,eff}. \tag{5.48}$$

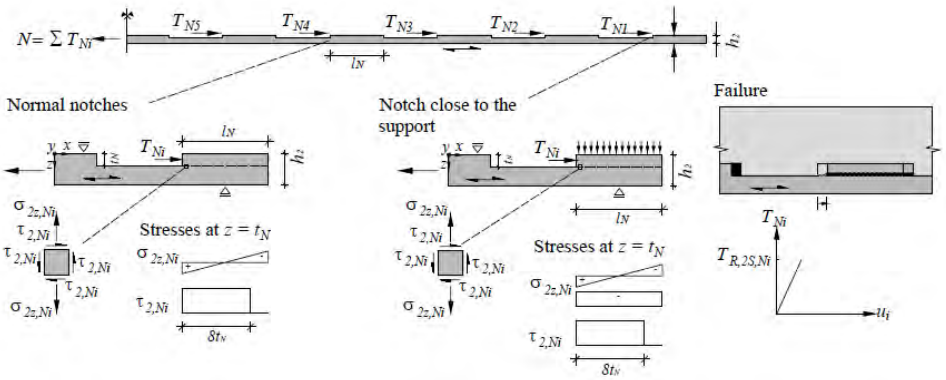

Figure 5.6: Cantilever model by Boccadoro for the prediction of Timber Shearing-off Failure (TSF) in the notch for traditional TCC floors with a 'thick' cracked concrete slab [4].

For the shearing-off failure mechanism of the timber (TSF), the shear stress $\tau_{2,Ni,Ed}$ is the most critical parameter. For the determination of $\tau_{2,Ni,Ed}$ a simplified rectangular stress distribution over the effective pre-timber length $l_v, eff = min(l_v, 8h_{n,eff})$ is used due to the noticed redistribution after the initial fracture and the observed, negligible shear transfer after $8 * h_{n,eff}$ and simplification reasons. Similar to the TCF, tensile stresses are present in the critical element. If these are relevant, the failure should again be analyzed in Bi-axial stress state using the Tensor Polynomial theory. With the assumption that no additional stresses in the x-direction are present in the area of shear transfer, the failure criterion can be formulated as shown in Equation (5.50). If the tensile stresses are not relevant, the notch resistance against TSF can be calculated by Equation (5.52). While for the traditional floors there is a clear critical element in the loaded notch area at the bottom of the notch concrete, which is $h_{n,eff} = h_n$ below the timber top surface, in the top layer of the CLT. For the conceptual floors

two elements will be checked; element A at the bottom of the concrete, which is $h_{n,eff}$ below the timber top surface, and at element B at the bottom of the notch insulation layer, which is h_n below the timber top surface. For the latter the effective pre-timber length will be determined, accordingly $l_v, eff = min(l_v, 8 * h_n)$. For the ED conceptual floor this means that element 2 is in the perpendicular second layer of the CLT and is therefore checked with the perpendicular compression and most importantly the perpendicular rolling shear strength. To the TSF check at element A and B will be referred as TSF-A and TSF-B respectively.

$$\tau_{2,Ni,Ed} = \frac{F_{v,Ni,Ed}}{b_n \cdot l_{v,eff})} \tag{5.49}$$

$$F_2 \cdot \sigma_{2,Ni,z,Ed} + F_{22} \cdot \sigma^2_{2,Ni,z,Ed} + F_{66} \cdot \tau^2_{2,Ni,Ed} > 1 \tag{5.50}$$

$$F_{66} = \frac{1}{f^2_{v,2}} \tag{5.51}$$

$$F_{Rd,TSF} = f_{v,0,d} \cdot b_n \cdot l_{v,eff}. \tag{5.52}$$

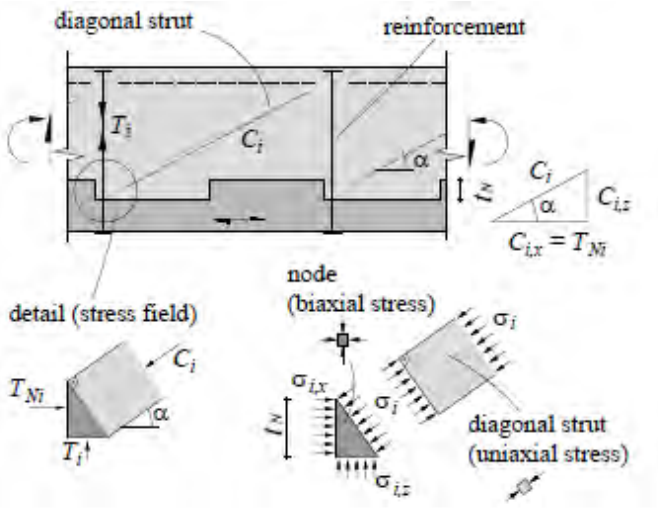

Figure 5.7: Strut-tie model by Boccadoro for the the prediction of Concrete Compression Failure (CCF) in the notch for traditional TCC floors with a 'thick' cracked concrete slab [4].

The prediction of the Concrete compression failure (CCF), also known as concrete crushing failure, for notches with fasteners is based on a strut-tie model. The critical bi-axial compression stress state can be found in the notch contact area due to the angled compression strut. Further derivation can provide the simple formula shown in Equation (5.53) which can be used for the calculation of the resistance against CCF. It assumed that this is also applicable for connectors without fasteners for which a cantilever model should be used.

$$F_{CCF,Rd} = f_{c,d} \cdot b_n \cdot h_{n,eff} \tag{5.53}$$

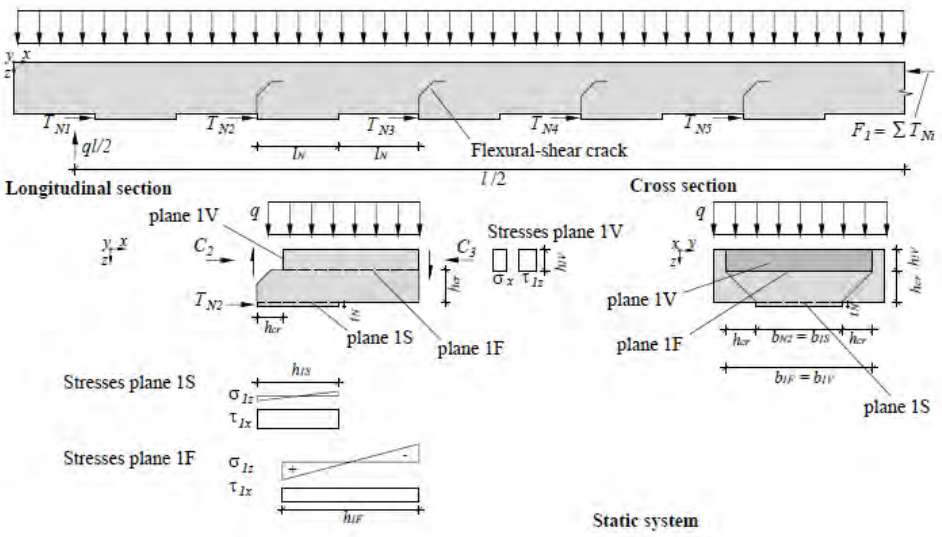

Figure 5.8: Cantilever model by Boccadoro for the prediction of Concrete Longitudinal Shear Failure (CLSF) at plane 1S, Concrete Diagonal Shear Failure (CDSF) at plane 1F and Concrete Vertical Shear Failure (CSVF) at plane 1V in the notch for traditional TCC floors with a 'thick' cracked concrete slab [4].

Boccadoro et al. mentions two approaches for the concrete shear failure in the notch based on the presence of vertical reinforcement. When this is present, the concrete can be modeled using the strut-tie method, which is also referred to as a truss model. For this configuration shear cracks near the notch are only initiated but do not lead to failure and it is assumed that all the tension in the tie is carried by the reinforcement. The tension in the tie can be calculated by Equation (5.54) and can be used to determine the Screw Tension failure (STF).

$$F_{z,Ni,Ed} = \frac{F_{v,Ni,Ed} \cdot e_{n,2}}{(l_n + l_s)} \tag{5.54}$$

For notches without vertical reinforcement three concrete shear failure types close to the notch will be considered based on a cantilever model. This however a very rough approximation due to the high variability in tensile strength of concrete aggregate interlock in cracks and flexural cracks which govern the failure. The modified Mohr-Coulomb criterion will be used to predict the failure load of these mechanisms. While this approach is thus aimed at the prediction of the concrete shear failure load for the un-reinforced conceptual floor, it will also be used for the determination of the initial crack formation, without propagation into actual failure, for the traditional floors.

The first failure mechanism is the Concrete Longitudinal Shear Failure (CLSF) over plane 1S shown in Figure 5.8. The equations for the determination of the present shear and vertical tensile stresses can be found in Equations (5.55) and (5.56) respectively. The corresponding

modified Mohr-coulomb criterium is shown in Equation (5.57), in which $\sin(\phi) = \frac{3}{5}$.

$$\tau_{1S,Ni,Ed} = \frac{F_{v,Ni,Ed}}{b_n \cdot l_n} \tag{5.55}$$

$$\sigma_{1S,Ni,z,Ed} = \frac{3 \cdot F_{v,Ni,Ed} \cdot h_{n,eff}}{b_n \cdot l_n^2} \tag{5.56}$$

$$\left(\sigma_{1S,Ni,z,Ed} + \frac{f_{c,d}}{2} - \frac{\sin(\phi) \cdot f_{ct,d}}{1-\sin(\phi)} - f_{ct,d}^2\right)^2 - \tau_{1S,Ni,Ed}^2 > \left(\frac{f_{c,d}}{2} - \frac{\sin(\phi) \cdot f_{ct,d}}{1-\sin(\phi)}\right)^2 \tag{5.57}$$

The second failure mechanism is the Concrete Diagonal Shear Failure (CDSF) over plane 1F, shown in Figure 5.8. This failure mechanism is characterized by the combination of shear, significant tensile stresses due to the eccentricity of the notch and alignment with cracks due to flexural tensile stresses at the bottom of the concrete. While Boccadoro et al. assumes a cracked concrete height h_cr, with a simplified crack angle of 45° due to the design featuring a 'thick' concrete slab, in this study designs with a 'thin' concrete slab without flexural cracks, and thus $h_cr = 0$, will be investigated. For the conceptual floor, it is assumed that the critical element is located at the height of the top surface of the timber on the contact surface. The shear stresses, vertical tensile stresses and corresponding failure criterion are shown in Equations (5.58) to (5.60).

$$\tau_{1F,Ni,Ed} = \frac{F_{v,Ni,Ed}}{b_n \cdot (l_n + l_s)} \tag{5.58}$$

$$\sigma_{1F,Ni,z,Ed} = \frac{6 \cdot F_{v,Ni,Ed} \cdot \left(h_{cr} + \frac{h_{n,eff}}{2}\right)}{b_n \cdot l_{v,CDSF}^2} \tag{5.59}$$

$$\left(\sigma_{1F,Ni,z,Ed} + \frac{f_{c,d}}{2} - \frac{\sin(\phi) \cdot f_{ct,d}}{1-\sin(\phi)} - f_{ct,d}^2\right)^2 - \tau_{1F,Ni,Ed}^2 > \left(\frac{f_{c,d}}{2} - \frac{\sin(\phi) \cdot f_{ct,d}}{1-\sin(\phi)}\right)^2 \tag{5.60}$$

The last considered failure mechanism is the Concrete Vertical Shear Failure (CVSF) over plane VF, shown in Figure 5.8. At this location shear and compressive stresses are present. However, since the compressive stresses have a uncertain positive effect on the shear resistance of the concrete, they should be neglected. Based on the moment equilibrium the formula for the shear force in the shear plane can be derived and is shown in Equation (5.61). The corresponding tensile stress, failure criterium and derived formula for the resistance against CVSF of the notch as shown in Equations (5.62) to (5.64).

$$V_{1V,Ni} = \frac{F_{v,Ni,Ed} \cdot e_{n,1}}{(l_n + l_s)} \tag{5.61}$$

$$\tau_{1V,Ni} = \frac{V_{1V,Ni}}{b_n \cdot (h_1 - h_{cr})} \tag{5.62}$$

$$\tau_{1V,Ni} > 4 \cdot f_{c,d} \tag{5.63}$$

$$F_{1V,Ni,Rd} = \frac{4 \cdot f_{c,d} \cdot b_{Ni} \cdot (h_1 - h_{cr}) \cdot (l_n + l_s)}{e_{n,1}} \tag{5.64}$$

To conclude, for the prediction of the four types of notch failure the calculation model by Boccadoro will be used. It includes formulas for the determination of the notch load based on the shear distribution shown in Equations (5.38) and (5.39), and a set of equations per type of notch failure to confirm if and with what notch load failure occurs shown in Equation (5.40) to (5.60).

5.1.4 Experimental bending test

Due to uncertainties in the prediction of the structural behavior, such as for the connection stiffness and failure mechanisms in the conceptual notch, a full floor experimental bending tests will be performed on a single specimen of the ED traditional and ED conceptual floor.

The designs of the ED traditional and conceptual are shown in Chapter 4. Both specimens are 6 meter in length, 0,5 meter in width and 0,3 m in height. The CLT used in the specimens is 7s-ply 220 mm (40-40-20-20-20-40-40) fully made of C24 timber manufactured by the CROSS-WORKS branch of Holzwerke van Roje GMBH & CO. KG. The concrete was poured by Geelen Beton and featured a strength grade of C50/60. Since both materials are parted of a standardized production process and no additional material testing will be done, the properties can assumed as given by EN 338 for the timber and given by EC3 for the concrete. The screws used in the traditional floor consisted of Eurotec TCC-II 9 screws with a diameter of 9 mm, a threaded length of 125 mm and a total length of 180 mm. Both specimens features a ∅6-100 mm horizontal reinforcement net to prevent shrinkage cracks. For the insulation material in the conceptual floor Rockfloor Base manufactured by ROCKWOOL B.V. was used and stapled to the timber. The notch sides of the conceptual floor also featured a PTFE strip to reduce friction between the timber and foil, and thus also the concrete layer. Furthermore, for the traditional specimen there was no foil in between the timber and concrete layers while for the conceptual specimen a 0,5 mm PE foil was present between the insulation and concrete layer. The concrete is thus fully loose on top of the insulation.

(a) Bare CLT element

(b) CLT element after placement of the PTFE strips, insulation layer, PE-foil and horizontal reinforcement.

Figure 5.9: Two fabrication stages of the conceptual floor specimen

The main advantage of the usage of a 6-point bending test over a 4-point bending test is the better alignment with a uniform distributed load assumed in the approach for prediction of the structural behavior. Figure 5.10 shows an overview of the bending test set-up.

While the structural scheme and dimensions are kept the same, the traditional and conceptual floor specimens are both tested in a slightly adapted test setup. The set-up for the traditional floor features a 150 kN computer controlled jack, this was against expectations however not enough to cause failure of the specimen. The set-up of the conceptual floor will therefore use a 250 kN manually controlled jack to ensure failure. Besides, a stiffer and symmetric frame will be used due to the increase of maximum load and observed axial rotation of the traditional floor due to uneven compression of the soft boards between the specimen and supports over their width caused by the asymmetrical set-up.

Both testing programs will feature the same loading pattern of three loops in the between 0 and 15 kN of jack force, with a loading rate of 1,2 mm/min, before continued increase of force until failure, with a loading rate of 2,4 mm/min. Based on the loops in the elastic domain, which approximately replicate $q = 5kN/m^2$ at its maximum, the elastic properties will be determined.

At last, both testing programs also feature a similar measurement set-up. Two pairs of Linear Variable Differential Transformers (LVDT's) are placed at the support, with one on the front and one on the back of specimen. They will possible displacement at the support, such

as settlement in the frame or compression of the intermediate soft boards. Furthermore four pairs of Mitutoyo digital indicators are placed at each loading point to capture the behavior over the span of the beam. The most critical deformation at mid span is captured by two LVDT's, or laser sensors for the set-up of the conceptual floor, at both sides of the specimen and by a draw wire sensor tensioned under the specimen at the center width. Due to the relatively very small scale of difference in accuracy between the LVDT's and laser sensors, its influence on the deformation results can be neglected. Furthermore, strain gauges are glued on the top of the concrete and bottom of the CLT at midspan. At last, the setup for the conceptual floor features two additional pairs of LVDT's which capture the compression of the insulation at midspan and at N3.

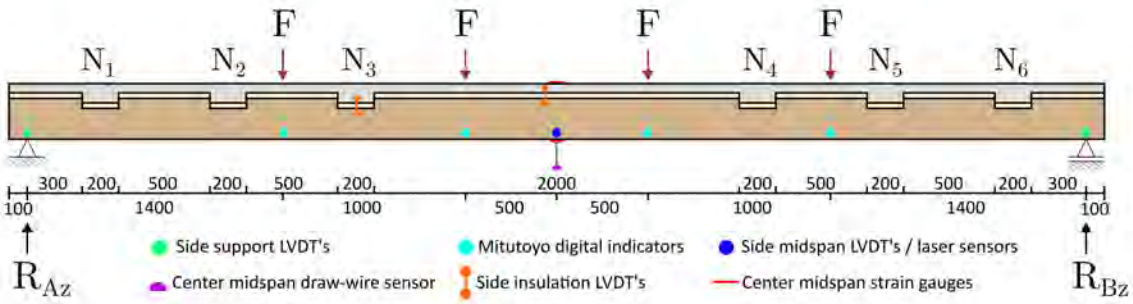

(a) Structural scheme, dimensions and measurement placement

(b) Test-setup for the traditional floor

(c) Test-setup for the conceptual floor

Figure 5.10: Test set-up of the experimental 6-pt bending test in the Structures Laboratory of the TU/e.

5.2 Results

In this chapter the results for the numerical push-out tests, analytical full floor evaluation and experimental 6-point bending tests will be discussed.

5.2.1 Numerical Push-out test

The load deformation diagrams of the numerical push-out test of the traditional and conceptual floors for the ED, LSD and LSD+ categories, as described in Section 5.1.1, are shown in Figure 5.11. Detailed results, such as stress and strain distribution through-out the specimen, and the modeling process can be be found in Appendix A.

The figure clearly shows the determination of the stiffness in the linear elastic zone. As expected there is a clear decrease of connection stiffness comparing the conceptual floor to the traditional floor between 24,92% and 38,12%. Based on findings by Lamothe et al. [33], it was expected that the ED-Conceptual floor would feature the highest decrease of connection stiffness due to the notch penetrating the much weaker second perpendicular layer for the conceptual version to create space for the notch-insulation. However, it featured the lowest decrease. This result thus indicates that the penetration of the notch depth in a perpendicular layer does not significantly influence the connection stiffness, as long as it is within the insulation height and thus not directly load bearing. However, more extensive research should be done to be able to fully understand and confirm this observation.

Besides, it is interesting to note that while the LSD and LSD+ floors feature the very similar results, the ED-floors features an higher stiffness. While it is easy to assume this is due to the increase concrete grade used in the ED floors, the concrete shows minimal strain in the elastic phase relative to the strain in the timber as shown in Appendix A. No further explanation could be found for this deviation in result.

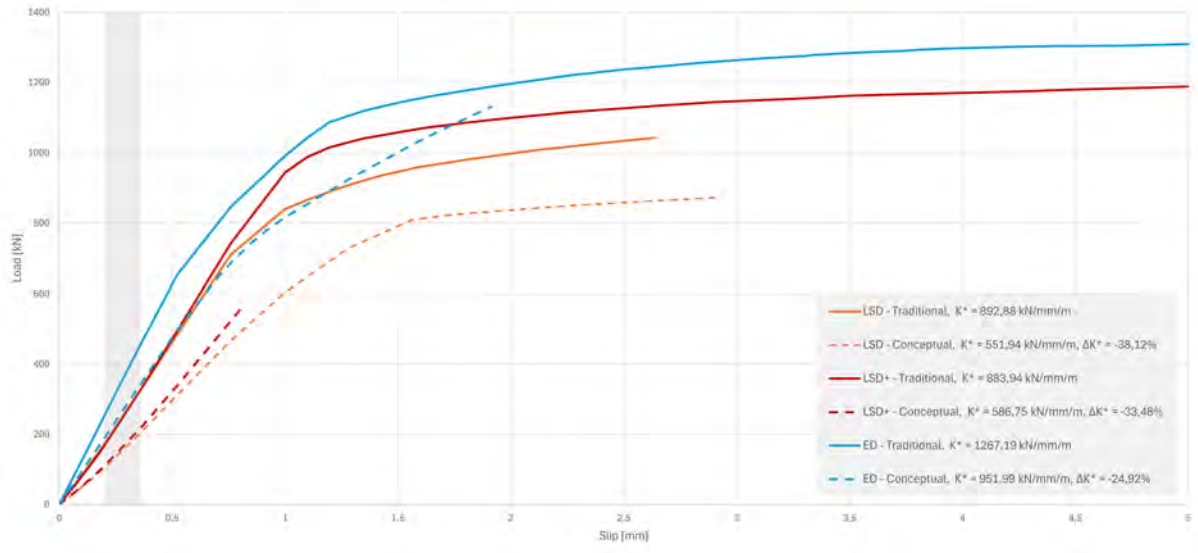

Figure 5.11: Load-deformation diagram of the numerical push-out test, including the stiffness determination domain, the corresponding equivalent connection stiffness per meter width K^* and the difference of the conceptual floor compared to the traditional floor ΔK^*.

5.2.2 Analytical results

This section discuss the performance of the different floor types for their serviceability limit state using the analytical separated- and extended gamma method in combination with the numerically determined connection stiffness K_{ser}.

First of all, Figure 5.12 shows the difference in bending stiffness calculated by the separated gamma method compared to the values calculated by the extended gamma method. For the conceptual and traditional floors, the instantaneous longitudinal effective bending stiffness EI_{eff} is $3,01\%$ to $6,12\%$ higher for the LSD and LSD+ floors using the separated gamma-method. While this is a marginal amount, for the same floor types in the ED floors this difference goes up to a significant 16%. This can be explained by the layer-limitations of the used base gamma-method in 'Step 1: determination of EI_{eff} of the CLT' and the following assumption of $\gamma = 1$ between the CLT layers, as explained in Section 5.1.2.1. Besides, for the decoupled floors only expected minimal differences between results for both methods can be observed. Due to the higher accuracy of the extended γ-method the upcoming results were found using this method. This choice is further elaborated in Section 5.3.2.1.

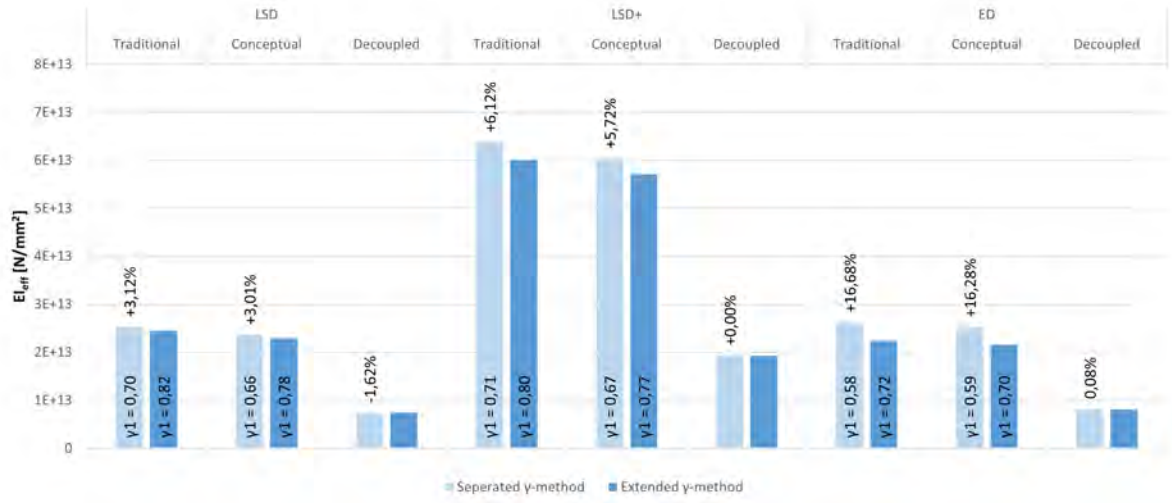

Figure 5.12: Instantaneous mean effective bending stiffness in the longitudinal direction for the nine studied floor types according to the separated- and extended gamma-method.

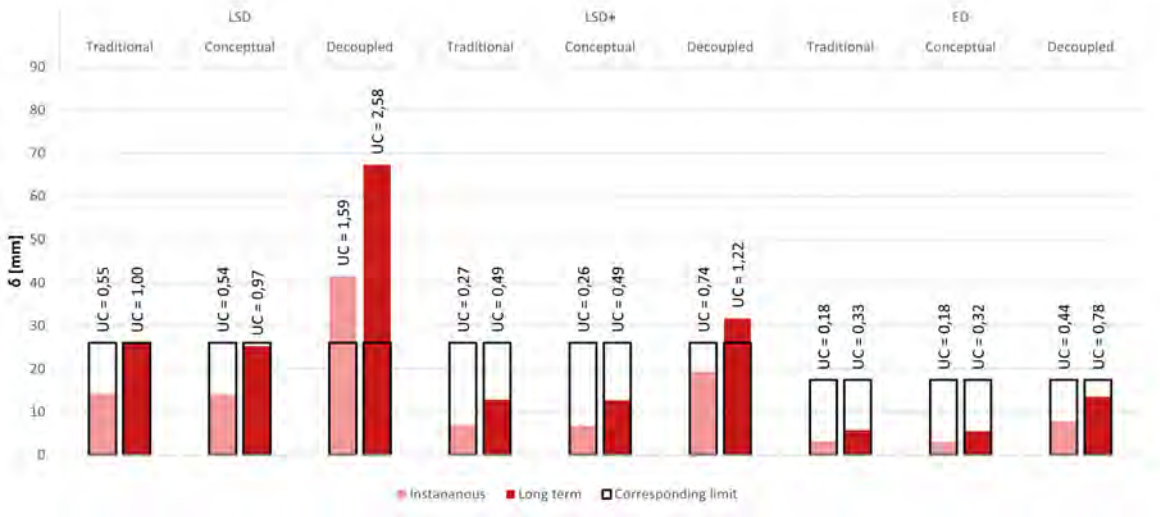

Figure 5.13: Instantaneous and long term maximum vertical deformation and corresponding limits with unity check values, for the nine studied floor types using the numerically determined K_{ser} values and the extended γ-method.

Figure 5.14 shows a comparison between the three floor types per design category to show the impact of the reduced connection stiffness for the conceptual floor and and the lack of composite interaction for the decoupled floor.

Comparing the conceptual floors to the traditional floors, it can be noted that although there is a significant impact on the connection stiffness by the addition of the resilient layer, the impact on the instantaneous effective bending stiffness EI_{eff} and the long term effective bending stiffness $EI_{eff,fin}$ is limited between $-4,23\%$ to $-6,33\%$ and $-4,13\%$ to $-6,58\%$ respectively. This can be explained by the fact that the $\gamma - value$ based on the connection stiffness only influences the additional bending stiffness due to the composite interaction, which is between the $62,58\%$ and $69,60\%$ of the total EI_{eff}. Besides, the $\gamma - value$ for both methods are also influenced negatively by an increase of the stiffness of the layers itself and positively by the increase of span of the system. The difference between the $\gamma - values$ is only between 0,02 and 0,04. The relation between the connection stiffness and bending stiffness is thus non-linear.

Furthermore, the conceptual design floors also features a significant reduction in mass due to the substitution of 20 mm concrete to mineral wool. In combination with the low imposed load for residential functions, the design load for SLS conditions is also decreased. For instantaneous situations this is a decrease between $6,56\%$ and $8,56\%$.

Combining the relatively low impact of the large decrease in connection stiffness on the bending stiffness and the reduction of load explains the similar structural performance in SLS conditions shown in Figure 5.13.

Comparing the decoupled floors to the traditional floors, much larger differences in bending stiffness can be noted. This is as expected due to the loss of composite interaction. For the LSD and LSD+ designs, it results in a (large) unsatisfactory deformation. However, the ED design still satisfies the deformation requirements due to its design on the 300 kg/m2 design guideline and its decreased span.

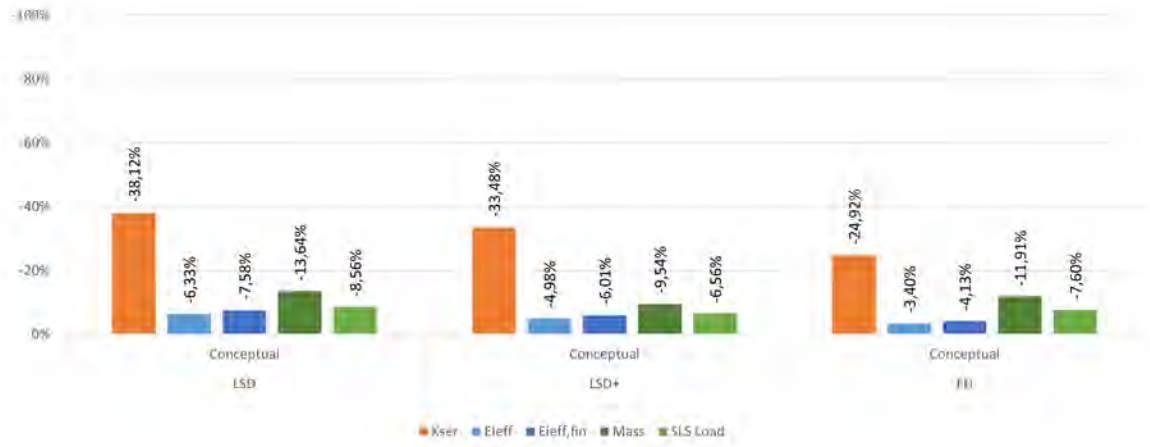

(a) Conceptual floors

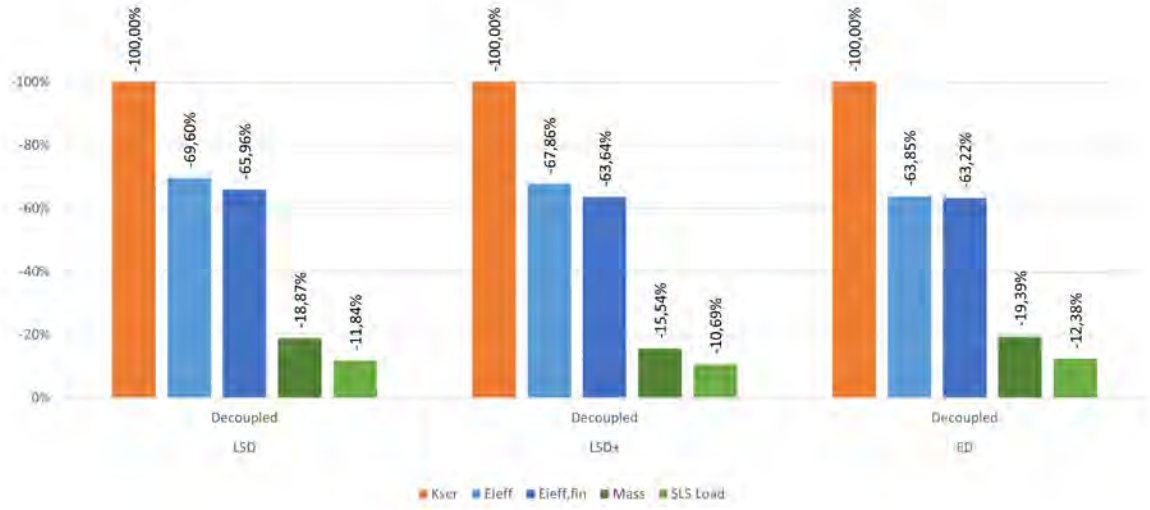

(b) Decoupled floors

Figure 5.14: Comparison of the conceptual and decoupled floors with the traditional floors as reference using the numerically determined K_{ser} values and the ext. γ-method.

5.2.3 Experimental bending test

In this section the results for the experimental 6-point bending test for the ED-Traditional floor and ED-Conceptual samples are discussed.

5.2.3.1 Traditional floor

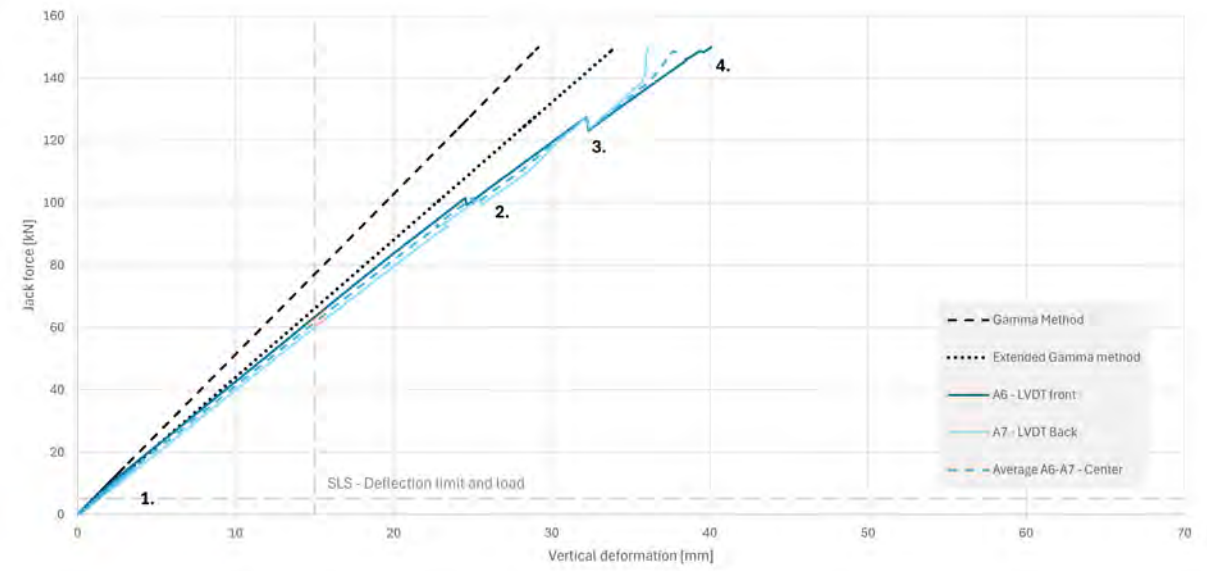

Figure 5.15: Load-deformation diagram of the experimental 6-point bending test for the ED-Traditional floor, including four points of interest.

The load-deformation diagram for the traditional floor is shown in Figure 5.15. It shows mainly linear elastic load-deformation relation and the following four points of interest:

1. **Elastic loops - 15 kN.**
   Three loops to 15 kN indicating the behavior at the high imposed load of $q = 5kN/m^2$ and stiffness determination.

2. **A loud bang, but no visual changes - 101 kN**
   Most likely from a sudden shift on the inside of the timber or concrete.

3. **Formation of fine hairline CDSF cracks - 127 kN**.
   Indicating initiation of concrete diagonal shear failure (CDSF). Located in notch N1, N2, N5 and N6. Most significant hairline crack and location are shown in Figure 5.16.

4. **Maximum of available jack force - 150 kN**
   No further visual changes, such as crack propagation or the hair line cracks. Likely due to the present vertical reinforcement.

(a) Hairline crack at N2

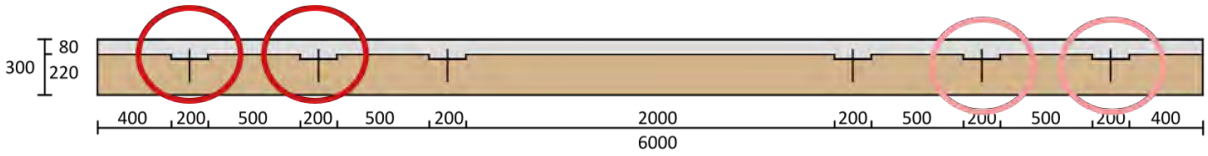

(b) Location of the cracks with the most significant hairline cracks highlighted in red and the minor hairline cracks highlighted in light red.

Figure 5.16: Diagonal concrete shear crack at 127 kN of the experimental bending test of the ED-traditional floor, indicating the most significant crack and the location of the cracks.

5.2.3.2 Conceptual floor

The load-deformation diagram for the conceptual floor is shown in Figure 5.17.

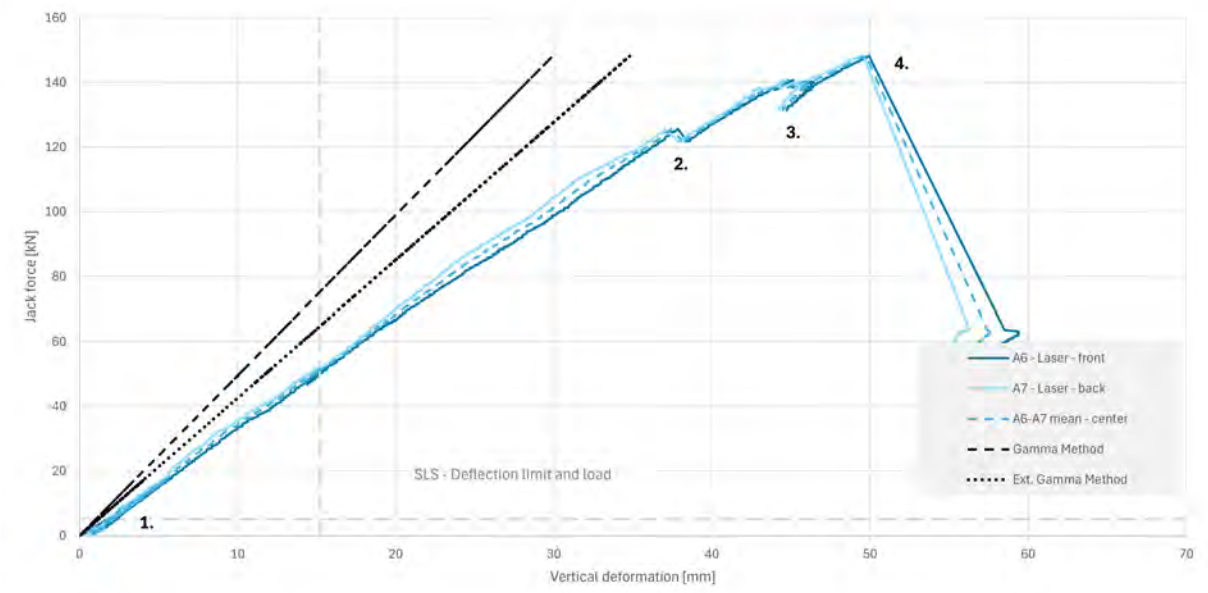

Figure 5.17: Load-deformation diagram of the experimental 6-point bending test for the ED-Conceptual floor, including four points of interest.

Similar to the traditional floor it shows a linear elastic load-deformation relation and again

four points of interest (POI):

1. **Elastic loops - 15 kN.**
   Three loops to 15 kN indicating the behavior at the high imposed load of $q = 5kN/m^2$ and stiffness determination.

2. **A loud bang, but no visual changes - 122 kN**
   Most likely from a sudden shift on the inside of the timber or concrete.

3. **CDSF crack formation and failure - 140 kN**.
   Hairline crack formation at 138 kN with instant propagation and full Concrete diagonal shear failure (CDSF) in N4, due to the lack of vertical reinforcement. Although N6 (and N1) should theoretically feature a higher notch force than N4, and thus a lower failure load, these notches likely did not failure first due to their position close to the notch and additional compressive stresses of the concrete towards the notch. This increases the shear resistance of the concrete. The failure and and location are shown in Figure 5.16.

4. **Complete failure - 148 kN**
   CDSF failure of N3, instantly followed by a combination of CDSF cracks and Timber shearing-off failure (TSF) in N2 and TSF in N1. The explanation for the unlikely CDSF in N3, due to the low notch force, is most probable due to a loss of composite interaction and a redistribution of stress after POI 3 which caused additional flexural tensile stress around N3 due to its location close to mid span. As described by Boccadoro et al., flexural bending stress and cracks are a strong enhancer of CDSF in notches [4]. The failure of N3, caused an increase of shear force and thus notch force in N2. Due the speed of the overloading, TSF occurred before a full CDSF failure could form. Most interestingly is the location of the TSF at the interface between the first longitudinal and second perpendicular CLT layer. This most probably shows that the influence of the lower shear resistance of the perpendicular CLT layer, due to the rolling shear, is stronger than the decrease of stress compared to the most stressed element at the height of the bottom of the notch-concrete. For the TSF of N1, the same applies with additional propagation of the shear failure through the perpendicular CLT layer due to its location to the support and the maximum shear stress at the neutral axis of the CLT.

(a) Broad view of notch failure

(b) Close-up of the notch failure

(c) Location of the failure

Figure 5.18: Diagonal concrete shear failure at 140 kN of the experimental bending test of the ED-conceptual floor.

(a) Broad view of notch failure N1-3

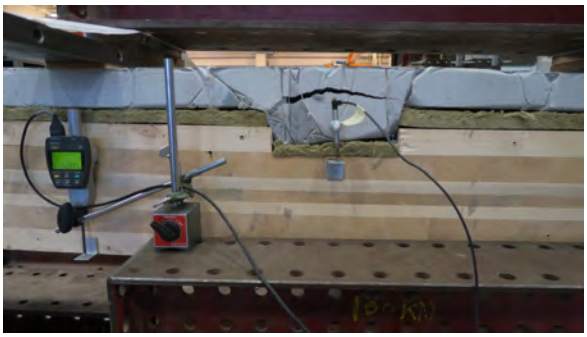

(b) Close-up of the notch failure at N3

(c) Location of the failures

Figure 5.19: Diagonal concrete shear failure at 148 kN of the experimental bending test of the ED-conceptual floor.

5.2.3.3 Bending stiffness

Next to the failure modes, the experimental bending test also provided some insights to the stiffness of the floor system. An overview of the results is given in Table 5.1. For the traditional floor it shows a large overestimation of the separated γ-method while the extended γ-method is quite accurate. The calculation values, and thus this result, includes the use of the numerically determined K_{ser} for both methods. For the conceptual floor, the difference of the separated γ-method to the extended γ-method is still similar while the gap between the separated- and extended γ-method to the experimental results has become larger. Most probable causes are a lower than calculated connection stiffness or the influence of the fabrication imperfections of the

sample, which lowered the notch contact area. This difference can also explain the larger than expected difference between the bending stiffness of the traditional and conceptual floor. These points are further disussed in Section 5.3.1.

		Experimental results	Seperated γ-method	Extended γ-method
Traditional				
EI_{eff}	$[N/mm^2]$	$2,175 \cdot 10^{13}$	$2,613 \cdot 10^{13}$	$2,239 \cdot 10^{13}$
$\Delta_{ext.\gamma-method}$		-2,89%	+16,70%	-
Conceptual				
EI_{eff}	$[N/mm^2]$	$1,880 \cdot 10^{13}$	$2,516 \cdot 10^{13}$	$2,163 \cdot 10^{13}$
$\Delta_{ext.\gamma-method}$		-13,12%	+16,68%	-
$\Delta_{traditional}$		-13,57%	-3,71%	-3,39%

Table 5.1: Overview of the mean experimental and calculated bending stiffness's for the ED-Traditional and ED-Conceptual floor in the 0-15 kN elastic domain.

5.3 Discussion

In this section the found results and their validity based on the used approach and comparison across approaches will be described. Firstly, the experimental analysis will be reviewed. It will be followed by a validation of the described approach for the determination of the stiffness. Finally, the prediction and design for ductile failure modes will be evaluated.

5.3.1 Experimental analysis

Several aspects should be noted about the experimental analysis. While the 6-point bending test more accurately captures the behavior under a uniform load, compared to 4-point bending tests it it not a perfect representation. Besides, the stiffness of the testing frame also impacts the results slightly, resulting in a slight increase of load per mm of sample deformation. While this effect is expected to be negligible, the frame for the testing of the traditional featured an asymmetric stiffness, resulting in a small rotation in the sample, as shown by the difference between the front and back LVDT's and Mitutoyo's in Figure 5.20a. By post-processing in the form of subtraction of the deformation at the supports, this effect was resolved as shown in Section 5.2.3. Indicating the additional positive or negative deformation due to rotation was only present in the timber soft boards between the sample and the steel frame. Due to the use of a stiffer and fully symmetric test frame for the conceptual floor, this effect was insignificant for this floor.

Furthermore, the draw-wire sensor underneath the CLT at mid span and center width of the floor featured a large deformation difference compared to the measurements of the midspan LVDT's. Based on the comparison of the results of the mitutoyo's sensors over the span of the beam, as shown in Figure 5.20b, it was concluded that the mean results of the front and back mid span LVDT's more accurately capture the floor behavior. For the conceptual floor, a similar phenomena was observed and tackled with the same approach, resulting in the use of the mean measurements of the front and back mid span laser sensors to quantify the behavior of the conceptual floor.

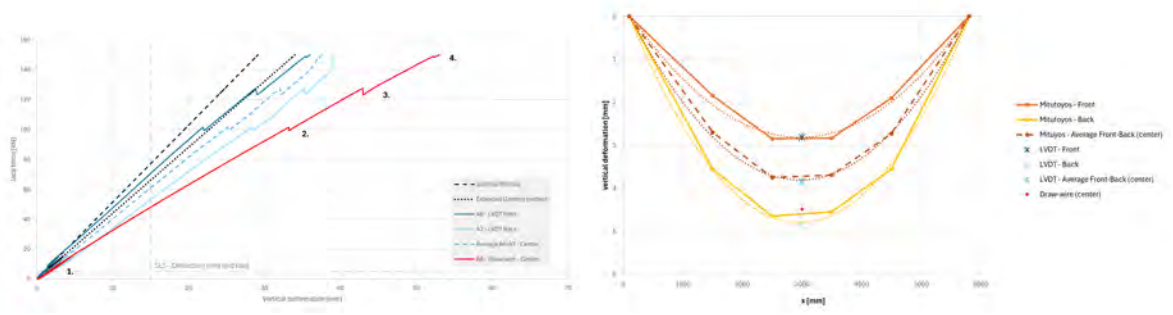

(a) Load-deformation diagram (b) Deformation over span

Figure 5.20: Unprocessed results of the experimental analysis of the ED - traditional floor.

Besides the testing frame and the sensor imperfections, the sample quality itself also has a large influence on the observed results. Firstly, for the traditional floor, shrinkage cracks were found at one or both top corners of all notches (Figure 5.21a). While these cracks are very thin, due to their position they can significantly enhance initiation of one of the concrete notch shear failures. In the conceptual floor no shrinkage cracks were observed.

Secondly, both specimens feature manufacturing imperfections in the CLT. One of these are circular holes in the bottom of the CLT of the traditional floor specimen close to mid span, similar to the circular holes at the top of the CLT for the conceptual floor, shown in Figure 5.21c. Other visual manufacturing imperfections are also screw (holes) in the sides, side indentations (Figure 5.21b), and notch imperfection due to folded and loosened PE-foil during concrete pouring (Figure 5.21d). Based on the results, the others do not seem to heavily influence the results while the latter can be the explanation for the lower than expected bending stiffness for the conceptual floor. While the foil was stapled to the insulation layer, its connection was not strong enough and the loosened foil prevented the notch to be completely filled. This lowers the contact area, and thus the connection stiffness between the two layers. Since this problem cannot be easily solved by nailing the foil through the insulation to the timber for a better bond, for further development the fabrication process should be re-considered.

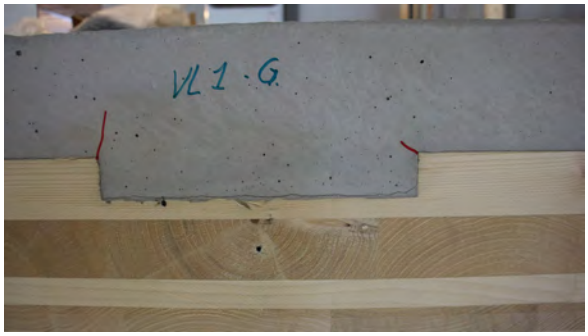

(a) Traditional floor: Shrinkage cracks

(b) Conceptual floor: side indentations

(c) Conceptual floor: on of two circular holes at the unloaded notch edge.

(d) Conceptual: Notch imperfections due to PE-foil.

Figure 5.21: Imperfections in the floor specimen

Furthermore, the compression of the insulation can also influence the behavior of the notch due it affecting the effective notch height. In unloaded situation the compression of the insulation was insignificant. For the loaded situation the load-compression diagram is shown in Figure 5.22. At high loads the compression of the insulation was considerable, especially measured at mid span where it reached the measurement limit of the LVDT. The larger deformation at midspan can be explained by the generally largest deformation of the concrete layer at mid span in combination with the location's distance to rotation restraining notches. The largest compression was however observed between mid span and N4 due to the local pressure of the loading point. However, even though there is an compression of the insulation at higher loads, and thus an increase of effective notch height, no significant influence on the bending stiffness shown in Figure 5.17 can be observed. More information about the point of interest in the figure can be found in Section 5.2.3 and Appendix C.

The combination of the insignificant impact on the bending stiffness and the maximum compression at 15 kN is only approximately 1 mm, it can be concluded that the compression of the insulation has minimal influence on the bending performance of the conceptual floor.

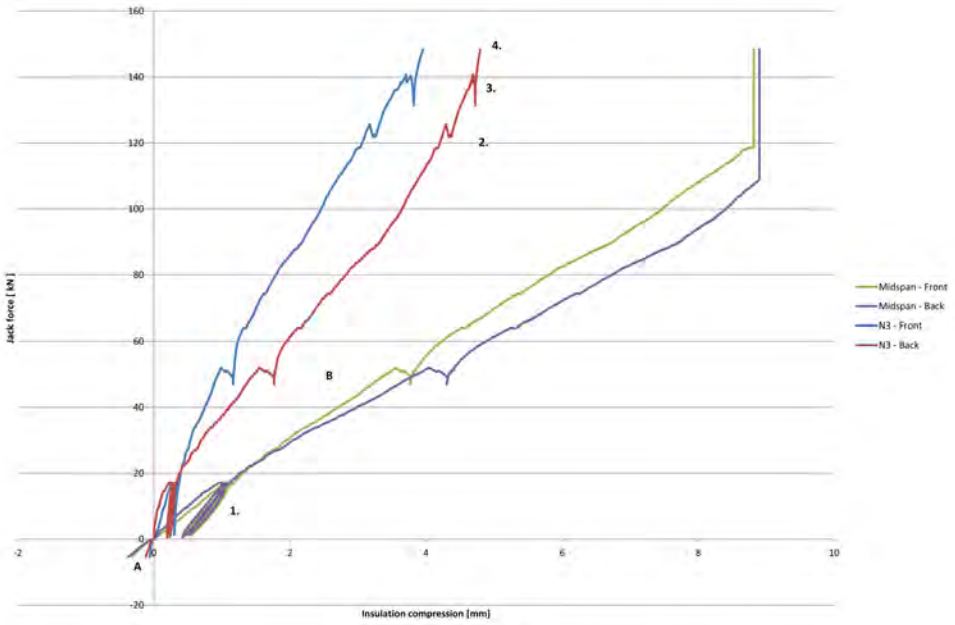

Figure 5.22: Load-compression diagram of the insulation layer of the ED-Conceptual floor during the experimental 6-point bending test.

5.3.2 Validity of the design and analysis approach

This section features an elaboration of the chosen design and analysis approach using the FEM modeling of push-out tests for determination of the connection stiffness, the separated- or extended γ-method for cross-section analysis, the draft TCC or Boccadoro-method for notch failure, and the step process, for the design of the traditional and conceptual floors for the LSD and LSD+ floors and the analysis of those and their decoupled and ED-floors.

5.3.2.1 Stiffness determination

First of all, the numerical analysis of a push-out test to determine K^*_{FEM} should be critically reviewed. The full modeling process and intermediate discussion points can be found in Chapter A.

In the preliminary modeling phase, in which it was attempted to replicate the results of three experimental investigations, a considerable difference of K^*_{FEM} compared to $K2^*_{exp}$ of -29,37% to -57,88% has been observed. No clear explanation was found for this large underestimation. However, the difference in K^* between the modeled geometries with and without insulation was found to be inline with the experimental results by Lamothe et al. [33]. Combining these results it was noted that the addition of an insulation featured a decrease in K^* of -9,56% to 20,97%.

Before determination of K^*_{FEM} for the ED/LSD/LSD+ floors, the final models were further developed. Firstly, a significant rotation and following transverse separation between the CLT and concrete was noted. While this is in practice tackled by the presence of the fasteners for the traditional floors, these are not modeled due to the low impact they have on the connection stiffness and the large impact they have on the model complexity [29], [53]. This is therefore tackled by the use of the 'no separation' contact type on the longitudinal interface between the CLT and concrete, which does not allow penetration and separation but does allow friction-less sliding. This featured an increase of stiffness of approx. 8%. This approach could however not be applied on the conceptual floors due to the insulation in between. To stabilize these models, an additional vertical roller was added at the unloaded end of the concrete. This brought the

observed difference in connection stiffness K^*_{FEM} between the conceptual and traditional version back from -57,12% to -20,97%, which is in line with the earlier found results. Furthermore, while in the studied experimental investigations the loading plate covered the full CLT-height, this is expected to overestimate the found stiffness compared to practice due to the possible force transfer through the full top layer of the CLT. After trial and error, it was chosen to reduced the top of the loading plate such that it aligns with the bottom of the notch. This is also in line with the extreme equilibrium states in push-out test as illustrated by Rasmussen [48]. Furthermore, it was also observed that an 2D model using shell elements and plain strain assumptions provides similar stiffness results as the described 3D model.

While it is difficult to predicate the accuracy of the models after the further developments, the determined stiffness for the traditional versions of the ED/LSD/LSD+ floors (K^*_{FEM} = 883,94 - 1267,19 kN/mm/m) are closer to the observed values for notches in CCC floors ($K^*_{exp,CLT}$ = 913,33 - 1630 kN/mm/m) than expected based on the initial replication. Furthermore, the decrease of connection stiffness due to the addition of insulation is higher for the final results than observed in the (replicated) experimental investigations. This can be explained by the difference in approaches. While the approach of Lamothe et al. added insulation in between the two materials while keeping the height of the concrete (and CLT) equal, in the conceptual floors the concrete height is reduced such that the total height stays the same. At last, it is important to note that according to Rasmussen the validity and applicability of push-out test and their wide variation in used set-up parameters are still a point of discussion in the field of TCC structures [48].

Although the results from the numerical analysis are thus expected to underestimate the actual connection stiffness and thus also the actual bending stiffness, the separated γ-method considerably overestimates and the extended γ-method slightly overestimates the experimental bending stiffness of the ED-traditional floor found in the 6-pt bending test, as shown in Section 5.2.3. The overestimation of the separated γ-method can be explained by the layer limitations and the used workarounds for CCC floors with 7-ply CLT. Most interestingly is therefore the observed slight overestimation for the extended γ-method, while thus a (small) underestimation was expected. Since the experimental results of the traditional floor are not expected to be majorly influenced by the sample quality, the most probable explanation can be found in the fundamental assumptions of the gamma-method. These assumptions include the assumption of a sinusoidal load distribution and perfectly smeared out connection spacing. Although the influence of the latter is already reduced by application of Equation (5.34) for the determination of the effective spacing, an overestimation is still expected based on earlier studies into the validity of the gamma method [8], [11], [39]. Due to the effects of the underestimated connection stiffness and the inherent overestimation of the γ-method, the combination of the applied numerical approach to determine the connection stiffness and the extended γ-method, or also the separated γ for CLT with less than 5 separated longitudinal layers, is found to be able to accurately predict bending stiffness of a CCC floor. The increased overestimation by approximately 10% of analytical results compared to experimental results for the conceptual floor are assigned to the lower notch quality of the sample.

At last, the adapted timber cross-section approach, proposed by Thai [53], was tested. This approach takes into account the removed part of the timber in the top layers due to the notch. While this is significant for investigation of notch CLT without concrete, for CCC floors this is often in the least effective area close to the neutral axis. This resulted in minimal differences

with the extended gamma method. This approach was therefore not continued for this study.

Furthermore, an additional indication on the validity of the stiffness determination for the ED-traditional and conceptual floors can be given by comparison of the natural frequency f_1 calculated from the reEC5-method, using the extended γ-method in combination with the results of the numerical push-out test, and the experimental vibration test described in Chapter 6. First of all, the natural frequency found using the reEC5-method aligns to the ones found in the experimental investigations of the two specimens. This thus indicates no significant disturbances in the determination of the stiffness. Furthermore, the decrease of $f_{1,exp}$ from the traditional to the conceptual floor roughly equals a 10% reduction in stiffness, which aligns with the found difference in the 6-pt bending test as expected.

Overall, several steps in the process for the determination of the bending stiffness of the system feature some major discussion points. This includes the accuracy of the numerical push-out test, the general validity of push-out tests, the overestimation in the separated- and extended gamma-method and the production quality of the tested specimen. However, even due to these discussion points, the bending stiffness was predicted adequately as showed by the results of the 6-pt bending test and the similarity of the obtained values for natural frequency from the reEC-5 method and experimental vibration test. Especially the found differences between the bending stiffness of the traditional and conceptual floor was consistent. It can therefore be concluded that the described methodology can give an adequate indication of the comparison of the structural performance of the traditional and conceptual floor.

5.3.2.2 Design for ductile failure

Tables 5.2 and 5.3 show the design loads and equivalent total force, comparable to the experimental jack force. The tables however show design loads, including characteristic strengths and stiffness's, safety- and modification factors. This explains the significantly lower calculated failure loads, particularly for the timber, as described in Section 5.2.3. Although these values are therefore not directly comparable, some interesting insights can still be taken from the comparison. First of all the the calculations confirm the experimental findings that for timber shearing off failure (TSF), the critical element is at the height of the interface of the first CLT (longitudinal) and second CLT (perpendicular) layer with low rolling shear strength, as opposed to the higher stressed element with higher shear resistance at the height of the bottom of the notch-concrete.

Furthermore, the experimental investigations both show the (initiation) of concrete diagonal shear failure (CDSF), while the calculations feature an incredibly high force to reach its failure. This is a result of the assumption in the Boccadoro-method that the concrete features flexural cracks. Since CDSF is heavily enhanced by flexural cracks, its calculation includes the crack height as parameter. In this study no flexural concrete cracking is assumed resulting in the observed difference.

Regarding the prediction of failure modes and loads and the corresponding criteria that TCF should be governing to achieve ductile failure, it was thus noted that the governing failure modes cannot be accurately predicted by the Boccadoro-method, the calculation for failure modes in the draft TCC is limited and is not applicable to notches without vertical reinforcement and FEM-modeling of the failure modes is very complex. In combination with the experience that the structural ULS are far from being the governing criterion, after structural SLS, vibration and acoustic criteria, the requirement for ductile failure should currently not be a main priority

in further design of the conceptual floors.

Table 5.2: Failure modes and design loads q_d as calculated with the combined ext. γ- and Boccadoro-method for the ED - traditional floor, including the equivalent total force $F_{d,eq}$ for a 6,0 by 0,5 m floor.

	Mode	Location	q_d [kN/m]	$F_{d,eq}$ [kN]		Mode	Location	q_d [kN/m]	$F_{d,eq}$ [kN]
1.	TSF-B	N1 or N6	14,61	34,48	9.	TSF-A	N2 or N5	88,51	248,80
2.	TSF-A	N1 or N6	30,15	79,53	10.	CLSF	N1 or N6	106,34	300.49
3.	TCF	N1 or N6	32,06	85,09	11.	CCF	N2 or N5	184,11	526,03
4.	TSF-B	N2 or N5	41,80	113,33	12.	CLSF	N2 or N5	270,81	777,45
5.	TBT	Midspan	43,67	131,00	13.	CDSF	N1 or N6	508,26	1466,05
6.	CT	Midspan	53.43	160.30	14.	CDSF	N2 or N5	1295,17	3748.12
7.	CCF	N1 or N6	72.29	201,75	15.	CDVF	N1 or N6	5251,81	15222,36
8.	TCF	N2 or N5	81,66	228,91	16.	CDVF	N2 or N5	13375,30	38780,47

Table 5.3: Failure modes and design loads q_d as calculated with the combined ext. γ- and Boccadoro-method for the ED - conceptual floor, including the equivalent total force $F_{d,eq}$ for a 6,0 by 0,5 m floor.

	Mode	Location	q_d [kN/m]	$F_{d,eq}$ [kN]		Mode	Location	q_d [kN/m]	$F_{d,eq}$ [kN]
1.	TBT	Midspan	13,48	40,43	9.	CLSF	N1 or N6	105,92	298,21
2.	TSF	N1 or N6	30,03	78,12	10.	STF	N2 or N5	150,87	428,57
3.	TCF	N1 or N6	31,94	83,66	11.	CCF	N2 or N5	183,39	522,87
4.	CT	Midspan	28,91	86,74	12.	CLSF	N2 or N5	269,75	733,31
5.	STF	N1 or N6	59,24	162,83	13.	CDSF	N1 or N6	506,27	1459,23
6.	CCF	N1 or N6	72,01	199,86	14.	CDSF	N2 or N5	1290,12	3732,38
7.	TCF	N2 or N5	81,34	226,92	15.	CDVF	N1 or N6	9179,31	26611,04
8.	TSF	N2 or N5	88,17	246,72	16.	CDVF	N2 or N5	23377,86	67786,80

5.4 Conclusion

The structural performance for each of the 3 floor types (traditional, conceptual, decoupled) for each of the three design categories (LSD, LSD+, ED) has been evaluated using a numerical push-out test for the determination of the connection stiffness, the separated- and extended γ-method for the cross-sectional analysis and the analytical calculation model of Boccadoro et al. has been used for the analysis of the failure mechanisms in the notch. The ED traditional and conceptual floor were also further analysed through a experimental 6-point bending tests. Based on these investigations the following conclusions can be drawn:

- For the approach for the determination of the stiffness of the system some key discussion points arose, including the accuracy of numerical push-out tests, the general validity of these tests, overestimation by the separated- and extended gamma-methods, and specimen production quality. However despite these issues, the bending stiffness was adequately

predicted, as confirmed by the experimental investigations. Notably, the consistent differences in bending stiffness between the traditional and conceptual floors validate the methodology for indicative comparison of their structural performance.

- The decrease of connection stiffness K^* due to the addition of an insulation layer, using the approach used by Lamothe et al. which simply adds the layer in between the timber and timber without adaptions resulting in an increased floor height, ranges from -10% to -20%. The approach used in this study for the design of the conceptual floor, where the concrete top layer is reduced by an equal amount such that the total floor height remains the same, features a reduction in K^* from -25% to -40%.

- Although the significant decrease in connection stiffness between the traditional and conceptual floor, the composite interaction, indicated by the γ_1-values, and the resulting effective bending stiffness feature a much less significant decrease up to approximately -10%. In combination with a decreased serviceability loading between -6% and -9%, for the conceptual floor in residential context due to the decrease in mass, indicates that the conceptual floors features a similar performance as their traditional counterparts for the SLS.

- For the traditional floor only hairline cracks in the concrete near the loaded notch corners were observed at the jack force maximum of 150 kN. While concrete diagonal shear failure (CDSF)was thus initiated, complete failure was prevented by the fasteners. For the conceptual floor CDSF failure was observed in N5 at 140 kN, which was followed by progressive notch failure of N3 by CDSF and N2 and N1 by timber shearing-off failure (TSF) at 148 kN. While this is a brittle failure mechanisms, it was found far above the UlS loading conditions. Furthermore, no new failure modes were observed in the conceptual floor.

- The described analytical approach for the evaluation of the failure mechanisms could not accurately predict the governing failure mode. In combination with the experience that the structural ULS is far from being the governing criterion, after structural SLS, vibration and acoustic criteria, the requirement of governing Timber Compression Failure (TCF) in the notch for ductile failure should therefore not be applied until improved failure prediction approaches are formulated.

- Due to the governing of the SLS for structural requirements, it can be concluded that the traditional floor and conceptual floor types feature a similar structural performance. Due to the loss of composite interaction, the decoupled floor featured a significant decrease in structural performance.

6 Vibrational performance

In this chapter the evaluation of the tactile vibration performance of the three floor types, for each of the three design categories is described. Section 6.1 describes the set requirements for the vibration performance according to the draft of the revised Eurocode 5. The method described in this code will also be used to analytically evaluate the floors. Furthermore, additional numerical vibrations analysis in the time and frequency domain will be done to provide better insights in the qualitative and relative behaviors of the floors. At last, this chapter will discuss the experimental vibration ball-fall test to validate the found insights. The results of these investigations will be described in Section 6.2 and their validity in Section 6.3. In Section 6.4 the conclusions regarding the vibration performance of these floors is described.

6.1 Methods and requirements

There has been much debate in the field of structural vibrations regarding the accuracy and applicability of different requirements and methods as can be read in Chapter 2. This section will outline the requirements and methods used by this study to evaluate the vibration performance. This will include a analytical analysis using the method mentioned in the draft for the revised Eurocode 5, time- and frequency dependent numerical analysis and experimental investigations to reinforce these predictive approaches.

6.1.1 Analytical analysis

Due to its recent development and likely future wide applicability, the requirements and analytical method described in the draft revised Eurocode 5 (reEC5) will be used in this study. The reEC5-method features a general minimal frequency requirement for floors and a class system based on (static) stiffness or floor response as shown in Table 6.1, with a corresponding requirement recommendation shown in Table 6.2. To quantify the floor response, the unit-less Response factor R is used. The Response factor should be calculated from the acceleration domain when the first eigenfrequency is higher or equal than 4,5 and lower or equal than 8 Hz. For floors with the first eigenfrequency higher than 8 Hz, the response factor should be calculated from the velocity domain. An overview of this process is given in Figure 6.1. It should be noted that this method and its requirements excludes the vibrations perceived by neighbours. Since the focus in the vibrational part of this study is on the structural vibration perceived by users of the same unit, this does not form an obstacle. Besides, with the scope of the study on multi-floor residential buildings, Class III will be used as threshold for satisfactory vibration performance.

Table 6.1: Floor vibration classification system of the reEC5-method [51].

	Floor performance levels						
Criteria	**I**	**II**	**III**	**IV**	**V**	**VI**	**VII**
Frequency f_1 [Hz] $\geq$	4.5						
Stiffness criteria w_{1kN} $[mm] \leq$	0.25		0.5	0.8	1.2	1.6	Unacceptable
Response factor R	4	8	12	16	24	32	Unacceptable
Acceleration criteria when $f_1 < 8$ [Hz] a_{rms}[m/s^2] $\leq$	R$\times$ 0.005						
Velocity criteria when $f_1 \geq 8$ [Hz] v_{rms} [m/s] $\leq$	R$\times$ 0.0001						

Table 6.2: Recommended selection of floor performance levels based on function [51].

Use category	Quality choice	Base choice	Economy choice
A (residential) multi-storey Single house	 level I, II, III level I, II, III, IV	 level IV level V	 level V level VI
B (office)	level I, II	level III	level IV

For the input parameters the values will be used as explained or calculated in Chapter 5. The most notable one is the effective bending stiffness EI_0 calculated by the extended gamma method for the traditional and conceptual floors. For the decoupled floors, the reEC5 states the same approached as applied in Chapter 5, which is to use the summation of the bending stiffness's of the layers without composite action. Similarly, for the bending stiffness of the Traditional floors with Floating Floor (F.F.) floor type, the individual stiffness of the concrete floating layer, without a component for composite interaction, will be added to the effective stiffness of the Traditional floor.

One of the parameters not previously calculated is the damping ratio. As explained earlier the damping of the floor system is one of the most influential parameters for vibration performance of floors. It is therefore present in the reEC5-method for the calculation of α_{rms} and β, which are used in the acceleration and velocity domain respectively. Since damping is used in many different forms, it is important to note that the damping in the reEC5-method is used in the form of modal damping ratio ζ based on the first eigenmode. Due to the complexity of determination of the damping ratio analytically, the damping ratio is often determined by extensive experimental investigations. To aid designers, the reEC5 provides modal damping ratios for different types of timber floor construction, shown in Table 6.3. Although these values are very generalized, these values will still be used in this study due to the lack of more accurate data corresponding to the investigated floors. For the Traditional floors $\zeta = 0.025$ will be used, while the Traditional floors with F.F. and Decoupled floors will use $\zeta = 0.035$. Since the Conceptual floors are expected to have a damping ratio in between these two values, they will be analyzed using both $\zeta = 0.025$ and $\zeta = 0.035$, such that an upper and lower performance boundary can be found. After obtaining the experimental data for the ED-Traditional and ED-conceptual floor, these floors will also be analyzed using their corresponding experimental damping ratio.

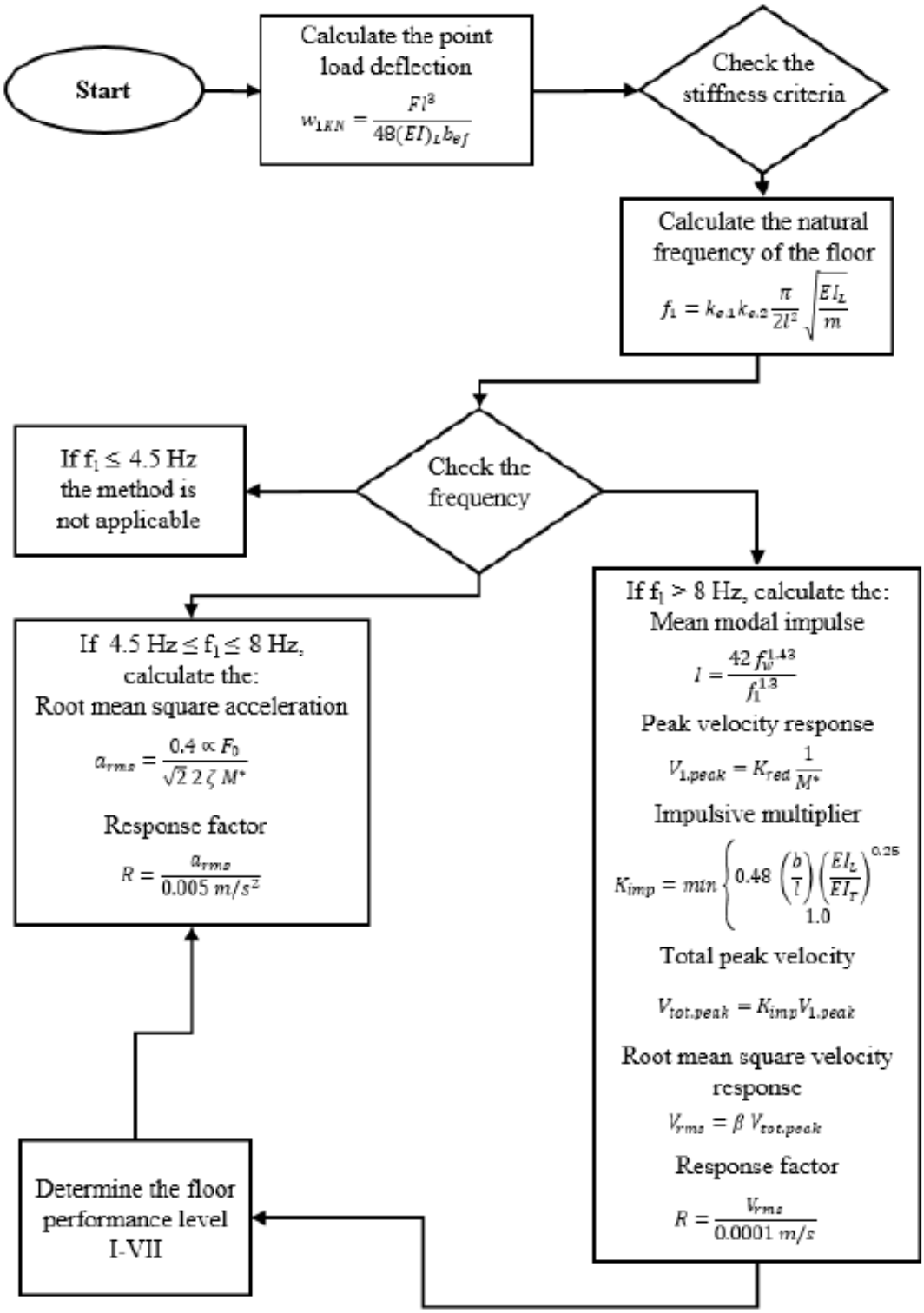

Figure 6.1: Schematic of the performance determination using the reEC5-method [51].

Table 6.3: Suggested values for the damping ratio according to rEC5 [51].

Modal damping ratio ζ	Floor structure
0.02	Joisted floors
0.025	Timber-concrete and massive floors
0.03	Joisted floors with a floating layer
0.035	Timber-concrete and massive floors with a floating layer
0.04	All floors with a floating layer and supported on all four sides

6.1.2 Numerical analysis

Due to the uncertainty of the applicability of the analytical method to the traditional and conceptual floor, an detailed FEM approach will also be applied. For the approach, the FEM software Ansys Mechanical will be used since this package easily allows vibration analyses.

The used model will be in 2D, using automatically generated quadratic rectangular and triangular elements. The element size will generally be 10 mm, but are refined around the notches to 5 mm. To accurately represent the single span direction with a large width of the floors, plain strain theorem is chosen. The material models used for the concrete and insulation layers will be modeled as linear isotropic. The timber will be modeled as linear orthotropic. The CLT will be modeled per layer with their corresponding direction. For the models for the Traditional floor type, the individual CLT layers using the 'bonded' contact type. This means that the elements, bonded to each other for penetration (or compression), separation (or tension) and sliding (or shear). For the contact areas of the CLT and Concrete at the sides of the edges, the 'frictionless' contact type will be used. This only bonds the edges for penetration, but allows separation and sliding without any friction. For the horizontal contact edges between the concrete and CLT the 'no separation' contact type is used, not allowing the edge elements to penetrate and separate. The latter resembles the vertical reinforcement normally used in TCC floors, which prevent separation between the concrete and timber. The contact however allows sliding without any friction. This makes sure all the shear interaction is through the notches and resembles the shear effect of the PE-foil in between the layers. For the conceptual floors, the CLT contact with the insulation will also use the 'bonded' contact type. Between the insulation and the concrete, the 'rough' contact will be used, fully bonding the edges for penetration and sliding. However, for this contact type the edges can separate from each which then also releases the sliding bond. More detailed information about the modeling process can be found in Chapter E.

Furthermore, the LSD and LSD+ floors have their horizontal and vertical supports at the bottom corners of the CLT with an horizontal distance of 8.7 meter. The ED floors have their supports 10 mm on the inside of these corners with an distance of 5,8 m in between, as similar to the experimental testing.

For the execution of the analysis each of the models will first be analysed by a modal analysis in Ansys to find the general modal behavior of the structure for a frequency range of 0-5000 Hz. Secondly, a Transient Structural and Harmonic response analysis will be executed using the data from the modal analysis. This will be further explained in the following paragraphs.

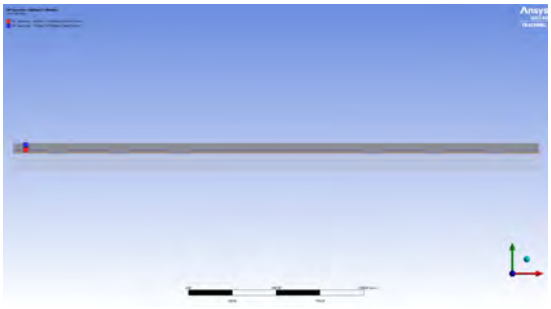

(a) Traditional - Horizontal CLT-Concrete contact: No separation

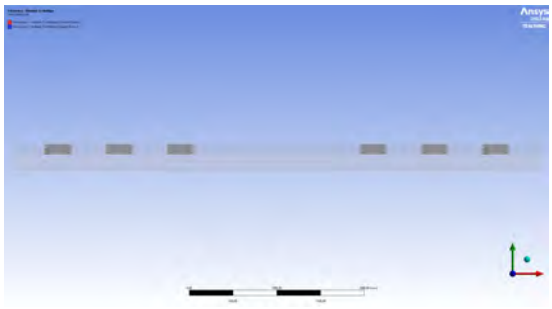

(b) Traditional - Vertical CLT-Concrete contact: Frictionless

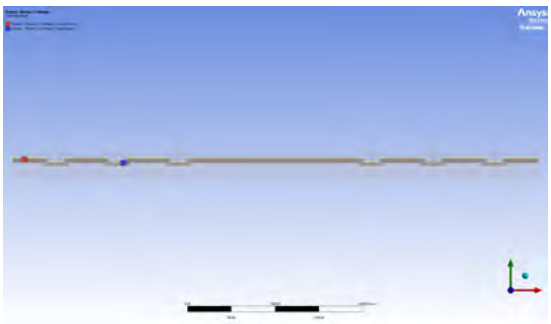

(c) Conceptual - CLT-Insulation contact: Bonded

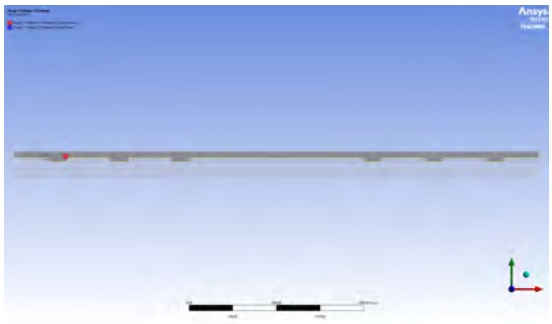

(d) Conceptual - Insulation-Concrete contact: Rough

Figure 6.2: Contact formulation

6.1.2.1 Transient Structural Analysis

A Transient Structural Analysis (TSA) is designed to find the dynamic response of a structure in the time domain. It therefore represents the actual behavior of when a force, like a footstep, hits the structure. Figure 6.3 shows the location of the boundary conditions and the load over time. The results will be measured at two vertices, the top vertice is located at midspan at the top of the concrete and the bottom vertice is located at the bottom of the CLT at midspan. Besides, the results will be measured in the domain of vertical deformation and vertical acceleration. The damping ratio is again an input of the analysis, the same approach as mentioned in Section 6.1.1 will be used, where the damping ratios are based on the reEC5. Furthermore, small time steps of 0,0005 seconds are applied to accurately capture the response.

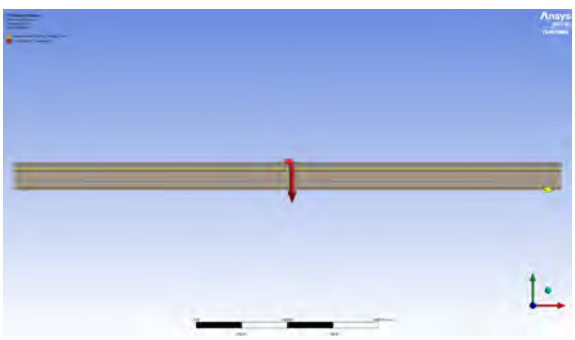

(a) Load and support location

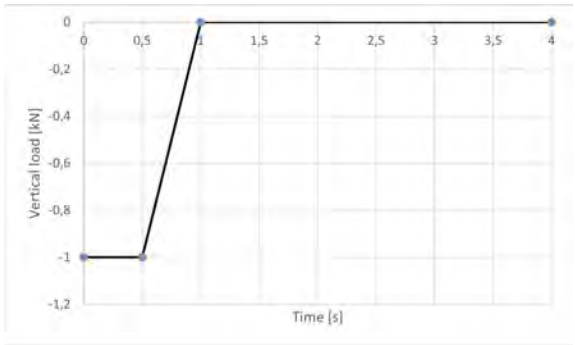

(b) Loading over time

Figure 6.3: Boundary conditions for the Transient Structural analysis

The results of the different floor types will be compared to each other by finding logarithmic ratio of the results of the top- and bottom vertices of the traditional floor $X(t)_{TSA}$, using the general relative unit of decibels defined in Equations (6.1) and (6.2). The corresponding values should not be confused with values for sound transmission or sound pressure levels, which also feature decibels as unit.

$$X_{TSA,\delta,i}(t) = 10log_{10}(\frac{\delta_{TSA,top,i}(t)}{\delta_{top,traditional}(t)}) \tag{6.1}$$

$$X_{TSA,a,i}(t) = 10log_{10}(\frac{a_{TSA,top,i}(t)}{a_{TSA,top,traditional}(t)}) \tag{6.2}$$

Besides, the signal frequency of the system can be determined from using the foundational relation Equations (6.3) and (6.4) between frequency and period [10].

$$f_{TSA,\delta} = 1/T_{TSA,\delta} \tag{6.3}$$

$$f_{TSA,a} = 1/T_{TSA,a} \tag{6.4}$$

6.1.2.2 Harmonic Response Analysis

A Harmonic Response Analysis features a different approach than the TSA and experimental analysis. It does not try to find the properties of the dynamic response by applying a transient load in a time domain, but by imposing a harmonic cyclic load. This harmonic load is changed in frequency and phase, while its amplitude will be be kept the constant. An example is shown in Figure 6.4. The results will thus show the magnitude of the floor response per excitement frequency and its corresponding phase. Peaks in the magnitude of the floor response therefore indicate the eigenfrequencies of the system. It is therefore an analysis in the frequency domain. Furthermore, the required computation time is heavily reduced compared to the transient analysis, due to it not requiring very small time steps. Besides, the response off higher modes can more clearly be analysed since they are isolated and the response is thus not dominated by the first eigenfrequencies.

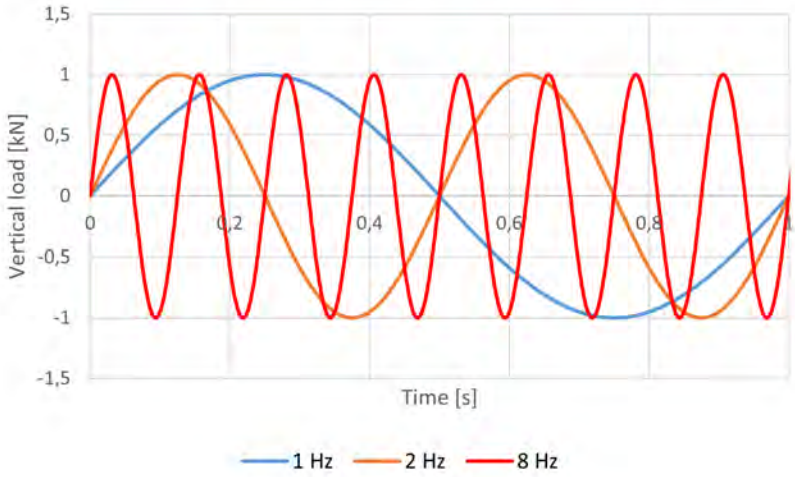

Figure 6.4: Example of harmonic loads with different frequencies.

The location of the load and boundary conditions is the same as in the TSA explained in the previous section. Next to the many interesting frequencies found by the modal analysis, extra user defined frequencies are added to create a finer resolution. For the range of 0-40 Hz, the added frequency step will be for each 0,5 Hz and from 40-5000 Hz the frequency step will be 10 Hz. For the tactile vibrations the analysis will be limited on the response of the top of the concrete for the 0-100 Hz range and the first four eigenmodes. For comparison across the floor types, the relation as defined in Equation (6.5) will be used.

$$X_{HRA,\delta,i}(f) = 10log_{10}(\frac{\delta_{HRA,top,i}(f)}{\delta_{HRA,top,traditional}(f)}) \tag{6.5}$$

6.1.3 Experimental analysis

To validate the found response in the analytical and numerical analysis, an experimental vibration test will be done. Both the test itself and the signal processing will be done in cooperation with Level Acoustics & Vibrations BV (LEVEL). As shown in Figure 6.5, for the vibration test the ED traditional specimen will be placed on two elevated supports with a similar span compared to the bending test of 5.8 m. The excitement will be provided by dropping a metal ball of 1,72 kg from a half meter height on a stiff rubber mat placed upon the specimen. Two drop positions will be used to excite and therefore visualize different modes. Both dropping position are at center-width of the floor, but differ in length position. Drop Position 1 (DP1) is located at $1/4L$ and Drop position 2 (DP2) is located at $1/2L$. For each position, the test will be done 6 times. To capture the floor response six triaxial accelerometers will be placed on the specimen in 3 pairs of 2 sensors. From each pair one sensor will be placed on the top- and bottom side of the specimen to capture the response of the concrete layer and of the CLT, respectively. All sensors will be directed such that their z-axis aligns the surface normal. Furthermore, the first pair (PCB 1/2) will be placed at $x = 1/2 \cdot L$, the second pair (PCB 3/4) at $x = 2/3 \cdot L$ and the third pair (BK1/2) at $x = 3/4 \cdot L$ such that a good indication is given of the response over the full span. All of the accelerometers will be placed at center span, in exception of the top sensor of pair 1 for DP2. For this situation this sensor is moved to approximately one fourth width to make space for the dropping position and its rubber mat. For pair 1 and 2 the PCB

Piezotronics Shear triaxial accelerometer Model 356A16, with sensitivity of 100 mV/g, will be used and for pair 3 the B&K Triaxial DeltaTron Accelerometer Type 4506, with sensitivity of 490 mV/g, will be used. Although both sensors feature a frequency range up to 5 kHz, the signal processing unit limited it to a maximum of 1024 Hz.

(a) Test-setup for the traditional floor (b) Test-setup for the conceptual floor

Figure 6.5: Set-up of the vibration ball-fall test in the Structures Laboratory of the TU/e.

The results from the accelerometers will be further processed to transform it into valuable data. First of all, a window function will be chosen. The window function is essential for processing of the signal from a time domain to a frequency domain through the used Fast Fourier Transformation (FFT). The goal of a FFT is to find the combination of linearly stacked harmonic functions with different frequencies, phases and amplitudes which most accurately corresponds to the actual signal. When this is done, the FFT plot will show how strong a specific frequency is present in the signal. The FFT however uses infinitely long functions, while the signal itself is only finite. This problem will be solved by infinitely duplicating the finite signal after each other. However, this would cause discontinuities. By multiplying the signal by a fitting window function, the values at the begin and end of the signal will both go to a specific value, which is often zero. Since the beginning and end of a signal now have the same value, it can be infinitely duplicated and thus analyses by a FFT. Since in this case the signal is caused by an impulse, the beginning is especially interesting while the values very close to zero are not and will interfere with the results. Therefore in this analysis a single window will be used, which will focus the processing around the impulse and the first part of the resonance. Furthermore, the quantity of acceleration in m/s^2 will be transformed into the quantity of Power Spectral Density over frequency, PSD(f), in decibels since this is a more generally captures the energy of a vibration. For this conversion the MATLAB(R) `'pwelch'` algorithm will be used. the Besides, the change to the log-scale used in decibels allows for more clearly visible trends.

6.2 Results

In this section the results for the tactile vibration performance will be discussed. It will include the observations made through the reEC-5 analytical method, the numerical Transient Structural and Harmonic Response analyses and finally the findings of the experimental ball-fall test.

6.2.1 Analytical analysis

In this section the results for the analytical vibration analysis using the reEC5-method will be discussed.

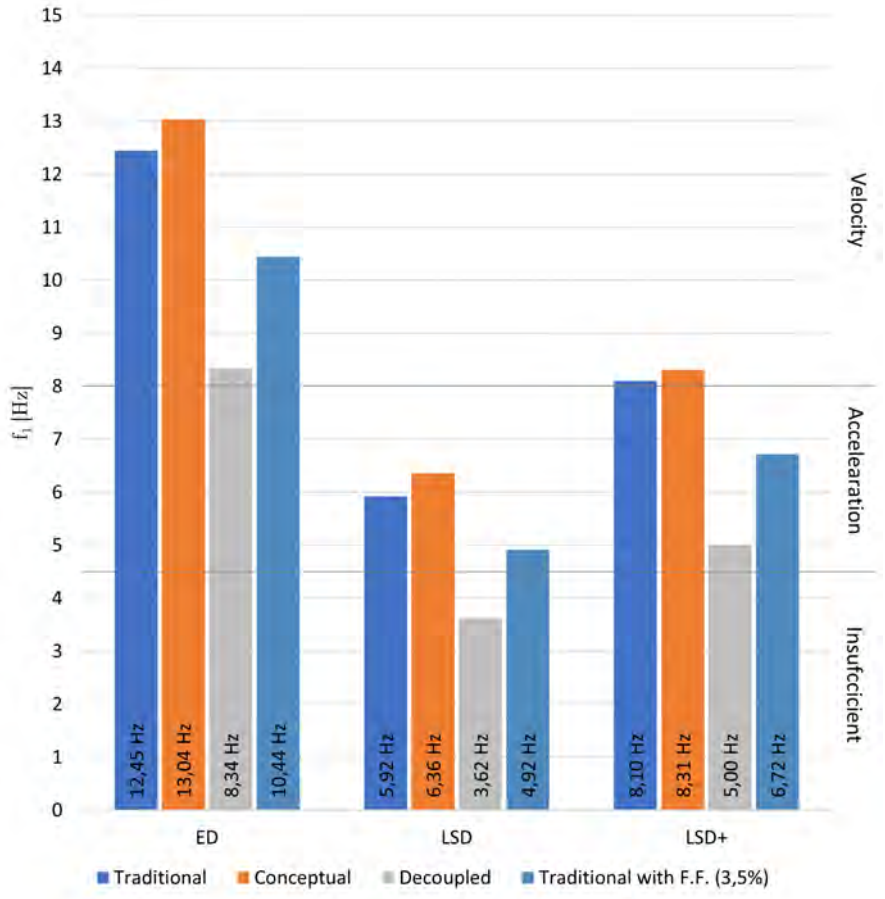

Figure 6.6: Values of the natural frequencies calculated using the reEC5-method.

Figure 6.6 show the predicted natural frequencies of the different floor types. The effect of increased dimensions, relative to its span, can clearly be observed by the lower frequencies found for the ED floor. The resulting increase of natural frequency indicates a stronger increase of stiffness than the increase in mass. Furthermore, it can be observed that there is trend in which the natural frequency is slightly increased relative to the natural frequency of the traditional floor. The decrease in mass is thus stronger than the decrease in bending stiffness. Next, the natural frequency for the decoupled floor is much lower than for the other floors, due to lack of composite action and thus heavily reduced bending stiffness. At last, the calculated natural frequency for the Traditional floors with F.F. also show decrease relative to the Traditional and Conceptual floor. This can be explained by a much stronger increase in mass than in bending stiffness since the concrete of the floating floor is fully decoupled without composite interaction with the other layers.

Figure 6.7 shows the response factors per floor types for the acceleration and velocity domain. In combination with the shown percentage differences relative to the traditional floor, it can be noted that there is a clear trend between the different floor types. First of all, the conceptual 2,5% floors perform worse (by featuring a higher R-factor), than their corresponding traditional floors, with an exception of the ED floor in the acceleration domain. This trend can be explained by the lower mass and bending stiffness of the conceptual floors compared to the traditional floors, while featuring an equal damping ratio. Secondly, the conceptual 3,5% floors perform

better than their corresponding traditional floors, especially in the acceleration domain. Showing the impact of the increase of damping ratio ζ. However, except for the ED conceptual 3,5% floor in the acceleration domain, both trends are not strong enough to impact the resulting vibration class.

Furthermore, it can also be noted that the ED-floors in acceleration domain feature a stronger positive performance difference compared to the other floors in this domain, resulting in the two mentioned exceptions. An explanation could be the lower reduction of bending stiffness going from the traditional floor to the conceptual floor as shown in Figure 5.14. It is however interesting that this trend is not found in the velocity domain, indicating a possible stronger influence of the bending stiffness on the acceleration response than on the velocity response. Since an extensive parameter study to investigate the acceleration and velocity domain is outside the scope of this project and the impact of this trend is of lesser importance for design practice since the ED floors should all be designed using the velocity domain, this is not further investigated.

Additionally, the LSD and LSD+ floors perform much better in the velocity domain as compared to the acceleration domain. This effect is strong enough to move the floors into one or two classes downwards. As described in Appendix B, in the design process for the LSD+ it was even governing to reach a natural frequency above 8 Hz to be able to calculate through the velocity domain and with its benefits reach the required Class III threshold. This trend is however not applicable for the ED design, possibly due to the lower span. As explained in the last paragraph, this is a point for further investigation.

When focusing on the results for the decoupled floors, it can be seen that they perform much worse than the other floors types. Even though they are calculated with an increased damping ratio, this is within exceptions since these floors feature a much lower effective bending stiffness due to the lack of composite action. Next to that, the decoupling effect does not feature extra benefits for the reduction of tactile vibrations.

The impact of the addition of a floating layer to the traditional floor can not only be seen in the natural frequency but also in the Response factor. As expected, the increase in mass generally features an improved vibration performance. The only exception is in the ED design category. However, most important is that the significant decrease in natural frequency also changes the governing calculation domain. The LSD+ floor therefore has to be calculated in the acceleration domain instead of the velocity domain, which results in a class change from the satisfactory Class III to unsatisfactory Class IV.

The analytical results for the Experimental Design Traditional- and Conceptual floors while using the experimental damping ratios, described in Section 6.2.3, are shown in Figure 6.8. For the acceleration domain, the results feature the same general positive trend as seen when the damping ratio provided by the reEC5; a significant decrease of R going from the traditional to the conceptual floor. Similarly to the ED-floors using the provided damping ratios, this results in a classification improvement from Class II to Class I. However, in the governing velocity domain, there is only a minimal improvement in floor response. For the floors using the experimental damping ratio, the earlier observed performance increase of the conceptual floor relative to traditional floor is still present but with a smaller magnitude. This indicates that a damping ratio increase for lower damping ratios has a larger impact on the final response factor. At last, similarly to the results using the provided damping ratio, it does not lead to a change in vibration

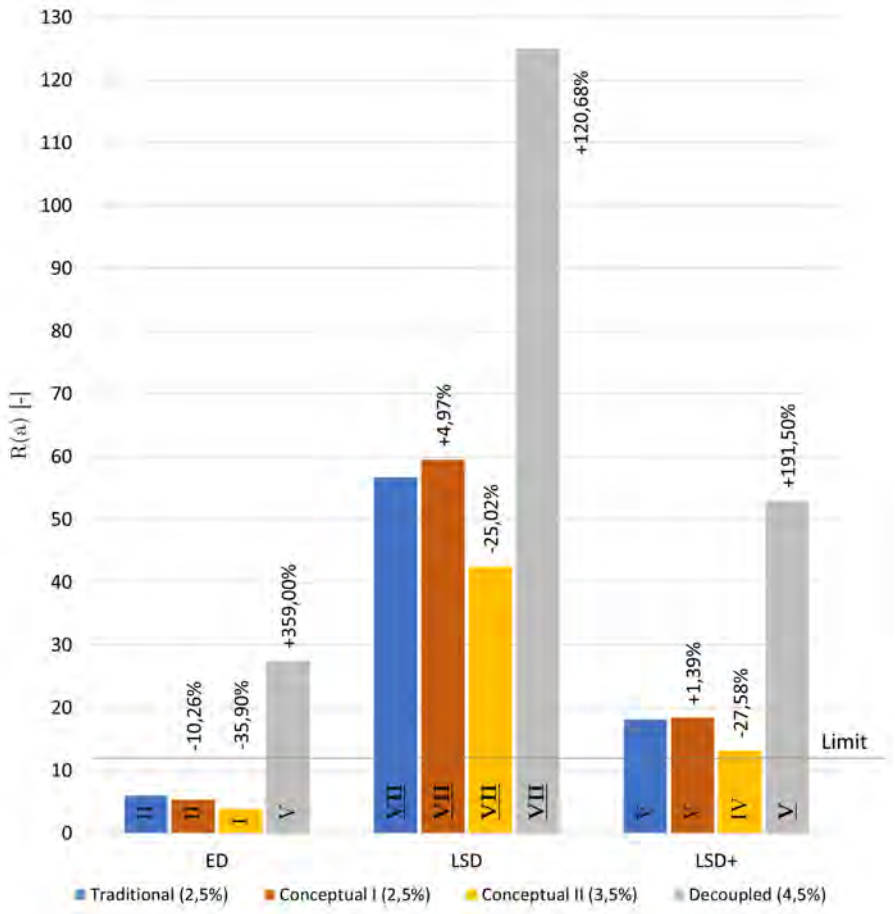

(a) acceleration domain

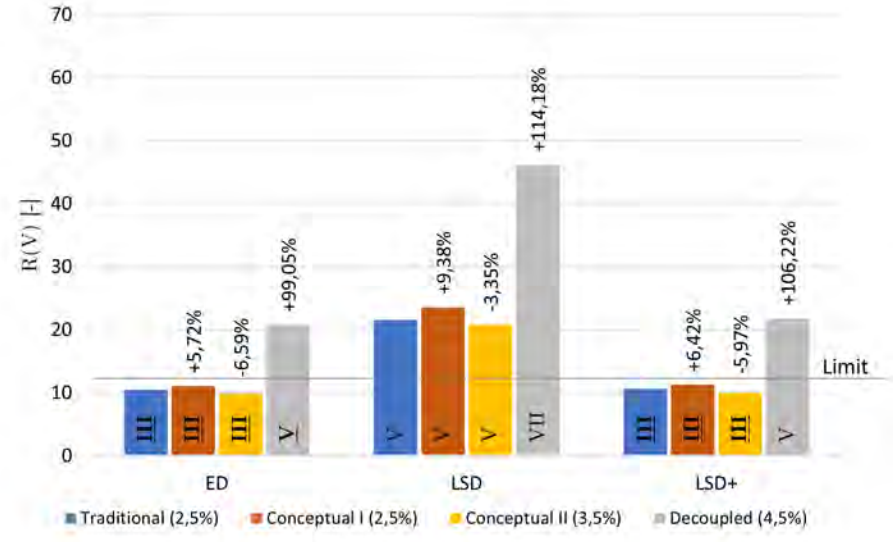

(b) velocity domain

Figure 6.7: Values of Response factor and vibration classes for each floor type and category using the reEC5-method, including highlighted governing classes and percentile differences compared to the corresponding traditional floor.

class.

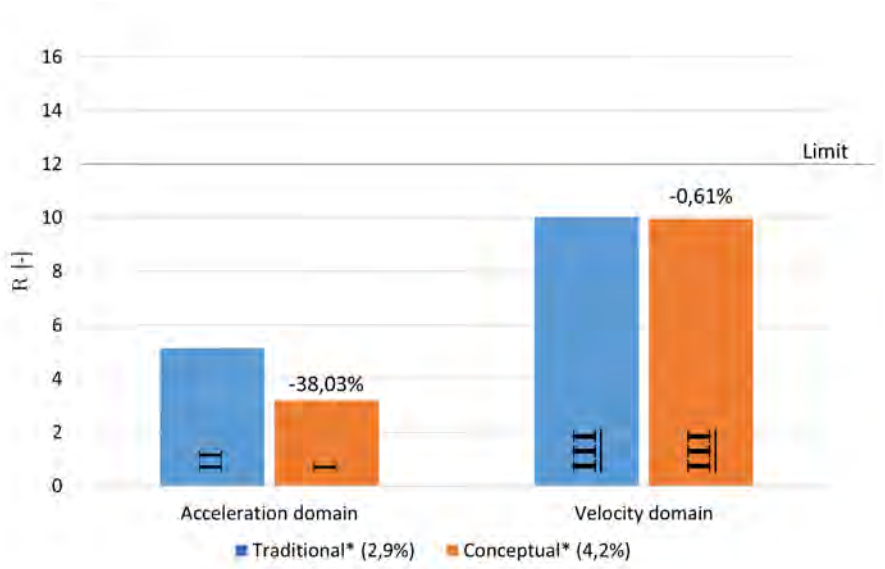

Figure 6.8: Values of Response factor and vibration classes for the ED Traditional and Conceptual floor using the reEC5-method and experimental damping ratios, including highlighted governing classes and percentile differences compared to the corresponding traditional floor.

All in all, based on the analytical analysis it can be noted that the conceptual floors with high damping feature a slightly improved vibration performance than the traditional, indicating that the improvement of damping is slightly stronger than the loss of bending stiffness and mass. The improvement is however not strong enough to improve the vibration class. It can therefore be concluded the improved vibration performance of the conceptual floors is insignificant. Furthermore, the addition of a floating for, possibly for acoustic reason, should be carefully considered since the increase in mass does not only decrease the floor response but also lowers the natural frequency.

6.2.2 Numerical analysis

This section will evaluate the results found in the Transient Structural Analysis and Harmonic Response Analysis done in the Ansys Mechanical FEM package. Extensive results for the analysis can be found in Appendix E.

6.2.2.1 Transient Structural Analysis

Before the results for the Transient Structural Analysis can be discussed, the data has to be further refined. As shown in Figures 6.9a and 6.10a the results for the first second are heavily influenced by the load configuration. There only the results after the first second will be considered. For this time frame the local maxima have been analyzed. From the local maxima the mean of the observed consistent period and resonance frequency are determined. Besides, the local maxima can be isolated to make a more clear distinction between the analyzed data. However, the refined graphs do not always have local maxima at the same time. Therefore an exponential trend-line is determined from the local maxima to predicts the response at all points in time, as shown in Figures 6.9c and 6.10c. Deviating local maxima, which were especially

present in the acceleration results, are excluded in the determination of the trend-line.

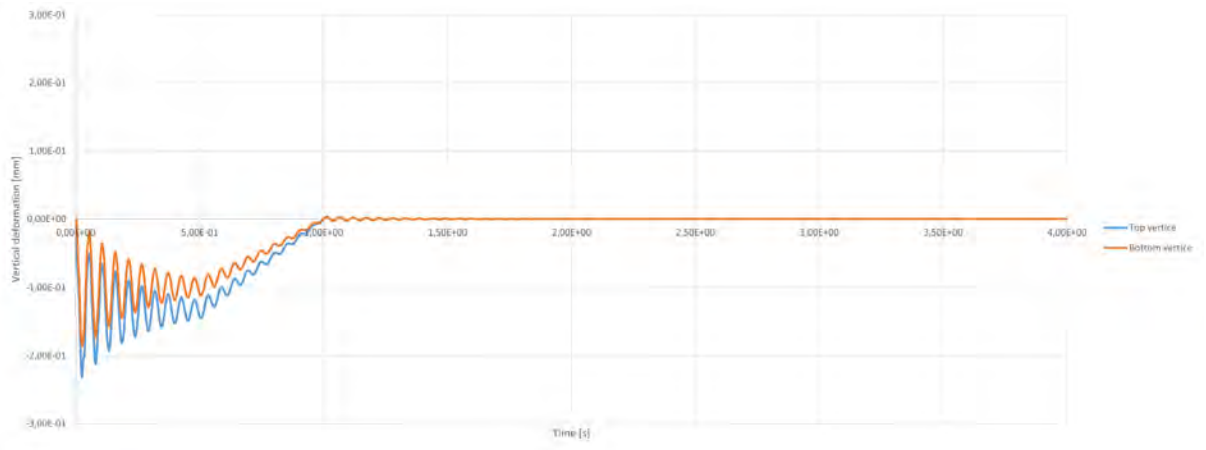

(a) Full time frame

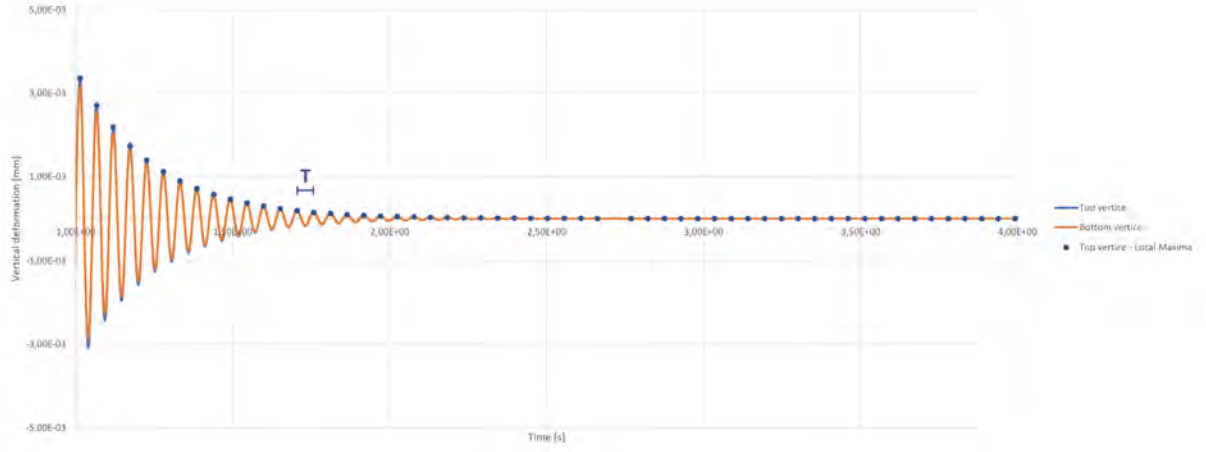

(b) Modified time frame

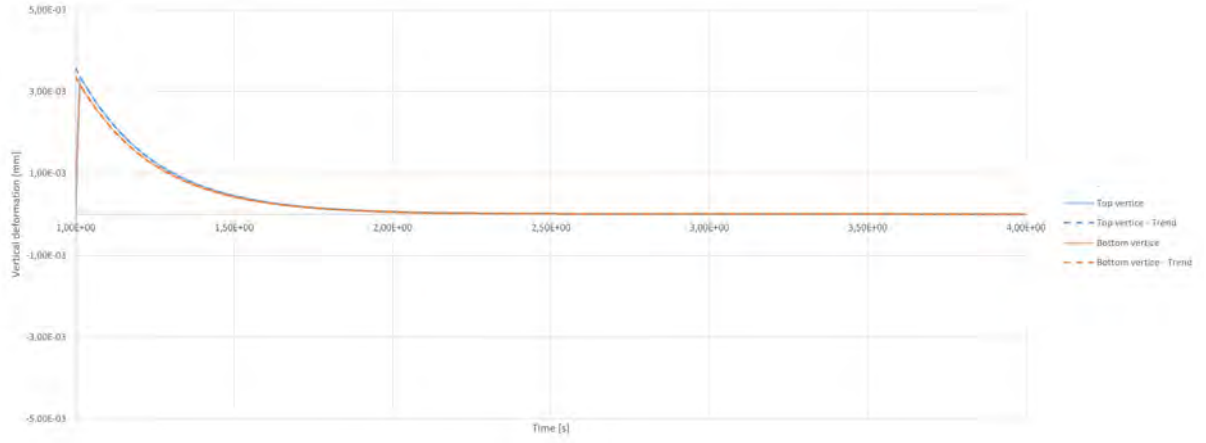

(c) Local maxima

Figure 6.9: Deformation results for the top of the concrete of the Transient Structural Analysis of the ED - Conceptual 3,5% floor.

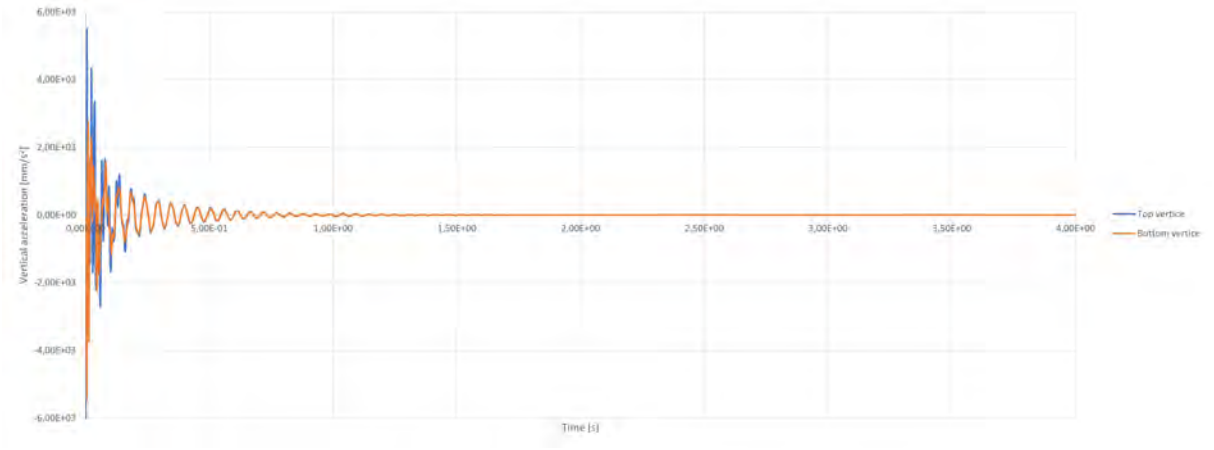

(a) Full time frame

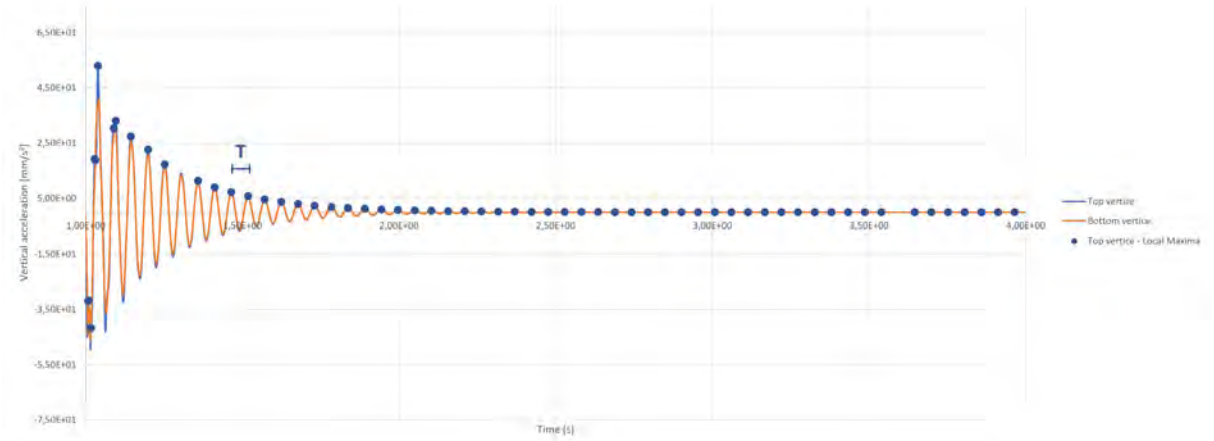

(b) Modified time frame

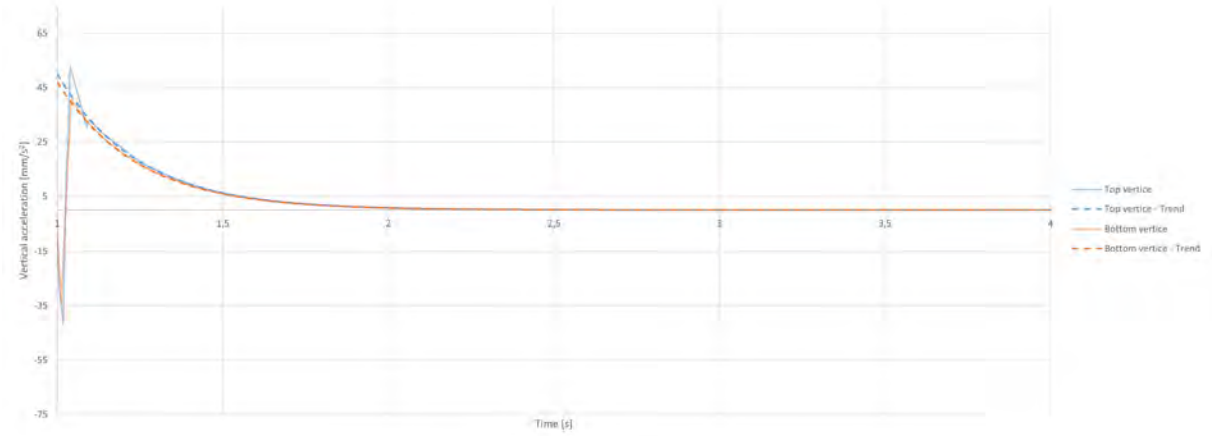

(c) Local maxima

Figure 6.10: Acceleration results for the top of the concrete of the Transient Structural Analysis of the ED - Conceptual 3,5% floor.

The results for the analysis or the Large Span Design floors are shown in Figures E.9 and E.10. Most notable from these results is the effect that the conceptual floor with 2,5% damping features slightly higher amplitudes, while the conceptual floors with 3,5% features significantly lower

vibration amplitudes. The former can be explained by the slightly lower stiffness and mass, without featuring an increase of damping. The latter shows the impact of that damping effect. The decoupled floor shows much higher vibration amplitude than the other floors, even though their 3,5% damping input, due to its lower bending stiffness and/or its fully decoupled concrete top layer.

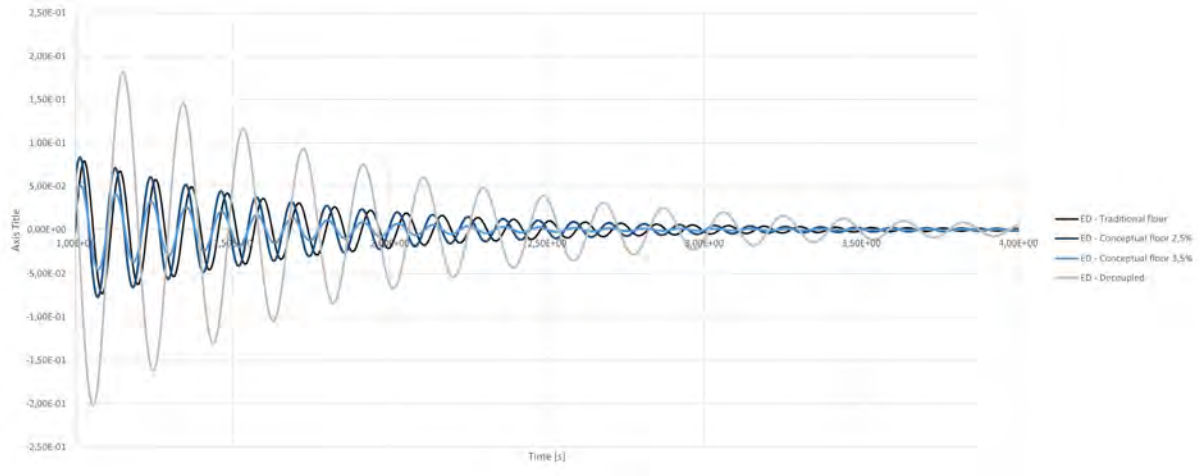

(a) Modified time frame

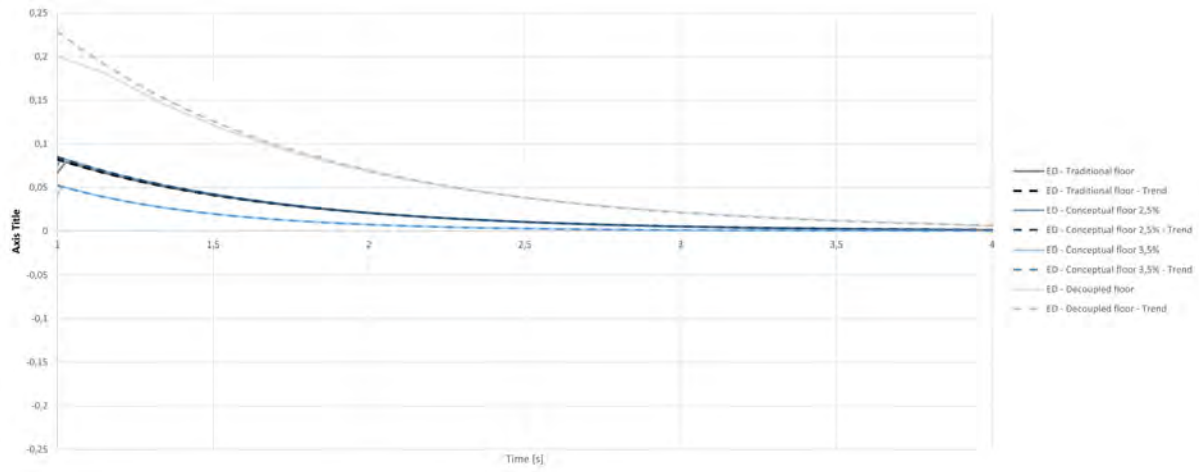

(b) Local maxima

Figure 6.11: Deformation results for the top of the concrete of the Large Span Design (LSD) floors.

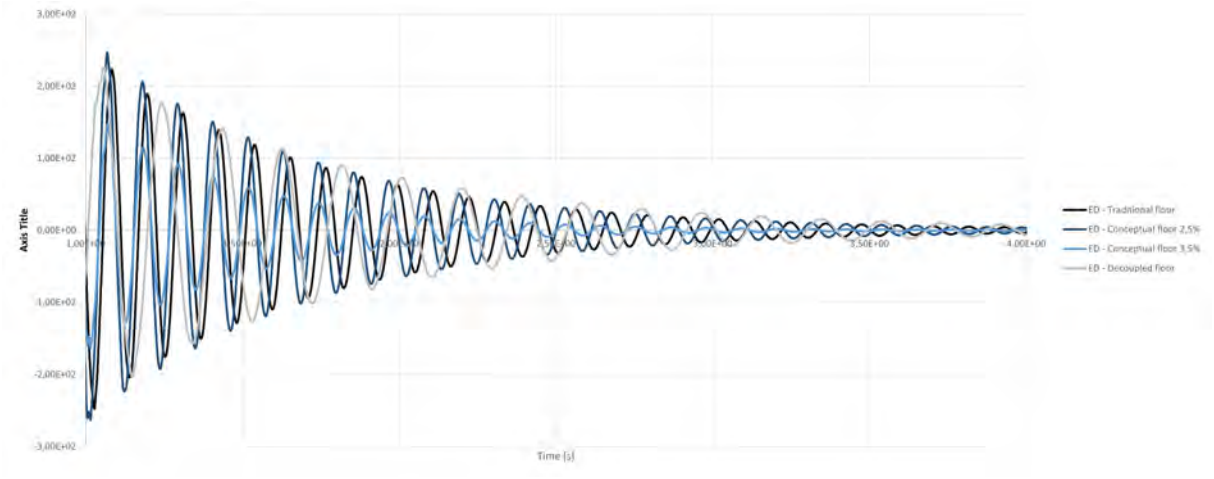

(a) Modified time frame

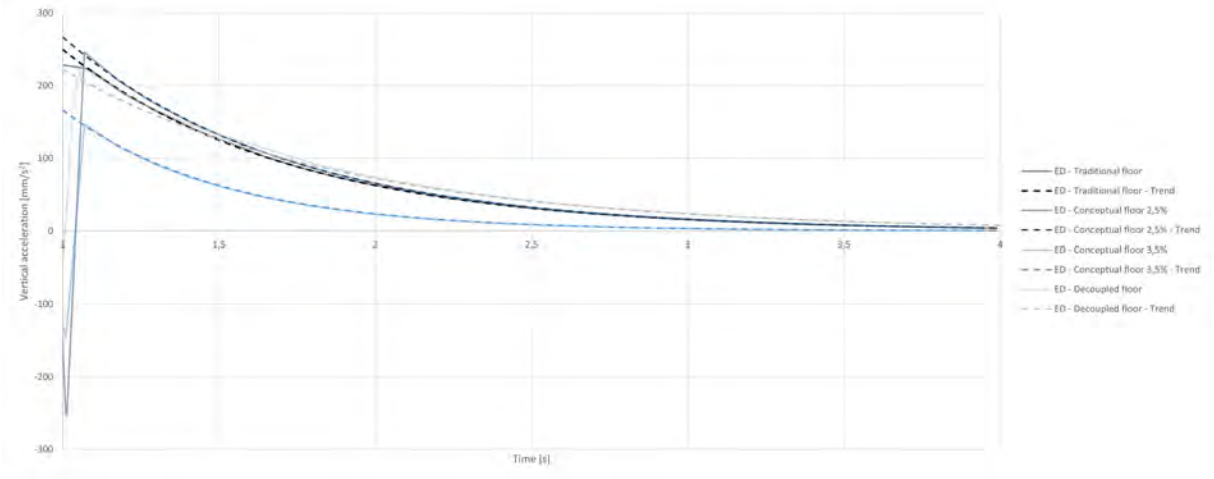

(b) Local maxima

Figure 6.12: Acceleration results for the top of the concrete of the Large Span Design (LSD) floors.

The results for the analysis or the Large Span Design+ floors are shown in Figure E.11. For these floors the same trends can be found as for the LSD floors. The difference in vibration amplitude for the conceptual 2,5% is even increased. One can also not the significant overall reduction of vibration amplitudes of the LSD+ floors compared to the LSD floors.

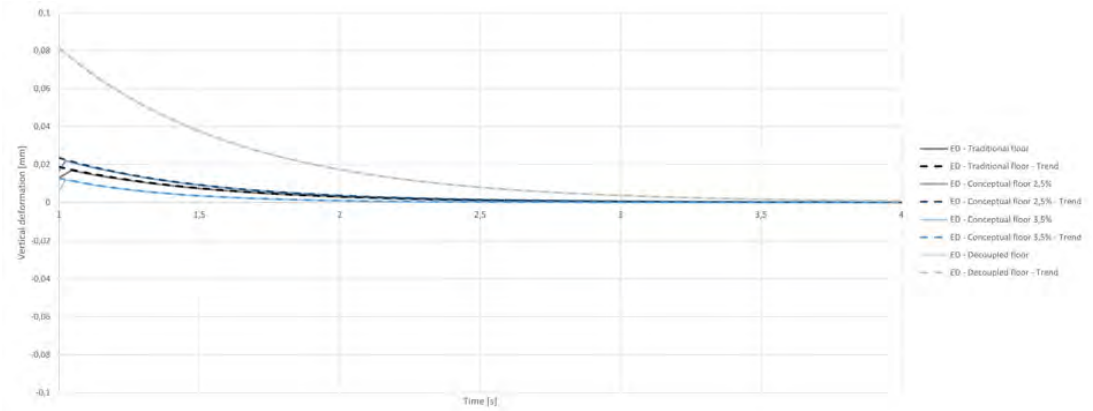

(a) Deformation

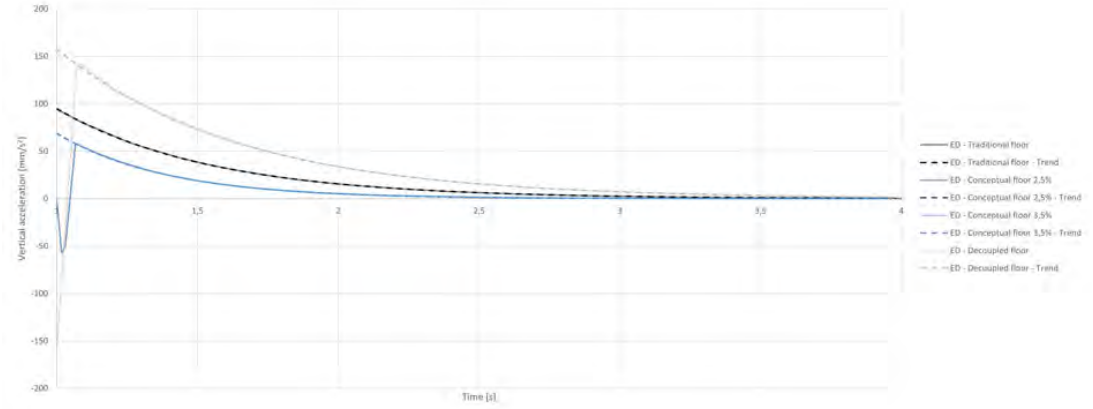

(b) Acceleration

Figure 6.13: Local maxima results for the top of the concrete of the Large Span Design+ (LSD+) floors.

The results for the analysis or the Experimental Design floors are shown in Figure E.5. Most interestingly is that for the results for the conceptual 3,5% and Traditional floors are much closer to each other than in the other design categories. Besides, the differences between the conceptual 2,5% floor is also larger. It implies that for this design category there is a higher reduction of bending stiffness of the conceptual by the addition of the insulation layer compared to the traditional floor than for the other design categories. This however contradicts with the results found in the Chapter 5, which describes the lowest reduction in stiffness in the ED floor. It however also describes the unexpected deviation in the form of an increase of connection stiffness K^* for the ED floors. Since this analysis is independent of the determined value for K^*, the connection stiffness in the vibration model might feature an expected lower value. This could explain the small difference in response for the discussed traditional and conceptual floor, due to the conceptual floor featuring a positive higher damping, but a negative decrease in bending stiffness which cancel out each other.

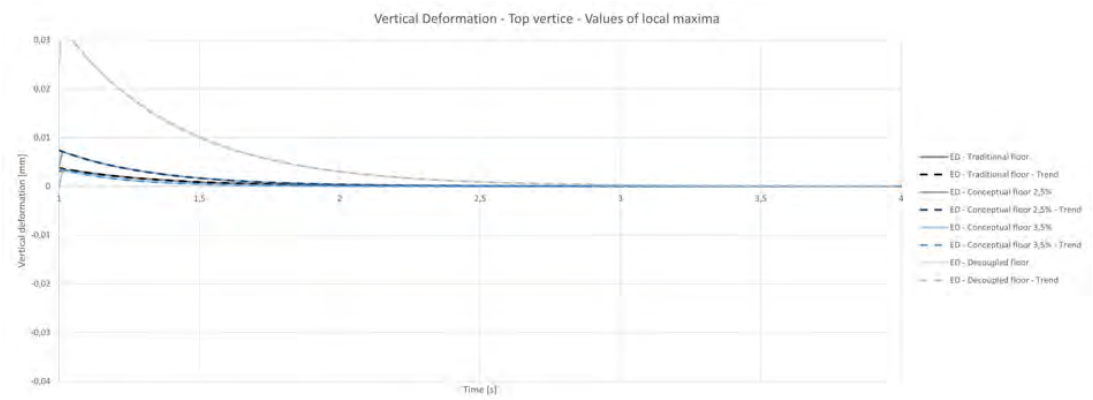

(a) Deformation

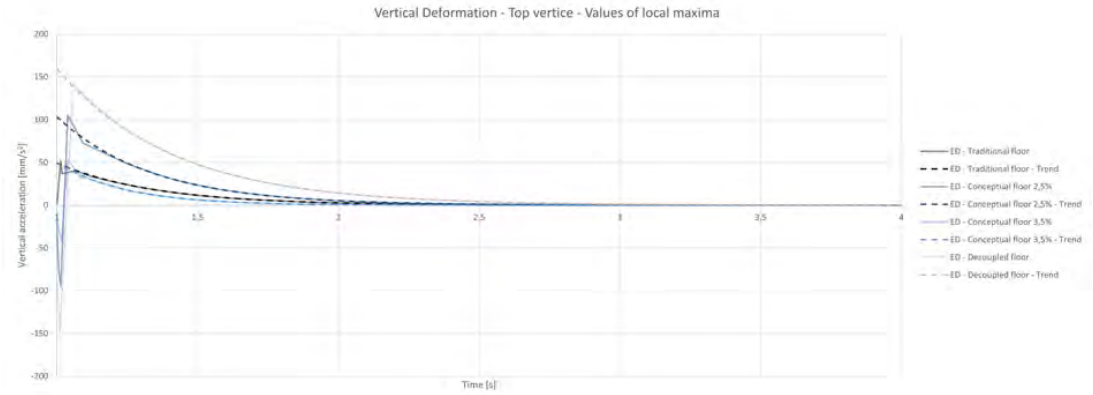

(b) Acceleration

Figure 6.14: Local maxima for the top of the concrete of the Experimental Design (ED) floors.

6.2.2.2 Harmonic Response Analysis

This section will show and evaluate the results for the Harmonic Response Analysis for tactile vibration performance.

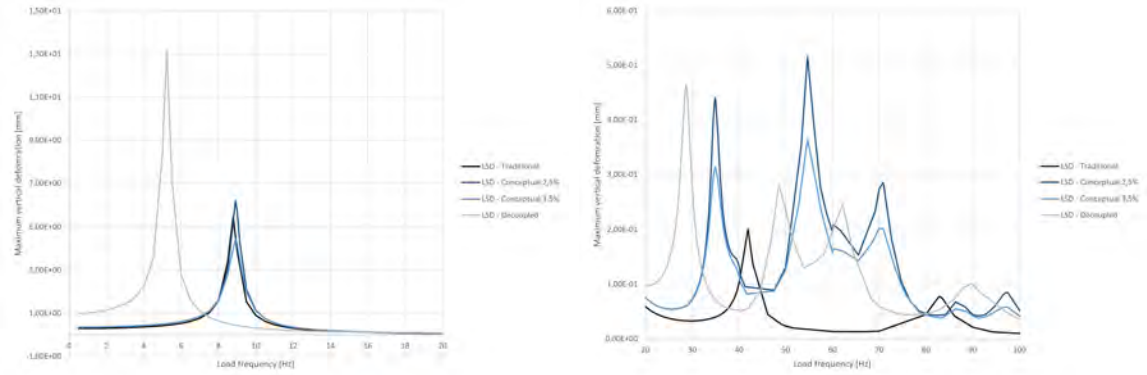

(a) 0-20 Hz (b) 20-100 Hz

Figure 6.15: Results of Harmonic Response Analysis of the Large Span Design (LSD) floors for low frequencies, measured at the top of the concrete.

The results for the Large Span Design floors are shown in Figure E.13. For the first eigenfrequency it can be noted that the the conceptual 3,5% has a reduced peak while the conceptual 2.5% has an increased peak relative to the peak of the traditional floor. The differences are however in-between 1 dB. Furthermore, the conceptual floors shows a slightly higher frequency. The most probable explanation is that the mass is more heavily reduced than the bending stiffness. The decoupled floor features a much lower eigenfrequency, which can be explained by the large reduction of bending stiffness due the lack of composite action.

For the higher modes the most notable observation is that the decoupled and conceptual floors feature 4 modes while the traditional floor only features 2 in the 20-100 Hz frequency range. These modes for the conceptual floor feature similar behavior as the ones for the decoupled floor but are shifted by the difference in bending stiffness. As shown in Figure 6.16 the response of the corresponding modes of the conceptual, and similarly observed for the decoupled floor, specifically in relate to concrete top layer, indicating decoupling behavior. The performance for this frequency range is therefore much lower compared to the traditional floor.

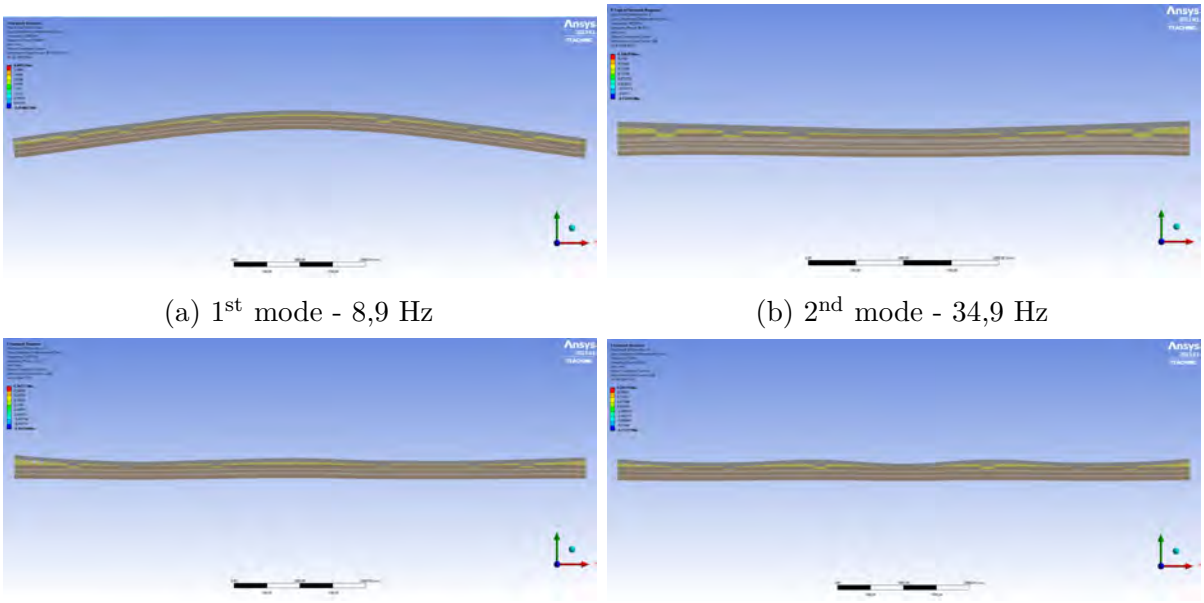

(a) 1st mode - 8,9 Hz (b) 2nd mode - 34,9 Hz

(c) 3rd mode - 54,7 Hz (d) 4th mode - 60,37

Figure 6.16: Modes of the Large Span Design (LSD) - Conceptual 3,5% floor determined with the Harmonic Response Analysis, including 70x and 200x deformation scale for the 1st mode and 2nd to 4th mode respectively.

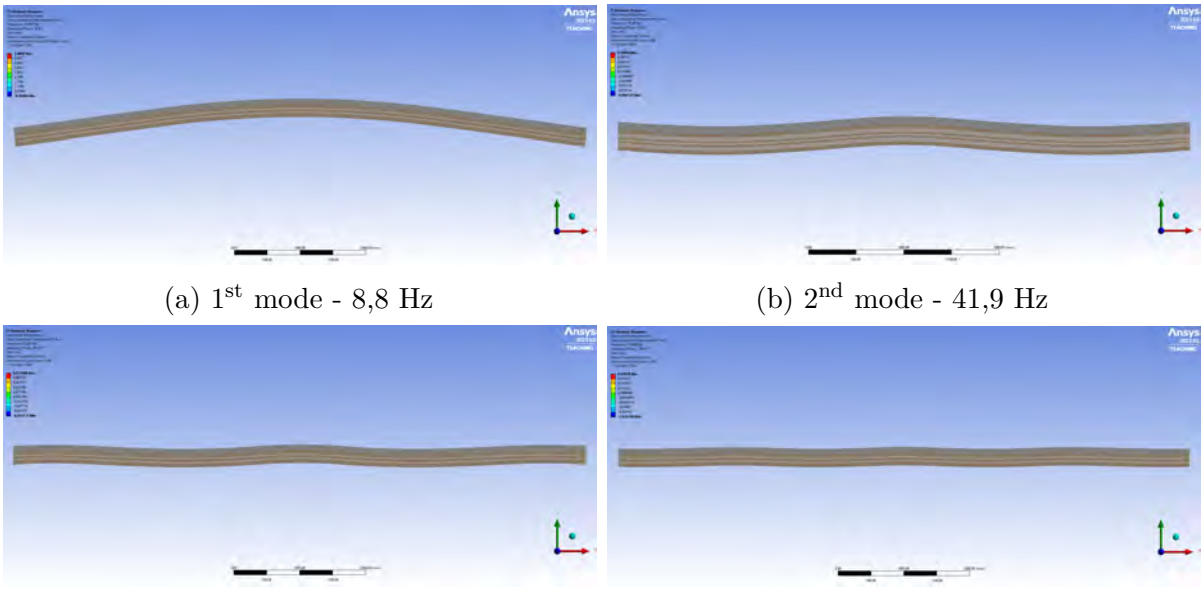

(a) 1st mode - 8,8 Hz (b) 2nd mode - 41,9 Hz

(c) 3rd mode - 88,4 Hz (d) 4th mode - 119,1 Hz

Figure 6.17: Modes of the Large Span Design (LSD) - Traditional 3,5% floor determined with the Harmonic Response Analysis, including 79x and 400x deformation scale for the 1st mode and 2nd to 4th mode respectively.

The results for the Large Span Design+ floors are shown in Figure E.14. For these floors similar observations can be made as done for the LSD floors. Besides, an increase in frequency can be observed. This implies a larger increase of bending stiffness than in mass. Furthermore, the peak values are considerable decreased compared to the LSD floors.

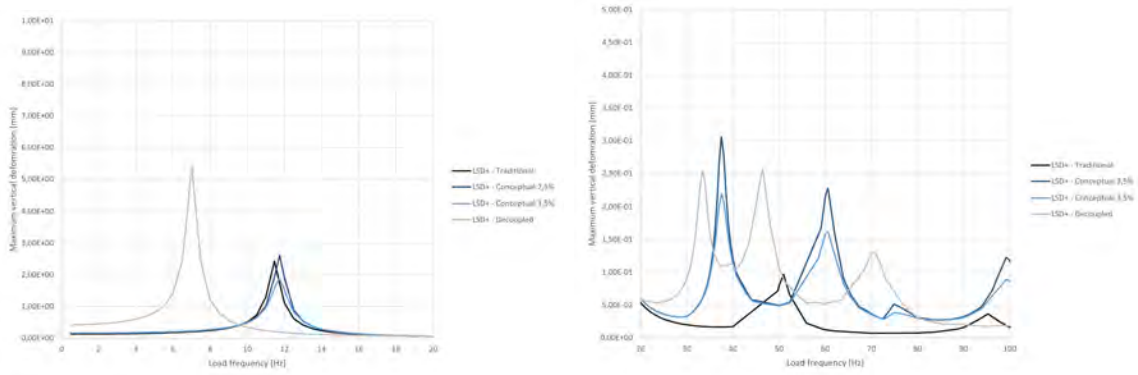

(a) 0-20 Hz (b) 20-100 Hz

Figure 6.18: Results of Harmonic Response Analysis of the Large Span Design+ (LSD+) floors for low frequencies, measured at the top of the concrete.

The results for the Experimental Design floors are shown in Figure E.22. Again, similar observations can be made as for the LSD and LSD+ floor although in a lesser extend. Next to that, it can be noted that the ED floors feature an higher floor frequency. Although it is likely to explain this using the 5,8 meter span, the actual cause is the different criteria used for the design,

causing relative larger dimensions. As noted, increased dimensions feature a stronger increase in bending stiffness than in mass resulting in a higher natural frequency. This also results in lower peak values.

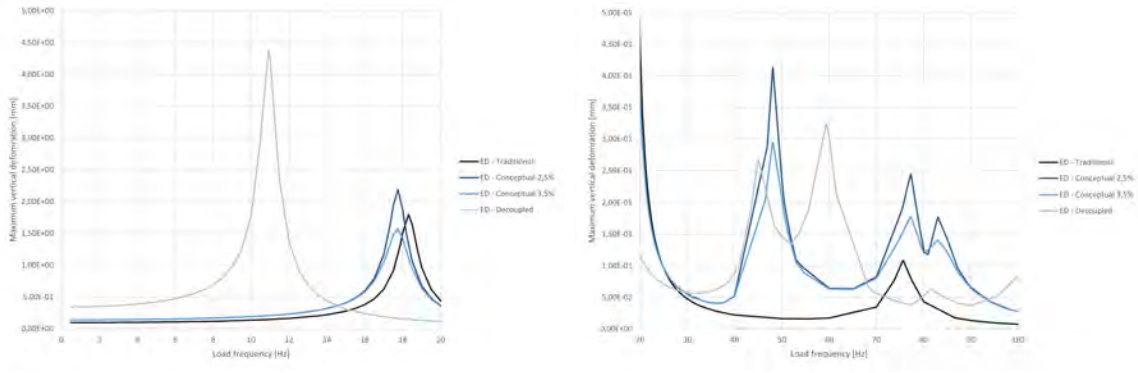

(a) 0-20 Hz (b) 20-100 Hz

Figure 6.19: Results of Harmonic Response Analysis of the Experimental Design (ED) floors for low frequencies, measured at the top of the concrete.

The results for the Experimental Design floors using the experimental damping ratios are shown in Figure E.16. Since only the damping ratio is adapted, similar behavior, such as peak frequencies, as for the original ED floors are visible. The peak values are however (positively) changed, including the difference between the traditional and conceptual floor.

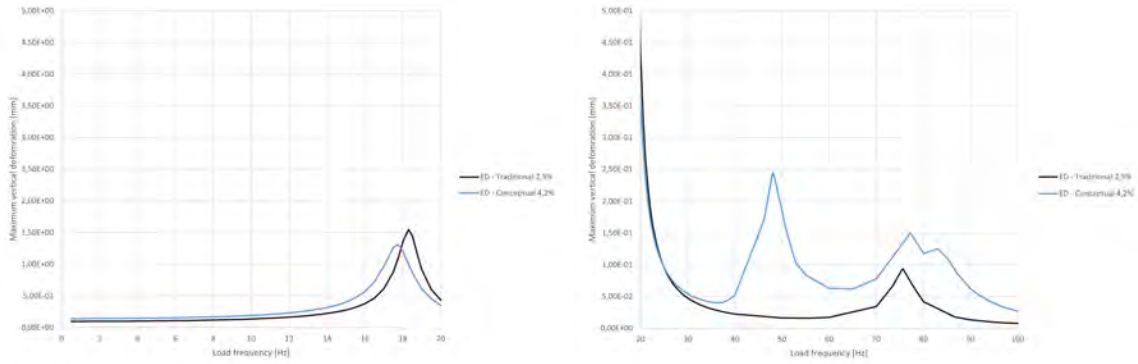

(a) 0-20 Hz (b) 20-100 Hz

Figure 6.20: Results of Harmonic Response Analysis of the Experimental Design (ED) floors for low frequencies, measured at the top of the concrete.,using the experimental damping ratios.

6.2.3 Experimental analysis

The results for the floor response of the first drop of series of the experimental ball-fall tests are shown in the time domain in Figures 6.21 and 6.22 and processed to the frequency domain in Figures 6.23 and 6.24 in order of drop position. Due to the lack of an available force meter in the experimental set-up and the uncertainties around the ball-drop excitement, the values on the y-axis cannot be accurately compared across measurements. However, the excitement is accurate

enough to analyze the general behavior of the floor response. Besides, due to the low coefficient of variance shown in Tables 6.4 and 6.5, the behavior of the first drop per floor type and drop position is representative for the other measurements in the same series.

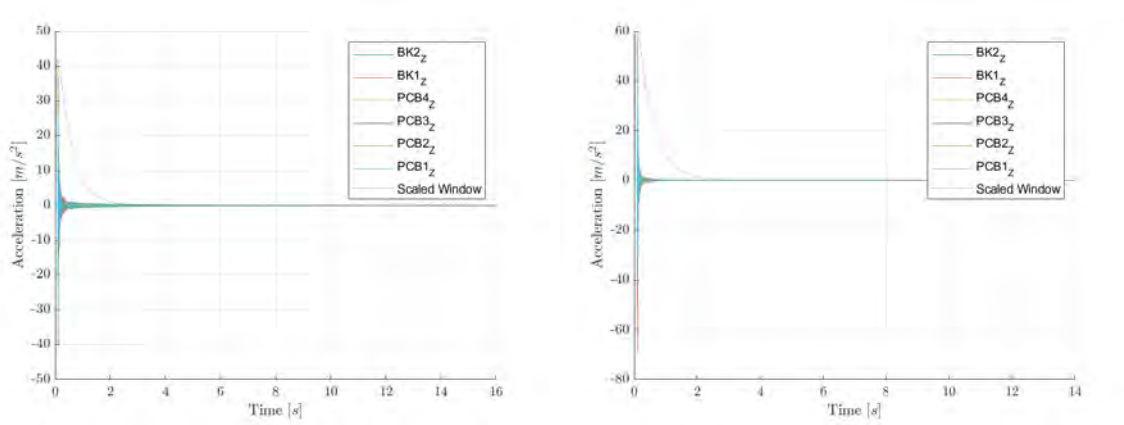

(a) Traditional floor (b) Conceptual floor

Figure 6.21: Results of floor response in time domain for drop 1 of the experimental vibration tests for drop position 1.

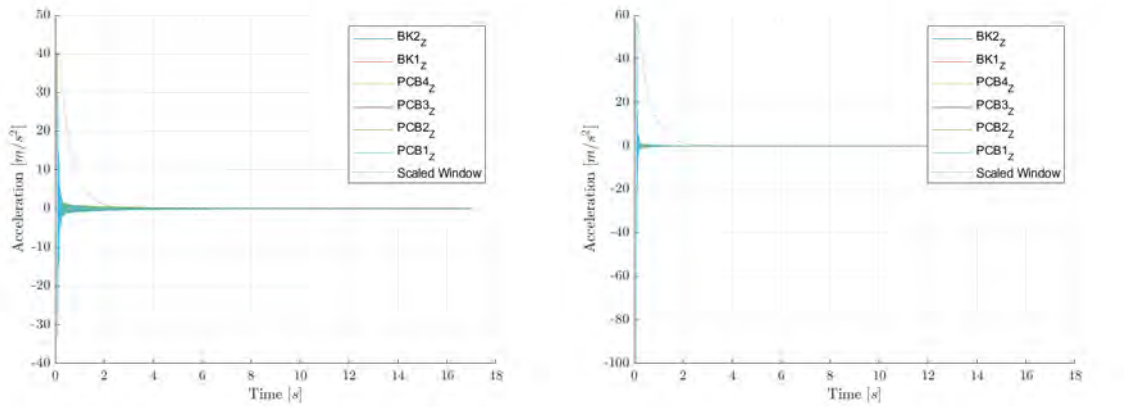

(a) Traditional floor (b) Conceptual floor

Figure 6.22: Results of floor response in time domain for drop 1 of the experimental vibration tests for drop position 2.

The main result taken from the time domain is that generally the Conceptual floor dampens out much quicker than Traditional floor, this is inline with the results on frequency domain which show an increased experimental damping ratio of the first mode. While for the traditional floor a $\zeta_{1,exp}$ of 2,9% could be found, the conceptual floor features an average $\zeta_{1,exp}$ of 4,2%.

The results of the processed floor response to the frequency domain, shown in Figure 6.23, show a slightly decrease of frequency of the conceptual floor for the first vibration mode. This can be explained by its lower mass and bending stiffness. The figure also shows that after the first peak of the natural frequency a significant second peak is present. For the traditional floor

this is in the form of a double peak at approximately 33 and 38 Hz. For the conceptual floor this in the form of a single peak at approximately at 26 Hz. This second mode is at $1/3L$ and $1/4L$ even stronger present than the first mode. This is due to the excitement of the floor of drop position 1 at $1/4L$ at the amplitude location of the second mode.

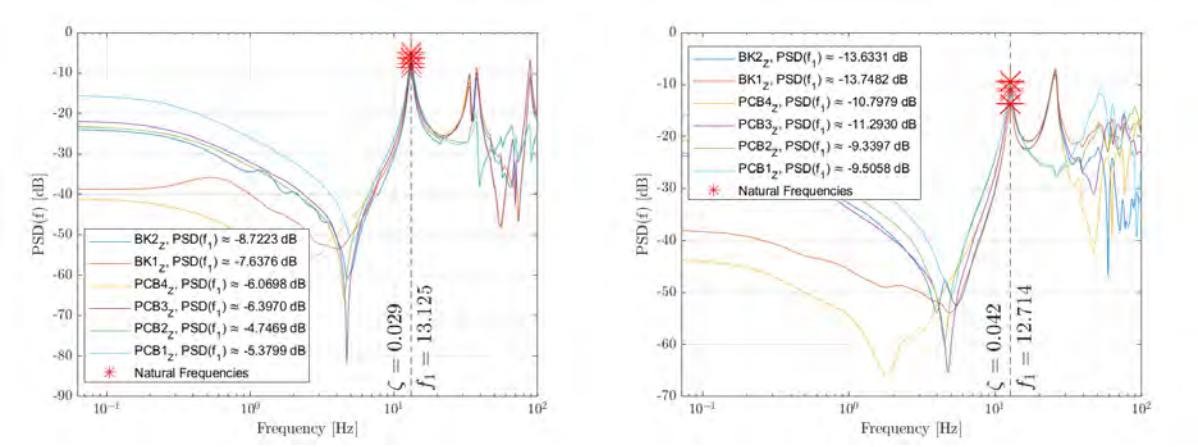

(a) Traditional floor (b) Conceptual floor

Figure 6.23: Processed results for floor response in frequency domain for drop 1 of the experimental vibration tests for drop position 1.

Table 6.4: Mean, standard deviation (SD) and coefficient of variance (CV) response parameters at the natural frequency of the 6 drops per floor type for drop position 1 of the experimental vibration test.

	$f_{1,exp}$ $[Hz]$	$\zeta_{1,exp}$ $[-]$	$PSD(f_{1,exp})$ $[dB]$ PCB1	PCB2	PCB3	PCB4	BK1	BK2
Traditional floor								
Mean	13,124	0,029	-5,4741	-4,8314	-6,4958	-6,1599	-7,7089	-8,8099
SD	0,003	0,000	0,0672	0,0623	0,0665	0,0639	0,0614	0,0632
CV	0,02%	0,00%	-1,23%	1,29%	1,02%	1,04%	0,80%	0,72%
Conceptual floor								
Mean	12,748	0,042	-9,4669	-9,3042	-11,2329	-10,7948	-13,6678	-13,6243
SD	0,017	0,000	0,1188	0,1175	0,1186	0,1219	0,1138	0,1250
CV	0,14%	0,00%	1,26%	1,26%	1,06%	1,13%	0,83%	0,92%

The results for drop position 2, shown in Figure 6.23 and Table 6.5, shows similar properties for the natural frequency. However, the peak for for the second vibration mode is not as strong anymore due to the excitement position not aligning to the amplitude location.

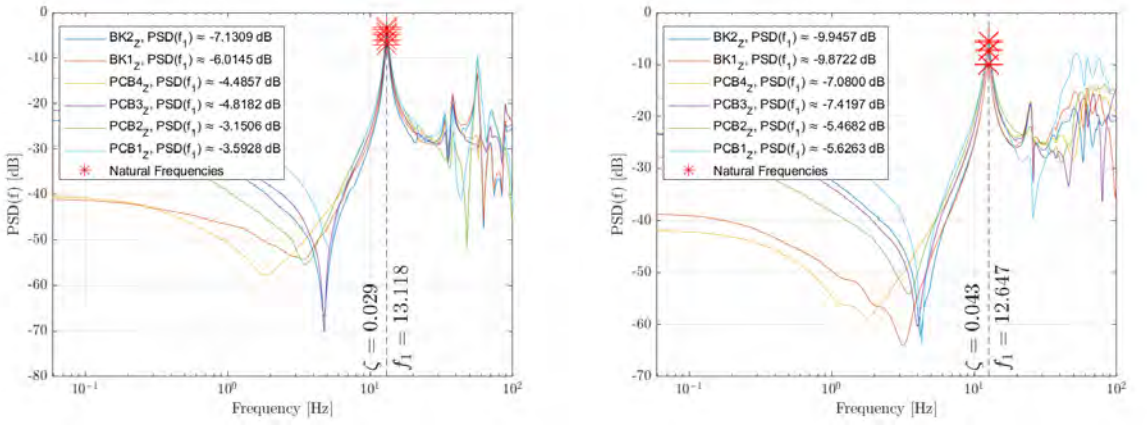

(a) Traditional floor (b) Conceptual floor

Figure 6.24: Processed results for floor response in frequency domain for drop 1 of the experimental vibration tests for drop position 2.

Table 6.5: Mean, standard deviation (SD) and coefficient of variance (CV) of the response parameters at the natural frequency of the 6 drops per floor type for drop position 2 of the experimental vibration test.

	$f_{1,exp}$ $[Hz]$	$\zeta_{1,exp}$ $[-]$	$PSD(f_{1,exp})$ $[dB]$ PCB1	PCB2	PCB3	PCB4	BK1	BK2
Traditional								
Mean	13,123	0,029	-3,0814	-2,6288	-4,2971	-3,9634	-5,4898	-6,6088
SD	0,003	0,000	0,3821	0,3855	0,3863	0,3862	0,3882	0,3881
CV	0,03%	0,00%	12,40%	14,66%	8,99%	9,74%	7,07%	5,87%
Conceptual								
Mean	12,651	0,043	-5,6510	-5,4846	-7,4372	-7,1038	-9,8885	-9,9592
SD	0,017	0,000	0,1823	0,1805	0,1829	0,1796	0,1811	0,1768
CV	0,13%	0,87%	3,23%	3,29%	2,46%	2,53%	1,83%	1,78%

6.3 Discussion

This section will compare the results between the analytical, numerical and experimental approaches and discuss their validity.

6.3.1 Damping

The first major discussion point is the assumed and present damping in the floor system. Interestingly the experimental damping of $\zeta_{trad,1,exp} = 2{,}9\%$ and $\zeta_{concep,1,exp} = 4{,}2\%$ is notably higher than the assumed $\zeta_{trad,1,reEC5} = 2{,}5\%$ and $\zeta_{concep,1,reEC5} = 2{,}5$-$3{,}5\%$, for TCC floors and TCC floors with floating layers respectively. Besides, the difference between $\zeta_{trad,1}$ and $\zeta_{concep,1}$ is also higher. However, the usage of these experimental values actually decreased the improved vibration performance of the conceptual floor relative to the traditional floor, in comparison to the use of the reEC-5 values for both floors. While the increase in damping ratio compensated for

the decrease in bending stiffness and mass and even provided a further response improvement, this improvement was not large enough to provide a significant vibration improvement. Interestingly, the experimentally found damping ratios were not only higher than the provided values for the reEC5 floors, the observed value found for the traditional floor is also significantly higher than values found for CCC floors with notches in literature, which fluctuated between $\zeta_1 = 0{,}6\text{-}1{,}2\%$ and for which the maximum was found for CCC floors with lower composite interaction causing more slip and friction [33], [53], [58]. These found values are thus higher than expected and due to its importance should be taken into account in further research.

6.3.2 Numerical analysis

In this paragraph the numerical modeling approach, the Transient Response Analysis and Harmonic Response Analysis and the validity of its results will be discussed.

First of all, the Transient Response Analysis requires attention. First of all, the 700 N used in the reEC5-method to replicate a footfall could not be replicated in the TSA due to convergence issues. Therefore, a 1 N force has been used. Furthermore, the results cannot be directly compared due to the pre-loading and gradual release excitement configuration instead of the use of an impulse. To not take into account the part where the load is effective, the first second has been left out of the analysis. The approach is therefore not applicable for the analysis of the vibration response in its most interesting 'forced' domain. Furthermore, due to a lack of available data on the viscous and hysteretic damping, the damping ratio for the first mode provided by the reEC5 and the experimental ball-test have been used as constant damping. Besides these attention points, it is generally still expected that the approach can provide an adequate qualitative and indication of the vibration response of the floor types relative to each other.

Furthermore, the CFL condition [28] for numerical time-dependent simulations has been checked and the approaches uses sufficiently small time steps to accurately capture the behavior. Besides, also the size of the mesh for vibration analysis has been checked by the commonly used relation of $h_mesh = 1/6 \cdot \lambda$ [59], and was found sufficient.

For the Harmonic response analysis similar convergence issues were found for the use of a 700 N cyclic load. However, due the load configuration not affecting the modal behavior, the observed qualitative and relative behavior is still valid. As described in Section E.2, the additionally found modes for the conceptual and decoupled floors in the 20-100 Hz range attributed to decoupled top floor response are aligned with the general formula for the vibration of a floating covering floor $f_{0,\mathrm{fl}} = 160 \cdot \sqrt{\frac{s'}{m'}}$ [52], in which s' is the dynamic stiffness of the resilient layer and m' the mass of the top floor. This indicates that the HRA can accurately capture the decoupled behavior of these floors. Although it does not impact the qualitative behavior it is recommended for future use of this approach to measure the acceleration and or velocity depending of the expected frequency to align it better to two governing parameters in the field of floor vibrations. At last, the same discussion points for damping and mesh size mentioned for the TSA apply.

While the modeling approach is generally considered valid, both the TSA and HRA feature similar results of the natural frequency which deviate from the analytically and experimentally found natural frequencies, as shown in Table 6.6. The higher natural frequencies found in the numerical approach indicates that the numerical approach creates stiffer models than in reality. No specific explanation for the difference could be found. Since the numerical analyses are only

used to find the qualitative behavior relative to the floor types, their conclusions are still valid and can be used to reinforce the findings of the other approaches.

Table 6.6: Summary of the natural frequencies found for the Experimental Design (ED) Traditional and Conceptual floor.

	$f_{1,exp}$ [Hz]	$f_{1,reEC5}$ [Hz]	$f_{1,TSA}$ [Hz]	$f_{1,HRA}$ [Hz]
Traditional	13,12	12,45	18,3	17,58
Conceptual	12,70	13,04	17,72	18,81
Decoupled	-	8,34	10,92	10,20

6.3.3 Experimental analysis

The experimental analysis also features some major attention points. First of all, due to the lack of a force meter in the set-up, the direct response over time could not be compared between the traditional and conceptual floor and the findings of the analytical approach. It can therefore also not provide additional insights on the visually observed increased initial response and increased damping of the conceptual floor in the time domain. Determining an single number value such as the root mean square acceleration might shed a different light on the currently observed conclusions. In contrast, the constraints of the ball-drop in the test are expected to be accurate enough to excite the floor in a similar way, enough that it can be qualitatively compared after the post processing.

Furthermore, although there are visible sample imperfections, the impact of these are expected to be acceptable. The most major impact can be seen in the decrease of the experimental natural frequency for the conceptual floor relative to the traditional floor, while for the analytical approach this is an increase. Assuming the mass is equal, this difference indicates a possible lower bending stiffness for the experimental specimen. Secondly, due to the imperfections and allowance of the specimen to move slightly, with friction, the damping of the specimen might be higher than for an perfectly produced floor. This difference in damping is however considered to be neglectable.

6.4 Conclusion

For the determination of the vibration performance of the studied floors an analytical analysis has been conducted using the method for the determination of the response factor as described by the draft of the revised Eurocode 5 for timber structures. Furthermore, a numerical approach using the time dependent Transient Structural Analysis (TSA) and excitement frequency dependent Harmonic Response Analysis (HRA) to provide extra insights in the qualitative behavior of the floors relative to each other. At last, an experimental vibration ball-fall test has been conducted to valid the approaches and its simplifications. Based on these investigations the following conclusions can be drawn:

- Based on validation with the experimental vibration test, the described analytical method was observed to be an accurate way to find the natural frequency of the traditional and conceptual floor.
- Due to limitations in the experimental set-up, the response magnitude could not directly be determined and the acceleration and velocity values determined from the reEC5-method,

which are used for the determination of the response factor and classification of the floor, could not be validated.

- The Harmonic Response Analysis shows potential to accurately describe the modal behavior of the three floor types and in qualitative comparison purposes.
- The Transient Structural Analysis as described can only be used for qualitative comparison purposes, while it requires a high computational time. It can however be provide valuable insights on the absolute response if the load configuration can be more accurately replicated.
- The analytical and the two numerical methods indicates similar relative behavior, where the conceptual 3,5% has a slightly better-, the conceptual 2,5% a slightly worse- and the decoupled floor has a much worse performance for tactile vibration performance.
- From the experimental investigation a damping ratio of 2,9% was found for the ED-Traditional floor and a damping ratio of 4,2% was found for the ED-conceptual floor. This is for both floors higher than the assumed reEC5-values of 2,5% and 3,5% respectively.
- The reEC5-method and the Harmonic Response Analysis show similar relative behavior, where the ED-conceptual 4,2% performs better than the ED-traditional 2,9% floors.
- The reEC5-method indicated that the addition of a floating for the traditional floor generally decrease floor response due to the added mass, but also lowers the natural frequency. If this results in a natural frequency below 8 Hz, the floor response has to be calculated in the acceleration domain which was for the long span floors observed to be unfavorable and cause the floor to be classified in a higher and possibility unsatisfactory response class.
- The investigations indicate an increased vibration performance of the conceptual floors compared to the traditional floor. However, due to the lack of absolute quantitative data, which can be related back to the reEC5-method on which the requirements are based, in the numerical and experimental investigations, they cannot provide insight on the absolute increase of vibration performance. Since the reEC5-method, while using experimental damping ratios, only indicated a small decrease of R(V) which did not increase the determined class, only the conservative conclusion that the conceptual floor features an equal vibration performance as the traditional floor can be made based on the approaches used in this study.

7 Acoustic performance

This chapter will discuss the acoustic performance of the nine studied floors. The acoustic performance referred to in this study focuses on the sound transmission through the floor system such that comfort in the residential unit a floor below is guaranteed. Perceivable sound in the lower residential unit can be categorized into two types based on their source. The first one is airborne sound whereby the floor system is indirectly excited through sound waves caused by for example speech, television or music. The second one is impact sound (transmission), which is when the floor is excited by impacts such as footfall, moving furniture or machinery. Both these sound types feature their own transmission behavior and are therefore evaluated separately. Besides, the transmission trough the floor can be characterized by two waves types, bending waves and longitudinal waves. The behavior of the bending waves can be described by the excitement causing the full element to bend, similar to tactile vibrations. The latter can be better described as the back and forth movement of particles of the materials in the direction of the wave. The total transmission is a complex combination of the two.

This chapter will first discuss the set requirements for the acoustic performance and the corresponding methodology, using an analytical, numerical and experimental approach, in Section 7.1. As explained in Chapter 4, the Traditional floor with Floating Floor (F.F.), will only be investigated with the analytical approach. The results of these approaches will be discussed in Section 7.2, after which the approach will be reviewed and the results compared in Section 7.3. Finally the conclusions are formulated in Section 7.4.

7.1 Requirements & methodology

This section described the requirements to reach satisfactory acoustic performance and the methodology on how this performance is evaluated. As described in Section 2.3, the acoustic performance of a floor is defined by its transmission of airborne sound and impact sound to the room located directly beneath. Although the sound transmission varies greatly based on the frequency due to the variation in floor performance and perception of sound over the frequency, it can be captured in two single number-values for each of the transmission types [9]. The first one is the Standardized Airborne Sound Level Difference $D_{nT,w}$, or more specifically $D_{nT,A}$ when A-weighting is used. It consists of the addition of the Standardized Airborne Sound Level Difference D_{nT} plus the spectrum adaptation term, described in ISO 717-1:2020, to tune the sound pressure level to our actual hearing based on the A-weighting curve. For impact sounds the main quantity is the Weighted Standardised Impact Sound Pressure Level $L_{nT,w}$, or similarly $L_{nT,A}$, which similarly consists out of the addition of the Standardised Impact Sound Pressure Level L_{nT} and the spectrum adaptation term described in ISO 717-2:202. While generally both these terms are evaluated in the 100-5000 Hz domain, it is advised for lightweight structures to start from 50 and even 25 Hz [9], [47]. Methodological limitations result in differing of the evaluated frequency domains, as described in their respective methodologies.

The satisfaction of the acoustic performance is based on the requirements set in the Dutch building code for the two single-number values. Due to the scope of this study, specifically the regulations regarding the transmission between two separate residential units are considered.

Further more, since the flanking transmission is outside the scope for the project, only the direct sound transmission will be evaluated. Since $D_{nT,A}$ is a difference in sound pressure levels, a minimum requirement is set, while $L_{nT,A}$ defines the sound pressure level in the room below for which thus a maximum requirement is set. The requirements for satisfactory acoustic performance are shown in Table 7.1.

Table 7.1: Requirements for the sound tranmission based on the Dutch requirements for sound insulation in residential buildings according to Bouwbesluit 2012 - Section 3.4 Sound insulation between rooms for new construction [41].

		Requirement
$D_{nT,A}$	[dB]	$\geq$52
$L_{nT,A}$	[dB]	$\leq$54

To determine the values of $D_{nT,A}$ and $L_{nT,A}$ for the 9 floor types, an analytical approach using the Bassist software will be used. However, due to the complexity of analytically determination of acoustic performance the approach is limited to basic floor configurations. The traditional and conceptual floor can therefore not be inserted directly. Therefore, additional numerical vibration analysis will be used to provide more qualitative information regarding the floor behavior for acoustics. At last, also an experimental investigation will be conducted on the ED traditional and vibrational floors to reinforce the qualitative numerical analysis with actual values.

7.1.1 Analytical analysis

For the determination of the single number-values for the airborne sound insulation $D_{nT,A}$ and impact sound pressure levels $L_{nT,A}$ the software program Bassist.Lab - 5.1 (Bassist) developed by Level.Tools, a trademark of Level Acoustics and Vibrations B.V., will be used. This program replicates results from experimental testing in acoustic laboratory conditions using a calculation model consisting of a collection of analytical equations and empirically found relations, which are among others based on the works of Gerretsen [35]. The empirical relations are mostly related to replicated the complex damping phenomena. In Bassist the single number-values are given for the 125-8000 Hz octave band range, including spectrum adaption terms to additionally include the 63 Hz octave band. The resulting single number-values will thus be conducted in a 44-11360 Hz.

An overview of the used properties of the base materials Table 7.2. The densities of the materials ρ and their Young's modulus E will be based upon the earlier described properties. For the insulation materials the Young's modulus was determined from Equation (7.1) [10] based on the described dynamic stiffness s' in the product specification [49].

$$s' = \frac{E}{t} \tag{7.1}$$

While the value for the longitudinal wave speed c_L of the CLT is based on the experience by LEVEL, the c_L for the concrete grades were determined from the simplified formula for the longitudinal wave speed through one dimensional solids shown in Equation (7.2).

$$c_L = \sqrt{\frac{E}{\rho}} \tag{7.2}$$

It is advised by the software manual to keep the Poisson ratio v and ratio of shear modulus and Young's modulus G/E equal to 0,3 and 0,385, respectively [35]. The loss factor η are based on information and experience of LEVEL. The flow resistance r_s in the insulation material can be approximated by Equation (7.3) for stone wool [35].

$$r_s = 50 \cdot \rho^1, 53 \tag{7.3}$$

Table 7.2: Material properties for the base materials in Bassist.

		CLT	C25/30	C30/37	C50/60	Rockfloor Base
ρ	[kg/m^3]	500	2400	2400	2400	100
E	[N/mm^2]	11000	31000	33000	37000	0,36[1]
c_L	[m/s]	3200[2]	3593,98[3]	3708,10[3]	3926,41[3]	-
G/E	[-]	0,385	0,385	0,385	0,385	-
η	[-]	0,015[2]	0,006[4]	0,006[4]	0,006[4]	0,25[4]
r_s	[kNs/m^4]	-	-	-	-	114,8154[5]

[1] $E = s'$

Furthermore, a span and width of 5 meter will be used as settings, as these are the maximum available dimensions in this version. Based on trial and error with dimensions of 8,7 by 8,7 meter with a developers version, an approximate difference for $D_{nT,A}$ and $L_{nT,A}$ of respectively -1 dB and +1 dB are expected.

Due to the uncertainty in the level of acoustic decoupling in the conceptual floor, an lower and upper performance boundary will be studied. The lower performance boundary will feature the same homogeneous floor approach as the traditional floor, assuming full acoustic coupling between the timber and concrete. The upper performance boundary will be calculated using the floating floor approach also used for the decoupled floor and thus assuming full acoustic coupling between the timber and concrete. The homogeneous floor- and floating floor approach will be described in the following sections.

7.1.1.1 Homogeneous floor approach for the Traditional- & lower bound Conceptual floors.

Since Bassist does not allow structural composite floors as direct input, an indirect input has to be used. For the traditional- and upper bound Conceptual floors this will be done by the determination of an equivalent homogeneous floor. This floor will then be inserted in the 'Base floor' structure type setting. Most important however is the determination of the equivalent properties. As shown in Equation (7.4), the equivalent density rho_{eq} is based on the total mass, including notches, M_n and the total height of the composite floor h_{tot}. Furthermore, Equation (7.2) can be rewritten to find the equivalent longitudinal wave speed $c_{L,eq}$, shown in Equation (7.5). For the determination of the bending stiffness the extended $\gamma - method$ will be used as described in Section 5.1.4. The equivalent loss factor can be determined from weighing the loss factors of the different materials over their Young's modulus and height, as shown in

Equation (7.6).

$$\rho_{\text{eq}} = \frac{M_n}{h_{\text{tot}}} \tag{7.4}$$

$$c_{L,\text{eq},1} = \sqrt{\frac{E_{\text{eff},1}}{\rho_{\text{equiv},1}}} \quad \text{with} \quad E_{\text{eff}} = \frac{EI_{\text{eff}}}{\frac{1}{12} \cdot b \cdot h_{\text{tot}}^3} \tag{7.5}$$

$$\eta_{\text{eq}} = \sum_{i=1}^{n} \eta_i \frac{E_i \cdot h_i}{\sum E_i h_i} \tag{7.6}$$

As described in Chapter 6, an experimental damping ratio $\zeta_{1,exp}$ has been found for the ED traditional and conceptual floor. An indication of the loss factor for these floors can then be found from the relation between the damping ratio and the loss factor shown in Equation (7.7) [10].

$$\eta_{exp} = 2 * \zeta_{1,exp} \tag{7.7}$$

7.1.1.2 Floating floor approach for the Decoupled- , upper bound Conceptual floors and Traditional floors with Floating Floor.

For the two acoustically decoupled floor types, the 'Base floor + floating floor' structure type setting will be used. This includes the input of a base floor, an interlayer and a top floor.

The insertion of the upper bound conceptual floor require again some additional steps. The interlayer will consist of the 20 mm Rockfloor Base material as described in Table 7.2. The top floor will consist out of the concrete properties corresponding to the concrete grade and height used in the design. However for the Base floor the described base CLT properties cannot be applied since the composite interaction will then not be considered. Therefore an equivalent base floor will be determined, including the full stiffness of the CLT and the stiffness of the concrete regarding the composite interaction. The formulas to determine the equivalent material properties as show in Equations (7.8) to (7.12). Since the mass of the concrete is determined in the program by the constant layer height and density, an equivalent mass will be used for the base floor, which thus includes the mass of the concrete in the notches in addition to the CLT mass.

$$EI_{2,\text{eq}} = EI_{\text{eff}} - EI_1 \tag{7.8}$$

$$E_{2,\text{eq}} = \frac{EI_{2,\text{eq}}}{I_2} \tag{7.9}$$

$$M_{(n,2,eq)} = M_n - M_{(n,1)} \tag{7.10}$$

$$\rho_{(2,eq)} = \frac{M_{(n,2,eq)}}{h_2} \tag{7.11}$$

$$c_{(L,2,eq)} = \sqrt{\frac{E_{(2,eq)}}{\rho_{(2,eq)}}} \tag{7.12}$$

$$\tag{7.13}$$

For the loss factor the same value as for the base CLT material will be used. However, for the additional investigation using the experimental damping ratio found for the ED-conceptual floor,

the loss factor will be adapted such that $\eta_{eq} = \eta_{exp}$. By rewriting Equation (7.6), Equation (7.14) can be found and $\eta_{2,eq}$ be determined.

$$\eta_{(2,eq)} = \frac{\eta_{(eq,exp)} \cdot (E_1 \cdot h_1 + E_{(2,eq)} \cdot h_2 + E_{insu} \cdot t) - \eta_1 \cdot (E_1 \cdot h_1) - \eta_{insu} \cdot (E_{insu} \cdot t)}{E_{(2,eq)} \cdot h_2} \tag{7.14}$$

For consistency the decoupled floor will be inserted using the same approach as the upper bound conceptual floor. This results in higher longitudinal velocities than for the base CLT described in Table 7.2. For comparison, the decoupled floors will additionally be evaluated using the standard practice of using the base CLT layer as base floor for the evaluation of the decoupled floor. This version will be referred to as 'Decoupled - reference'.

As last, the Traditional floor with additional floating floor will also be calculated using the Floating floor approach. It features the same properties for the base floor as calculated for the modeling of the Traditional floor as equivalent base floor using the 'homogeneous base floor' approach described in previous section. For the interlayer the 20 mm Rockfloor Base will again be used, and for the floating top layer the lower grade C25/30 concrete will be used, with equal thickness as the top floor of the decoupled floor. The dimensions of all the floors are described in Chapter 4.

7.1.2 Numerical analysis

Similar in the analysis of vibration performance, the analytical method is not expected to accurately capture the acoustic performance of the conceptual floor. Therefore next to a limited experimental analysis, an numerical analysis will be done. For this the same two analyses types as for the vibration performance, described in Section 6.1.2 will be used: a Transient Structural Analysis and a Harmonic Response Analysis (HRA) in the software package of Ansys mechanical. While for the tactile vibration performance the vibration of the top of the concrete is most important, for acoustic performance the response of the bottom of the CLT and the difference between the top and bottom response are critical.The latter provides an indication of the transmission of (sound) waves through the floor. To compare the response at the bottom of the CLT in between floor types, Y(t) has been defined in Equations (7.15) to (7.17) using a logarithmic ratio is decibels.

$$Y_{TSA,\delta,i}(t) = 10log_{10}(\frac{\delta_{TSA,bot,i}(t)}{\delta_{bot,traditional}(t)}) \tag{7.15}$$

$$Y_{TSA,a,i}(t) = 10log_{10}(\frac{a_{TSA,bot,i}(t)}{a_{TSA,bot,traditional}(t)}) \tag{7.16}$$

$$Y_{HRA,\delta,i}(f) = 10log_{10}(\frac{\delta_{HRA,bot,i}(f)}{\delta_{HRA,bot,traditional}(f)}) \tag{7.17}$$

To compare Top-Bottom Transfer between floor types, G(t) has been defined in Equations (7.18) to (7.20) also using a logarithmic ratio is decibels.

$$G_{TSA,\delta,i}(t) = 10log_{10}(\frac{\delta_{TSA,bot,i}(t)}{\delta_{top,i}(t)}) \tag{7.18}$$

$$G_{TSA,a,i}(t) = 10log_{10}(\frac{a_{TSA,bot,i}(t)}{a_{TSA,top,i}(t)}) \tag{7.19}$$

$$G_{HRA,\delta,i}(f) = 10log_{10}(\frac{\delta_{HRA,bot,i}(f)}{\delta_{HRA,top,i}(f)}) \tag{7.20}$$

At last, it should be noted that the analyses are originally a setup for vibrational analysis and therefore only provide indicative acoustic insights. Furthermore, the observed frequency range for the HRA will now be 0-5000 Hz.

7.1.3 Experimental analysis

Similarly to the numerical analysis, to provide an indicative insight in the acoustical performance in an experimental setup the same vibration experimental as described in Section 6.1.3 will be used. The only difference is the result processing. For this analysis the top-bottom transfer is again the most important parameter. For the experimental analysis the top-bottom transfer per frequency per pair will be found by finding the response of the top sensor of the pair $PSD_{top,i}(f)$ and the response of the bottom sensor of the pair $PSD_{bot,i}(f)$. This dimensionless ratio, will than be converted back to decibels. The experimental top-bottom transfer $H(f)$ is therefore defined as shown in Equation (7.21). A negative value of $H(f)$ indicates that there is a positive weaker bottom response than top response.

$$H_i(f) = 10log_{10}(\frac{PSD_{bot,i}(f)}{PSD_{top,i}(f)}) \tag{7.21}$$

To determine if the floor response at a given frequency can be defined as 'coupled' or 'decoupled' a threshold for top bottom transfer of +- 5 dB is established. From this threshold outwards, the difference in top and bottom response can actually be perceived.

At last, since the top and bottom transfer is only a relative term defining the relation of the top and bottom accelerometers of each pair, the inaccuracy of the excitement method does not impact the the values of $H(f)$ and thus can be compared across dropping positions and floor types.

7.2 Results

In this section the results of the Analytical approach using Bassist, the numerical approach using the Transient Structural Analysis and Harmonic Response analysis and the experimental vibration test will be discussed.

7.2.1 Analytical analysis

An overview of the calculated single-number values of the airborne sound insulation and impact sound pressure levels are shown in Figure 7.1. Several interesting trends can be observed from this figure.

First of all, it can be clearly noted that the impact sound is governing over the airborne sound insulation. Especially the LSD+ floors show great performance in the airborne sound

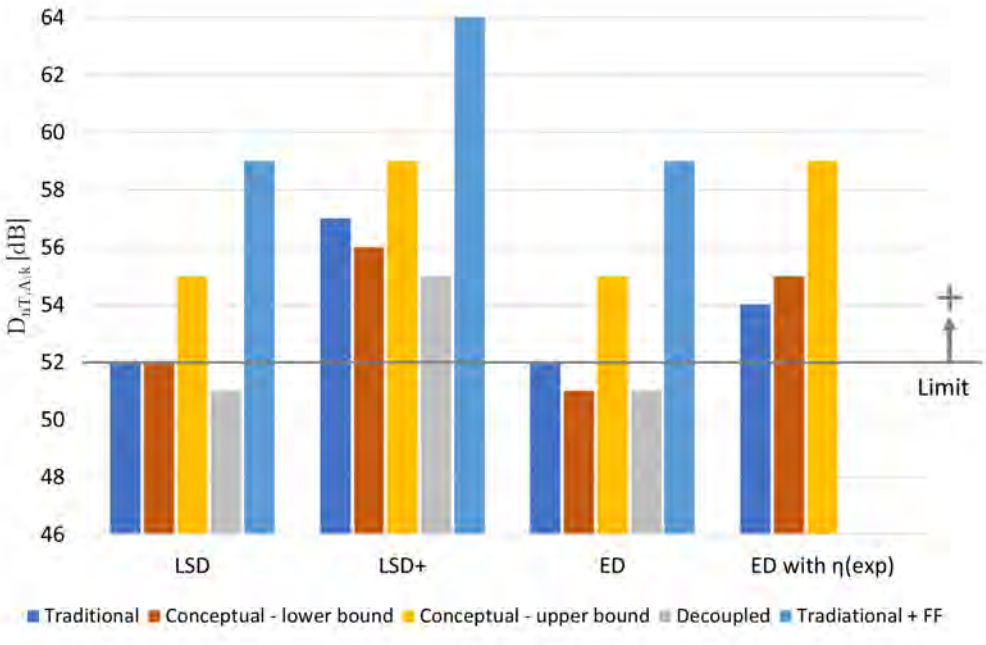

(a) Airborne sound insulation

H

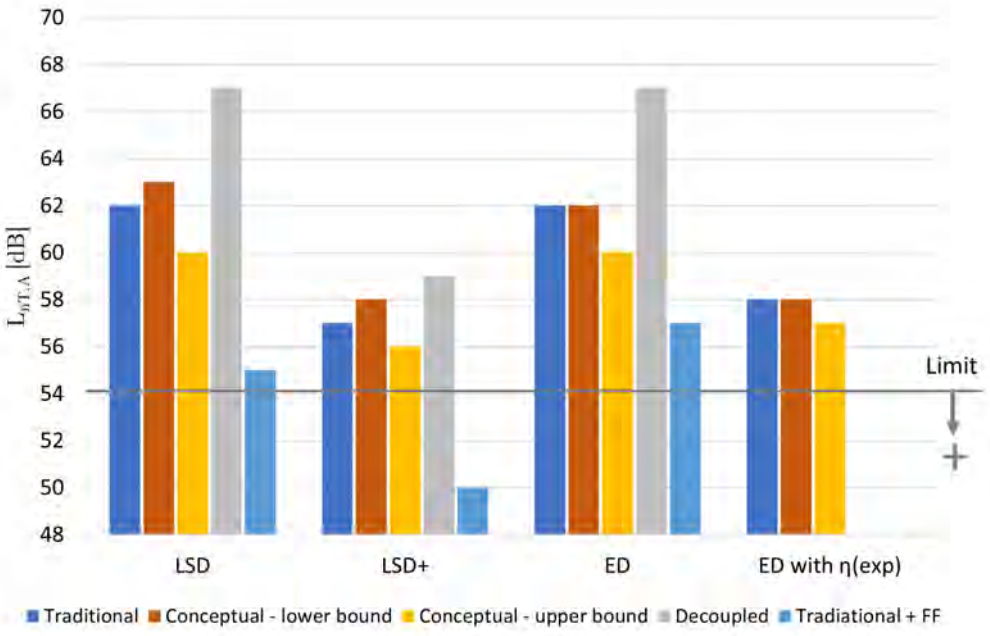

(b) Impact sound pressure level

Figure 7.1: Overview of the single number-values calculated in Bassist, including the lower limit for satisfactory Airborne sound insulation and upper limit for satisfactory Impact sound pressure level.

criteria. While for the impact sound criteria it also features the best performance, it is not low enough to reach the upper limit.

Secondly, it can be observed that the lower bound conceptual floor, assuming full acoustic coupling, features a similar performance as the traditional floors with differences in the range from -1 dB to +1 dB for $D_{nT,A}$ and 0 dB to +1 dB for $L_{nT,A}$. The upper bound of the conceptual floor, found by the floating floor approach, performs much better with an increase of $D_{nT,A}$ between +2 dB and +4 dB and a decrease of $L_{nT,A}$ between -1 dB to -2 dB. While the behavior of the lower bound conceptual floor was similar to the traditional floor, the upper bound features a more similar behavior to the decoupled floor as shown for the ED-floors, which are also indicative for the general behavior of the floor types in the other design categories, in Figure 7.1. This behavior difference mainly results in a considerable improved performance above the 125 Hz octave band. The positive decrease of $L_{nT,A}$ is however limited due to a peak formation at the 125 Hz octave band. Since the actual conceptual floor is expected to partly feature the coupled and decoupled acoustic behavior, the governing peak observed in the fully decoupled state might be reduced at the cost of the less critical performance in the upper frequencies.

Thirdly, the decoupled floors perform worse than expected compared to the the conceptual upper bound floor, which also uses the floating floor approach. It can be noted that there is no specific negative behavior change, but a worse performance in general. Although the decoupled floor features a slightly lower mass than the conceptual floors due to presence of extra concrete in the notches of the latter (between 15,72 and 23,59 kg/m^2) it is not expected to be significant to create the observed difference. The other major difference is the integration of the additional stiffness of composite action part of the concrete to the regular stiffness of the CLT for the conceptual floor to represent the increased bending stiffness of the composite floor. This addition of this additional bending stiffness in the upper bound conceptual floor can be seen in the form of a flatter peak at 125 Hz compared to the decoupled floor. However, the way of how the additional composite interaction is integrated did not only change the bending stiffness but affected the elastic modulus E_2, eq of the material. It therefore improves the performance in low frequencies where the bending stiffness features an high impact, but also at higher frequencies where bending stiffness is less impactful. Besides, the equivalent loss factor η_{eq} of the combined layers is based on the height and elastic modulus of the layers. Due to the much higher elastic modulus of the CLT and equivalent base floor, used for the decoupled and conceptual floor respectively, the higher loss factor of the CLT, compared to the concrete, is more present and thus results in to a increased η_{eq} of the system. The significantly worse performance of the decoupled floor compared to the upper bound conceptual floor, both featuring the floating floor approach, is most probable caused by a combination of a slight decrease in mass, a lower (equivalent) elastic modulus for the base layer and a lower equivalent loss factor of the system.

Fourthly, the decoupled floor also performs significantly worse compared to the coupled traditional and lower bound conceptual floor featuring the homogeneous approach, while an better performance was expected due the acoustical decoupling. Similar to the findings of the comparison of the upper bound conceptual floor to the coupled floors, a much better performance was found for the frequencies above the 125 Hz octave band. This can most likely be attributed to the decoupling effect. However, although the increased performance for the middle- and high frequencies, the decoupled floor feature worse single-number values. Critical for the general weak performance is thus the poor performance in the low frequency domain consisting of the 63 Hz and 125 Hz octave bands. The results for the low frequency domain can be explained by the low bending stiffness of the decoupled floor and the negative impact of the decoupling due to

resonance frequency of the top floor.

Fifth, the improvement of the acoustic performance of the traditional floor with floating floor can be seen clearly. It features increased decoupling and mass, while it maintains the bending stiffness of the traditional floor. Especially the latter two parameters features positive influence on the critical low frequencies where bending waves are governing.

At last, it can be noted that the usage of the increased equivalent loss factor determined from the experimental damping ratio $\zeta_{1,exp}$ features a significantly better acoustic performance for the ED-floors.

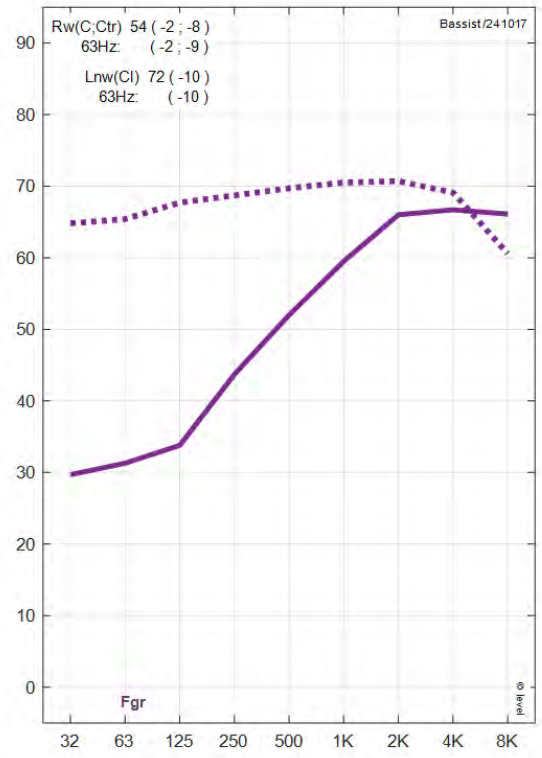

(a) Traditional

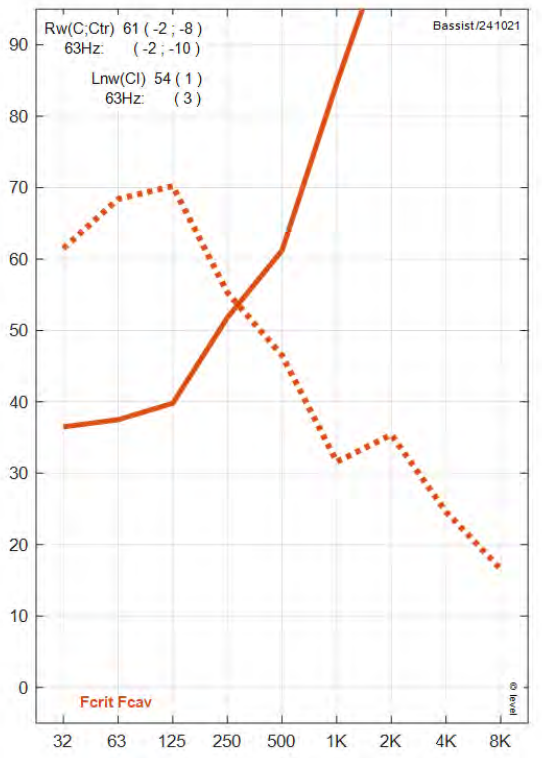

(b) Traditional with Floating Floor

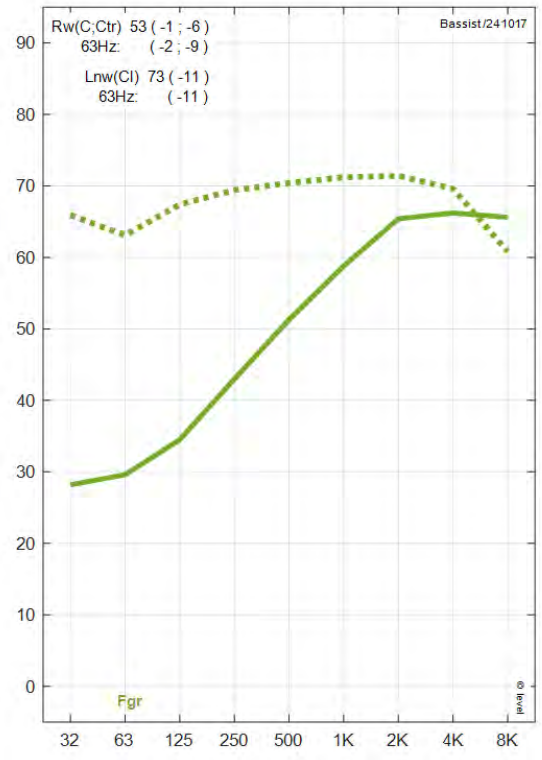

(c) Conceptual - lower bound

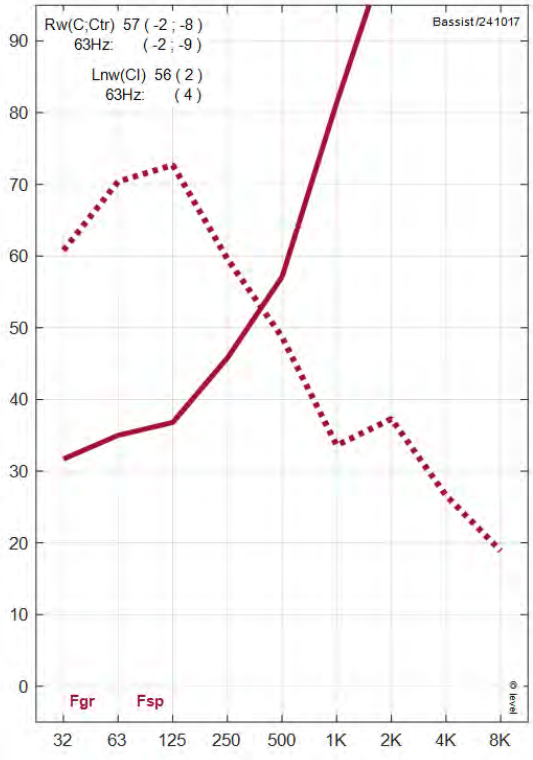

(d) Conceptual - upper bound

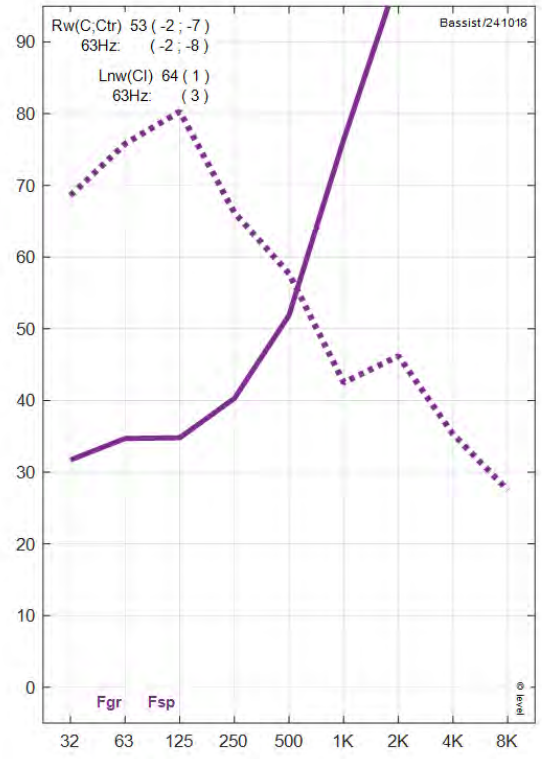

(e) Decoupled

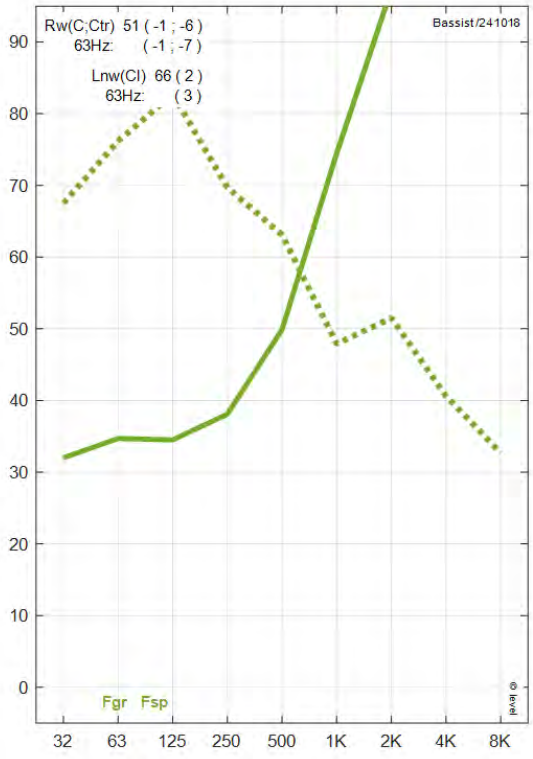

(f) Decoupled - Reference

Figure 7.2: Airborne sound insulation and Impact sound pressure level per octave band of frequency calculated by Bassist for the floors in the Experimental Design (ED) category.

7.2.2 Numerical analysis

This section discusses the results of the numerical vibration analyses conducted to provide an indication of the relative sound transmission due to bending waves. First the results of the time-dependent Transient Structural analysis will be discussed and secondly the frequency dependent Harmonic Response analysis.

7.2.2.1 Transient Structural Analysis

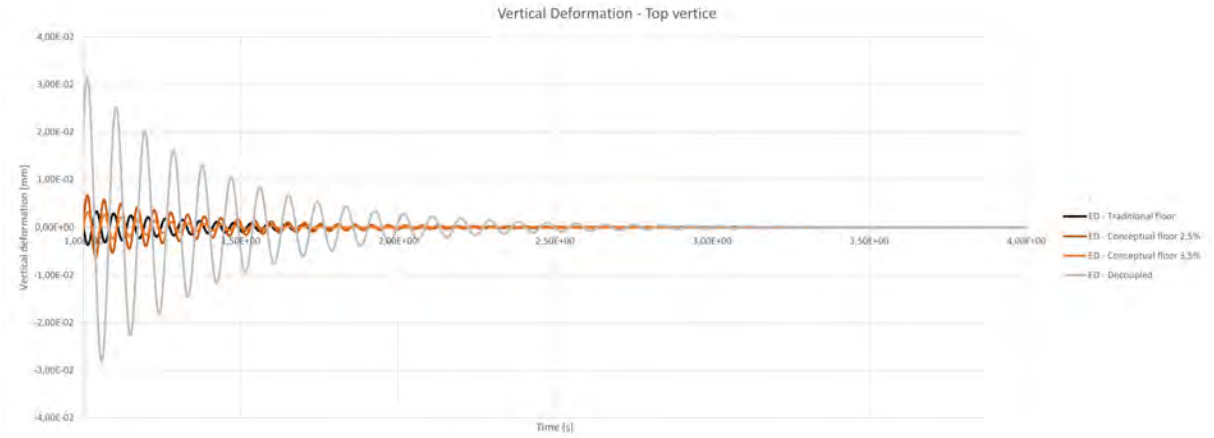

(a) Modified time frame

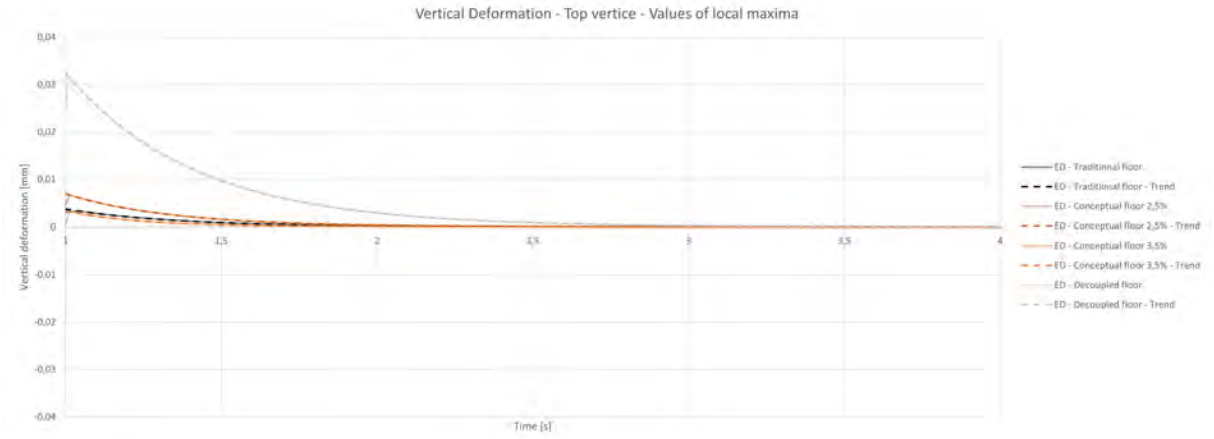

(b) Local maxima

Figure 7.3: Deformation results for the top of the concrete of the Experimental Design (ED) floors.

The results for the Transient Structural Analsys (TSA) of the Experimental Design (ED) floor can be seen in Figure E.5 and features similar trends as observed for the LSD and LSD+ design categories. Extensive results for the three design categories can be found in Section E.1.

It can be observed that the conceptual 3,5% floors featured the lowest vibration response at the bottom of the CLT. This was followed-up by the traditional and conceptual 2,5%, respectively. For the ED floor the traditional floor featured more similar behavior to the Conceptual 3,5% floor. However, for the LSD and LSD+ floors the traditional floor almost perfectly align with the conceptual 2,5% floor. The worst bottom CLT response was found for the decoupled floors. These results can be explained by the fact that this analysis set-up can only capture

the behavior of bending waves for first natural frequencies. This is mainly the result of the excitement configuration of releasing a downward force at top of the concrete, located at the center of floor span. The floor is therefore in pre-bended state and will after excitement decay on its own. Due to the vibration decaying on its own, the first and possibly second natural frequency will dominate the observed response. The was confirmed by the frequency of the vibration, which aligned with the first eigenfrequencies found in the Harmonic Response Analysis. For this type of wave the mass and effective bending stiffness of the floor are the governing parameters, and the decoupling of top and bottom floor barely has effect. This was confirmed by the minimal difference between top and bottom response in the conceptual and decoupled floors. This explains why the traditional floor features similar responses as the conceptual floors. The improved performance of the conceptual 3,5% thus comes solely from its increased damping ratio. It also explains the poor performance of the decoupled floor, which is now punished for its lower mass and significantly lower bending stiffness without getting major benefits from the increased decoupling.

Figure 7.4a shows a comparison between the three design categories. The decreased performance observed for the LSD floors can be related to its significant lower bending stiffness relative to its span compared to the other two design categories. Although the ED floor features a much lower bending stiffness compared to the LSD+ floor, it is also analysed for a 6 meter span instead of an 8,7 meter span. This is considered as the main cause for the observed best performance for the ED floors.

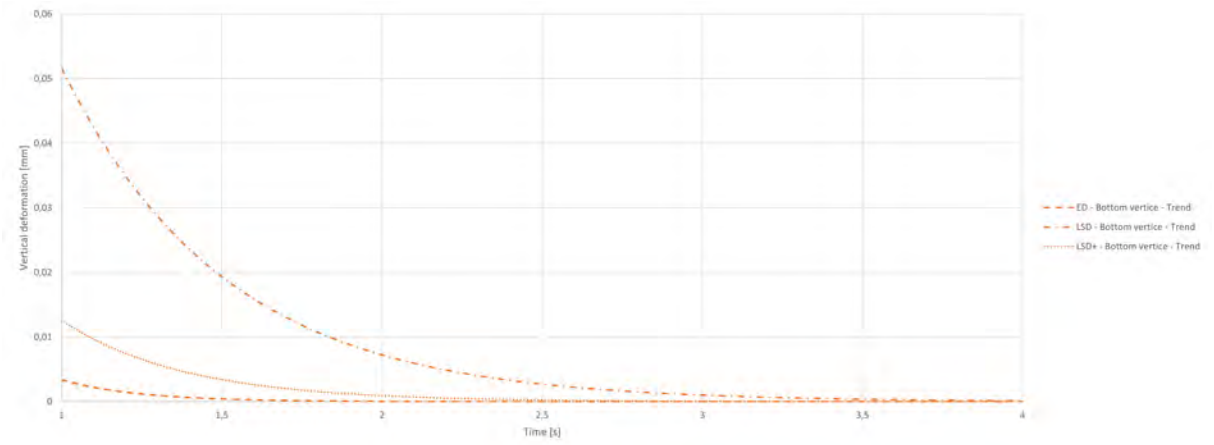

(a) Bottom response for the conceptual 3,5% floors for each design categories using the Transient Structural Analysis.

7.2.2.2 Harmonic Response Analysis

In this section the results regarding the approach using the Harmonic Response Analysis to provide an indication for the sound transmission are discussed.

Figure 7.5 shows the maximum response at the bottom of the CLT per floor type and design category. The most prominent observation is the almost constant magnitude of the conceptual floors in between the values found for the traditional and decoupled floors. Besides, its response is formed by the governing response trends in the traditional and decoupled floors, such as in 2500-3000 Hz and 3700 Hz for the conceptual LSD floors.

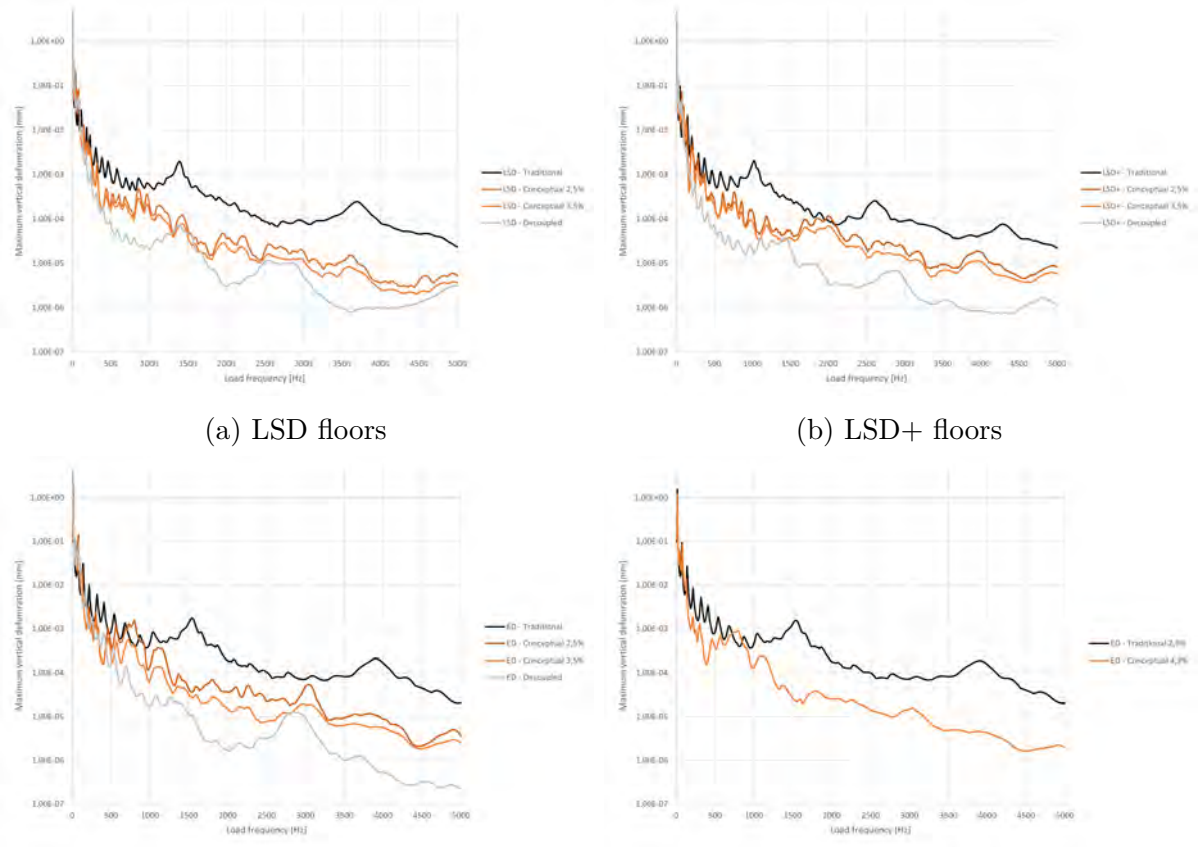

(a) LSD floors

(b) LSD+ floors

(c) ED floors

(d) ED floors using ζ_{exp}

Figure 7.5: Results of response at the bottom of the CLT per floor type using the the Harmonic Response Analysis of the per floor design category.

These observations are in line with the results shown for the Top-Bottom Transfer indicating the bottom response relative to top response Figure 7.6.

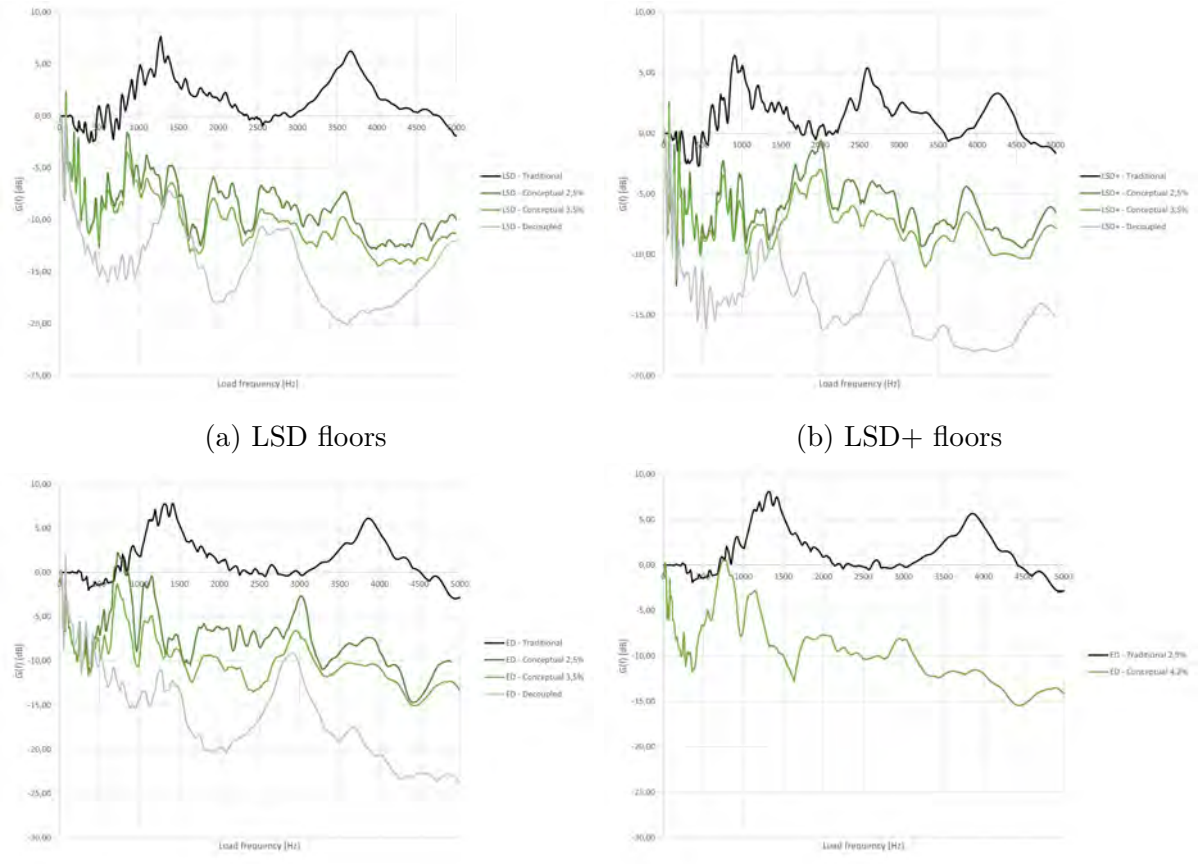

(a) LSD floors

(b) LSD+ floors

(c) ED floors

(d) ED floors using ζ_{exp}

Figure 7.6: Top-Bottom transfer $G(f)$ of the floor types based on the results of the Harmonic Response Analysis of per floor design category.

A more detailed response of the ED floors per frequency range is shown in Figures 7.7 and 7.8. It shows the insignificant impact of the decoupling on the first 40 Hz compared to a decreased bending stiffness. The conceptual 3,5% only outperforms the traditional floor in this region due to its increased damping ratio. After 40 Hz, the first decoupling effects are visible for the decoupled floor as well as the conceptual floors. This results in a decrease of performance due to the introduction of extra modes, as well as a positive performance due to a decreasing transfer over frequency. Between 70 and 100 Hz the positive effects begin to govern the response, resulting in an improved acoustic performance for the decoupled and conceptual floor relative to the traditional floor.

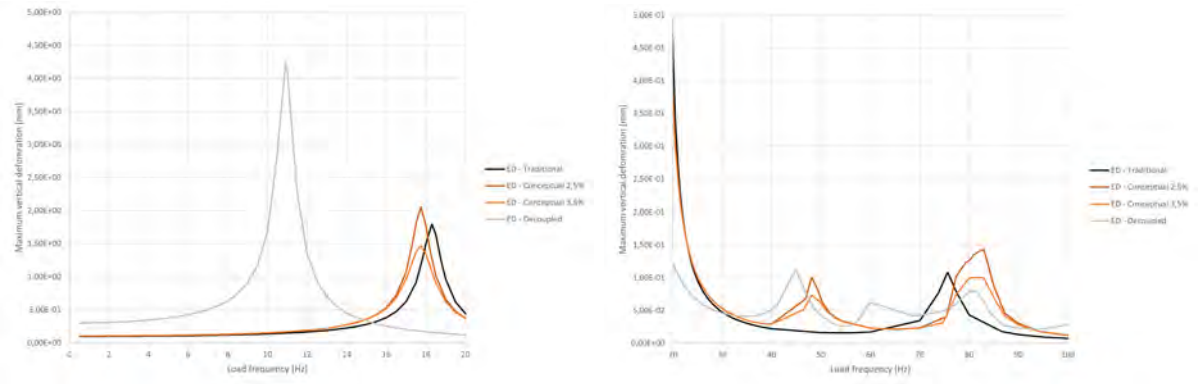

(a) 0-20 Hz (b) 20-100

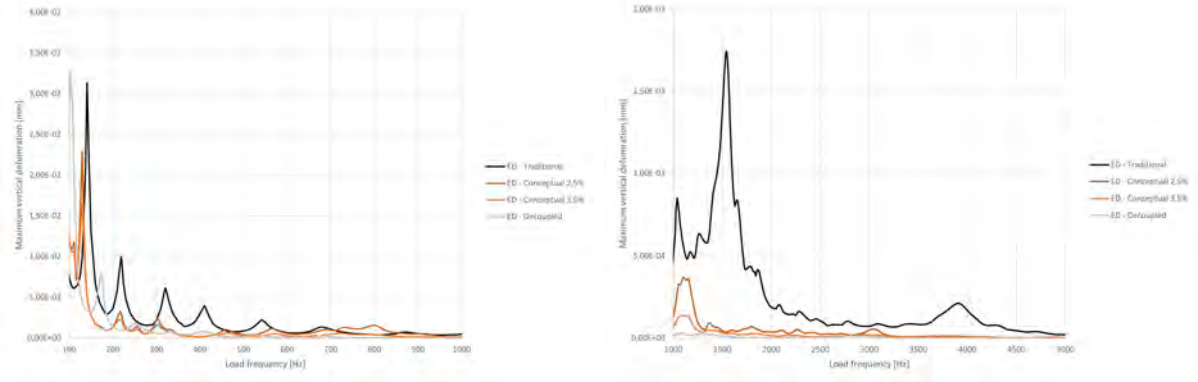

(c) 100-1000 Hz (d) 1000-5000 Hz

Figure 7.7: Results of the Harmonic Response Analysis for the Experimental design (ED) per floor type.

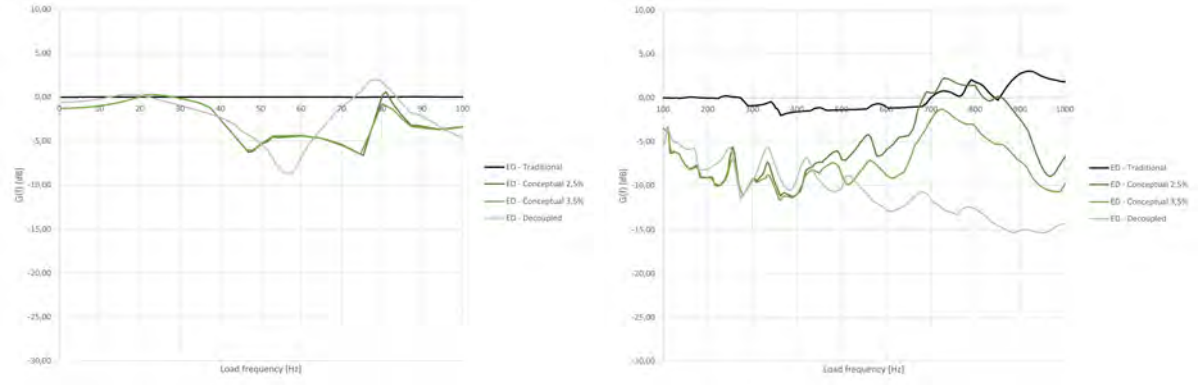

(a) 0-100 Hz (b) 100-1000 Hz

Figure 7.8: Top-Bottom transfer $G(f)$ based on the results of the Harmonic Response Analysis of the Experimental design (ED) per floor type.

At last, it it surprising to see a significant positive Top-Bottom Transfer at around 1500 Hz for the traditional floor and around 740 Hz for the conceptual floor 2,5% of the Experimental Design category. The corresponding modes are shown in Figure 7.9. This observation can be

explained due to the characteristic of the CLT as build-up element with weak transverse layers, resulting in variation in the response of its layers.

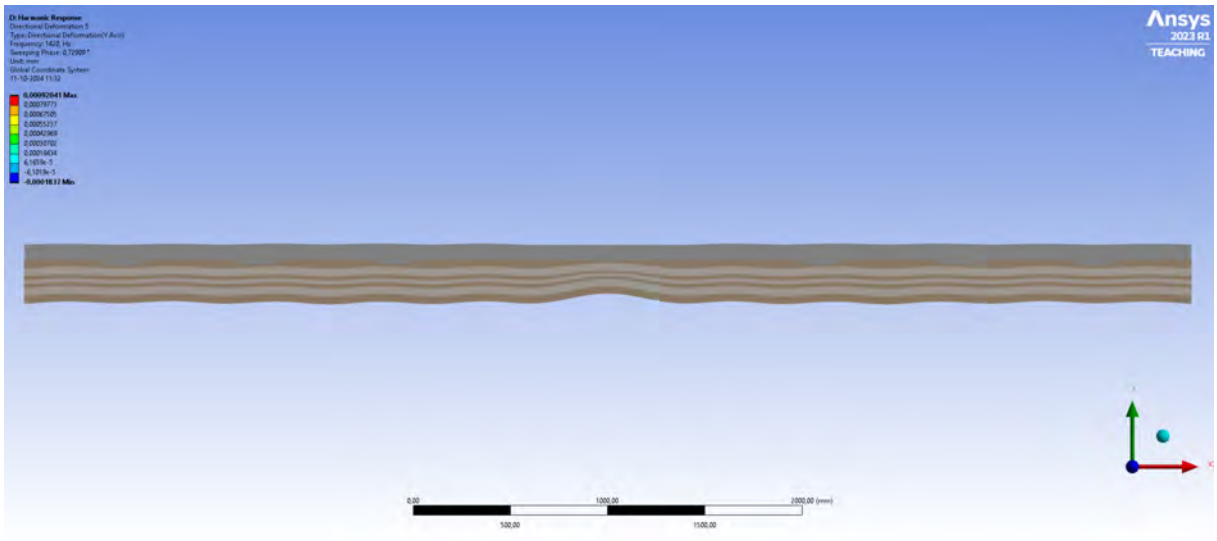

(a) Traditional floor - 1500 Hz

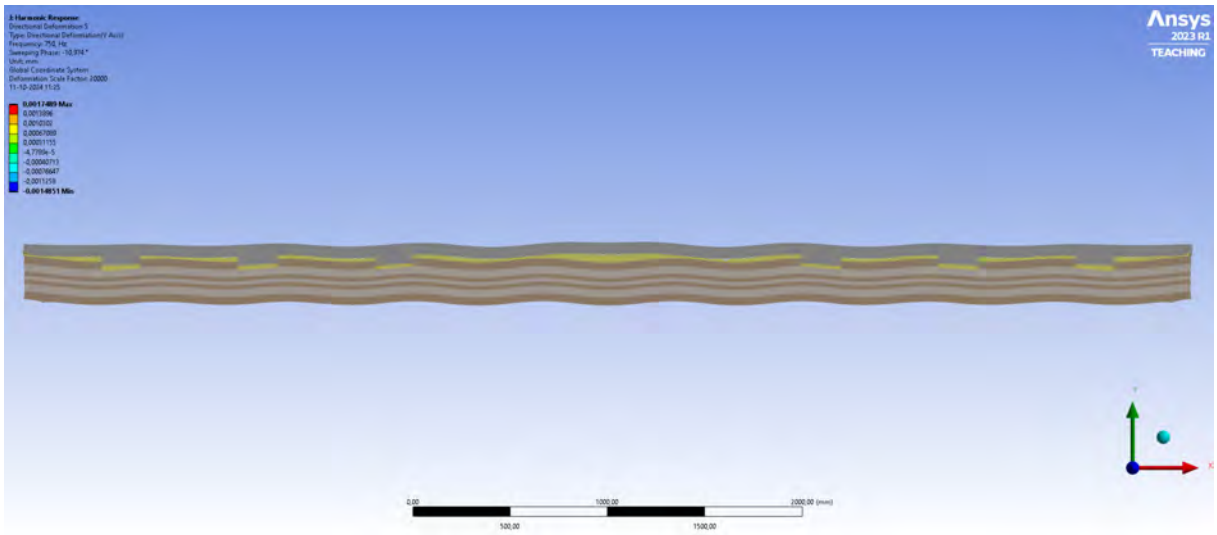

(b) Conceptual 2,5% floor - 740 Hz

Figure 7.9: Modes, with an increased deformation scale, for a positive Top-Bottom transfer $G(f)$ based on the results of the Harmonic Response Analysis of the Experimental design (ED).

7.2.3 Experimental analysis

The results for top-bottom transfer for the traditional floor are shown in Figures 7.10 and 7.11. To properly read these figures it should be noted that $H(f)$ is based on the PSD(F). As explained earlier, the latter is found by a FFT of the original signal in time domain and shows the strength of harmonic vibrations per frequency. Contrary to $G(f)$ used in the acoustic numerical analysis, $H(f)$ thus does not show if the top of the floor vibrates stronger/weaker than the bottom of the floor but only if that specific frequency is present.

For the results of the Traditional floor with DP1, excluding the first 20 Hz due to frequency

hearing range and exclusions the last 200 Hz due to sensor limit accuracy, it can be seen that there are only three slim peaks at approximately 320, 480 and 540 Hz go beyond the 5 dB threshold. For the Traditional floor response from excitement at DP2 larger positive and negative differences can be seen with more peaks (slightly) over of near the threshold. However, the behavior of the traditional floor in both situation should be seen as coupled.

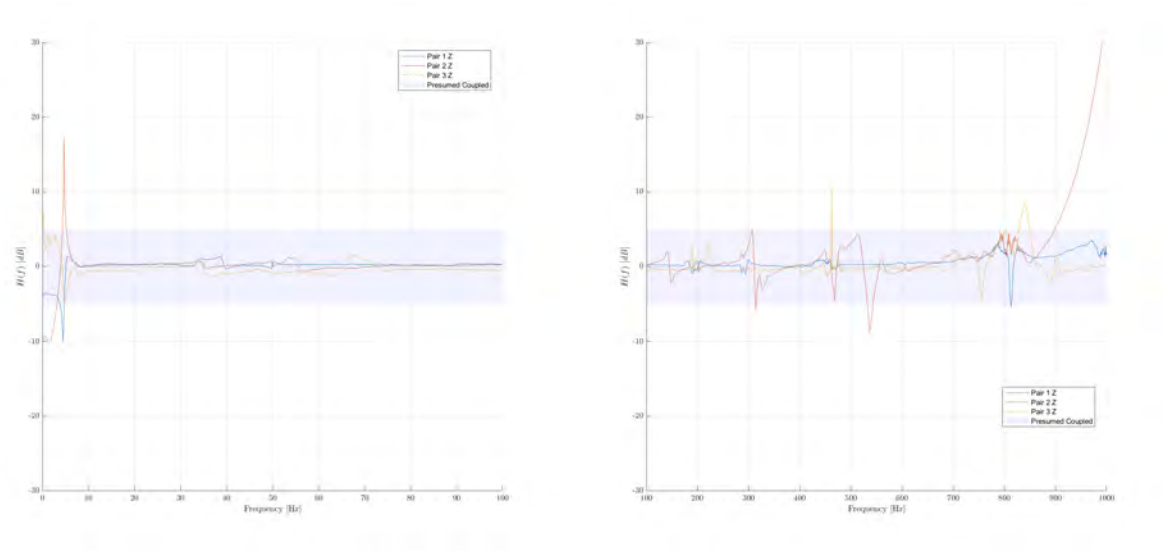

(a) 0-100 Hz (b) 100-1000 Hz

Figure 7.10: Transfer function processed from the floor response in the frequency domain for drop 1 for DP1 of the experimental vibration tests of the Traditional Floor.

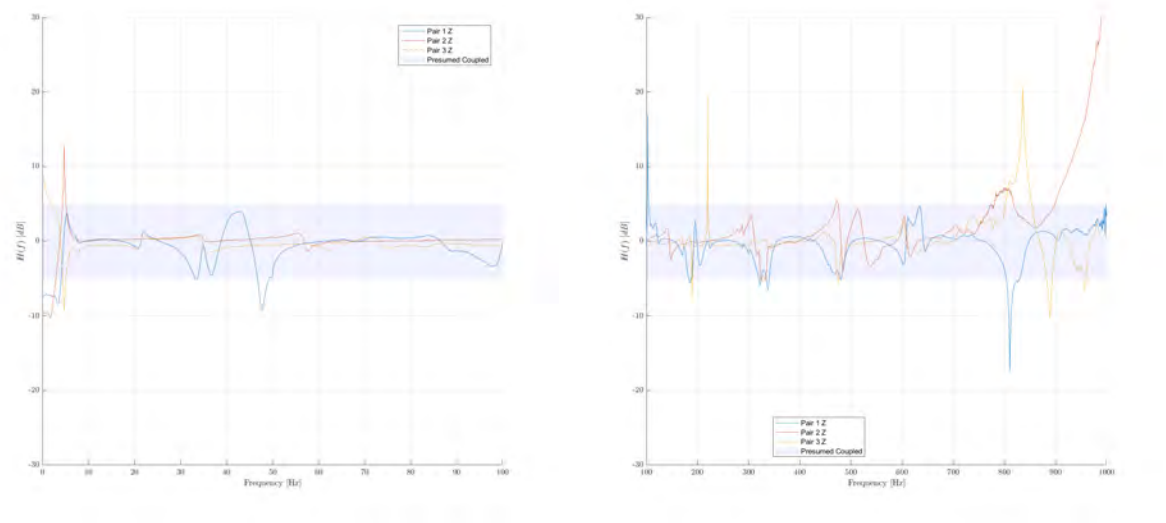

(a) 0-100 Hz (b) 100-1000 Hz

Figure 7.11: Transfer function processed from the floor response in the frequency domain for drop 1 for DP2 of the experimental vibration tests of the Traditional Floor.

The results for top-bottom transfer for the conceptual floor are shown in Figures 7.12 and 7.13. The response following from excitement at DP1 starts again for low frequency as fully coupled

behavior with a with a $H(f)$ close to zero. However, between 25 and 100 Hz decoupling behavior starts to appear. This behavior only reaches a continuous decoupling effect for pair 3 at 1/4L. Interestingly, the values of $H(f)$ for pair 1 and 2 start to become positive after 75 Hz.

The $H(f)$ of pair 1 even goes over the positive threshold, meaning that at those frequencies there is a stronger presence of the bottom impulse response than in the top impulse response. This does not directly mean a negative acoustic performance. Contrary, it even indicates presence of decoupling, and thus positive acoustic performance, since it means that there is a difference in the general behavior of the CLT and concrete layer.

The $H(f)$ of pair 1 even goes over the positive threshold, meaning that at those frequencies there is a stronger presence of the bottom impulse response than in the top impulse response. While this may seem as a negative and unexpected phenomena for the sound transmission if the ratios were based on results of the response per excitement frequency, as is the case in standard acoustic testing and is used in the numerical HRA analysis, the shown ratio is based on two time-dependent responses from a single excitement. As explained in Section 7.1.3, these signals were then processed using a FFT into a frequency domain. It therefore only show the presence and magnitude of the frequencies to replicate the time-dependent signal. For example, if the top response would only have a peak at 8 Hz, and the bottom response only have a peak at 12 Hz. The graph of the ratio would then provide a positive peak at 8 Hz and a negative peak at 12 Hz. A positive peak thus indicates that the response top and bottom response do not have a peak at the same frequency. This indicates different responses and thus also decoupling.

Similar to the traditional floors, the results for top-bottom transfer for excitement at DP2 features much more fluctuations compared to excitement from DP1. This could possibly be explained by the reduction of the notches and thus contact points in the center of the floor where DP2 is located.

The larger fluctuations, and specifically larger negative peaks, for the conceptual floor indicate a (partially) decoupled behavior.

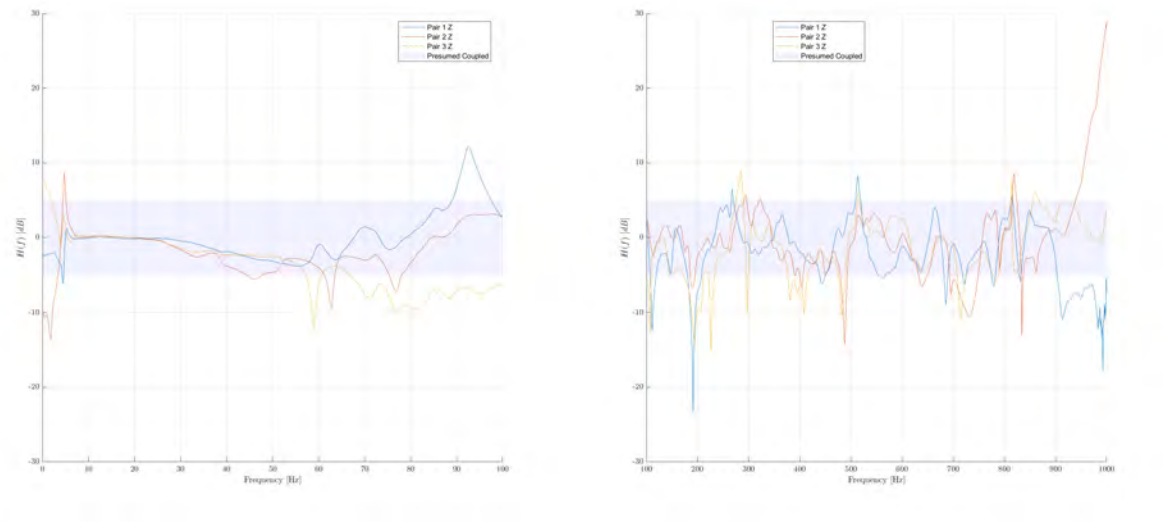

(a) 0-100 Hz (b) 100-1000 Hz

Figure 7.12: Transfer function processed from the floor response in the frequency domain for drop 1 for DP1 of the experimental vibration tests of the Conceptual Floor.

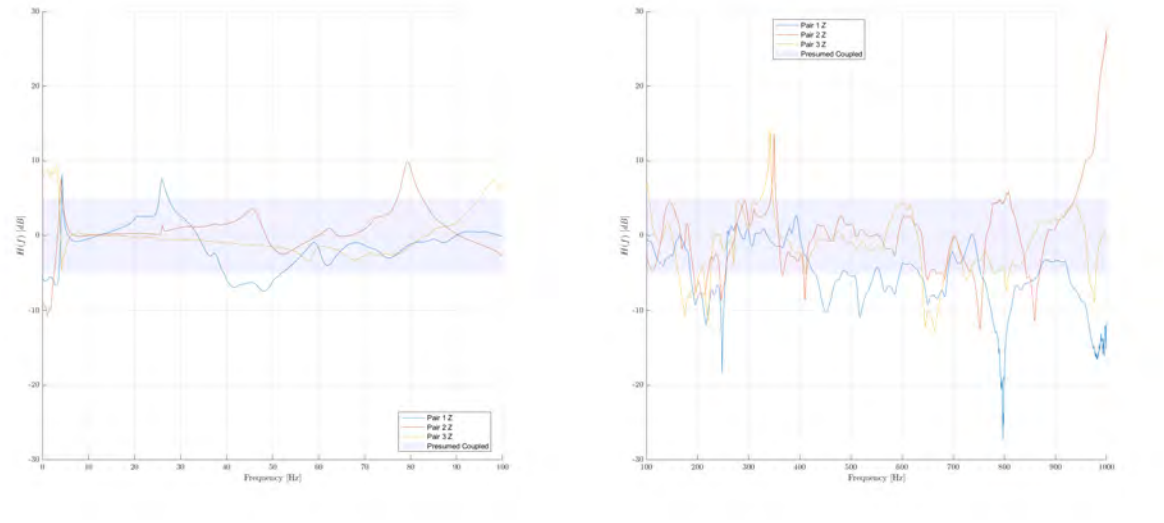

(a) 0-100 Hz (b) 100-1000 Hz

Figure 7.13: Transfer function processed from the floor response in the frequency domain for drop 1 for DP2 of the experimental vibration tests of the Conceptual Floor.

7.3 Discussion

In this section the found results and their validity based on the used approach and comparison across approaches will be described. Firstly, the analytical approach will be reviewed with specific focus on its two used approach to gain representative floor behavior. Secondly, the numerical analysis approach will be discussed with additional attention to its relation with the acoustic performance. Similarly, this will also be discussed for the experimental vibration test

in combination with other influencing factors. At last, all the results will be compared to each other.

7.3.1 Analytical approach

As already indicated in the methodology, which can be found in Section 7.1.1, the traditional and upper/lower bound conceptual floors cannot be directly inserted in the software. Therefore, the homogeneous floor approach and the floating floor approach featuring equivalent layers with equivalent material properties have to be used.

The validation for the determination of the equivalent base layer consisting out of the sole CLT or CLT with an improved stiffness due to integration of the composite action of the concrete are oversimplified. This is due to the use of the effective Young's moduli E_{eff} and $E_{2,eff}$ determined from the effective bending stiffness EI_eff divided by the second moment of are of the full system I_tot. This approach contrasts with one of the fundamental assumptions of the gamma method for calculating an effective cross-section I_eff, as explained in Section 5.1.4.

This effect is thus also present for the decoupled floor where the $E_{eff,CLT}$ determines the equivalent longitudinal wave speed. To get an indication of the effect it is compared to the practice standard approach in which the advised value for the longitudinal wave speed of the CLT is used. Figure 7.14 shows the comparison between the two decoupled floors. A significant difference in the two can be observed for both the airborne and impact sound insulation, indicating an overestimation due to the usage of the floating floor approach.

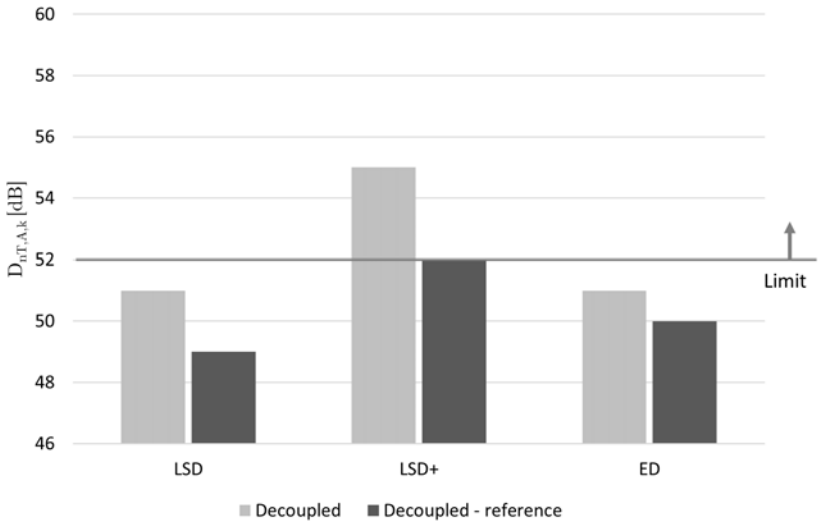

(a) Airborne sound insulation

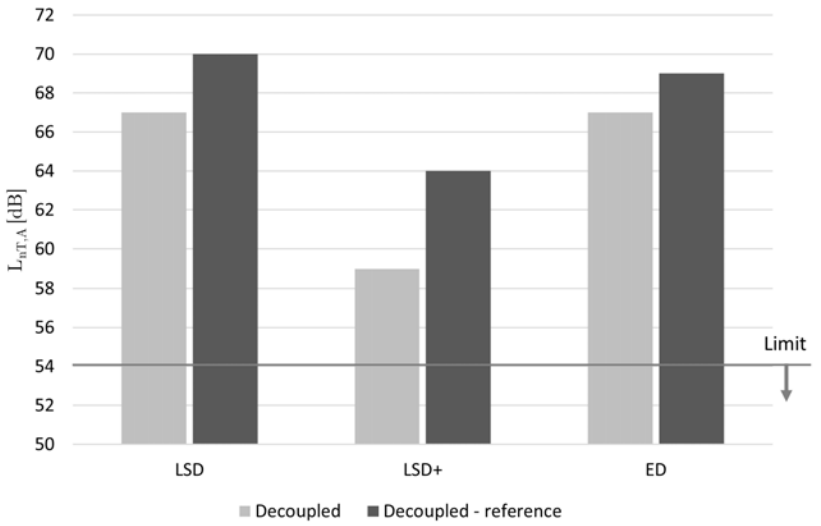

(b) Impact sound pressure level

Figure 7.14: Comparison of the single number-values calculated for described and standard approach of the decoupled floors.

Furthermore, for the conceptual floor using the floating floor principle even more complex effects are present. Due to the integration of the composite action of the concrete in $E_{2,eff}$ with the aim to properly take into account the effective bending stiffness EI_{eff} of the floor, other parameters which are only influenced by the sole Young's modulus, instead of its combination with the cross-section stiffness, might be influenced too. This could be the case for the longitudinal wave transmission, which can possibly cause an overestimation of the acoustic performances. However, based on the found results and the bath-tub principle it was observed that the single number-values are heavily determined by the frequencies with the worst performance. For upper boundary conceptual floor this was was in the low frequency region. In this region the bending

stiffness has a large influence on the performance. It is therefore crucial that this is properly accounted for, as is done in the used approach. An overestimation in the non-critical higher frequency is thus acceptable.

Therefore, the absolute acoustic performance cannot be accurately captured by this method due to the limitations in the calculation model, requiring the determination of equivalent material properties. However, due to the results showing explainable behavior, which are also inline with the results found for traditional and decoupled TCC floors in literature [26], it is expected that the results feature an adequate indication for the comparison of the floor behavior between the traditional, conceptual and decoupled floor.

7.3.2 Numerical analysis

While the the general discussion points regarding the numerical modeling, Transient Analysis and Harmonic Response Analysis, are discussed in Section 6.3.2, this section will focus on the applicability of these approaches to provide an valid indication for the acoustical performance.

First of all, as stated in Section 7.2.2 the Transient Structural Analysis is only applicable for the indication of the response regarding bending waves in the frequency range around the first natural frequency due to its approach of analysis of a decaying signal. The range of numerically found natural frequencies for the nine studied floors was between 4,26 and 18,39 Hz, which are also an overestimation of the actual natural as described in Section 6.3.2. As discussed in Section 7.1, the lower limit of the frequency range for sound transmission is between 25-50 Hz, due to the limitations in human hearing. The described approach using the Transient Analysis is therefore not applicable for the determination of the acoustic performance.

While the described approach using the Harmonic Response Analysis can also only capture the response of bending waves, it can do so based on a varying excitement frequency. The usage of a cyclic load especially replicates airborne sound, and only in a lesser extend the impact sound from a footstep. The found results using this analysis type can all be explained, indicating that the approach of determine the bottom response and its relation with the top response using the Harmonic response Analysis can provide an adequate indication the acoustic performance.

7.3.3 Experimental analysis

Next to the points discussed in Section 6.3.3, there are three main discussion points for the experimental analysis regarding its ability to indicate acoustic performance.

First of all, the test-up is a vibration test and not an acoustic test. The main difference is the excitement through a single impulse from which the decaying signal is analyzed to determine the combination of present harmonic loads with differing frequency, phase and magnitude. It can thus only predict the natural frequencies of the system, while not the actual response at that frequency. Therefore it can also not convert its results into a sound pressure levels for airborne and impact sound and their corresponding single number values.

Secondly, the experimental program missed the testing of a decoupled floor specimen. This would have resulted in a better understanding of the location of the conceptual floor response in the spectrum of a fully coupled and a fully decoupled system.

Thirdly, the lower sample quality around the notch might result in an underestimation of the found decoupling. This is especially the case when the concrete does not cleanly follow the side of the surface insulation, but due to its weight and effects in the foil compress it as its edges, as shown in Figure 5.21d. This could have resulted in decreased resilience of the insulation layer or even direct contact.

7.3.4 Comparison of the results

In this section the results found by the different approaches are compared to each other. In the analytical approach, using the Bassist software, the most important take away is the difference in behavior of the traditional- and lower boundary conceptual floors, for which both full acoustic coupling is assumed, and the behavior of the upper boundary conceptual-, the decoupled-, and traditional floors with floating floors, for which fully decoupled behavior was assumed. While the coupled floors featured a relative constant behavior over the frequency, the floors with decoupling featured an critical peak in the 125 Hz octave band after which the performance rapidly improved over the frequency. Due to this behavior change the upper boundary conceptual floors featured a generally improved single value number value for acoustical performance compared to its lower boundary counterpart and traditional floor. The improvement was however limited by its peak around 125 Hz. For the decoupled floors, the reduced bending stiffness due to the lack of composite action proved detrimental for the 63 and 125 Hz octave band, resulting in significantly worse performances compared to the other floor types. Although it was anticipated that the low frequencies, governed by the bending stiffness, were critical, it was still expected that the decoupled floors feature the best acoustic performance.

These main findings for the numerical approach using the Harmonic Response Analysis, partly agree and partly contradict these findings. While the decoupling effect present in the decoupled floor were also found to have minimal positive impact and an negative extra mode in the lowest frequencies, it already begins to start providing significant from 70 Hz onwards. This results that the decoupled and conceptual floors already start to outperform the traditional floor from 70 Hz instead of from the 125 Hz octave band (88-177 Hz). If the results from the numerical model are more valid for reality than the results gained from the analytical method, this movement of the critical peak and earlier positive impact of the decoupling can mean an significant improvement in acoustic performance due to the the A-weighting more heavily reduces peak for lower frequencies.

The experimental vibration test also neither agree or disagree with the described observations from the other approaches. When the excitement was located at 1/4L decoupling effects in conceptual floor already become significant from 60 Hz. However, the decoupling also faded between 80-100 Hz and become relevant again at 110-120 Hz. While the early presence of the positive effects from decoupling aligns with the HRA, its quick fading is possibly due to a resonance peak in the resilient layer which in combination with the bathtub principle can explain the poor performance found for the 125 Hz.

Overall, there is a clear agreement that the conceptual floor features similar decoupling effects as the decoupled floor, resulting in significantly improved acoustic performance for frequencies above the 125 octave band. For the critical frequencies below this threshold, the presence and effect of the decoupling was much more difficult to capture, resulting in unclear results regarding its actual behavior. If this effect is present in its most positive form of the spectrum, it can also heavily increases the acoustic performance in lower frequencies. If this effect is present in its most negative form, it negates the positive effects found for the higher frequencies and it negates the positive effects found in the higher frequency and result in detrimental acoustic performance for decoupled floors. However, since the conceptual floor features a similar bending stiffness as the traditional floor, the poor performance in the low frequencies is limited. Still, with a reduced performance for the low-frequency range, it results in a overall better performance of

the conceptual floor compared to the traditional floor.

7.4 Conclusion

To provide an indication of the acoustic performance for each of the floor types for each of the three design categories (LSD, LSD+, ED) a number of different investigations have been conducted. An analytical approach using the Bassist software has been used to find an indication for the airborne and impact sound transmission, $D_{nT,A}$ and $L_{nT,A}$. The ED traditional and conceptual floor were also further analyzed through a experimental vibration test. Based on these investigations the following conclusions can be drawn:

- In the analytical analysis using Bassist, the traditional floor was evaluated using an equivalent homogeneous floor approach. The decoupled floor was modeled using an equivalent floating floor approach. The conceptual floor was modeled using both approaches. At last, for the traditional floor with floating floor (F.F.) the equivalent floating floor approach was also applied, including the usage of the equivalent homogeneous of the traditional floor as base floor. It was observed that the traditional and conceptual floor using the homogeneous approach featured very similar and constant performance for the governing impact sound insulation over the frequencies. The decoupled, traditional floor with F.F. and conceptual floor using the floating floor approach also featured similar behavior compared to each other, but also featured a significant performance improvement after the 125 Hz octave band. This was however compensated by a relative worse performance in the 63 and 125 Hz octave bands. As explained by the bath-tub principle, the worst performance is critical and due to the lack of bending stiffness it resulted for the decoupled floor in very poor single-number values for airborne sound $D_{nT,A}$ and impact sound $L_{nT,A}$. While for the conceptual floor using the same approach, the poor performance in the low frequencies limited its improvement in the single number values, it still featured better overall results than the homogeneous floors. Due the increased decoupling, significant increase in mass and its maintained high bending stiffness, the traditional floor with F.F. featured overall increased acoustic performance. The most improvement was found in the critical low frequency area.

- Considering the numerical analysis, the main conclusion is that the response of the conceptual floor is located in between the high response of the traditional floor and the low response of the decoupled floor, which can be explained by the observed presence of the (partial) decoupling effects. This resulted in major performance increases compared to the traditional floor from 70 Hz onwards. Between 25 and 70 Hz it featured a worse performance due to the presence of extra modes.

- From the experimental vibration test it was observed that there was significant decoupling present in the conceptual floor from 60 Hz onwards. It was however also noted that the amount of decoupling was heavily subjected to variation over its frequency, for example decreasing significantly again in the 80-100 Hz region.

- The three approaches were in agreement that the conceptual floor showed significant improvement in acoustic performance from the 177 Hz to 5000 Hz, similar to the decoupled floor. For the critical 44-177 Hz frequency range its performance was however not consistent

over the different approaches. In the worst case scenario, the features a relatively poor performance for this range in regard to the higher frequencies and limit the overall acoustic performance improvement compared to the traditional floor. In its best case scenario, earlier decoupling is present and the resilient layer resonance is present at a lower frequency increasing the performance in this low frequency range considerably. The result would be an significant overall improvement of acoustic performance compared to the traditional floor.

- Overall, these findings indicate that the traditional and decoupled floor barely fall short to satisfy the requirements for airborne sound transmission, while they considerably fall short for the requirements of the impact sound transmission. Due to the conceptual floor featuring (partial) decoupling in combination with its high stiffness due to composite interaction, it features much improved acoustic performance. The results indicate that the conceptual floors comfortably satisfy the airborne sound requirements across all design categories. However, while an improvement regarding the traditional floor is observed for the impact sound transmission, it also falls short to meet its requirements.

8 Conclusion

This master thesis introduces an innovative way of improving the vibro-acoustical behavior for CLT-Concrete Composite (CCC) floors by integrating a resilient layer in between two structural composite layers. The study consists of two major phases.

The first phase focuses on the understanding and current state of the art of the design aspects regarding structural, vibro-acoustical and practical in CCC floors and the preliminary design of the connector detail and floor build-up.

The second phase focuses on the evaluation of the static structural performance, tactile vibration performance and acoustic performance of a CCC floors with the designed resilient rectangular notch connections. This has been done for three floor types; a traditional CCC floor with a fully coupled CLT and Concrete layer, a decoupled CLT-Concrete floor with a resilient layer under the concrete and the conceptual floor which also features the resilient layer to gain acoustic decoupling and increased damping and the design connector to maintain the composite interaction and thus its structural properties. These three floor types were replicated for three design categories. Firstly, the Long Span Design (LSD) category features floor designed on the threshold of the structural performance for a 8.7 meter span. Secondly, the Long Span Design+ (LSD+) category features floors design on the threshold of the vibration performance for a similar span. At last, the Experimental Design (ED) category consists out of floors of which its dimensions are based on the provided 6 m long test specimen for the traditional floor type. Governing for this specimen was the 300 kg/m^2 practice guideline for the minimum weight of a base floor to reach satisfactory acoustic performance after a floating floor is added.

The structural performance was assessed by using requirements for the serviceability limit state and the ultimate limit state. The former will focus on instantaneous and long term deformation, while the latter will focus on cross-sectional stresses, notch failure mechanisms and ductile failure. The used methodology consists of numerical modeling of a push-out test for the determination of the connection stiffness, an analytical approach using the separated and extended γ-method for cross-sectional analysis, an analytical calculation model for the prediction of notch failures and an experimental program using a 6 point bending test. The vibrational performance is evaluated using the requirements and analytical method prescribed by the draft of the revised Eurocode 5. Besides, additional numerical vibrations analysis in the time and frequency domain have been done to provide better insights in the qualitative and relative behaviors of the floors. At last, an experimental vibration ball-fall has been conducted to validate the found insights. The acoustic performance is evaluated by usages of the analytical calculation software for sound transmission Bassist and the numerical and experimental vibration investigations.

Based on these investigations the found indicative performances are shown in Figure 8.1 and the following conclusions were found:

- Based on the comparison of the several (improved) commonly used and conceptual shear

connections types, it was concluded that an improved version of the commonly used continuous rectangular notch features the most potential to facilitate acoustic decoupling while maintaining the shear connection stiffness for the composite actions. The final detail included a 20 mm mineral wool layer on the CLT surface and in the notch with a moisture retaining foil on top of it. The sides of the notch were further covered by Teflon strips, to reduce the friction in the notch contact area.

- for the structural Serviceability Limit State it was noted that although the conceptual floors feature a large decrease in connection stiffness and a smaller concrete cross-section relative to their traditional floor counterparts, the impact on the effective bending stiffness is much less significant with a decrease up to approximately -10%. Including the reduction in mass, the difference in governing long term deformation in residential context is even less reduced. Overall, this indicates that the conceptual floors feature a similar structural performance as their traditional counterparts in the governing serviceability state. As expected, the decoupled floors featured a significant decrease in bending stiffness and thus structural performance, due to the lack of composite action.

- For the structural Ultimate Limit State, it was found that the tested traditional floor did feature hairline cracks in the concrete around the notch, but did not fail at a load of 150 KN. The corresponding conceptual floor, did feature Concrete Diagonal Shear and progressive Timber shearing-off failures of the notches in the 140-148 kN domain, likely due to the lack of vertical reinforcement. While this is a brittle failure mode, the failure loads were considerably higher than the ULS loading conditions and thus do not impact the structural design significantly. In combination with the difficultly to predict these failure loads using the current state of the art, it is not advised to take into account the requirement for ductile failure behavior, by ensuring that the Timber Compression Failure in the notch is governing, in the initial design phase for CCC conceptual floors.

- For the relative vibration performance it was observed from the experimental vibration fall-test that the conceptual floor features an approximate damping ratio of 4,2% while the traditional floor only features a damping ratio of 2,9%. Although this resulted in a overall increase of vibration performance for the conceptual floor, this was limited by its reduced bending stiffness and mass. The indicated increase in performance relative to the traditional floor could therefore not be judged as significant based on the used methods. Further investigations can provide more insight in the magnitude of the significance of the improvement. Similar as to the structural performance, the decoupled floor featured poor vibration performance due to the lack of composite action. Besides, while the Traditional floor with Floating Floor (F.F.) featured an increase mass with positive effects on the floor response, combined with a minimal increase in bending stiffness it can also lower the natural frequency. If this results in a natural frequency lower than 8 Hz, the response has to be determined from the generally unfavorable acceleration domain.

- Based on the acoustic evaluation it was found that the decoupling effect was present in the conceptual floor and provided the conceptual and decoupled floor with a substantial increase of acoustic performance above 177 Hz, relative to the traditional floor. However the decoupling effect also introduced an extra critical mode in the 44-177 Hz region and in combination with the impact of bending waves, the decoupled floor performed very poorly and this governed its overall indicative airborne sound performance $D_{nT,A}$ and

impact sound performance LnT, A. Due to the conceptual floor maintaining its bending stiffness, it performed much better in this frequency range. The performance was however still relatively poor compared to its great performance in the higher frequency range, limiting the overall indicative performance gain relative to the traditional floor. Based on limited investigations, due to the present decoupling, significant increase in mass and its maintained high bending stiffness, the traditional floor with Floating floor featured an overall increased acoustic performance as expected. Importantly, the most improvement relative to the conceptual floor was found in the critical low frequency area. Further development of the conceptual floor regarding the low frequency domain could potentially increase the acoustic performance sufficiently that no additional acoustic measures have to be taken.

Overall, it can be said that the integration of Vibro-Acoustical resilient behaviour in CLT-Concrete Composite floors with resilient notched connections has much potential to increase the acoustic transmission performance, while replacing 20 mm of heavy concrete by 20 mm of light mineral wool and not requiring addition total floor height. However, since the vibration performance has to be assumed as equal to the traditional floors, the conceptual floors still have to feature the increased LSD+ dimensions to satisfy for vibration performance. Therefore, there is no significant dimension and material reduction in the structural floor itself. The main benefit of the system for the structural floor is therefore that the mass and concrete usage is significantly decreased. This can however still feature a considerable impact on the sustainability of a multi-residential buildings.

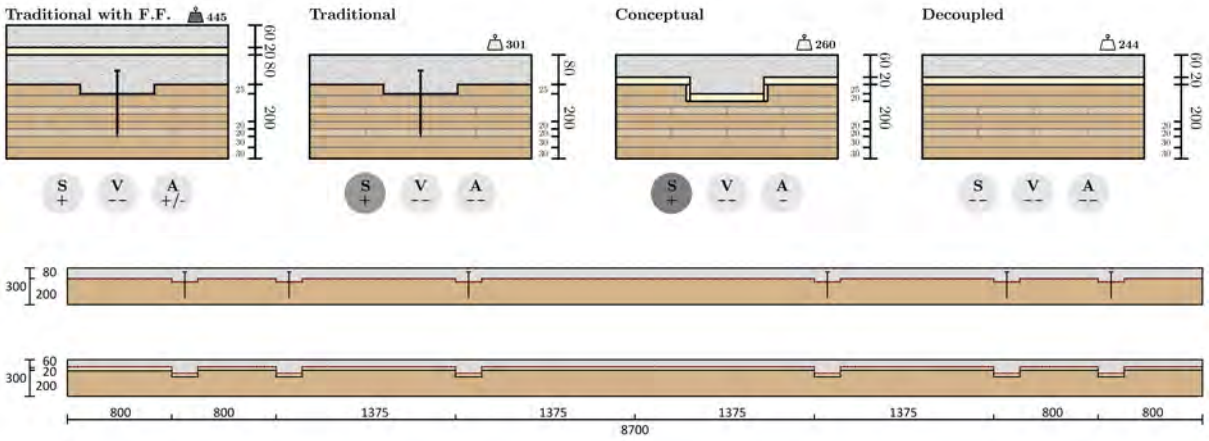

(a) Large Span Design floors

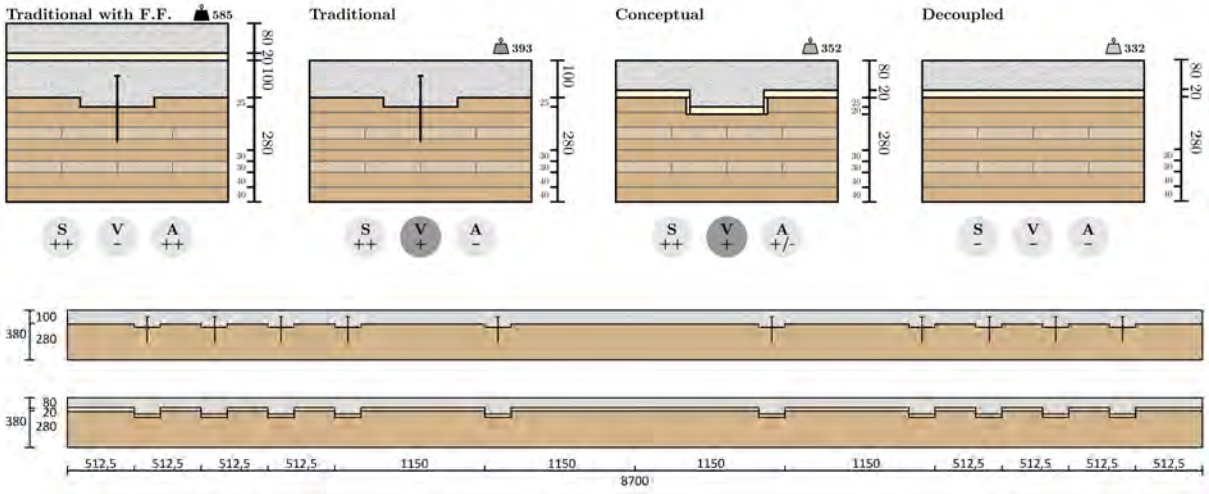

(b) Large Span Design+ floors

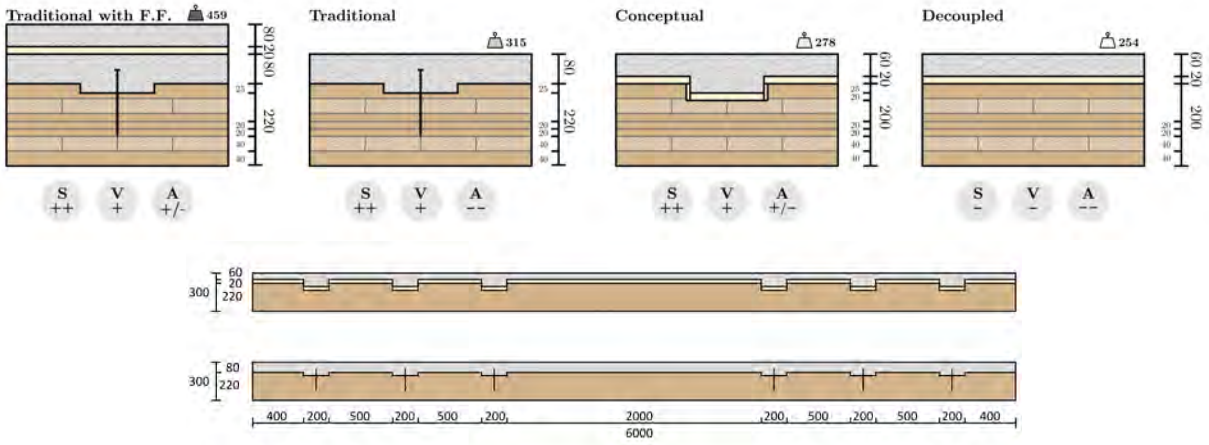

(c) Experimental Design floors

Figure 8.1: Overview of the derived indicative Structural (S), Vibration (V) and Acoustic (A) performance for the studied floors types and design categories.

9 Recommendations

Given the exploratory nature of this study on the integration of a resilient layer in CLT-Concrete Composites, and the conclusion that it demonstrates promising results for improvement of the acoustical and possibly also the vibration performance, the primary recommendation is to pursue further development of this concept. This development should focus on a combination of the following aspects. A connection detail featuring a combination of the different mentioned recommendations can be found in Figure 9.1.

First of all, further development should focused on the design of the conceptual floor and its connection detail in regard to the acoustic performance in the 44-177 Hz frequency range. This range was shown to be critical and limited improvement of the acoustic performance, due to the indicated presence of a resonance peak in the top floor. This should be conducted by experimental acoustic testing in a large span environment to find more accurate and absolute results. The requirement of the large span testing environment complicates the acoustical testing program since most acoustic laboratories only allow for smaller dimensions, but is critical due to the influence of the span dependent bending waves in this region. The improvement can possibly be found in the variation in type and thickness for the insulation in general or in the relative variation in type and thickness between the surface and notch insulation. Furthermore, it is expected that the amount and stiffness of the connectors does not only influence the bending stiffness but also the degree of acoustic coupling. This could for example be done by an investigation comparing continuous and discrete notches, as discrete notches are found to feature a higher connection per mm notch width, described in Chapter A. while reducing the acoustic contact area. More understanding in the relation between these parameters can provide better understanding to design floors in such a way that it is most beneficial for the acoustic performance in the 44-177 Hz range.

Secondly, the structural failure mechanism of the floor type should be better understood such that it can be accurately predicted. While the failure modes for traditional CCC floors are already difficult to predict, the increase of total notch depth for placement of the notch insulation further interferes with strain and stress distributions. Furthermore, although it was noted that fasteners are not required to prevent separation, an improvement to the notch capacity and ductility could be the integration of a stirrup in the concrete. This could prevent the brittle concrete diagonal shear failure to happening before timber compression failure.

Thirdly, attention should be given to the fabrication side of the conceptual floors. Since the PE-foil is difficult to be properly secured due the softness of the insulation layer, it easily folds and round-off corners. In combination with the soft surface insulation for which the weight of the concrete can compress its corners, it can cause the concrete to not properly follow the intended geometry. An option could be to use a stiff U-profile inside the notch. This can be placed in the notch after the insulation and foil is placed and create a geometrical correct and stiff mould for the concrete. This profile would preferably be made of densified timber or another bio-based material which is stiff enough to not cause extra compressive strain in the load transfer zone.

Fourthly, the hygrothermal behavior, such as moisture and shrinkage effects, and propping effects are not taken into account in this study. As described by Dias [8], this could have considerable effects on the structural performance by causing additional inelastic strains and concrete cracking in unfavourable situations. This has also been noted for the experimentally tested traditional floor where the concrete diagonal shear hairline crack was propagated from a shrinkage crack at the notch corner. Additional research is recommended to ensure the integrity of the specimens in practice.

Fifth, its integration in other building systems should be properly developed. Especially support conditions and its connection to other structural elements are likely to become governing for vibrations and acoustics over the direct perception and transmission. Besides, the floor system shows great potential for the usage in two spanning systems due to the CLT and Concrete both featuring beneficial stiffness in transverse direction. This impact of this aspect is however governed by the exact configuration as a all-side supported slab, for which the vibration and acoustic bending wave performance might be improved significantly,or a point supported slab, which can result in the reverse.

Sixth, the used methodology should be considered carefully. To more accurately validate the stiffness determination approach, an extended experimental push-out test program should be performed. For this program the mentioned improvement such as variation in insulation thickness, addition of stirrups and improvements of the detail regarding the fabrication process could be taken into account. For further vibration experiments, a wider floor specimen and a force meter should be used to have the ability to not only qualitatively analyse the found behavior but also use the values absolutely. At last, as said in the first paragraph, for the determination of the acoustic performance long span acoustic testing is essential.

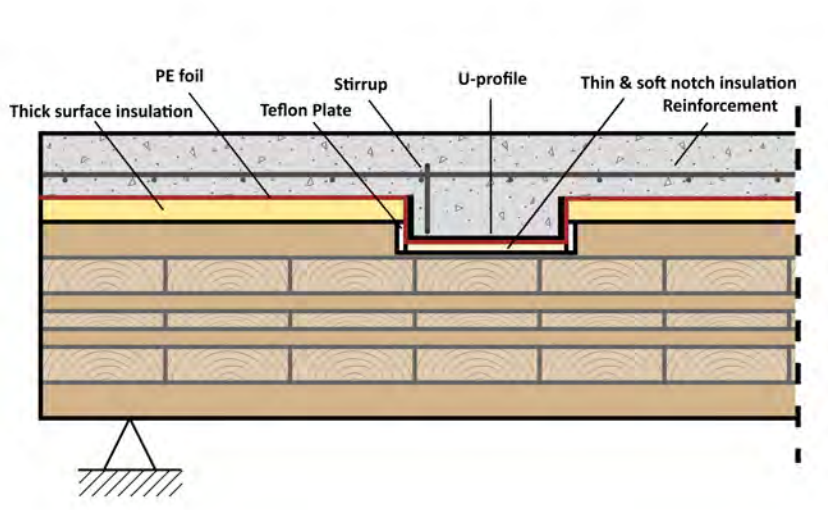

Figure 9.1: Connection detail including a combination of design recommendations for further development.

References

[1] Arup, *Designing and engineering the Netherlands' tallest timber-hybrid residential building*. [Online]. Available: https://www.arup.com/projects/haut/.

[2] Y. Bao, W. Lu, K. Yue, H. Zhou, B. Lu, and Z. Chen, "Structural performance of cross-laminated timber-concrete composite floors with inclined self-tapping screws bearing unidirectional tension-shear loads," *Journal of Building Engineering*, vol. 55, Sep. 2022, ISSN: 23527102. DOI: 10.1016/j.jobe.2022.104653.

[3] L. Boccadoro, R. Steiger, S. Zweidler, and A. Frangi, "Analysis of shear transfer and gap opening in timber–concrete composite members with notched connections," *Materials and Structures/Materiaux et Constructions*, vol. 50, no. 5, pp. 1–15, 2017, ISSN: 13595997. DOI: 10.1617/s11527-017-1098-3.

[4] L. Boccadoro, S. Zweidler, and A. Frangi, "Timber-concrete composite slabs made of beech laminated veneer lumber," Ph.D. dissertation, ETH Zurich, 2016, ISBN: 9783903039001.

[5] Building Acoustics Group, *IBPM Sound*, Eindhoven, 2017.

[6] CEN/TC 250, A. Dias, M. Fragiaceomo, *et al.*, "Working draft of Eurocode 5: Design of Timber Structures - Structural design of timber-concrete composite structures - Common rules and rules for buildings," European Committee of Standardization (CEN), Tech. Rep., 2019.

[7] Comsol, *The Finite Element Method (FEM)*, 2016. [Online]. Available: https://www.comsol.com/multiphysics/finite-element-method.

[8] COST Action FP1402 / WG4, *Design of timber-concrete composite structures*, A. Dias, J. Schänzlin, and P. Dietsch, Eds. ShakerVerlagGmbH, 2018, ISBN: 978-3-8440-6145-1.

[9] COST Action TU0901 - Integrating and Harmonizing Sound Insulation Aspects and in Sustainable Urban Housing Constructions., *Building acoustics throughout Europe Volume 1: Towards a common framework in building acoustics throughout Europe*, B. Rasmussen and M. Machimbarrena, Eds. Brussels: COST Office, 2014, vol. 1, p. 257, ISBN: 978-84-697-0158-4.

[10] L. Cremer, M. Heckl, and B. A. T. Petersson, "Structure-Borne Sound Structural Vibrations and Sound Radiation at Audio Frequencies 3 rd edition," Tech. Rep.

[11] S. Cuerrier-auclair, *Design Guide for Timber-Concrete Composite Floors in Canada*. Pointe-Claire, QC: FPInnovation, 2020, p. 116, ISBN: 9780864885937.

[12] D/O Architects, "Acoustic Testing of CLT Composite Floor Assemblies for TMBR © Minneapolis," Minneapolis, Tech. Rep., 2021, p. 33.

[13] A. M. Dias, J. W. Van de Kuilen, S. Lopes, and H. Cruz, "A non-linear 3D FEM model to simulate timber-concrete joints," *Advances in Engineering Software*, vol. 38, no. 8-9, pp. 522–530, 2007, ISSN: 09659978. DOI: 10.1016/j.advengsoft.2006.08.024.

[14] A. Dias, "Mechanical behaviour of timber-concrete joints," Ph.D. dissertation, Technicshe Universiteit Delft, 2005, p. 303, ISBN: 909019214X.

[15] D. DJOUBISSIÉ DENOUWÉ, A. MESSAN, E. FOURNELY, and A. BOUCHAIR, "Influence of Interlayer in Timber-Concrete Composite Structures with Threaded Rebar as Shear Connector-Experimental Study," *American Journal of Civil Engineering and Architecture*, vol. 6, no. 1, pp. 38–45, Jan. 2018, ISSN: 2328-398X. DOI: 10.12691/ajcea-6-1-5.

[16] European Commission Directorate-General for Research and innovation, M. Feldmann, C. Heinemeyer, and M. Lukić, "Human-induced vibration of steel structures (Hivoss)," Tech. Rep., 2010. DOI: doi/10.2777/79056.

[17] European Committee for Standardization, *EN-1991-1-1 (2004) Eurocode 1, Actions on Structures—Part 1-1: General Actions —Densities, Self-Weight, Imposed Loads for Buildings*, Brussels, 2002.

[18] European Committee for Standardization, *CEN/TS 19103 - Eurocode 5: Design of Timber structures - Structural design of timber-concrete composite structures - Common Rules and rules for buildings*, Brussels, 2021.

[19] European Committee of Standardization (CEN) - TC 124, "Timber structures - Joints made with mechanical fasteners - General principles for the determination of strength and deformation characteristics (ISO 6891:1983)," Tech. Rep., 1991.

[20] M. Feldmann, C. Heinemeyer, C. Butz, *et al.*, "Design of floor structures for human induced vibrations," Tech. Rep., 2009, p. 75.

[21] A. R. Gerber, "TIMBER-CONCRETE COMPOSITE CONNECTORS IN FLAT-PLATE ENGINEERED WOOD PRODUCTS," University of Britisch Columbia, Vancouver, Tech. Rep., 2016, p. 163.

[22] U. A. Girhammar, "A simplified analysis method for composite beams with interlayer slip," *International Journal of Mechanical Sciences*, vol. 51, no. 7, pp. 515–530, 2009, ISSN: 00207403. DOI: 10.1016/j.ijmecsci.2009.05.003. [Online]. Available: http://dx.doi.org/10.1016/j.ijmecsci.2009.05.003.

[23] W. de Groot, "7PP4M0 Advanced Timber Structures," Eindhoven University of Technology, Master Architecture, Building and planning, Unit of Structural Engineering an Design, Tech. Rep., 2022.

[24] A. Gustafsson, R. Crocetti, A. Just, *et al.*, *The CLT Handbook*, 1st ed., E. Borgström and J. Fröbel, Eds. Stockholm: Swedish Wood, 2019, p. 188, ISBN: 978-91-983214-4-3.

[25] K. Hagberg, T. Tomi, and STB Team, "Design Guide – Silent Timber Build – WWN + Summary," Tech. Rep., 2017.

[26] A. Homb, C. G. Carter, and A. Rabold, "Impact sound insulation of cross-laminated timber/massive wood floor constructions: Collection of laboratory measurements and result evaluation," *Building Acoustics*, vol. 24, no. 1, pp. 35–52, 2017, ISSN: 20598025. DOI: 10.1177/1351010X16682966.

[27] L. J. Hu, Y. H. Chui, and D. M. Onysko, "Vibration serviceability of timber floors in residential construction," *Progress in Structural Engineering and Materials*, vol. 3, no. 3, pp. 228–237, 2001, ISSN: 1365-0556. DOI: 10.1002/pse.69.

[28] T. J. Hughes, *The Finite element method*, ISBN: 0-13-317025-X.

[29] Y. Jiang and R. Crocetti, "CLT-concrete composite floors with notched shear connectors," *Construction and Building Materials*, vol. 195, pp. 127–139, Jan. 2019, ISSN: 09500618. DOI: 10.1016/j.conbuildmat.2018.11.066.

[30] J. Klaassen, "Dynamic behavior of timber-concrete floors causes by walking loads. A study into the influence of the transverse stiffness of a timber-concrete composite floor on the dynamic behaviour and vibration comfort.," Ph.D. dissertation, Eindhoven University of Technology, 2019, p. 228.

[31] R. Kliger, M. Johansson, R. Crocetti, *et al.*, *Design of timber structures*, 3rd ed., P. Godonou, Ed. Stockholm: Swedish Wood, 2022, vol. Volume 1: p. 256, ISBN: 978-91-637-0055-2.

[32] H. Kreuzinger and J. Raadschelders, *B11-1 Samengestelde liggers en kolommen.pdf*, 1998.

[33] S. Lamothe, L. Sorelli, P. Blanchet, and P. Galimard, "Engineering ductile notch connections for composite floors made of laminated timber and high or ultra-high performance fiber reinforced concrete," *Engineering Structures*, vol. 211, May 2020, ISSN: 18737323. DOI: 10.1016/j.engstruct.2020.110415.

[34] S. Lamothe, L. Sorelli, P. Blanchet, and P. Galimard, "Lightweight and slender timber-concrete composite floors made of CLT-HPC and CLT-UHPC with ductile notch connectors," *Engineering Structures*, vol. 243, no. April, p. 112 409, 2021, ISSN: 18737323. DOI: 10.1016/j.engstruct.2021.112409. [Online]. Available: https://doi.org/10.1016/j.engstruct.2021.112409.

[35] Level.Tools, "Handleiding Bassist Handleiding Bassist.Lab versie 1.0," Tech. Rep., 2022.

[36] Y. Li and S. Ren, Eds., *2 - Basic Properties of Building Decorative Materials*. Woodhead Publishing, 2011, vol. i, pp. 10–24, ISBN: 978-0-85709-257-1. DOI: 10.1533/9780857092588.10.

[37] F. Ljunggren, "Innovative solutions to improved sound insulation of CLT floors," *Developments in the Built Environment*, vol. 13, Mar. 2023, ISSN: 26661659. DOI: 10.1016/j.dibe.2022.100117.

[38] E. Lukaszewska, "Development Prefabricated Timber-Concrete Floors Timber-Concrete Composite," Ph.D. dissertation, Lulea University of Technology, 2009, p. 318, ISBN: 9789186233853.

[39] J.-W. van Maanen, "Timber Concrete composite floor slab on point supports," Ph.D. dissertation, Eindhoven University ofT echnology, Eindhoven, Nov. 2023, p. 218.

[40] K. Q. Mai, A. Park, and K. Lee, "Experimental and numerical performance of shear connections in CLT–concrete composite floor," *Materials and Structures/Materiaux et Constructions*, vol. 51, no. 4, Aug. 2018, ISSN: 13595997. DOI: 10.1617/s11527-018-1202-3.

[41] Ministerie van Binnenlandse Zaken en Koninkrijksrelaties., *Bouwbesluit 2012*, 2012. [Online]. Available: https://rijksoverheid.bouwbesluit.com/Inhoud/docs/wet/bb2012.

[42] National Oceanic and atmospheric administration, *Understanding Ocean Acoustics*, 2022. [Online]. Available: https://oceanexplorer.noaa.gov/explorations/sound01/

background/acoustics/acoustics.html#:~:text=Sound%20moves%20at%20a%20faster,of%20water%20differ%20from%20air..

[43] Nederlandse Organisatie voor Toegepast Natuurwetenschappelijk Onderzoek (TNO), "Model ter berekening van de lucht- en contactgeluidisolatie," Tech. Rep., 2007. [Online]. Available: Lichtbouwen.nl.

[44] Nederlandse Organisatie voor Toegepast Natuurwetenschappelijk Onderzoek (TNO), *Trillingen*, 2007. [Online]. Available: http://www.lichtbouwen.nl/prestatiebepaling/vuistregels/trillingen.

[45] O. Neve and L. Spencer-Allen, "Shaking up dance floor design with timber–concrete composites," *Proceedings of Institution of Civil Engineers: Construction Materials*, vol. 168, no. 4, pp. 204–212, 2015, ISSN: 17476518. DOI: 10.1680/coma.14.00048.

[46] Nieman De Raadgevende Ingenieurs and D. Roelofsen, "Geluidwering tussen ruimten & installatiegeluid," Nieuwegein, Tech. Rep., 2020, pp. 1–14. [Online]. Available: https://www.planviewer.nl/imro/files/NL.IMRO.0356.OVRH2020002-VA02/b_NL.IMRO.0356.OVRH2020002-VA02_Bijlage26...27022020.pdf.

[47] R. Öqvist, "Measurement and Perception of Sound Insulation from 20 Hz between Dwellings," Ph.D. dissertation, Luleå tekniska universitet, 2017, p. 156, ISBN: 978-91-7583-868-7 (ISBN). [Online]. Available: http://urn.kb.se/resolve?urn=urn:nbn:se:ltu:diva-62843%0Ahttp://ltu.diva-portal.org/smash/get/diva2:1086459/FULLTEXT01.pdf.

[48] P. K. Rasmussen, J. H. Sørensen, L. C. Hoang, B. Feddersen, and F. Larsen, "Notched connection in timber-concrete composite deck structures: A literature review on push-off experiments & design approaches," *Construction and Building Materials*, vol. 397, Sep. 2023, ISSN: 09500618. DOI: 10.1016/j.conbuildmat.2023.131761.

[49] ROCKWOOL B.V., "Rockfloor Base - Technisch productblad," Tech. Rep. [Online]. Available: https://p-cdn.rockwool.com/syssiteassets/rw-bnl/downloads-nl/downloads/technische-productbladen/vloer/technisch-productblad-rockfloor-base-nl.pdf?f=20221208103900.

[50] M. Roks, "The dynamic behaviour of timber-concrete composites," Ph.D. dissertation, Eindhoven University of Technology, 2017, p. 165.

[51] W. Schirén and T. Swahn, "Vibrations in residental timber floors," p. 100, 2019.

[52] C. van der Steen, *Het (Dek)vloerenboek*, 2010th ed. Den Haag: Bedrijfschap Afbouw, 2010, p. 118.

[53] M.-V. Thai, "Evaluation of the vibration behavior and optimization of the conception of CLT-concrete floors," Ph.D. dissertation, Universitéde Bordeaux & Universitédu Québecà Chicoutimi, 2022, p. 153. DOI: NNT:2021BORD0338. [Online]. Available: https://archivesic.ccsd.cnrs.fr/U-BORDEAUX/tel-03738322v1.

[54] University of Wisconsin, *Acoustic Impendence*, 2009. [Online]. Available: https://www4.uwsp.edu/physastr/kmenning/Phys115/Link5-09_acoustic_impedance.pdf.

[55] R. Verhaegh, M. Vola, and J. d. Jong, "Haut - A 21-storey Tall Timber Residential Building," *International Journal of High-Rise Buildings*, vol. 9, no. 3, pp. 213–220, Sep. 2020, ISSN: 22889930. DOI: 10.21022/IJHRB.2020.9.3.213.

[56] M. Wallner-Novak, M. Augustin, J. Koppelhuber, and K. Pock, *Wallner-Novak et al. - 2018 - CLT structural design volume 2*, ISBN: 978-3-902320-96-4.

[57] D. Yeoh, M. Fragiacomo, M. De Franceschi, and K. Heng Boon, "State of the Art on Timber-Concrete Composite Structures: Literature Review," *Journal of Structural Engineering*, vol. 137, no. 10, pp. 1085–1095, 2011, ISSN: 0733-9445. DOI: 10.1061/(asce)st.1943-541x.0000353.

[58] L. Zhang, J. Zhou, Y. H. Chui, and G. Li, "Vibration Performance and Stiffness Properties of Mass Timber Panel–Concrete Composite Floors with Notched Connections," *Journal of Structural Engineering*, vol. 148, no. 9, Sep. 2022, ISSN: 0733-9445. DOI: 10.1061/(asce)st.1943-541x.0003450.

[59] O. Zienkiewicz, R. Taylor, and D. Fox, *The Finite Element Method for Solid and Structural Mechanics*. Elsevier, 2014, ISBN: 9781856176347. DOI: 10.1016/C2009-0-26332-X. [Online]. Available: https://www.sciencedirect.com/book/9781856176347/the-finite-element-method-for-solid-and-structural-mechanics#book-info.

Appendices

A Modelling of Push-out test

This chapter discusses the process of establishing the FEM models which replicate experimental push-out test to determine the connection stiffness K of notch connections. For this the FEM software package Ansys 2024 R1 was used. Next to static analysis, this software also allows easy-access dynamic analysis options and therefore allowed continuity between the modelling of the push-out test and the planned vibration analysis. For the replication of Push-out test the 'Static structural' analysis will be used.

A.1 Preliminary modelling and validation

This section will describe the steps taken to develop an accurate model. For this it was chosen to replicate completed experimental investigations as close as possible. The approach is mainly based on three prior studies in the modelling of TCC push-out tests by Dias et al. in 2006 [13], Jiang and Crocetti (JC) in 2018 [29] and Thai in 2021 [53]. For the validation of the models against experimental results of the study of JC and Thai into rectangular notches will be used in addition to a study of Lamothe et al. in 2020 in triangular notches with high-performance concrete (HPC) and Ultra-high-fiber-reinforced concrete (UHFRC) with and without an insulation inter-layer [33].

The following paragraph outlines the material approach for the replicated models. Firstly, similar to JC and Thai, the CLT will be modelled as bonded individual layers. Secondly, the timber is modelled as a simplified orthotropic bi-linear material, shown in Figure A.1a, using the van Hill criterion for plasticity, as advised by Dias, JC and Thai. The former two provided the following corresponding relations; $R_{11} = \sigma_0/\sigma_{eq} = 1.0$, $R_{22} = R_{33} = \sigma_{90}/\sigma_{eq} = 0.19$ and $R_{12} = R_{13} = R_{23} = \sqrt{3} * \sigma_v/\sigma_{eq} = 0.38$. According to Dias, the yield strength in longitudinal direction σ_0 is considered equal to the embedment strength, which can be calculated using the provided formulas in Eurocode 5 based on the density of the timber and the diameter of the fasteners. Since the force transfer is not done by any fasteners, for the latter an 8 mm diameter was assumed. Furthermore, due to software limitations, the behavior in tension was considered equal to the behavior in compression. Due to an equal elastic response in compression as in tension, this is not expected to be impact-full to the results. For simplicity and convergence reasons, tension failure was not modelled. If not all the required timber material data is available in the corresponding study or the product specifications, the data was filled in by estimation of the most representative timber class according to EN 338 or the following relations; $E_{xx} = 30E_{zz} = 30E_{yy}$, $G_{yz} = G_{xy}/10$.

The concrete was modelled as an isotropic material. Thai does not consider the plasticity of the concrete due to minimal expected impact, JC advises the use of the Hognestad model, while Dias advises the use of a tri-linear model as shown in Figure A.1b. Due to possible high stress concentrations plasticity was considered and the tri-linear model was chosen due to a better integration into the Ansys software. Furthermore, due to software limitations, the behavior in tension was considered equal to the behavior in compression. For simplicity and convergence reasons, failure mechanisms such as compressive crushing considered by Dias and tensile cracking considered by JC were not taken into account. Although the elastic stiffness of the concrete is

equal in both compression and tension, the lack of implemented low strength tensile failure might make the model too stiff. If not all the required concrete material data is available in the corresponding study or the product specifications, the data was filled in by estimation of the most representative concrete class described by EC2 based on the compressive strength or elastic modulus. At last, based on the study by Thai, a Poisson ratio of 0,2 will be used for the concrete.

As mentioned by JC and Thai, the contribution of the screws to the elastic behavior is minimal and will therefore not be modelled.

The insulation material will be modelled as simple elastic isotropic materials. If the required elastic moduli not is available in the corresponding study or the product specifications, it was determined from the relation to the dynamic stiffness $s' = E/h_{insulation}$ or its required load for 10% compression. A Poisson ratio of 0,0 will be used. The impact of the these parameters are however expected to be minimal.

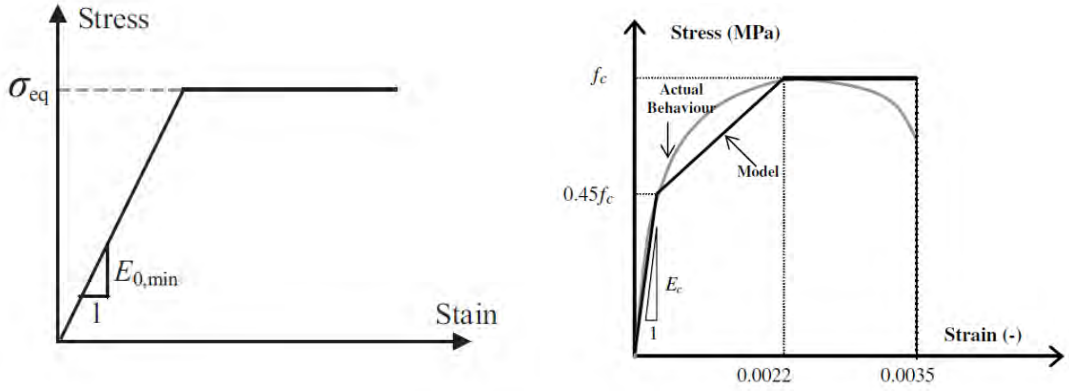

(a) Bi-linear timber model [29]. (b) Tri-linear concrete model [13].

Figure A.1: Used material models

For the all the replicated FEM models, the boundary conditions were kept similar to their experimental investigations. While JC performed a symmetric push-out test where the stable geometry and friction created transverse stability, Lamothe et al. and Thai performed asymmetric push-out test in which stability was assured by extra transverse rollers in the opposing corners of the vertical supports. In the FE-model, the longitudinal support and loading plate will also feature a transverse displacement constraint to replicate the experimental boundary conditions. Besides, due to the difference in the stiffness of the CLT layers, the introduction of the load was done by by displacement of a steel loading plate against the full height of the timber in 3 steps; 0,2 mm at t=1s, 1mm at t=2s and 5 mm at t=3s.

For the models without insulation the contact surfaces were modelled as 'bonded' for the interfaces of the CLT-layers and the for the interface between the steel loading plates and the CLT/Concrete. The 'bonded' contact type indicates that the no penetration (compression), no separation (tension) and no sliding (shear) is allowed between between the elements, similar to gluing them together. The interface between CLT and Concrete was modelled as 'friction-less'. This contact type is opposite to 'bonded', only disallowing penetration, but allowing separation and free sliding. This is done to replicate the presence of PE-foil for moisture. This approach is essential since the combination of friction and the eccentricity of the asymmetric push-out test could increase the observed connection stiffness up to 10% [38], [53].

Furthermore, the models will be made in a 3D environment, as is also done by Dias, JC and Thai. Besides, the mesh will be generated using the 'linear' element order setting in Ansys, resulting in mostly solid hex-8 elements. The general mesh size was 10 mm, which was refined in the notch area to 5 mm. The setting 'Large deflection' will be used. Besides, only half the specimens will be modelled, using symmetry in the width-direction to cut down computational time.

At last, the three experimental investigations by JC, Thai and Lamothe all used the loading pattern as described by EN 26891, in which the specimen has to be loaded until 40% of the expected maximum load F_{max}, from which the load has to be reduced until to only 10% of F_{max} before increasing the load until failure. This allows the determination of two stiffness indications; $K1$ for the initial loading up to $0,4F_{max}$ and $K2$ for the second loading up to $0,4F_{max}$ as shown in Figure A.2. The reasoning is the possible underestimation of the stiffness by $K1$ due to initially present settling effects in the set-up and specimen. Although the use of $K2$ is therefore more widespread, $K1$ is also used due to its conservative nature as for example by Thai. Similar to the modelling approach of JC, this 'loop' will not be modelled since settling effects are not present in FEM models. The connection stiffness K from the models, will be determined based on the two data points closest to where the experimental investigations initiated the decrease of load. Since the used notch widths vary between the three used experiments and the width is generally assumed to have a linear impact on the connection stiffness [53], the connection stiffness's will be converted to connection stiffness per meter width K^* for comparison.

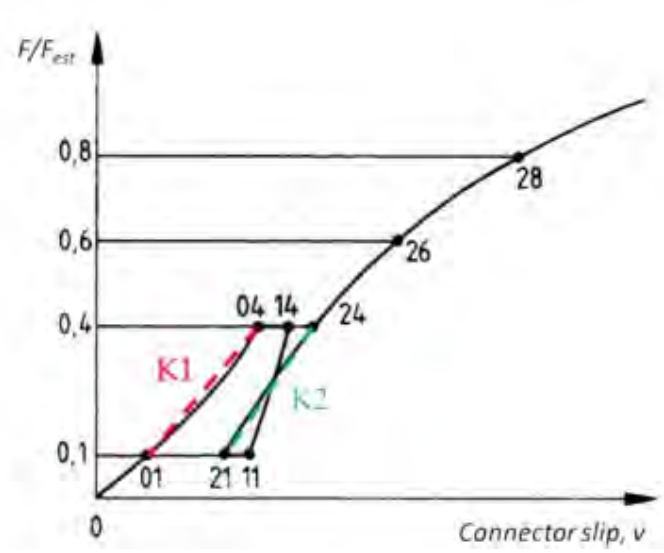

Figure A.2: Loading pattern and stiffness determination according to EN 26891 [19], [53].

A.1.1 Replication of Jiang and Crocetti, 2018.

As mentioned one of the studies used to validate the modelling approach is the study of Jiang and Crocetti in 2018 into CCC floors with rectangular notches, for which among others the latter were experimentally investigated using symmetric push-out tests [29]. Besides the experimental push-out test, they also built and validated an accurate FE-model in the Abaqus software. The set-up of these two, together with the set-up of the replicated Ansys model are shown in Figure A.3. Similar to the Abaqus model, the replicated model features an additional symmetry in longitudinal direction applicable due to the symmetric push-out test setup. Besides,

since no foil was used in the experimental investigations, a friction coefficient of 0.57 was used for the CLT-Concrete interface. This was therefore also done in the replicated model using the 'frictional' contact type. The main differences between the two FE-models is the integration of concrete post-failure in tension by using tension stiffening and the inclusion of the stirrup placed in the notch in the form of a beam element. These two differences should however not have impact on the elastic region. Due to its 5-ply configuration and the outlier results for N180-1, the N180-2 specimen will be used to validate the model.

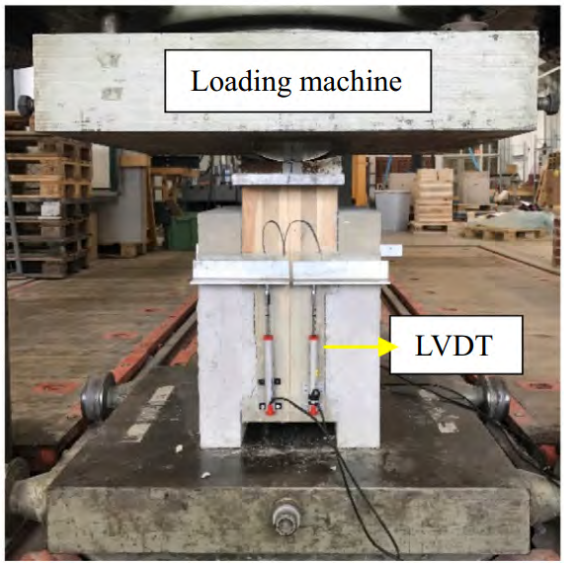

(a) Experimental set-up

(b) Specimen before pouring of the concrete

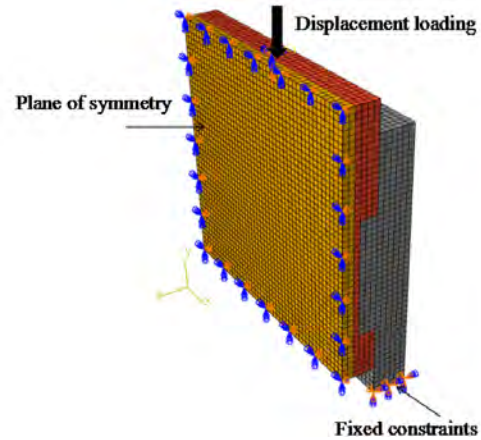

(c) Abaqus model

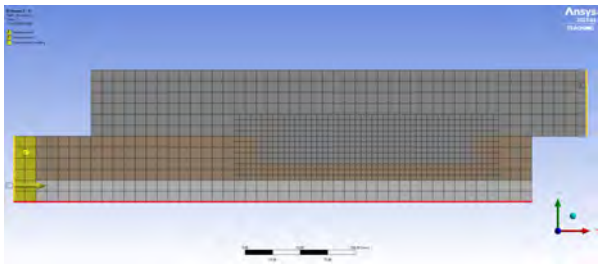

(d) Side view of replicated 3D FEM model.

Figure A.3: Set-up of the experimental investigations and Abaqus model studied by JC [29] and the corresponding replicated FEM model with supports in yellow, longitudinal-symmetry surface in red and view on the width-symmetry surface.

Figure A.4 shows the approximate results of the experimental investigations, which are also valid for the Abaqus results due to high accuracy, and the result obtained from the replicated FE-model. As expected, a large difference in failure load can be observed. However, most important is observable underestimation of the connection stiffness per meter width K^*

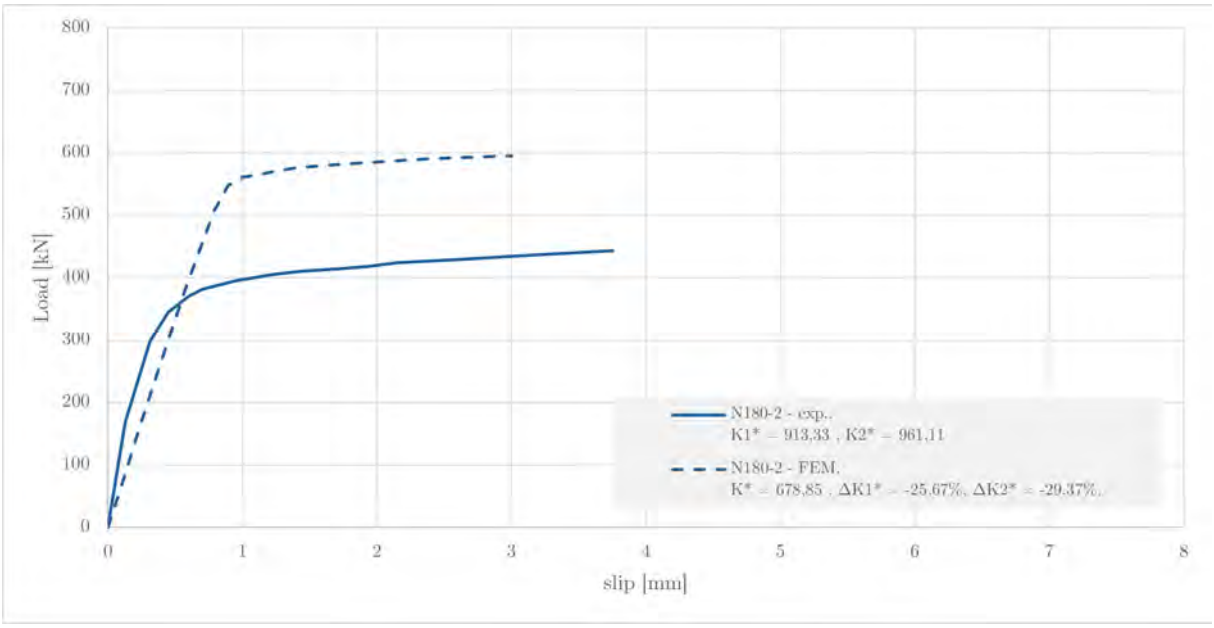

Figure A.4: Load-slip diagram showing the experimental results found by Jiang and Crocetti [29] and the replicated FEM results.

A.1.2 Replication of Thai, 2021.

The second study used to validate the modelling approach is the study of Thai in 2021 into vibration behavior and optimization of design of CCC floors [53]. For this study also different parameters for rectangular notches for CCC floors were investigated using experimental asymmetrical push-out tests. Similar to JC, the experimental investigation was also used to validate a FE-model to continue broader investigations. The Abaqus software package was used for this again. While the model is very similar to the one used by JC, it does not feature concrete plasticity and other failure mechanisms due to the focus of the study on the elastic stiffness. Besides, due to the presence of PE-foil between the concrete and CLT, the contact were modelled as friction-less. At last, an upper and lower boundary were established using the maximum and minimum values, respectively, of the Young's modulus E and compressive strength σ_{xx} found in experimental material tests. The by Thai chosen notch dimensions of series I, which are also similar to the ones used in the N180-2 specimen of JC, will be replicated. At last, an adapted version of the series I of Thai including the insulation type 1 approach of Lamothe et al. is also modelled. This approach is further elaborated in next section.

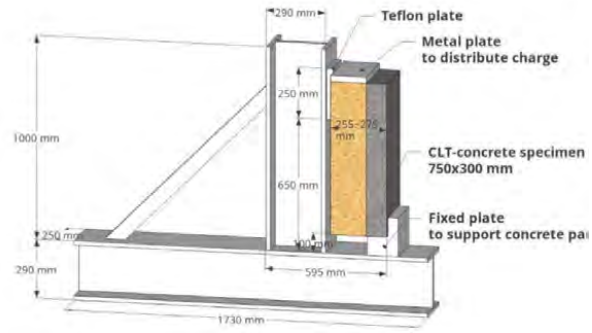

(a) Experimental set-up

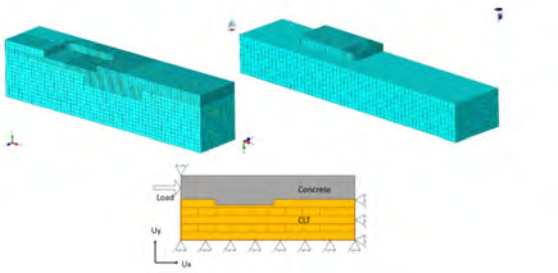

(b) Overview of the Abaqus model

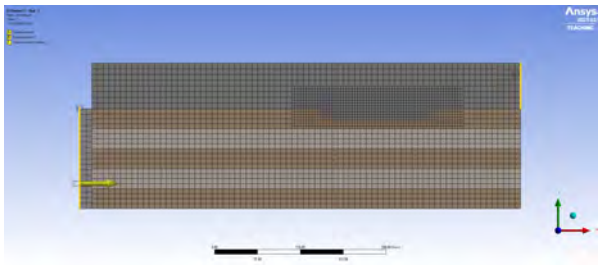

(c) Side view of replicated 3D FEM model.

Figure A.5: Set-up of the experimental investigations and Abaqus model studied by Thai [53] and the corresponding replicated FEM model with supports in yellow and view on the width-symmetry surface.

The load slip diagram for the experimental investigation, upper and lower boundary based on the Abaqus model of Thai and the replicated model in Ansys are shown in Figure A.6. As was noted by the Thai, the experimental investigations were close to the results of the lower-boundary Abaqus model, and were were in agreement up to approximately 6 mm. Besides, Thai also noted an increase of connection stiffness per meter notch width compared to the results of JC, using equal notch dimensions, and mentioned the most probable cause was the use of continuous notches over the width by JC while Thai used discrete notches where the specimen was on both sides 50 mm wider. The loaded part of the timber was therefore not only constrained by the timber underneath but also at its sides.

Furthermore, the replicated model again showed an underestimation of the observed stiffness. Furthermore, the version with insulation featured an expected decrease in stiffness.

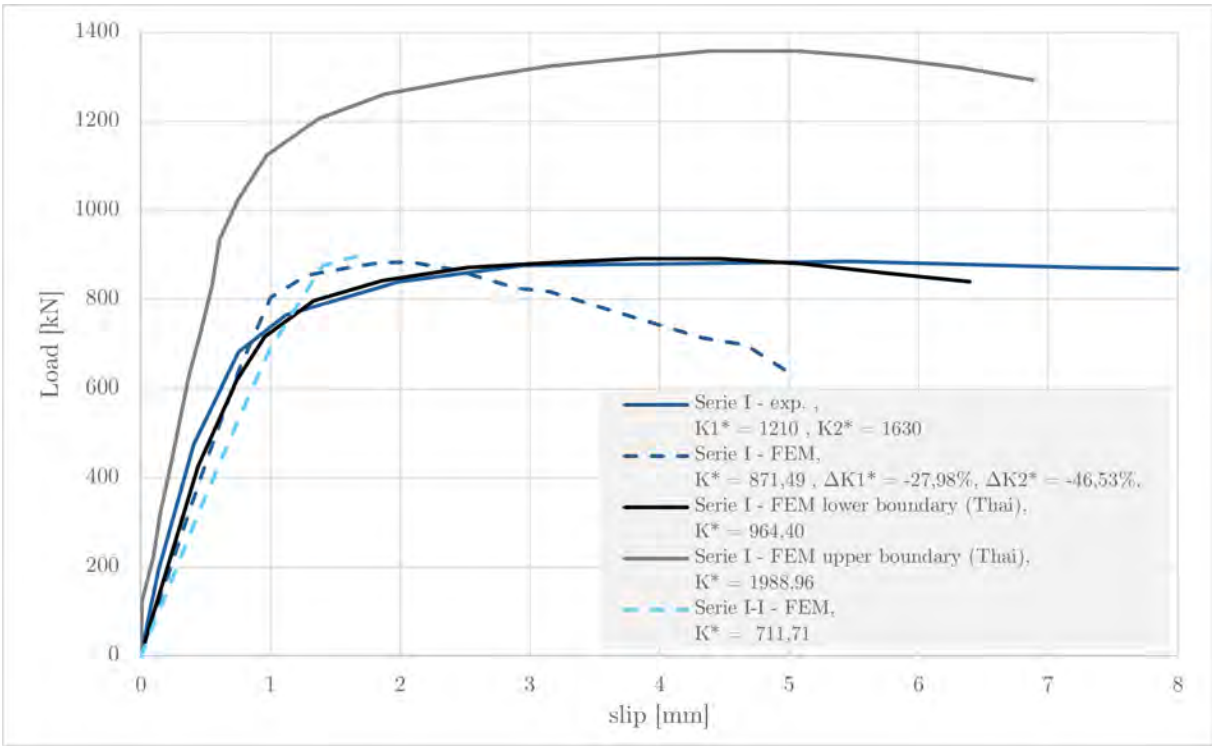

Figure A.6: Load-slip diagram showing the experimental results found by Thai [53], the replicated FEM results and the FEM results of the geometry with added Insulation type 1 (I) based on the approach of Lamothe et al. [33].

A.1.3 Replication of Lamothe et al., 2020.

The last study used to validate the modelling approach is the study of Lamothe et al. in 2020 into the design and engineering of ductile triangular notch connections using HPC and UHFRPC notches with and without an insulation inter-layer [33]. Besides, the study uses two timber types, 5-ply CLT and glue laminated timber (GLT). The insulation versions were only applied to the GLT specimens. Similar to specimen design of Thai, the notches are discrete and 100 mm smaller then the specimen width, creating a 50 mm residual width on both sides. The versions with insulation layer featured one of two wood fibre panel as insulation layer; type 1 using a 19 mm layer of SONOpan II and type 2 using a 25 mm layer of SONOclimat Eco 4. The insulation was added in between the timber and concrete, while these layers kept their original dimensions. This thus increases the total thickness of the specimen. Although the effective height of the notch, which is the height of contact between the CLT and concrete, stays the same, the total height will be increased. For the insulation versions, the replicated model featured the 'bonded' contact type for the interface between the CLT and insulation for stability reasons and the 'friction-less' contact type between the insulation and concrete, since a PE-foil is present between these two layers. The contact of Concrete and CLT in the notch is also still modelled as 'friction-less'. Due to convergence issues no valid replicated FEM model could be made using the type 2 insulation. Furthermore, an additional version was made in FEM of the CLT with insulation type 1 due to the scope of the project.

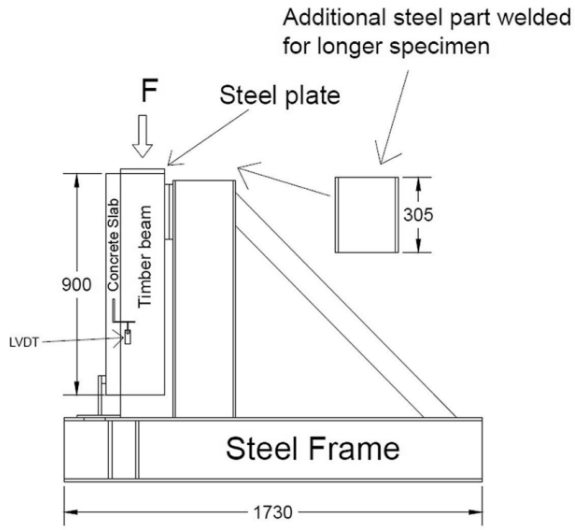

(a) Experimental set-up

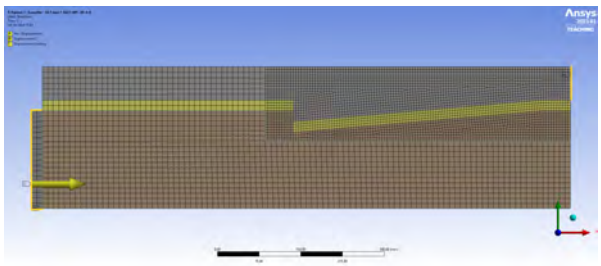

(b) Side view of replicated 3D FEM model for the GLT-HPC-20-4-I.

Figure A.7: Set-up of the experimental investigations by Lamothe [33] and the corresponding replicated FEM model with supports in yellow and view on the width-symmetry surface.

The load slip diagram for the experimental investigation and the replicated model in Ansys are shown in Figure A.8. Although the graph indicates an considerable overestimation of K1, the experimental investigations featured a much higher K2 value. Compared to K2, the replicated FEM model still underestimates the connection stiffness.

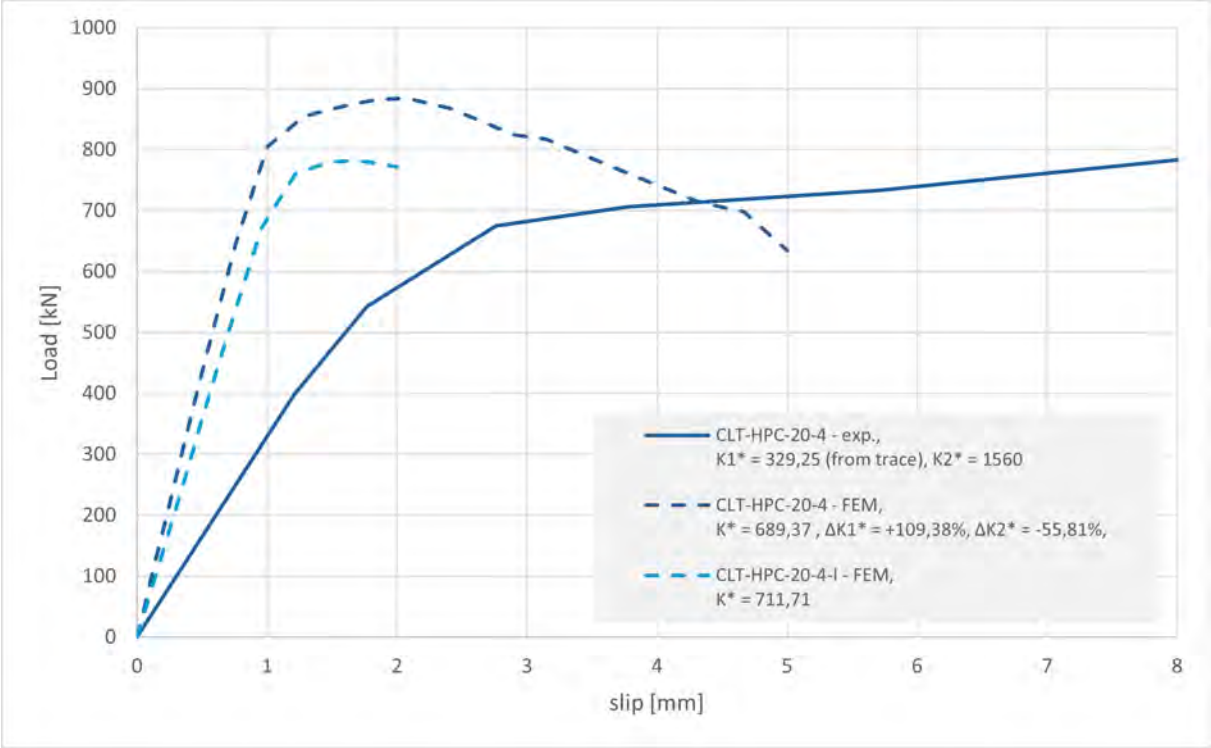

(a) CLT

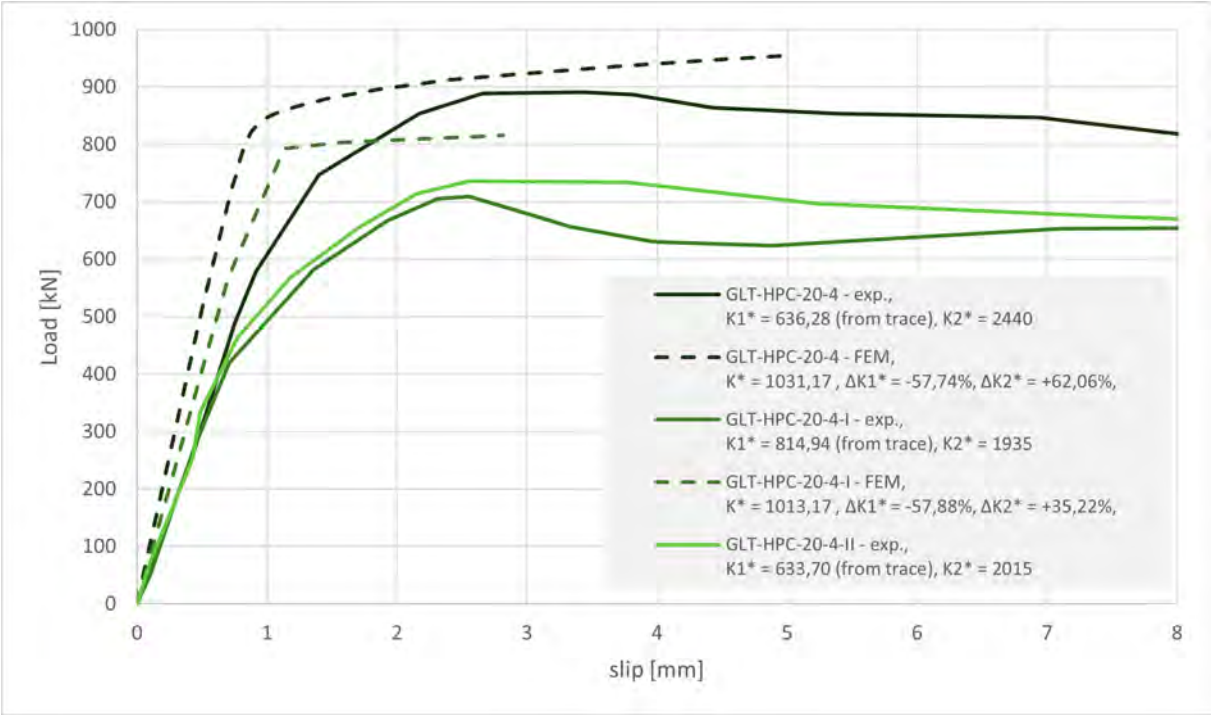

(b) GLT

Figure A.8: Load-slip diagram showing the experimental results found by Lamothe et al [33], the replicated FEM results and the additional FEM results of the CLT-HPC-20-4 series with added Insulation type 1 (I).

A.1.4 Validation

Figure A.9 shows the percentile differences between the K^* values of the replicated models and the $K1^*$ and $K2^*$ values of the corresponding experimental investigations. While, the negative $\Delta K1^*$ values for the JC and Thai specimens is in line with the trend of the $\Delta K2^*$ values, the $\Delta K1^*$ values for the Lamothe specimens show a large overestimation. The most probable reason is an unreliable much lower value for $K1^*$ relative to the value for $K2^*$. Besides, based on their own Abaqus-model Thai observed that the FEM results better align with the values of $K2^*$ then the values of $K1^*$. This is as expected due to the presence of settling effects for $K1^*$. The combination of unreliable $\Delta K1^*$ values and the better observed aligned of FEM results with $K2^*$ suggest the latter should be used for validation. The described modelling approach therefore significantly underestimates by featuring a difference of -29,37% to -57,88% compared to experimental results for $K2^*$. Although thoroughly checked, no specific cause could be found for this large underestimation.

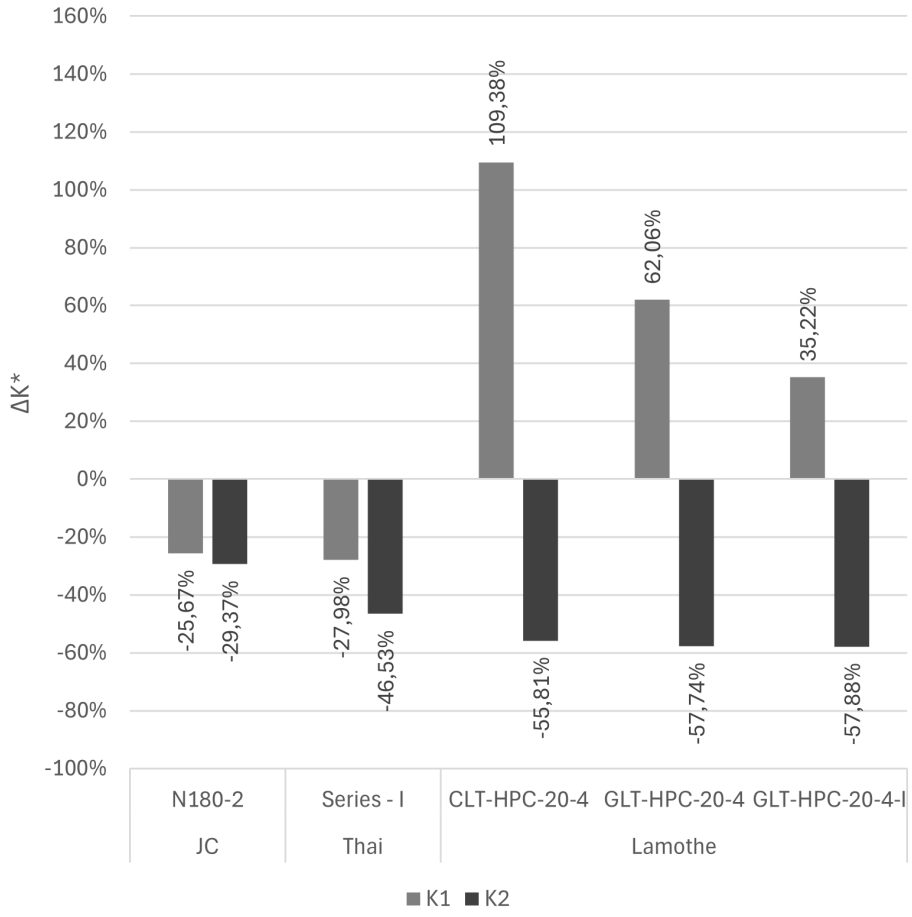

Figure A.9: Difference between the connection stiffness per meter width K^* found in the replicated FEM results as compared to the $K1^*$ and $K2^*$ values of the corresponding experimental investigations.

However, the model is inline with the experimental results for the difference between the versions with insulation and the versions without insulation as shown in Figure A.10. Neglecting the outliers showing an illogical increase of K^*, the addition of the insulation features a decrease

in connection stiffness of -9,56% to 20,97%.

(a) FEM

(b) Experimental investigations by Lamothe et al. [33].

Figure A.10: Difference between the connection stiffness per meter width K^* of the specimens with added insulation type 1 or 2 as compared to their counterparts without insulation.

A.1.5 Additional investigations

After the replication of the experimental results additional investigations were done to improve the modelling approach. These investigations were done in a lighter 2D model. Most importantly, the models now mainly use 4-node shell elements and plain strain assumptions were used to replicate the width of the floor specimens. Comparing the results for the 3D models to the results of the 2D models shown in Figure A.13 for the 6 floors with notches, it can be concluded that the 2D model accurately represents the 3D model. These additional investigations are done using the geometry and properties of the three versions of LSD v1 floor.

Firstly, it was observed that the models showed significant outward rotation, which caused separation between the concrete and timber. This phenomena is not accurate representation for the actual behavior since it will be prevented by the addition of the fasteners. While these fasteners do not directly impact the connection stiffness as described above, they thus influence the stability of the FEM model and therefore indirectly affect the found connection stiffness. This second function was replicated by using the 'no separation' contact type instead of the 'friction-less' contact type for the longitudinal interface between the concrete and CLT as shown in Figure A.11a. This contact type similarly does not constrain sliding, but it does constrain separation next to penetration. This resulted in an approx. 8% increase in connection stiffness. This effect might also explain the smallest observed difference between the experimental and replicated FEM results for the JC specimen, which featured a symmetrical push-out test in which the timber was constrained for ration due to symmetry.

For the conceptual floor this phenomena was also noted, but can not be tackled by changing the contact type of the CLT and concrete for the longitudinal surface since there is no contact

due to to presence of the insulation layer in between. Although the conceptual floor design does not feature fasteners, the transverse rotation was still assumed too large to get an accurate value for the connection stiffness. It was therefore chosen to also constrain the unloaded end of the concrete in the vertical direction. This resulted in an 84,32% increase in connection stiffness compared to the unstabilized model. The conceptual floor therefore only featured a difference in connection stiffness of -20,97% instead of -57,12%, which is again in line with results found earlier. Furthermore, it was tested if different configuration of contact types between the CLT and insulation and concrete and insulation influenced the results, e.g. changing from 'friction-less' to 'bonded' or 'rough'. The latter allows separation, but does not allow any sliding (shear) when there is contact between the elements. It was observed that these changes had no significant on the results due to relative insignificant stiffness of the inter-layer. However, fully bonding both layer to the insulation might influence the separation mechanisms and is thus less applicable. Furthermore, the using a 'bonded' contact with the CLT and 'rough' contact with the concrete showed better model convergence compared to using 'friction-less'.

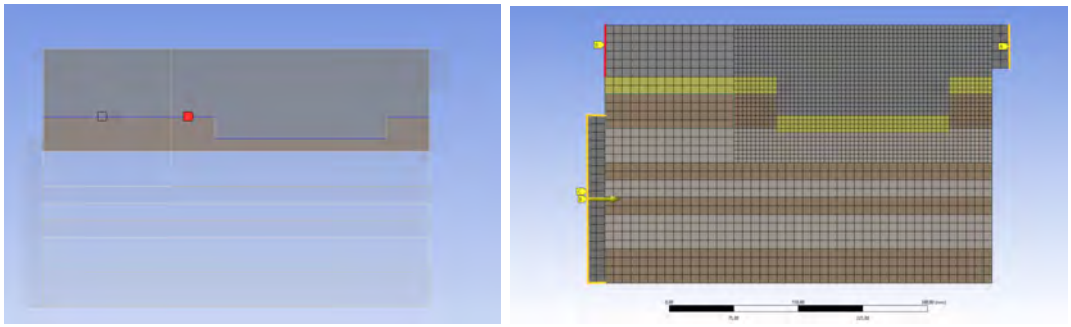

(a) Longitudinal CLT-Concrete interface featuring the 'No-separation' contact type in the FE-model.

(b) Boundary conditions of the conceptual floor, including the additional vertical support of the concrete in red.

Figure A.11: Measures taken for the stabilization of the push-out models for the traditional (a) and conceptual floor (b).

Secondly, the impact of the dimensions of the load- and support plates were investigated. Next to the base configuration of these plates over the full height of the timber and concrete, called plate configuration (PC-A), four other configurations were considered. In PC-B, the loading plate at the CLT was shortened at the top and the concrete was shortened at the bottom at 30 mm, such that the CLT-plate reached exactly the second CLT layer. For PC-C, this was only the case for the plate at the CLT, while the plate at the concrete had the same dimensions. PC-D, featured a full height concrete-plate while the CLT-plate was limited to the notch depth, representing the continuous part of the timber. At last, the plates in PC-E are shortened based on the approximate center of axial force in the timber and concrete based on the stress diagrams obtained from the separated gamma-method using the K^*-value based on PC-A.

Table A.1: Results for the LSD v1 traditional design using the different load and support plate configurations.

		PC-A	PC-B	PC-C	PC-D	PC-E
K^*	[kN/mm]	1417,93	875,68	883,14	1086,80	180,52
K^*_{PC-A}	[%]	-	-38,24	-37,2	-23,35	-86,24

From the results shown in Table A.1 it can be seen that all the additionally investigated configurations decrease the stiffness. This is due to PC-A mainly uses the unrealistic full height of the first CLT layer for the force transfer, while the others can only use a limited height and/or have to transfer it through its weak second layer. The difference in stiffness between the first and second layer can be seen in the large local stress increase for PC-D, in which almost all the force is transferred through the residual height of first layer. Furthermore, the similar results of PC-B and PC-C show the minimal impact of the concrete plate dimensions. Furthermore, PC-E was not further investigated due the extremely large decrease in connection stiffness in combination with convergence issues. All in all, the loading and support plate configuration has significant impact on the results of the connection stiffness. This is inline with the conclusions of Rasmussen in his literature study on the validation of experimental push-out test [48]. The plate configuration D will be chosen over plate configuration B, due to the large positive impact of residual height of the first CLT layer, as was also mentioned by Lamothe et al. [33], and a better alignment with the extreme equilibrium states illustrated by Rasmussen.

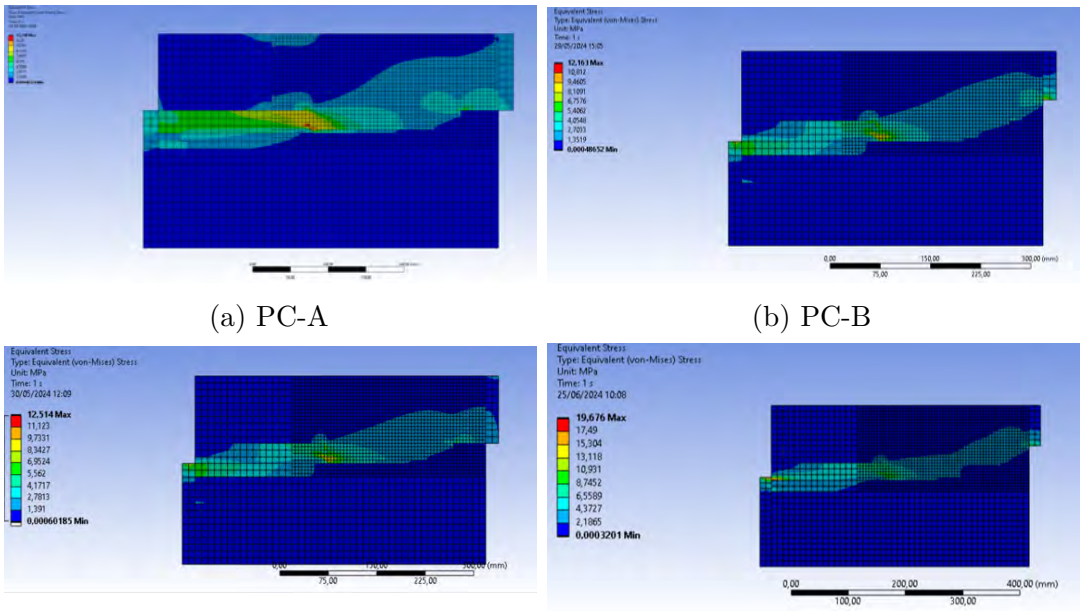

(a) PC-A (b) PC-B

(c) PC-C (d) PC-D

Figure A.12: Equivalent Von Mises stress at 0,2 mm deformation of the numerical push-out test for the LSD v1 traditional floor with the different plate configurations.

A.2 Final modelling and results

Based on the experiences with preliminary modelling, the final modelling approach for the ED/LSD/LSD+ floors thus consists out of the creation of a 3D model, using linear 8-node solid elements, in which the timber is displaced by a steel loading plate covering the full timber excluding the notch height and the concrete is supported by a steel support plate. The timber is modelled as a elastic-perfectly plastic material using the Hill-criterion and the concrete is modelled as a tri-linear material. Further failure mechanisms are omitted due to the scope of the study on the elastic range. Fasteners are left-out of the model due their minimal direct impact of the shear behavior. To replicate their function to prevent separation, the longitudinal surface between the CLT and concrete will be modelled using the 'no separation' contact type. The perpendicular CLT and concrete surface will be modelled keep the 'friction-less' contact type and the individual CLT-layers will be glued together using the 'bonded' contact type. This is similar to the conceptual floor, which additionally feature a 'bonded' CLT-insulation contact surface and a 'rough' insulation-concrete contact surface. To stabilize the models of the conceptual floors, an additional vertical roller was added at the unloaded concrete end. Besides, it was also found that a 2D model using plain strain assumptions aligns well with the results of the 3D-model of the full specimen.

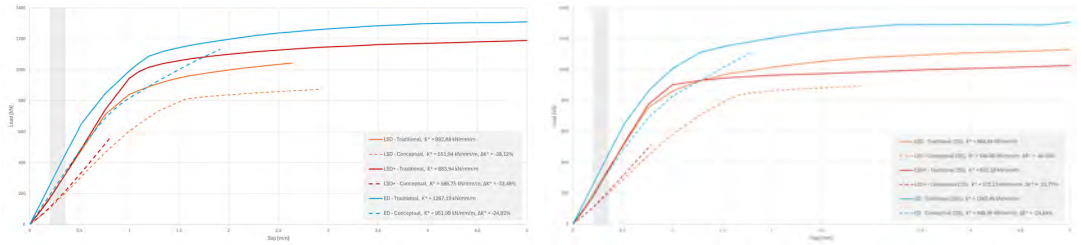

(a) 3D (b) 2D

Figure A.13: Load-deformation diagrams of the numerical push-out test for the 3D and 2D models, including the stiffness determination domain, the corresponding equivalent connection stiffness per meter width K^* and the difference of the conceptual floor compared to the traditional floor ΔK^*.

Although not extensively investigated, the figure shows the influence of the floor design on the stiffness while the notch dimensions are kept the same. This variation is mainly present in the case of the ED - Traditional floor. While the most apparent reason would be the higher concrete grade used in the ED floors, the general strain in the concrete was found to be minimal compared to the strain in the timber shown in the figures below. To explain the deviation for the ED floors and the low variation between the LSD and LSD+ floors, the exact impact of the parameters should be further investigated.

A.2.1 ED floors

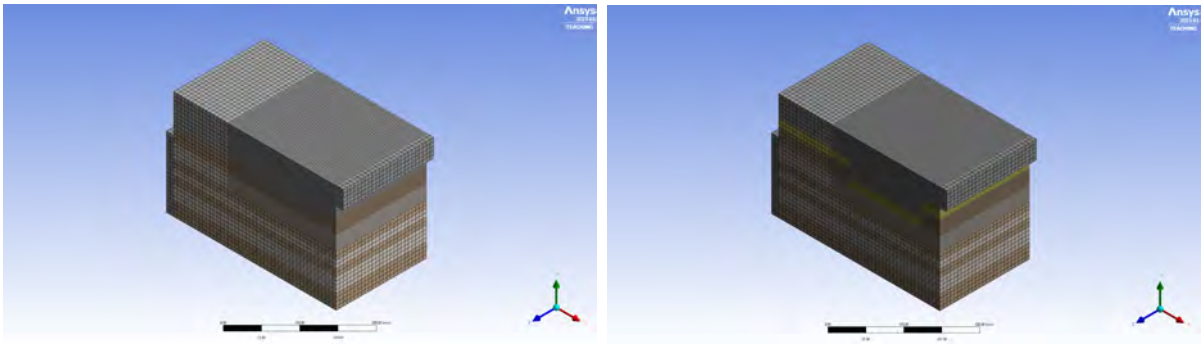

(a) 3D view

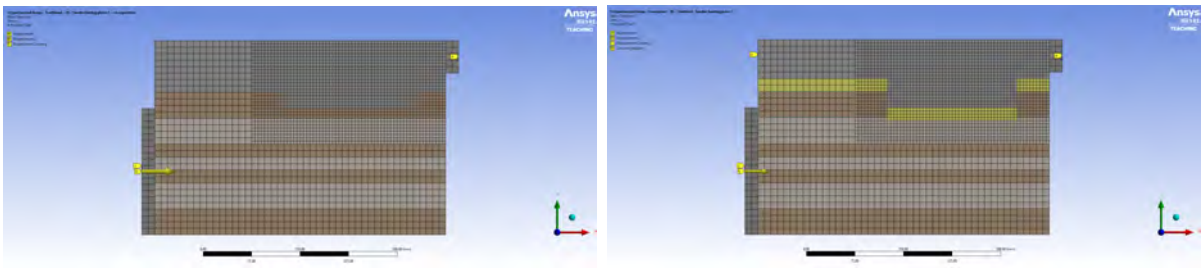

(b) Side view

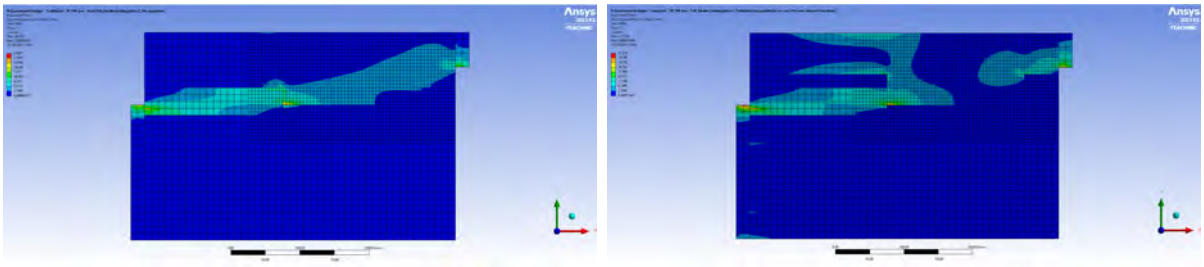

(c) Equivalent stress at 0,2 mm (elastic)

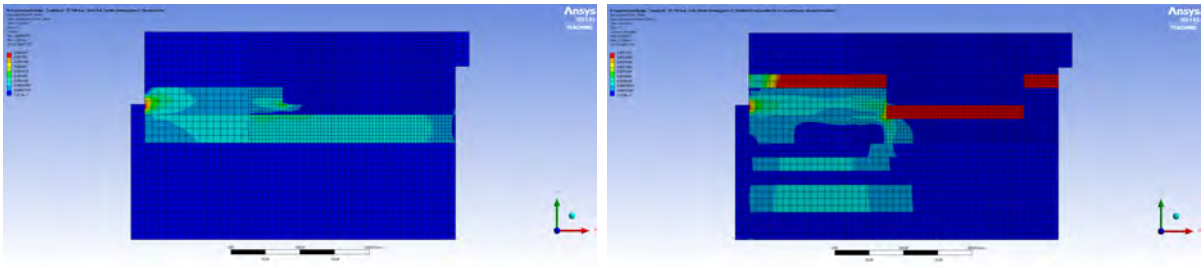

(d) Equivalent strain at 0,2 mm (elastic)

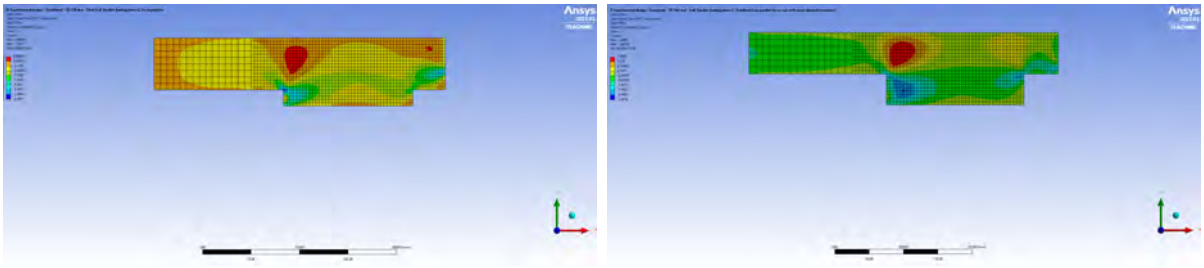

(e) Shear stress in concrete at 0,2 mm (elastic)

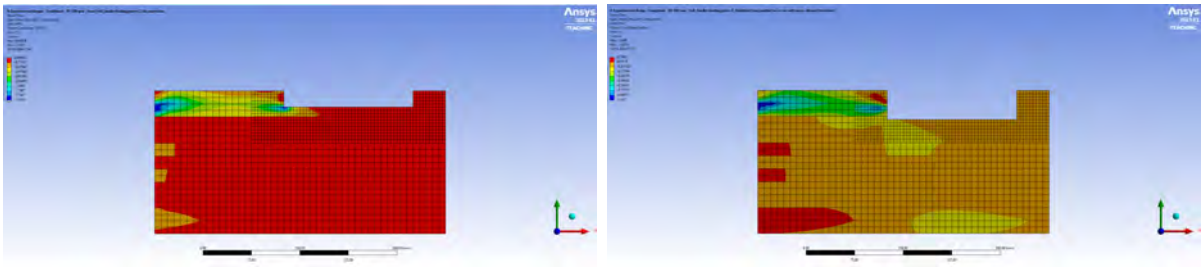

(f) Shear stress in CLT at 0,2 mm (elastic)

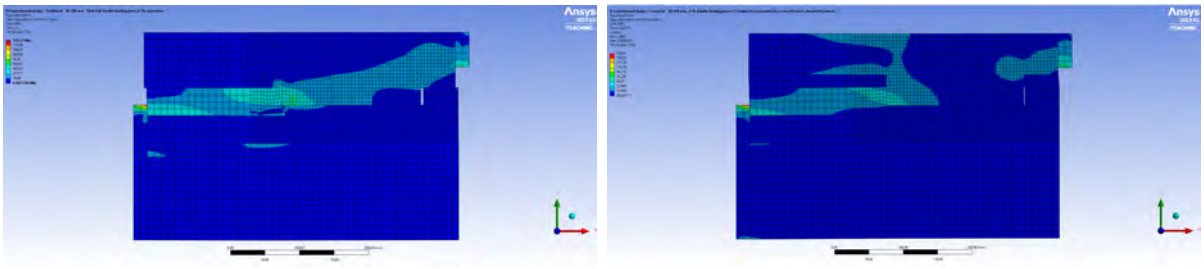

(g) Equivalent stress at 5 mm & 1,9 mm (plastic)

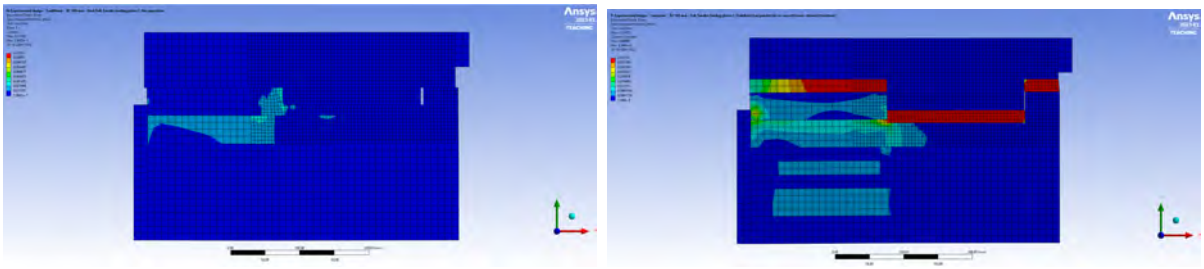

(h) Equivalent elastic strain at 5 mm & 1,9 mm (plastic)

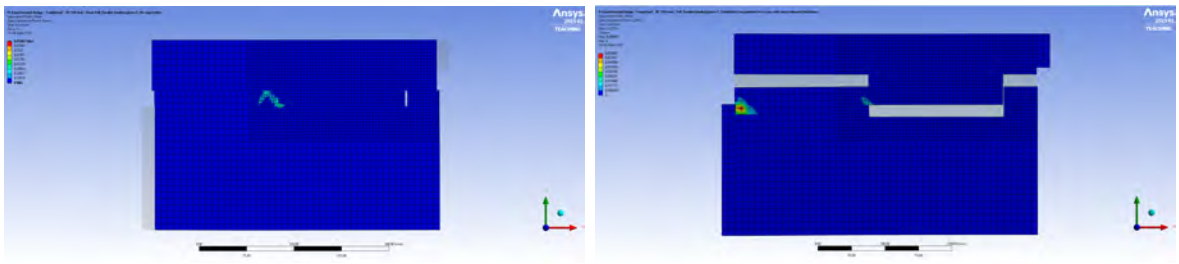

(i) Equivalent plastic strain at 5 mm & 1,9 mm (plastic)

Figure A.14: Overview of the push-out test of the ED floor with the traditional floor on the left and conceptual floor on the right.

A.2.2 LSD floors

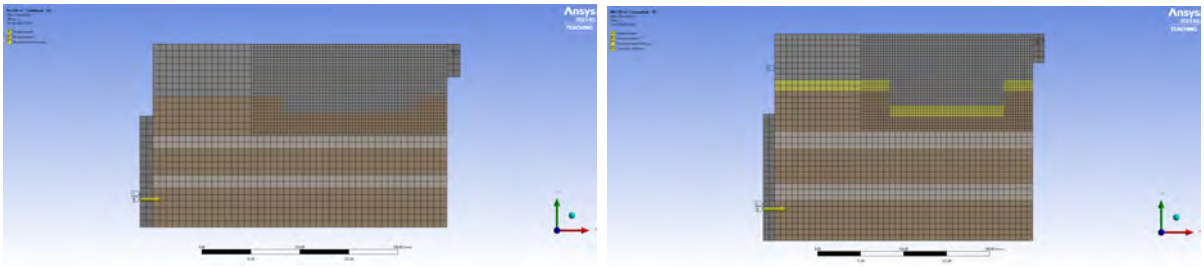

(a) Geometry and boundary conditions

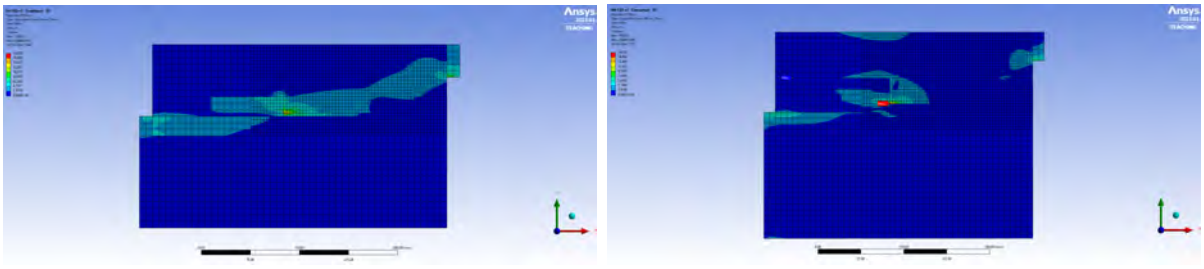

(b) Equivalent stress at 0,2 mm (elastic)

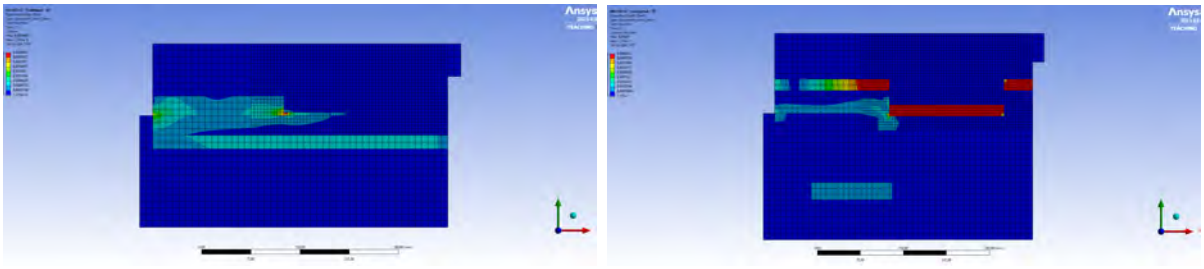

(c) Equivalent strain at 0,2 mm (elastic)

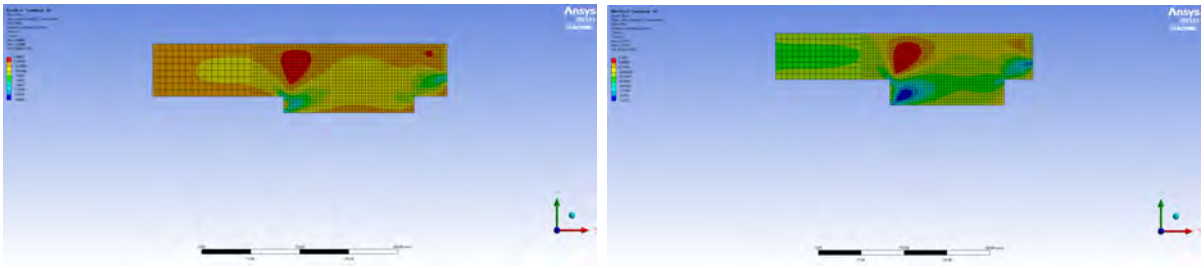

(d) Shear stress in concrete at 0,2 mm (elastic)

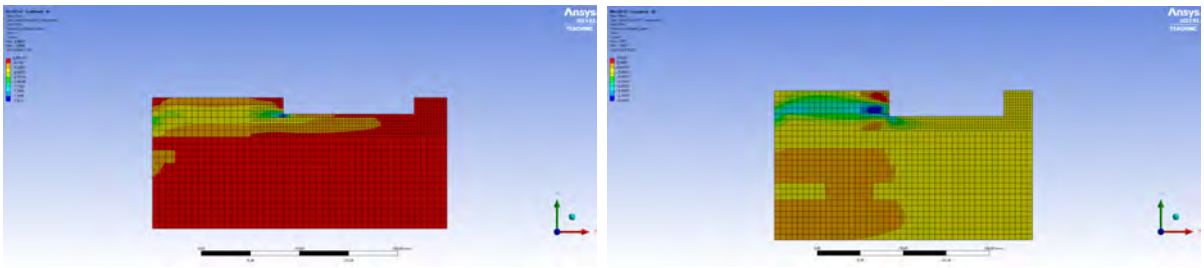

(e) Shear stress in CLT at 0,2 mm (elastic)

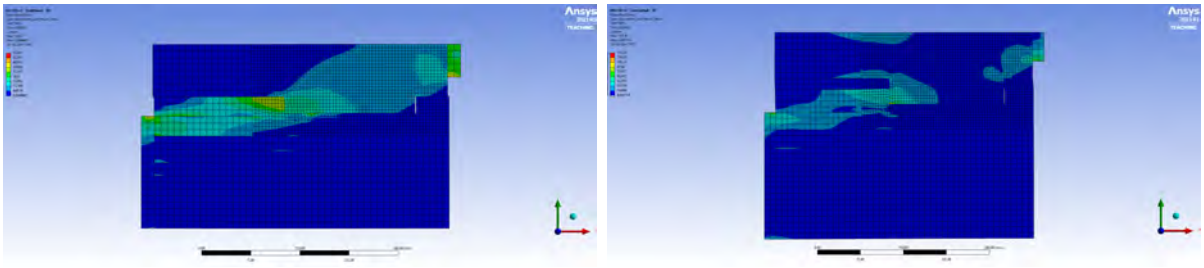

(f) Equivalent stress at 2,6 & 2,15 mm (plastic)

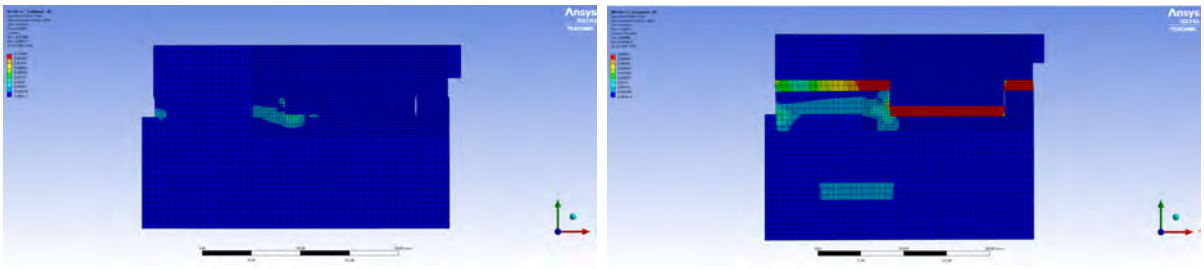

(g) Equivalent elastic strain at 2,6 & 2,15 mm (plastic)

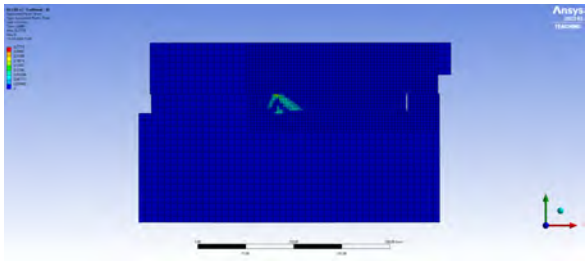

(h) Equivalent plastic strain at 2,6 (plastic)

Figure A.15: Overview of the push-out test of the LSD floor with the traditional floor on the left and conceptual floor on the right.

A.2.3 LSD+ floors

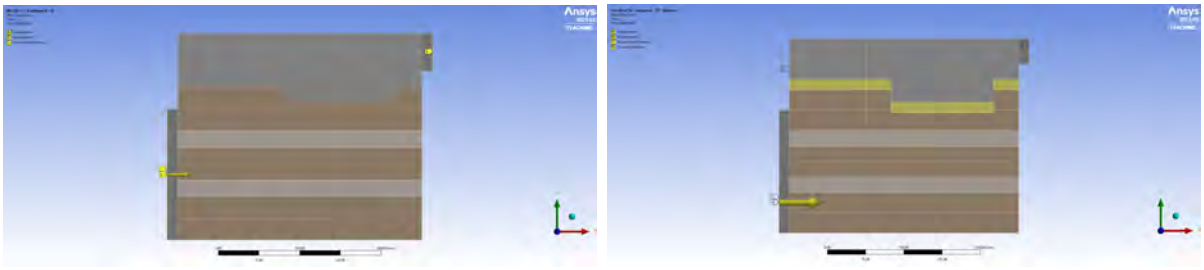

(a) Geometry and boundary conditions

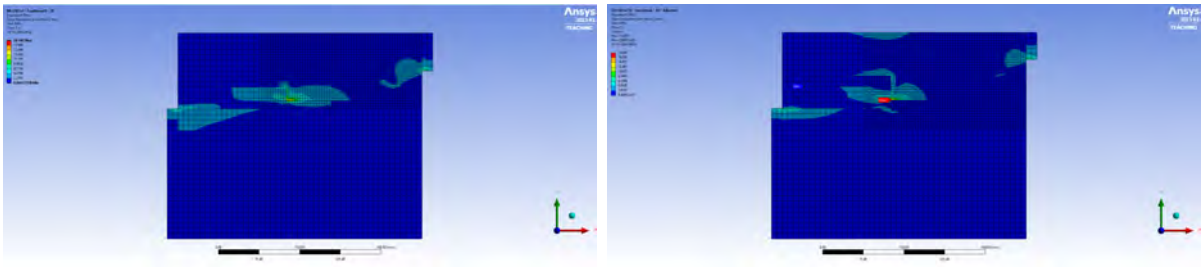

(b) Equivalent stress at 0,2 mm (elastic)

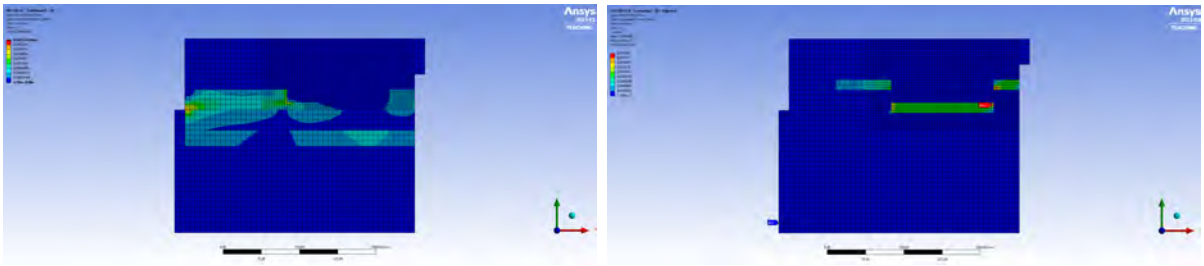

(c) Equivalent strain at 0,2 mm (elastic)

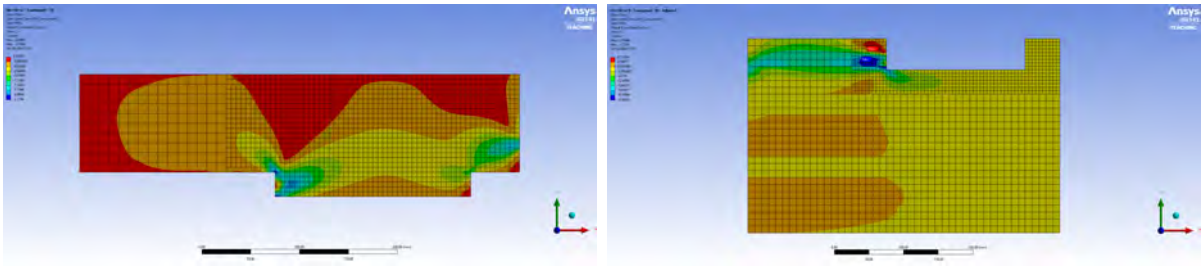

(d) Shear stress in concrete at 0,2 mm (elastic)

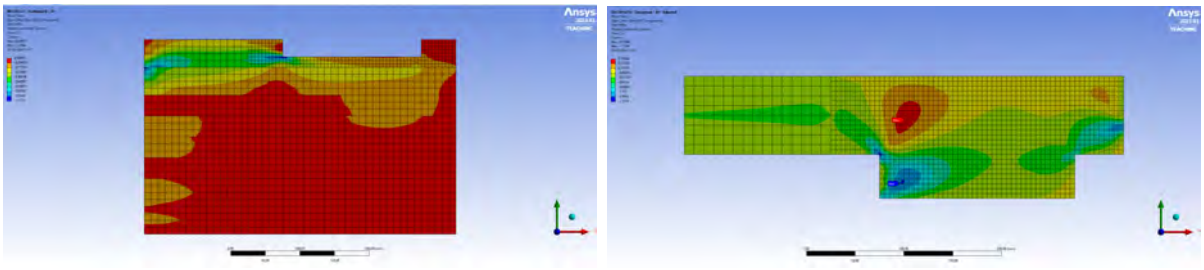

(e) Shear stress in CLT at 0,2 mm (elastic)

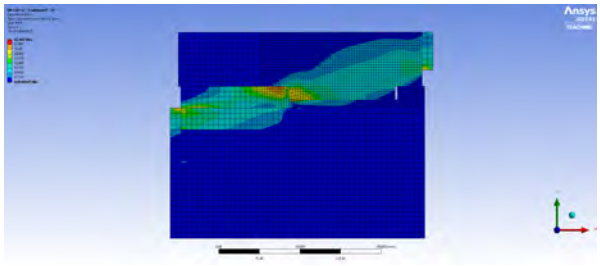

(f) Equivalent stress at 5 mm (plastic)

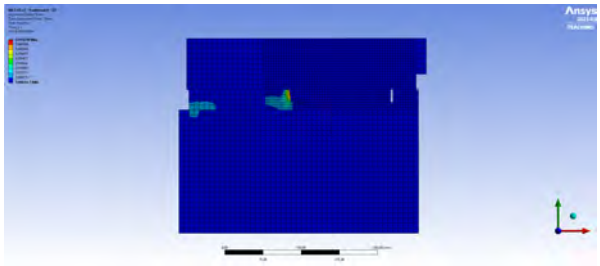

(g) Equivalent elastic strain at 5 mm (plastic)

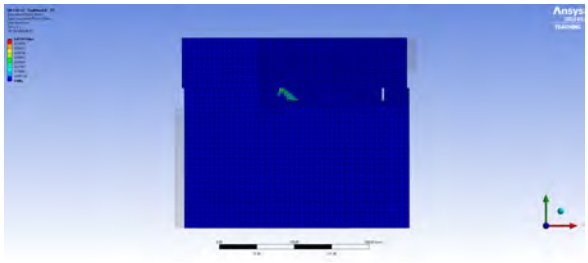

(h) Equivalent plastic strain at 5 mm (plastic)

Figure A.16: Overview of the push-out test of the LSD+ floor with the traditional floor on the left and conceptual floor on the right.

B Design of the LSD and LSD+ floors

In this appendix the iterative design processes for the determination of the LSD and LSD+ floors are elaborated. While the LSD design process focuses on the design of floor which are on the edge of structural unity checks and fulfills the failure order criteria, the LSD+ floors are designed on the edge of the vibration criteria while also fulfilling the structural criteria.

B.1 Design of the LSD floor

As introduced in Chapter 4, the aim of the Large Span Design categories is to design a structural and conceptual floor which just fulfills the structural requirements. The structural requirements are described in Section 5.1. For the determination of the stiffness firstly an push-out test will be replicated which provide the value for the connection stiffness K used in the second step of calculation of the floor properties using the γ-method. Besides, it was mentioned that the effective spacing for connector with a spacing larger then 5% of the floor span should feature adapted zoning. Besides, it is also advised to distribute the spacing following the shear distribution over the length. As described in this study the 2-zone approach was used. Furthermore, as described notch failure should also be taken into account to ensure the Timber Compression Failure (TCF) in the notch is governing.

However, the design such a floor is a iterative process since it requires a starting geometry to numerically model as push-out test. The results of the push-out test using the starting geometry, in the form of connection stiffness, should then be implemented. With these values a build-up can be designed which approach unity checks of 1,0. However, this new geometry should then again be modeled to find its actual connection stiffness. Due to the high influence of geometry on connection stiffness, the connection stiffness likely differs significantly and the has to be adjusted for the unity checks to approach 1,0 again. This continues with each step lowering the differences until a satisfactory built-up is found which approach 1,0 with its actual connection stiffness.

This was thus also the case for the design of the LSD floor, in combination that the approach was adapted over time. It results in three phases as shown in Table B.1.

Table B.1: Overview of the three phases of the design process for the LSD floors.

	Connection stiffness	Spacing	Cross-section analysis	Connection failure	Result	
					Traditional	Conceptual
LSD v1	FEM model of literature Push-out test	Constant 400 mm	Separated Gamma method	-	100 0 180	70 25 180
LSD v2	FEM model of LSD v1	Adjusted spacing in two zones	Extended Gamma method	Boccadoro-method	80 0 200	60 20 200
LSD v3	FEM model of LSD v2	Adjusted spacing in two zones	Extended Gamma method	Boccadoro-method	80 0 200	60 20 200

For the starting geometry the geometry of Series I in the study by Thai into experimental push-out tests of CCC floors with rectangular notches [53] was chosen. Although actual values

of the experimental push-out test are available, the results from the numerical approach to determine the connection stiffness is used for consistency. For the conceptual floor the same starting geometry was used while just adding 20 mm of insulation in between. Furthermore, LSD v3 features the same build-up as previous step, since the redone numerical modeling resulted in a connection stiffness which did not impact the final UC's significantly. This thus concluded the process.

The steps in each iteration to design the build-up firstly focused on the check for instantaneous and long-term deflection. If the build-up did not fulfill the deflection UC's, the concrete grade and/or height was increased in steps of 5 mm. If the concrete reached it maxed thickness of 100 mm or cracking occurred, the timber was heightened with steps of 10 mm, possibly switching between 5s-, 7s-, 7ss- and 8ss-ply CLT.

When some build-ups were determined which feature a UC of 0.9-1,0, the following step was to look at the cross-section failure in combination with the notch failure load to see which had a lower UC and was thus governing. The goal was to create a floor design which was governed by Timber Compression Failure (TCF) in the notch, since it is the only ductile failure mode in the system. Firstly, it was quickly noted that a minimum concrete grade of C25/30 was needed to make Timber Compression Failure governing over all the other notch failures. Then the second challenge was to make it governing over concrete cracking. Since an increase in concrete height, and in some occasions, grade also increased its relative contribution to the stiffness, it resulted in higher flexural tensile stresses and thus concrete cracking. The main focus on making TCF governing over concrete cracks was to mainly focus on increasing the spacing which results in larger shear force transfer per notch. However, an increase in spacing also results in a decrease in bending stiffness, requiring increase in concrete-height. As can be expected this can result in dead-ends of the design process, therefore also the timber was upped sporadically in steps of 10 mm. This process resulted in several options with differing timber and concrete heights, concrete grades and spacings. The several options which all satisfied the deflection, stress and failure order criteria. The final choice of the traditional and conceptual LSD floors was based on a build-up with UC between 0,95-0,1, since it is thus a configuration on the edge of the criteria, a build-up with equal timber height, total height and spacing for the traditional and conceptual floor making it the best comparable floors.

As mentioned inChapter 4, the decoupled floor featured the same layer build-up as the conceptual floor and the Traditional floor with F.F. was just the configuration of the Traditional floor with the 20 mm insulation layer used in this study and a floating concrete layer with the same thickness as used in its conceptual and decoupled counter parts made of the lowest considered concrete grade C20/25.

B.2 Design of the LSD+ floor

As introduced in Chapter 4, the aim of the Large Span Design+ categories is to design a structural and conceptual floor which just fulfills the vibration requirements. This was done by the combination of the stiffness determination approach mentioned in previous section and the reEC5-method explained in Section 6.1. For the determination of the build-up for the LSD+ floors, the full stiffness determination approach, thus including the zoning spacing, the extended *gamma*-method and Boccadoro-method, was used from the start and the geometry of the LSD v3 traditional and conceptual floors were used as starting point.

The aim for the LSD+ design process is again to find floor configurations with minimal amount of material. Therefore, similar to the LSD floors design process, the timber was only increased after one or two best concrete-spacing configuration were found. After it was found, the process was repeated for a 10 mm thicker CLT configuration and find again the optimum concrete-spacing configurations. In the end it results in a couple of good option for which the one was chosen which will be used in the study.
To increase the vibration performance the bending stiffness and mass of the floor can be increased. However, even more extreme then for the LSD floors, simply increasing the concrete height/grade or decreasing the spacing was not as straight forwards. As shown in Table B.2, it requires mainly balancing of the concrete height and spacing. In the design process it was especially noted that the required Class III could be reached when the natural frequency is above the 8 Hz threshold and the Response factor can be calculated through the velocity domain.

Table B.2: Example of a step in the determination of the LSD+ floors

			E2E	E3	E3B	E4	E5	E6
Properties	Concrete	[-]	C25/30	C25/30	C25/30	C25/30	C25/30	C25/30
	h_1	[mm]	**60**	**80**	**80**	90	100	100
	CLT	[-]	8-ply	8-ply	8-ply	8-ply	8-ply	8-ply
		[-]	-30-20-30-30-20-30-30--	-30-20-30-30-20-30-30--	-30-20-30-30-20-30-30--	-30-20-30-30-20-30-30--	-30-20-30-30-20-30-30--	-30-20-30-30-20-30-30--
	h_2	[mm]	**220**	**220**	**220**	**220**	**220**	**220**
	t_1	[-]	**20**	**20**	**20**	**20**	**20**	**20**
	h_{tot}	[mm]	300	320	320	330	340	340
	Connector	[-]	-	-	-	-	-	-
Structural	K_{ser}	[N/mm]	8,61E+05	8,61E+05	8,61E+05	8,61E+05	8,61E+05	8,61E+05
	s_{z0}	[N/mm]	800,00	800,00	600,00	800,00	800,00	512,50
	s_{z1}	[mm]	**800,00**	**800,00**	**600,00**	**800,00**	**800,00**	**512,50**
	s_{z2}	[mm]	**1375,00**	**1375,00**	**600,00**	**1375,00**	**1375,00**	**1150,00**
	s_{eff}	[mm]	1197,35	1197,35	684,00	1197,35	1197,35	848,85
	C_{ser}	[N/mm2]	**7,19E+02**	**7,19E+02**	**1,26E+03**	**7,19E+02**	**7,19E+02**	**1,01E+03**
	Source	[-]						
	$\gamma_{gov.0}$	[-]	0,75	0,69	0,80	0,66	0,64	0,72
	$EI_{eff.0}$	[Nmm2/m]	3,04E+13	3,69E+13	3,89E+13	4,02E+13	4,38E+13	4,56E+13
	$\gamma_{gov.90}$	[-]	0,00	0,00	0,00	0,00	0,00	0,00
	$EI_{eff.90}$	[Nmm2/m]	8,16E+11	1,58E+12	1,58E+12	2,14E+12	2,84E+12	2,84E+12
	w_{gov}	[mm]	Long term - 19,57	Long term - 18,28	Long term - 17,59	Long term - 17,71	Long term - 17,18	Long term - 16,64
	$UC_{w,gov}$	[-]	0,75	0,70	0,67	0,68	0,66	0,64
	$\sigma_{gov.1}$	[N/mm2]	C: -6,53	C: -6,11	C: -6,22	C: -5,98	C: -5,88	C: -5,92
	$UC_{gov.1}$	[-]	0,39	0,37	0,37	0,36	0,35	0,36
	$\sigma_{gov.2}$	[N/mm2]	T+B: 3,13	T+B: 3,05	T+B: 3,06	T+B: 3,00	T+B: 2,96	T+B: 2,96
	$UC_{gov.2}$	[-]	0,24	0,23	0,24	0,23	0,23	0,23
	γ_1	[-]	0,83	0,81	0,87	0,80	0,80	0,84
	$EI_{eff.0}$	[Nmm2/m]	2,95E+13	3,56E+13	3,75E+13	3,88E+13	4,22E+13	4,39E+13
	$\gamma_{1.90}$	[-]	0,00	0,00	0,00	0,00	0,00	0,00
	$EI_{eff.90}$	[Nmm2/m]	1,27E+12	2,03E+12	2,03E+12	2,59E+12	3,29E+12	3,29E+12
	w_{gov}	[mm]	Long term - 20,12	Long term - 18,83	Long term - 18,17	Long term - 18,26	Long term - 17,73	Long term - 17,20
	$UC_{w,gov}$	[-]	0,77	0,72	0,70	0,70	0,68	0,66
	$\sigma_{gov.1}$	[N/mm2]	C: -6,33	C: -5,95	C: -6,01	C: -5,84	C: -5,76	C: -5,77
	$UC_{gov.1}$	[-]	0,38	0,36	0,36	0,35	0,35	0,35
	$\sigma_{gov.2}$	[N/mm2]	T+B: 3,24	T+B: 3,15	T+B: 3,17	T+B: 3,10	T+B: 3,05	T+B: 3,06
	$UC_{gov.2}$	[-]	**0,30**	**0,29**	**0,29**	**0,29**	**0,28**	**0,28**
	$F_{v,Ed,Ni}$	[N]	1,50E+05	1,59E+05	1,31E+05	1,62E+05	1,64E+05	1,16E+05
	$UC_{v,Ni,gov}$	[-]	TCF - N1: 0,40	TCF - N1: 0,43	TCF - N1: 0,35	TCF - N1: 0,44	TCF - N1: 0,44	TCF - N1: 0,31
Vibrations	f_0	[Hz]	7,07 = OK	6,95 = OK	7,0 = OK	7,0 = OK	7,05 = OK	7,11 = OK
	w_{1kN}	[mm]	5,18E-8 = Class I/II	4,28E-8 = Class I/II	4,05E-8 = Class I/II	3,92E-8 = Class I/II	3,60E-8 = Class I/II	3,46E-8 = Class I/II
	ζ	[-]	0,035	0,035	0,035	0,035	0,035	0,035
	$R_{a/p}$	[-]	30,29 = Class VI	25,43 = Class VI	23,98 = Class V	23,18 = Class V	21,19 = Class V	20,24 = Class V
Acoustics	M_n	[kg/m2]	269,72	317,72	329,52	341,72	365,72	373,59
	$L'_{nw+c150-:}$	[dB]	51,14 = OK	46,88 = OK	45,93 = OK	44,98 = OK	43,21 = OK	42,66 = OK
			Make it nice distribution. (sz0 to 600 (&sz2 to 1475) does not work)	Increasing concrete to the 'max' 80 mm	Lowering spacing not really possible for failure order. But works for class increase	Increasing concrete to higher class	Increasing concrete to max	cannot decrease spacing

C Experimental bending analysis

This Appendix shows additional information on the experimental bending tests.

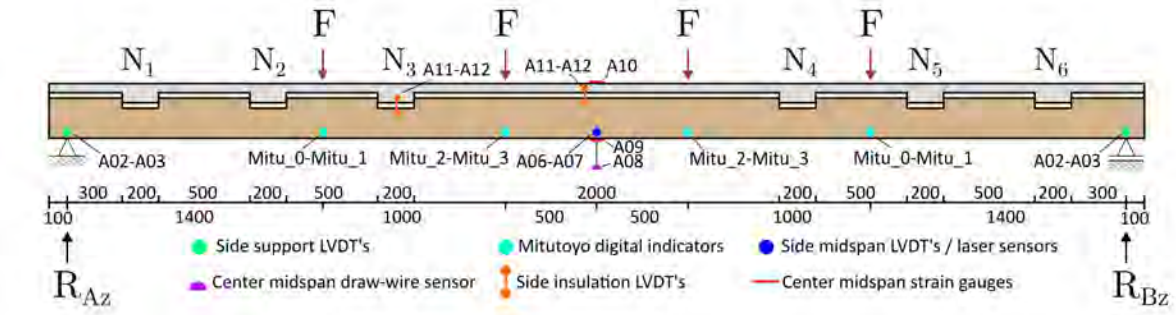

Figure C.1: Measurement placement and ID's for the experimental bending tests

C.1 ED - Traditional floor

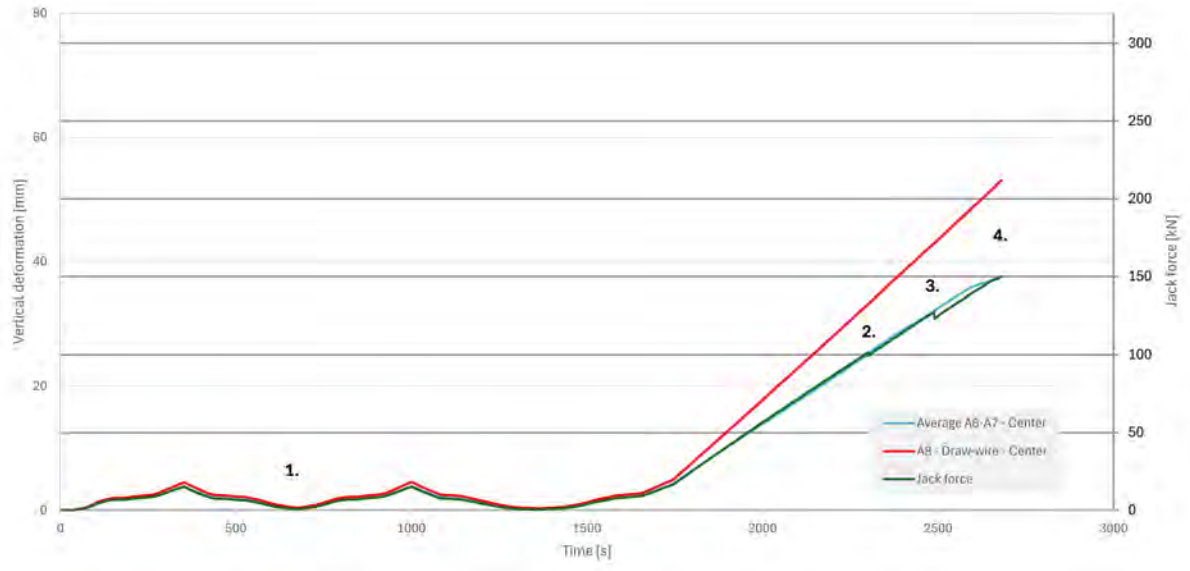

Figure C.2: Jack force and displacement over time.

C.2 ED - Conceptual floor

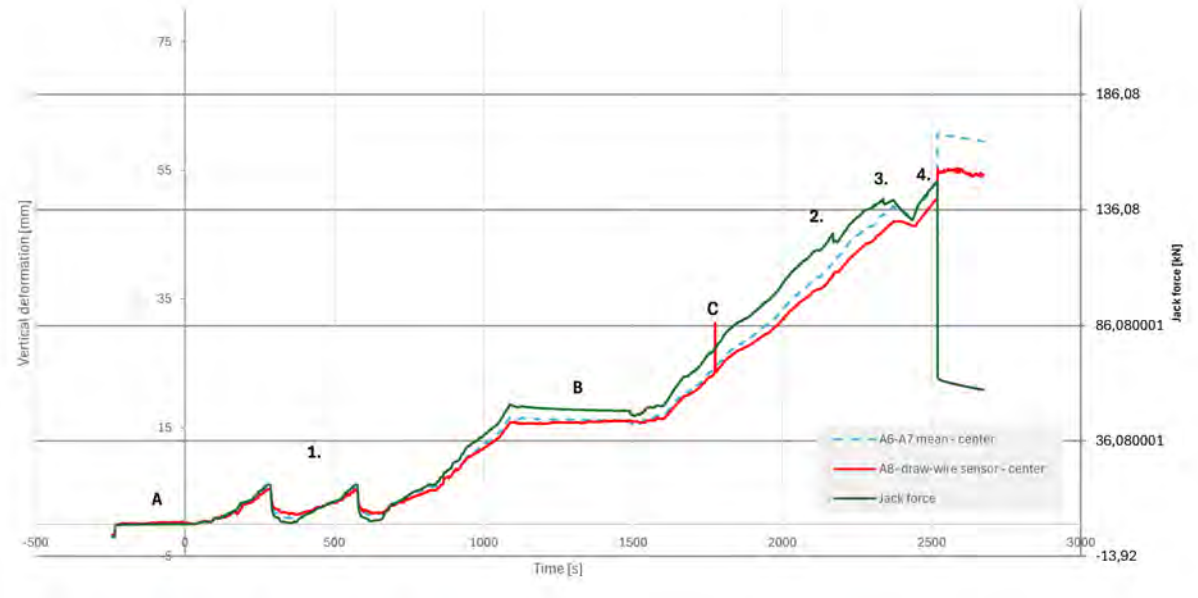

Figure C.3: Jack force and displacement over time.

Additional points of interest

- A. Calibration of the jack force due to start of measurement before the pressure frame had contact with the floor and was thus hanging from the jack. The raw measurement thus started while in a tensile state. Calibration from point of contact.
- B. Oil change in manual check.

D Experimental vibration analysis

D.0.1 Traditional floor

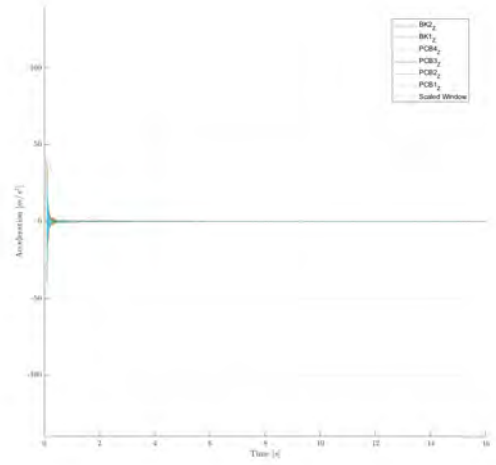

(a) Pure signal

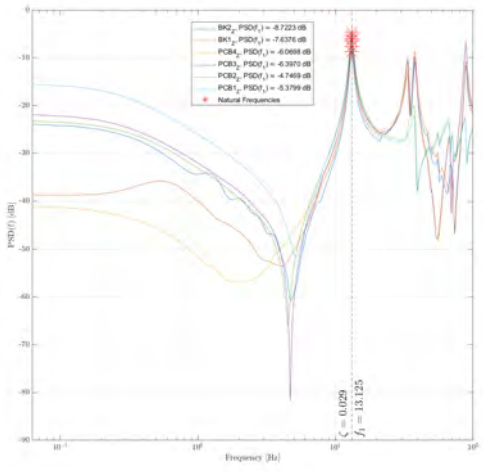

(b) PSD over frequency - 0-100 Hz

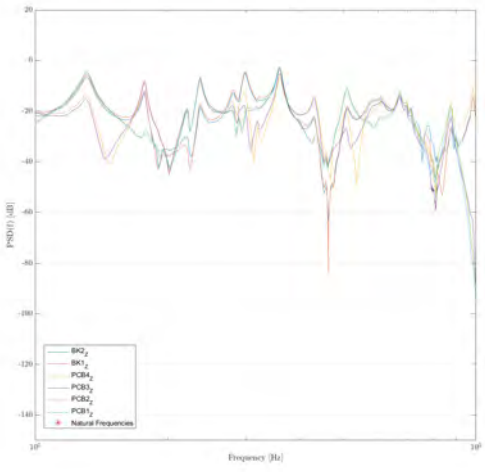

(c) PSD over frequency - 100-1000 Hz

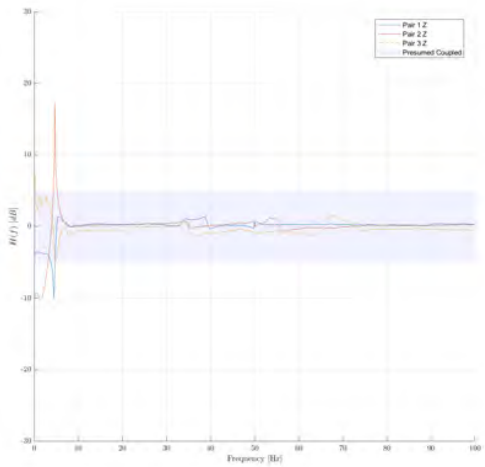

(d) Top-Bottom transfer - 0-100 Hz

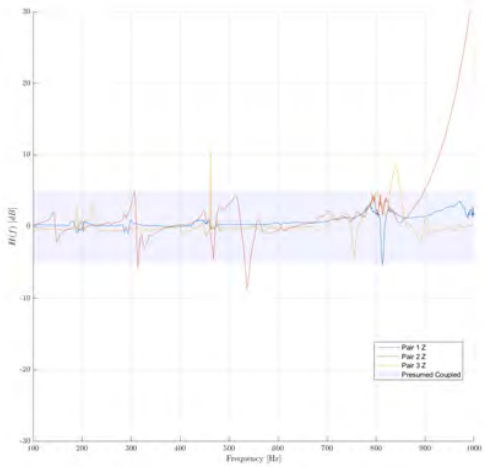

(e) Top-Bottom transfer - 100-1000 Hz

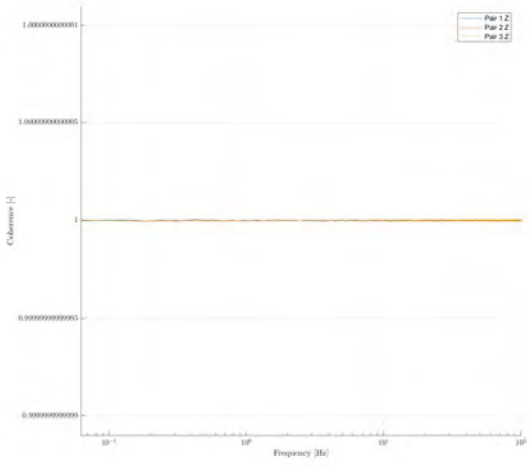

(f) Coherence - 0-100 Hz

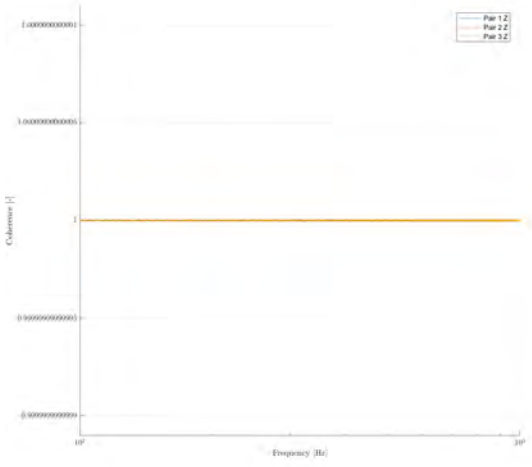

(g) Coherence - 100-1000 Hz

Figure D.1: Results of the experimental vibration analysis for the Experimental Design (ED) - Traditional floor - Drop position 1 - Measurement 1

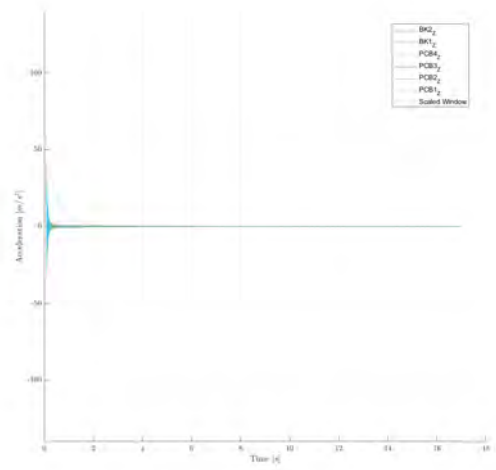

(a) Pure signal

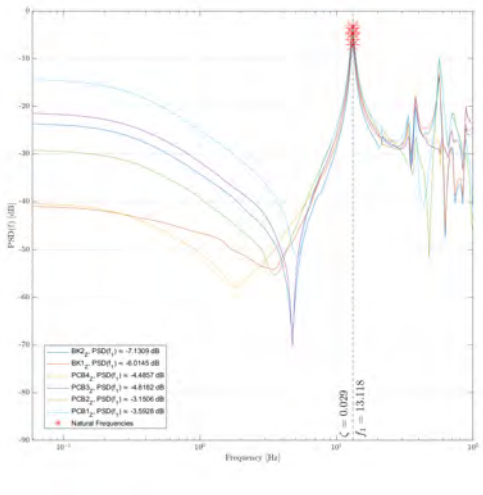

(b) PSD over frequency - 0-100 Hz

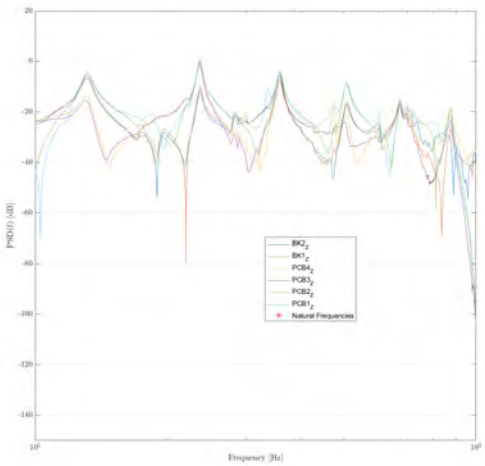

(c) PSD over frequency - 100-1000 Hz

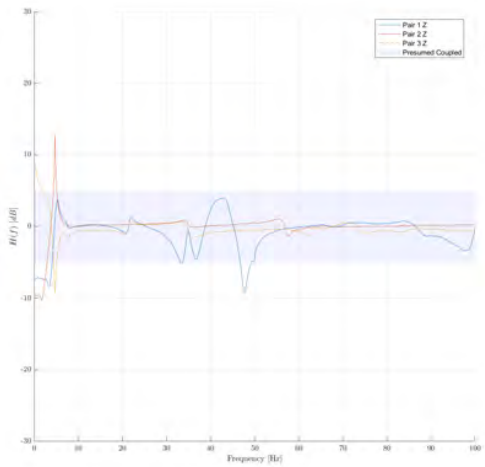

(d) Top-Bottom transfer - 0-100 Hz

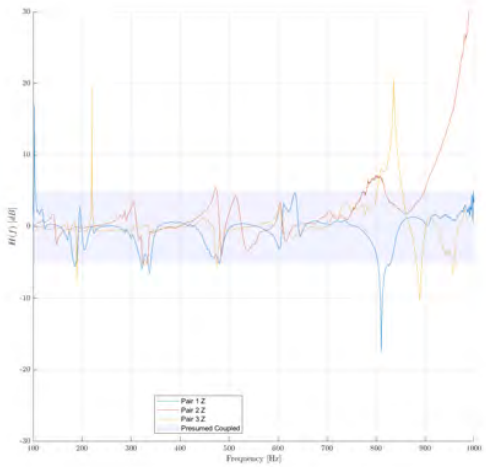

(e) Top-Bottom transfer - 100-1000 Hz

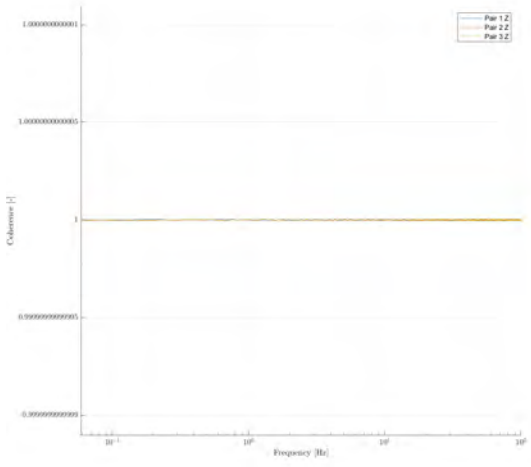

(f) Coherence - 0-100 Hz

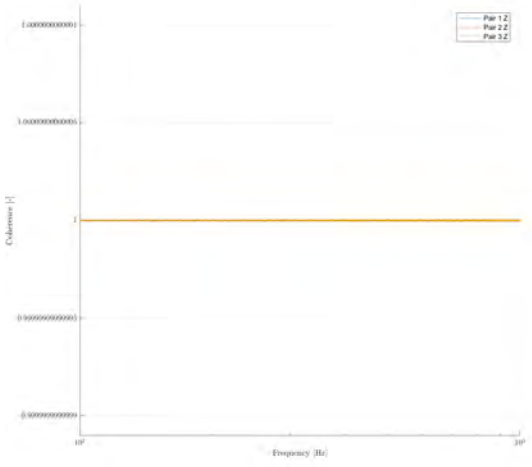

(g) Coherence - 100-1000 Hz

Figure D.2: Results of the experimental vibration analysis for the Experimental Design (ED) - Traditional - Drop position 2 - Measurement 1

D.0.2 Conceptual floor

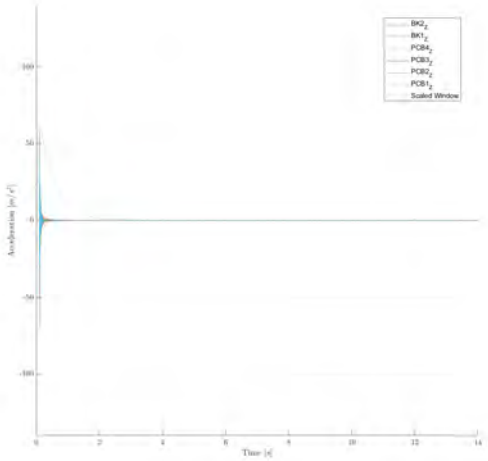

(a) Pure signal

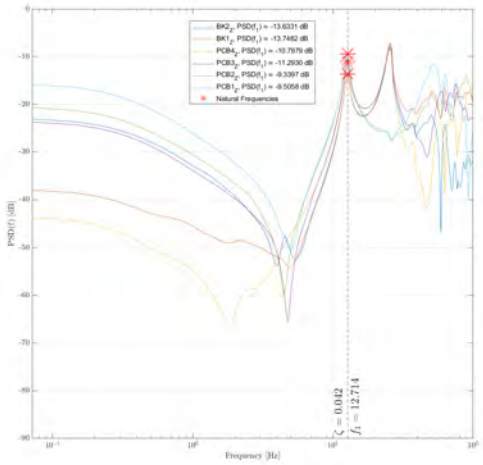

(b) PSD over frequency - 0-100 Hz

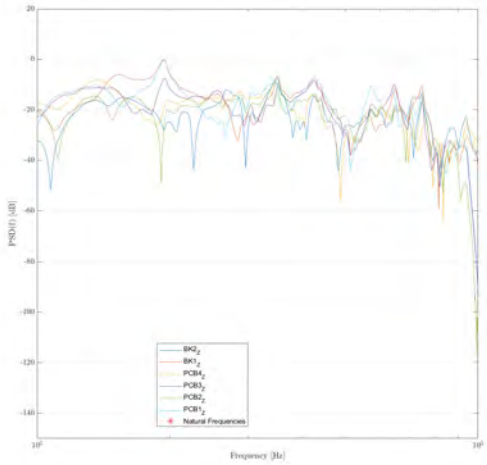

(c) PSD over frequency - 100-1000 Hz

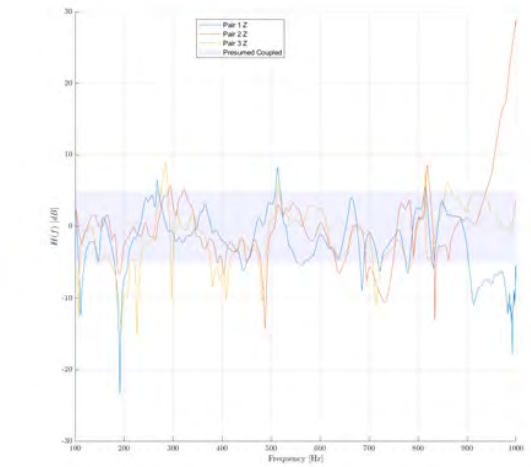

(d) Top-Bottom transfer - 0-100 Hz

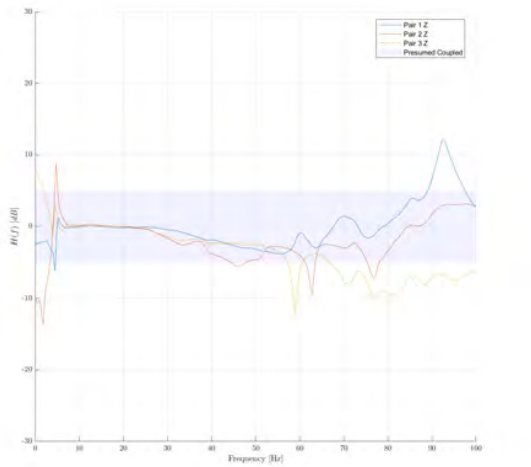

(e) Top-Bottom transfer - 100-1000 Hz

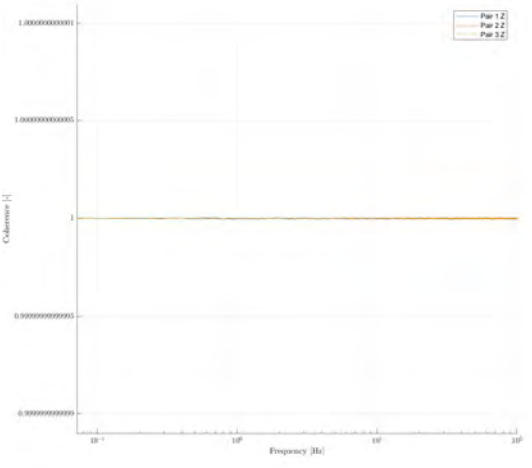

(f) Coherence - 0-100 Hz

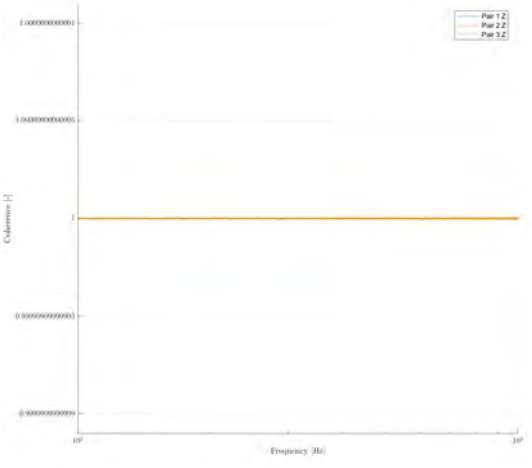

(g) Coherence - 100-1000 Hz

Figure D.3: Results of the experimental vibration analysis for the Experimental Design (ED) - Conceptual - Drop position 1 - Measurement 1

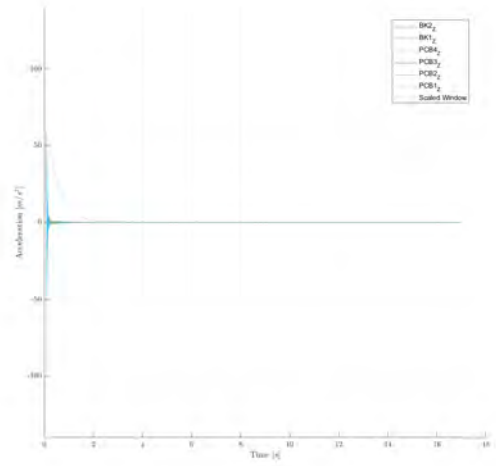

(a) Pure signal

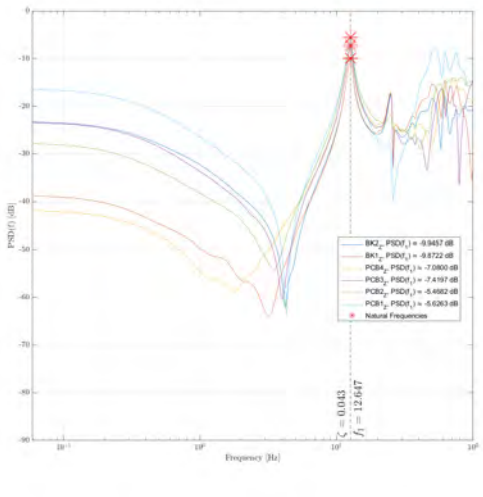

(b) PSD over frequency - 0-100 Hz

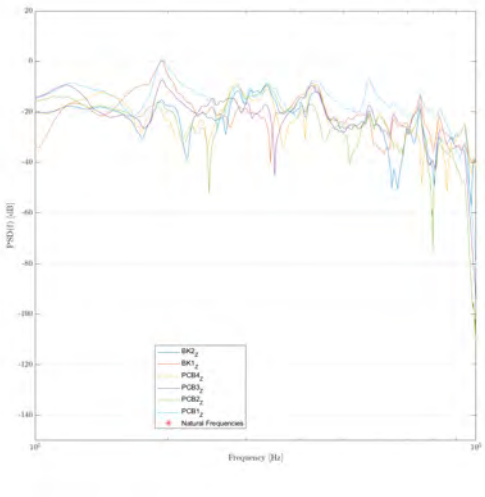

(c) PSD over frequency - 100-1000 Hz

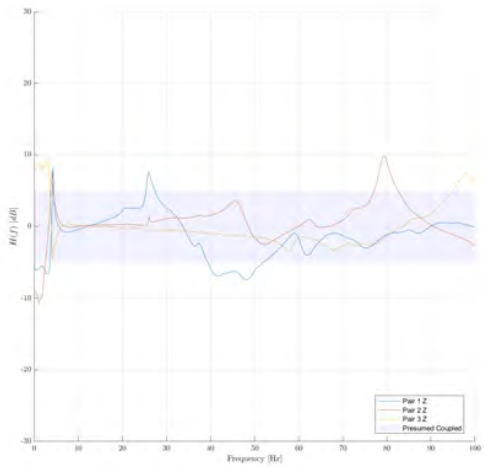

(d) Top-Bottom transfer - 0-100 Hz

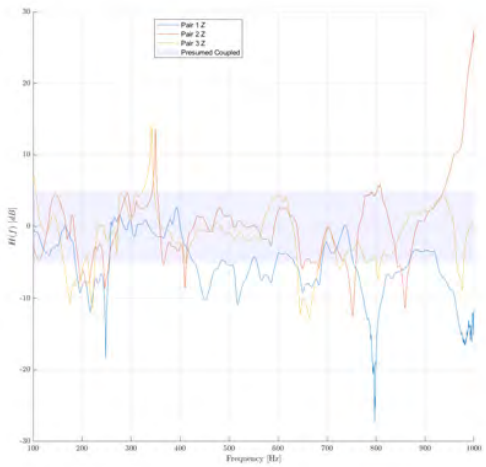

(e) Top-Bottom transfer - 100-1000 Hz

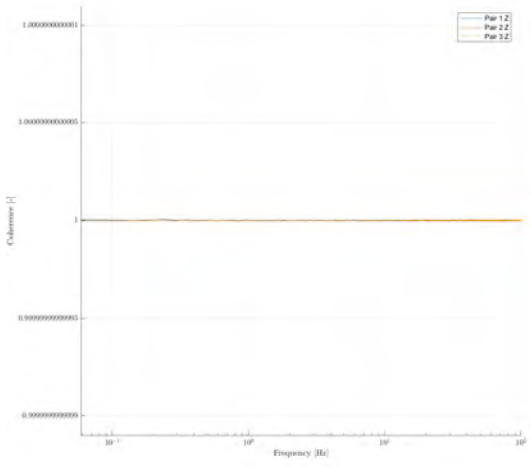

(f) Coherence - 0-100 Hz

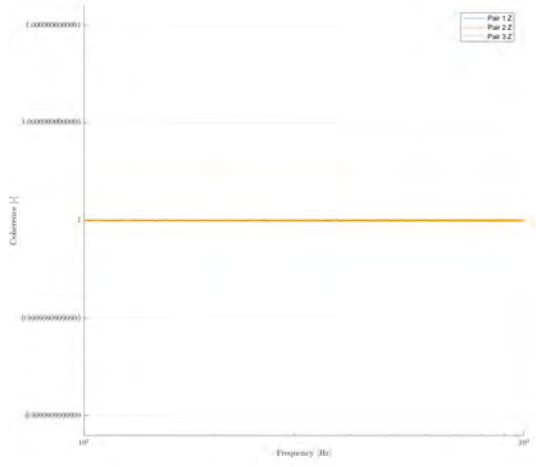

(g) Coherence - 100-1000 Hz

Figure D.4: Results of the experimental vibration analysis for the Experimental Design (ED) - Conceptual - Drop position 2 - Measurement 1

E Numerical vibration analysis

E.1 Transient analysis for for vibration and acoustic performance

E.1.1 Top response

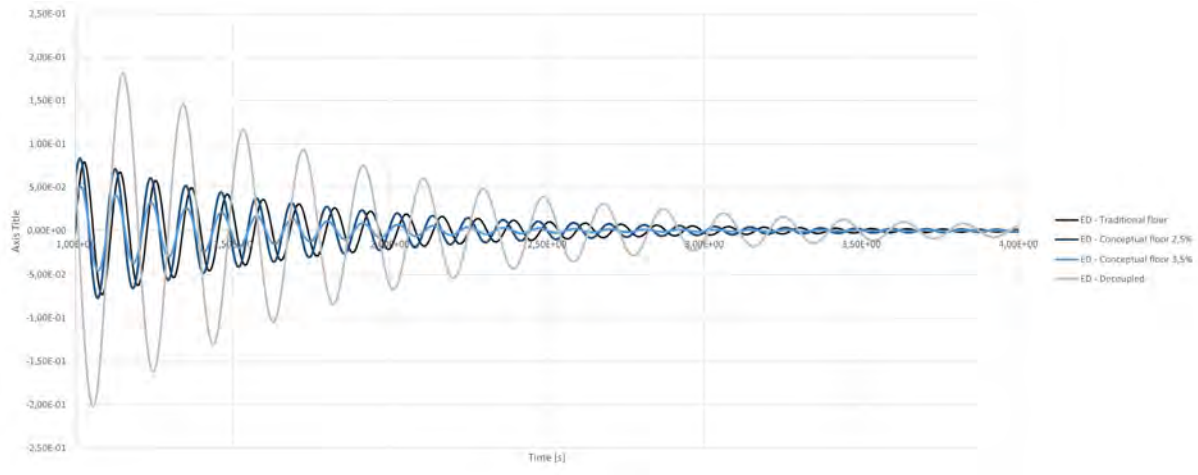

(a) Modified time frame

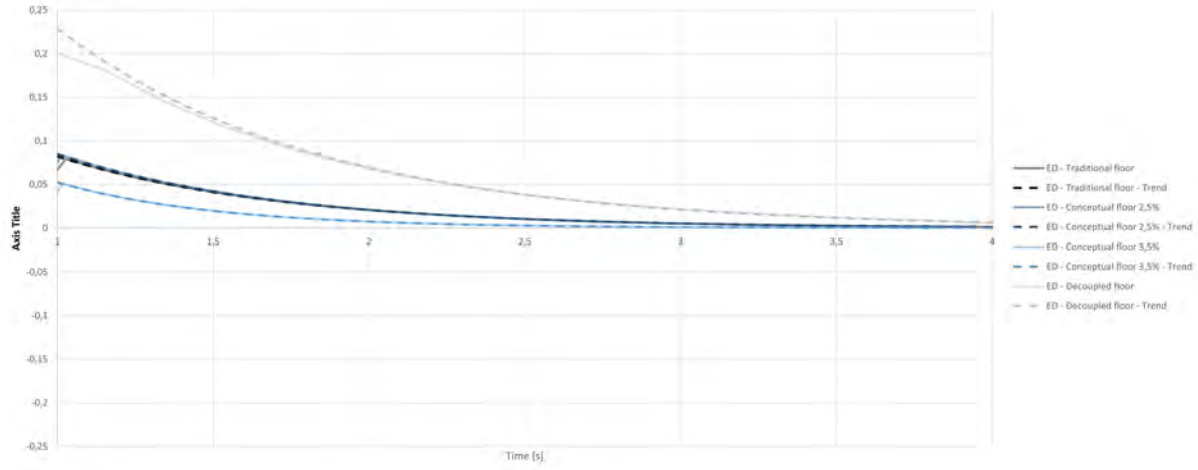

(b) Local maxima

Figure E.1: Deformation results for the top of the concrete of the Large Span Design (LSD) floors.

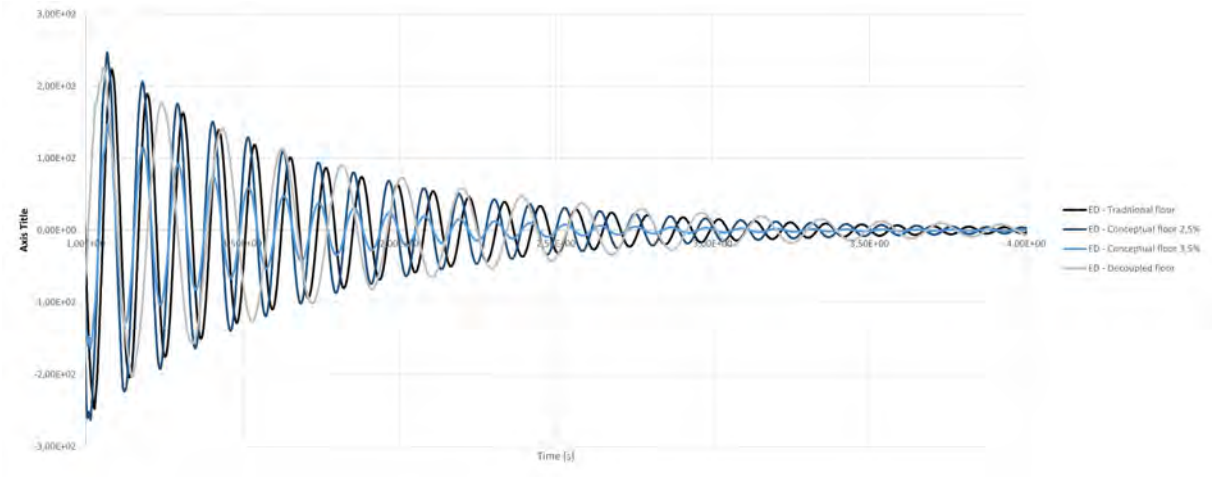

(a) Modified time frame

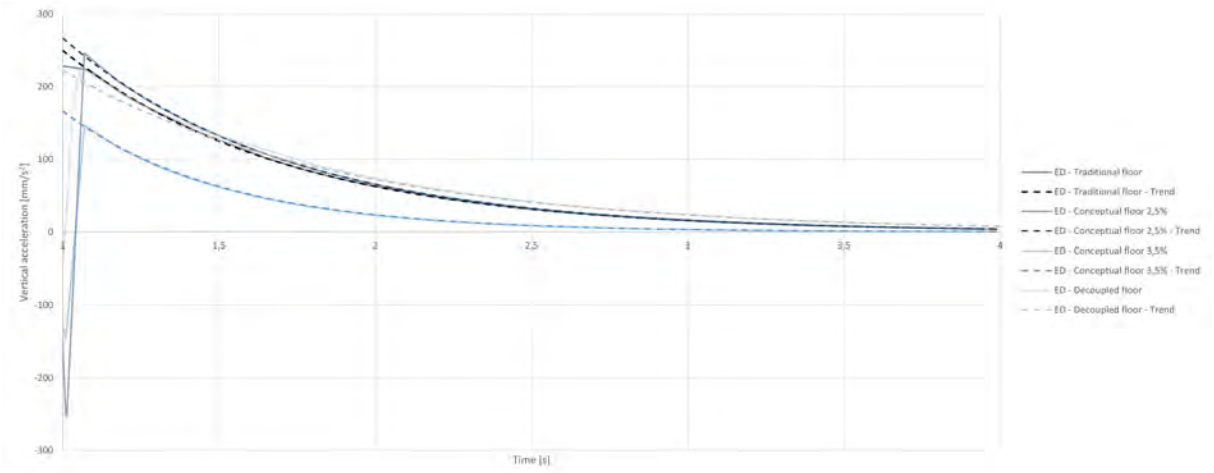

(b) Local maxima

Figure E.2: Acceleration results for the top of the concrete of the Large Span Design (LSD) floors.

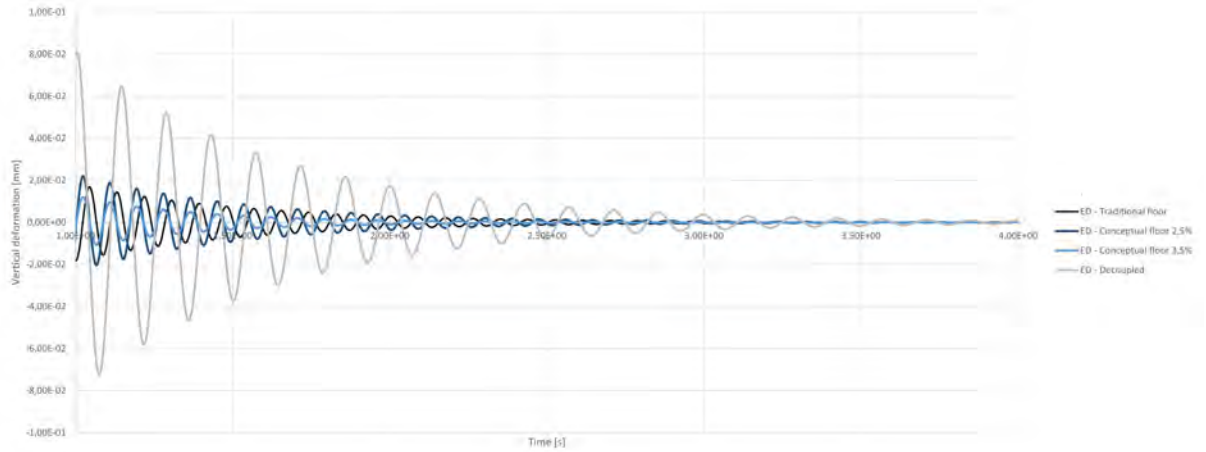

(a) Modified time frame

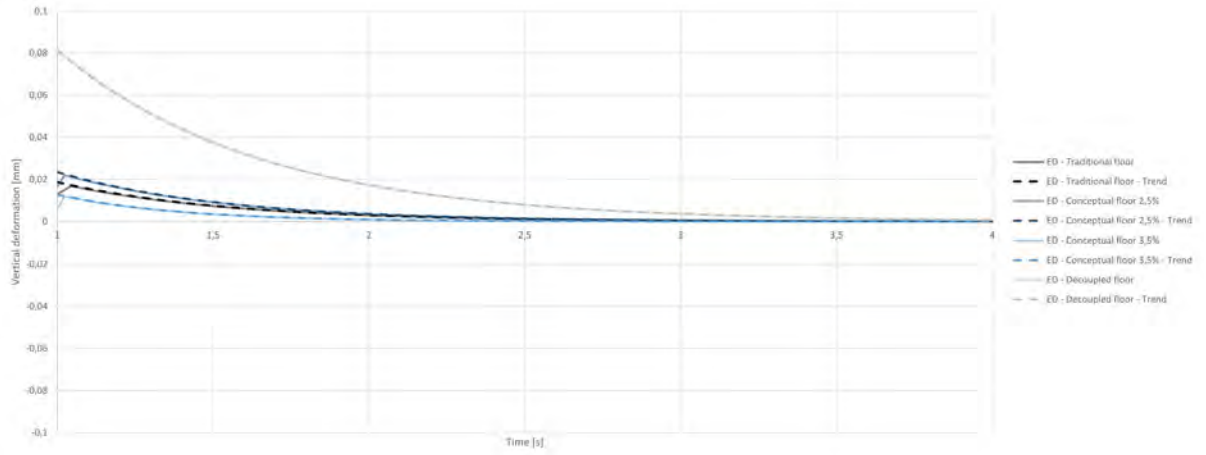

(b) Local maxima

Figure E.3: Deformation results for the top of the concrete of the Large Span Design+ (LSD+) floors.

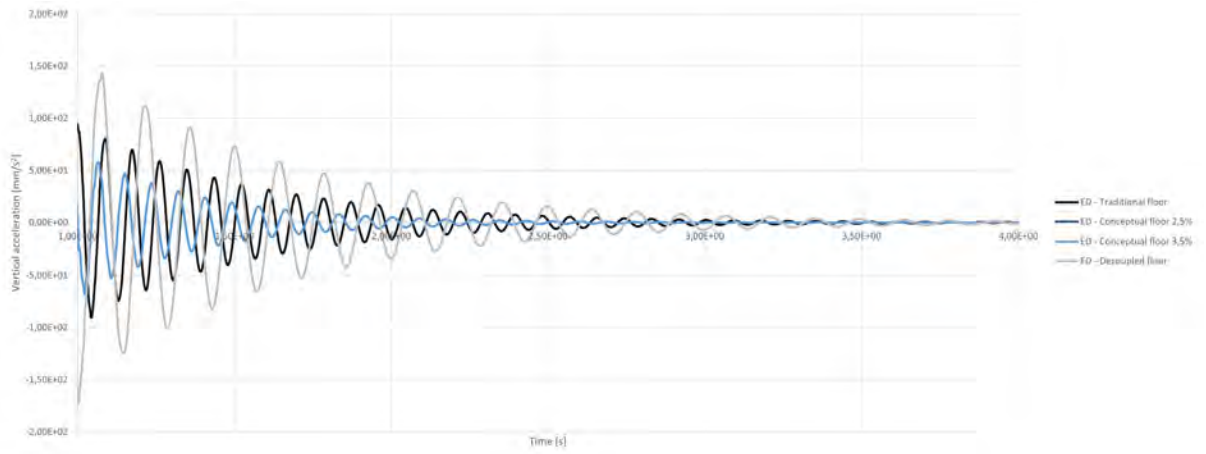

(a) Modified time frame

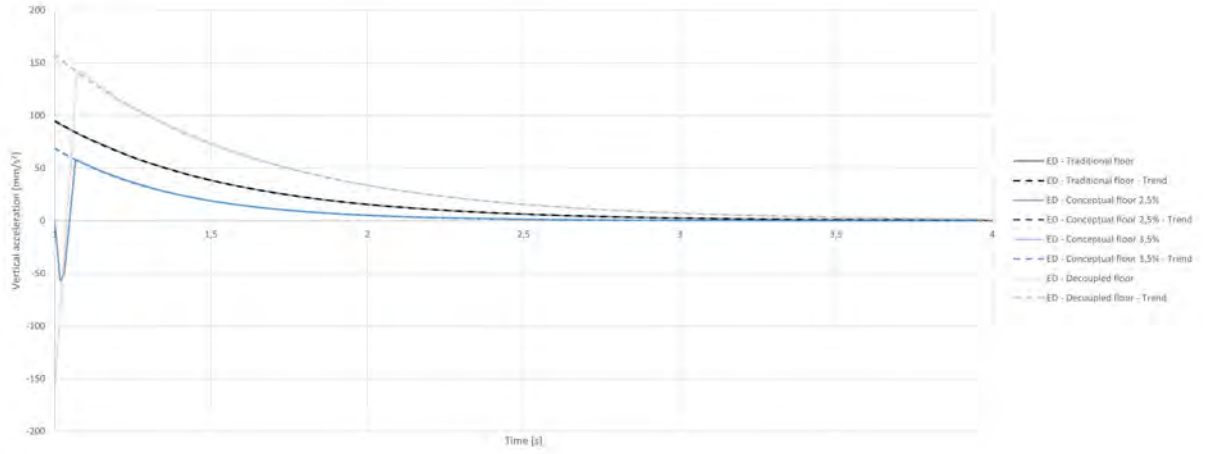

(b) Local maxima

Figure E.4: Acceleration results for the top of the concrete of the Large Span Design+ (LSD+) floors.

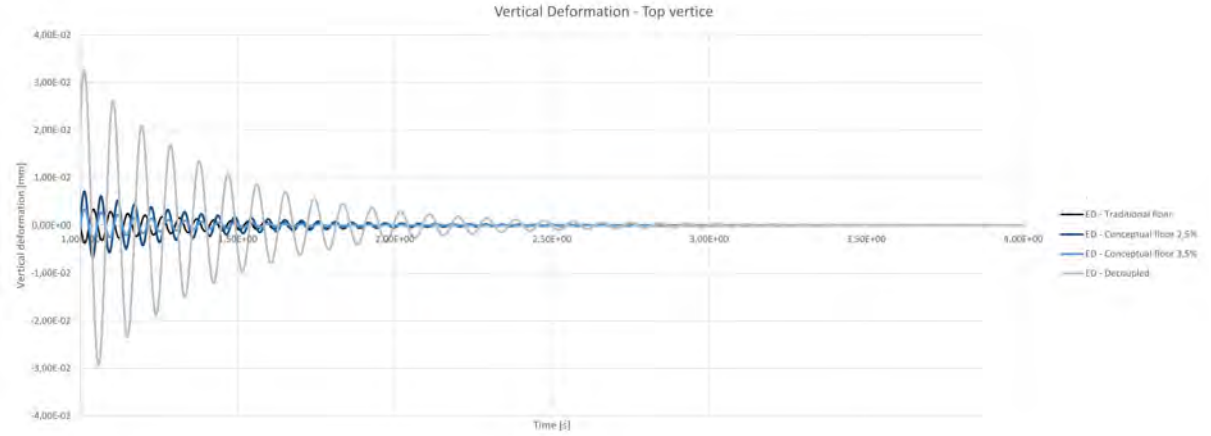

(a) Modified time frame

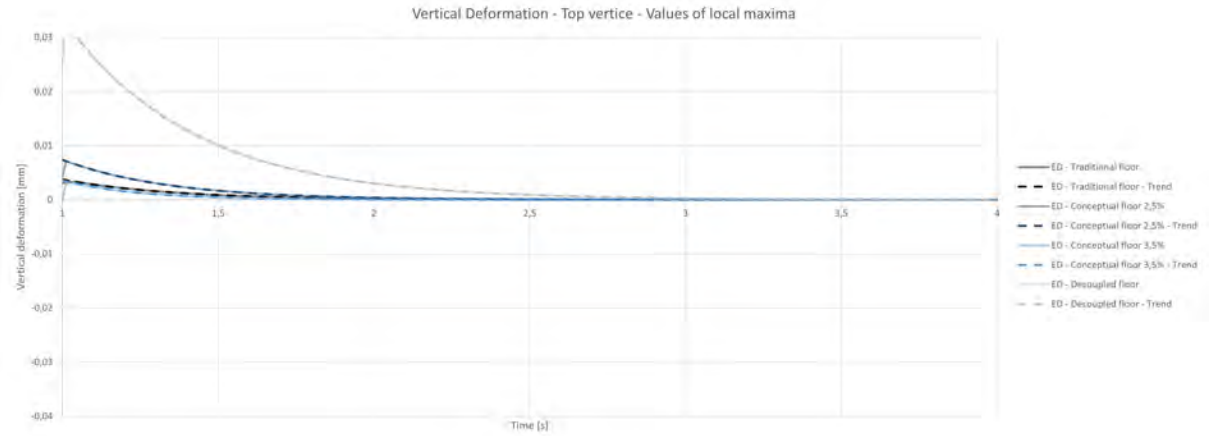

(b) Local maxima

Figure E.5: Deformation results for the top of the concrete of the Experimental Design (ED) floors.

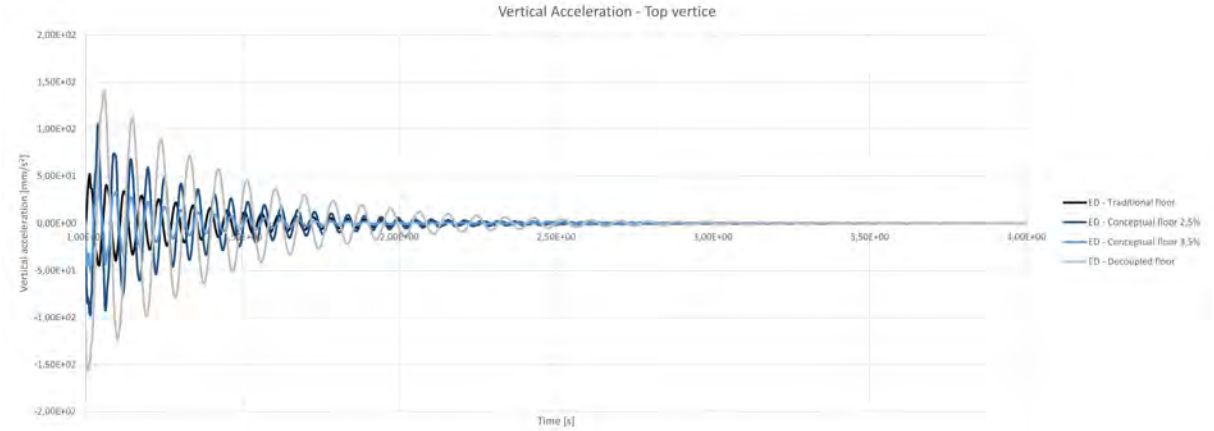

(a) Modified time frame

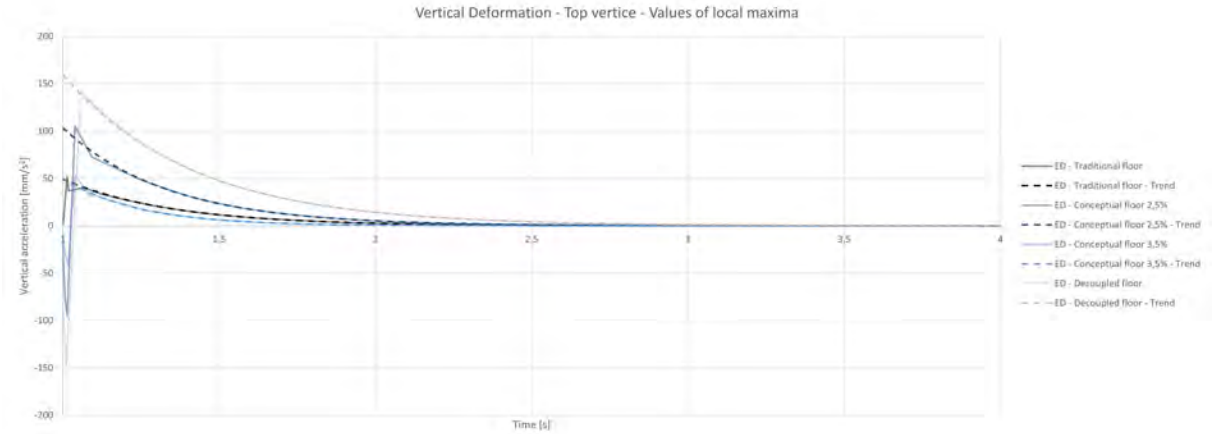

(b) Local maxima

Figure E.6: Acceleration results for the top of the concrete of the Experimental Design (ED) floors.

E.1.2 Bottom Response

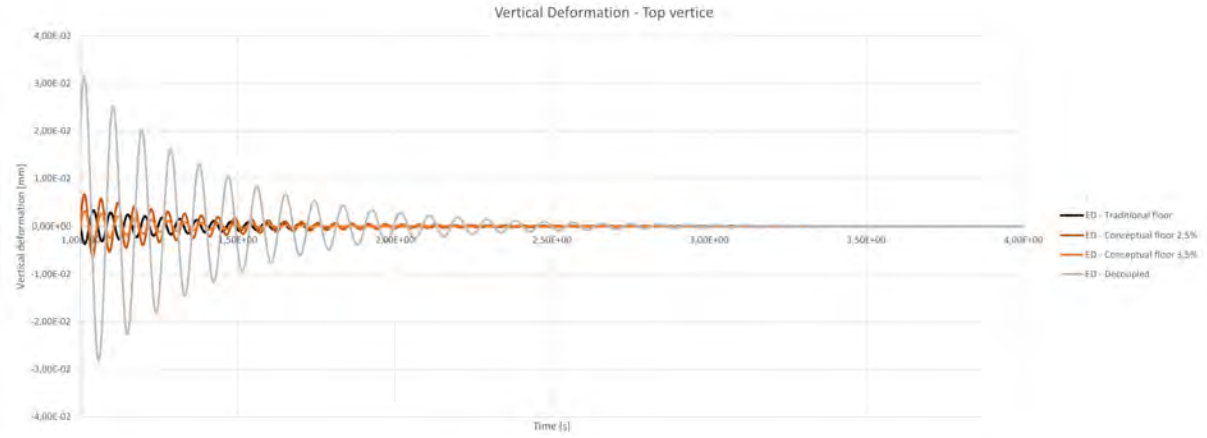

(a) Modified time frame

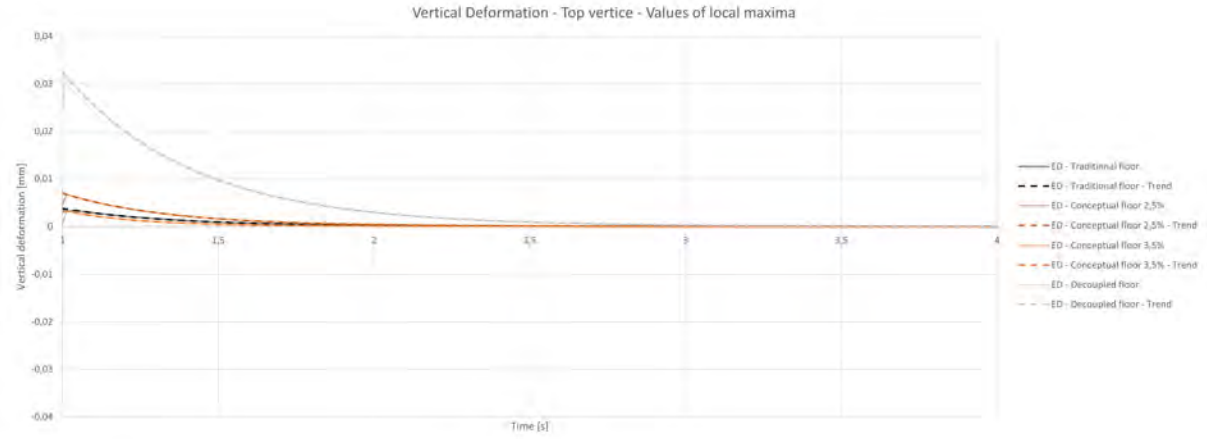

(b) Local maxima

Figure E.7: Deformation results for the top of the concrete of the Experimental Design (ED) floors.

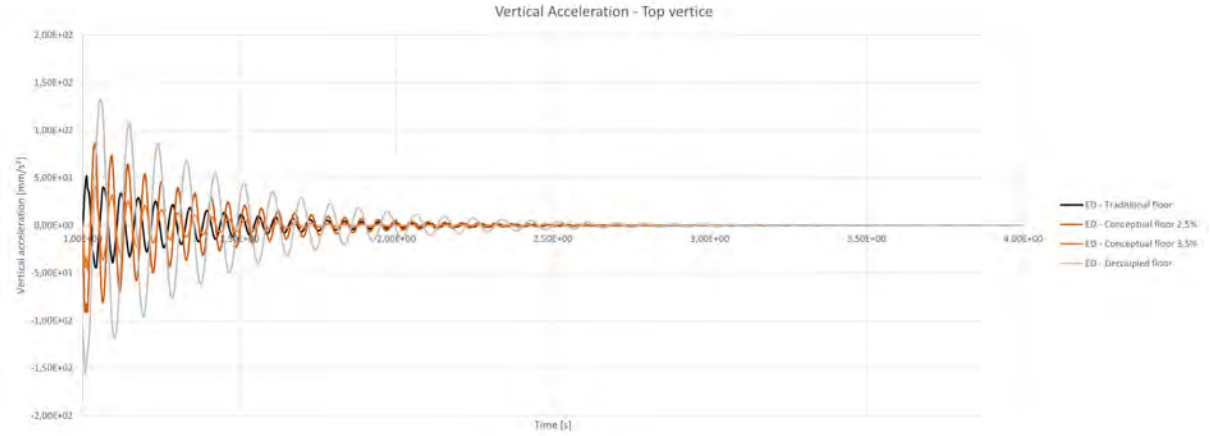

(a) Modified time frame

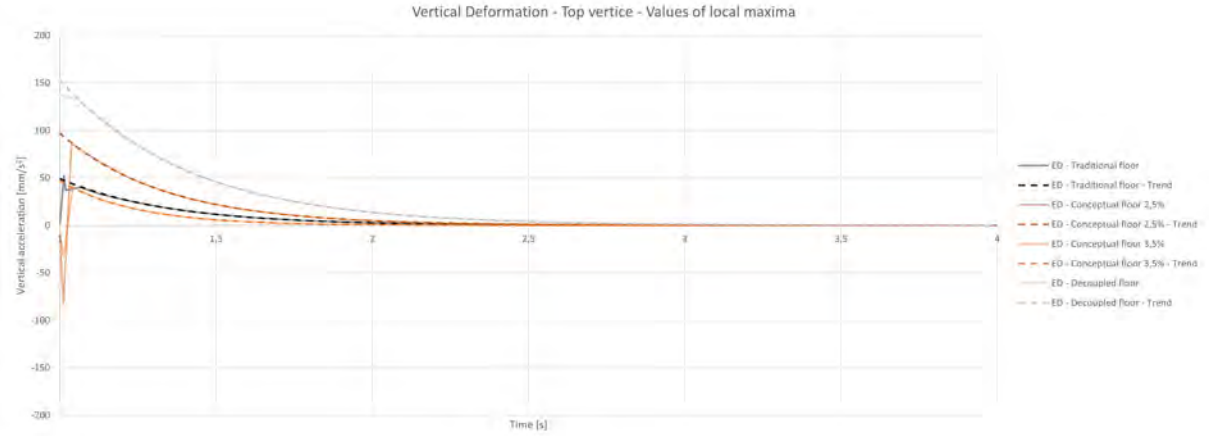

(b) Local maxima

Figure E.8: Acceleration results for the bottom of the CLT of the Experimental Design (ED) floors.

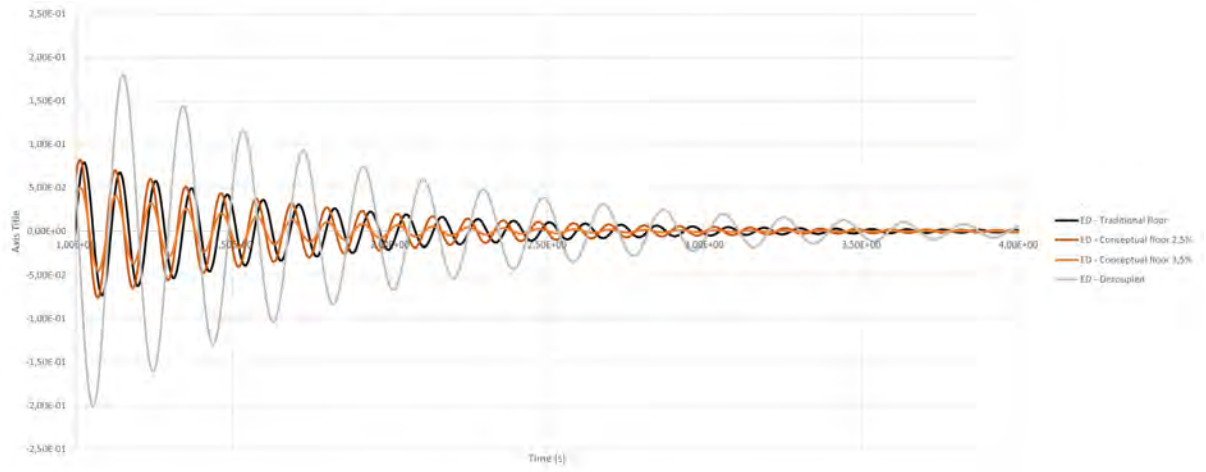

(a) Modified time frame

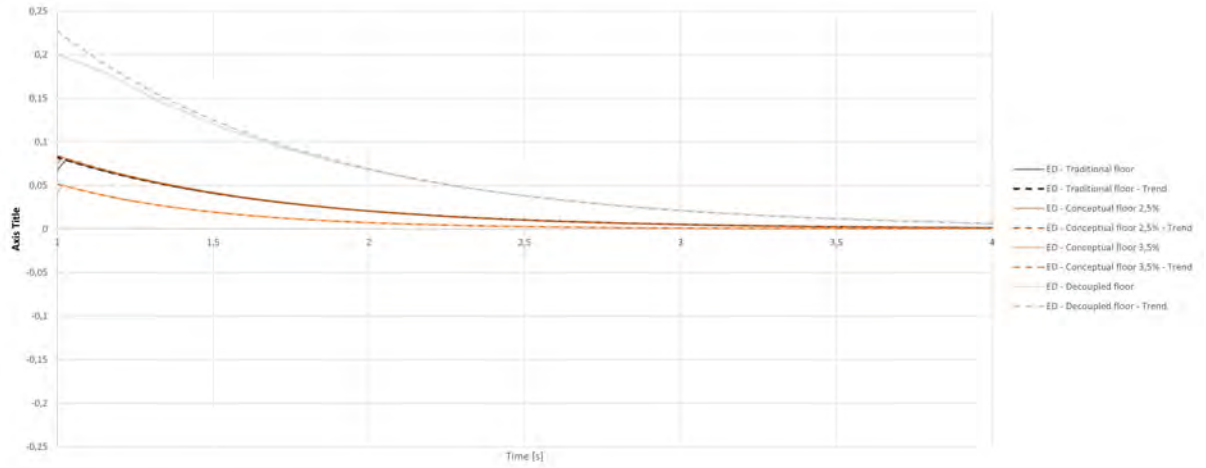

(b) Local maxima

Figure E.9: Deformation results for the top of the concrete of the Large Span Design (LSD) floors.

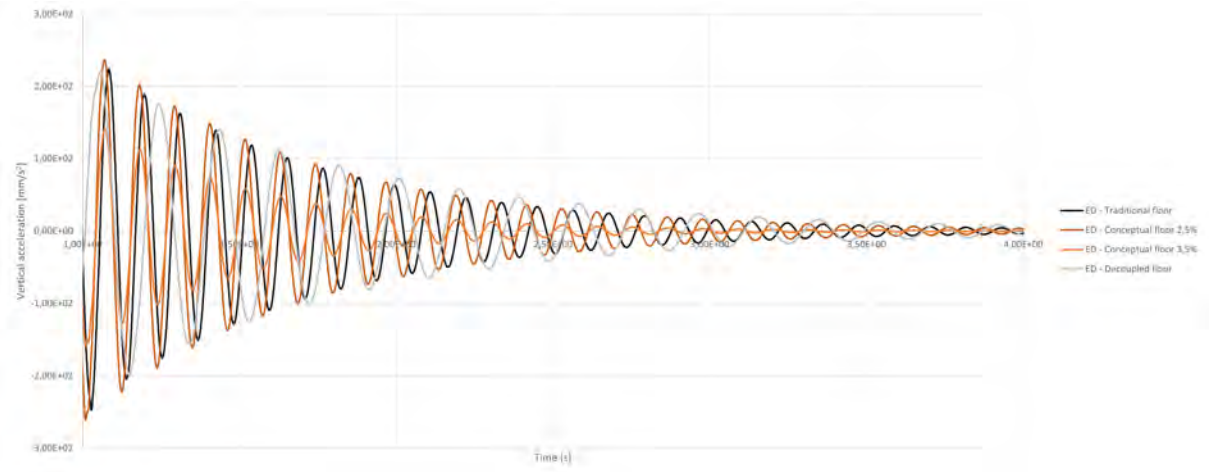

(a) Modified time frame

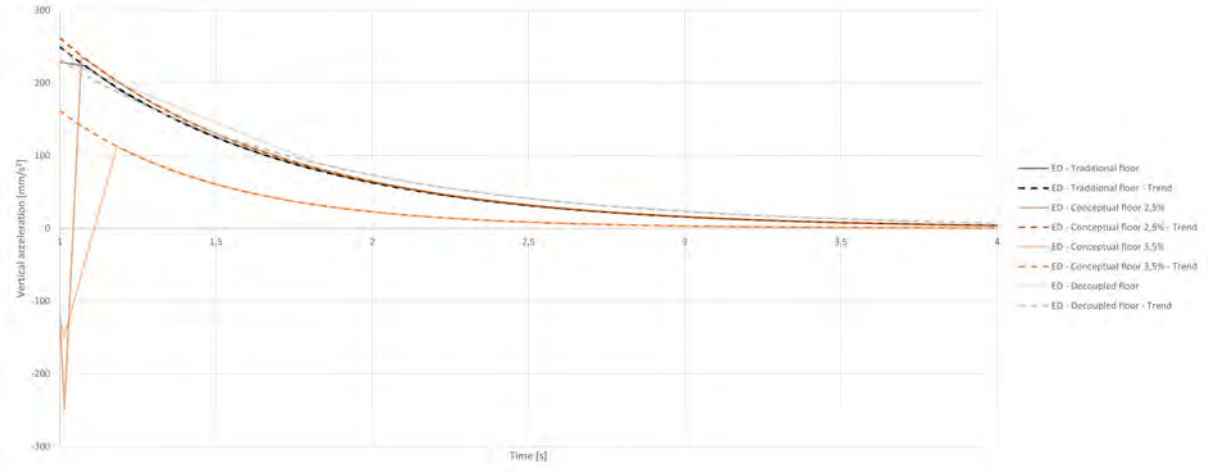

(b) Local maxima

Figure E.10: Acceleration results for the top of the concrete of the Large Span Design (LSD) floors.

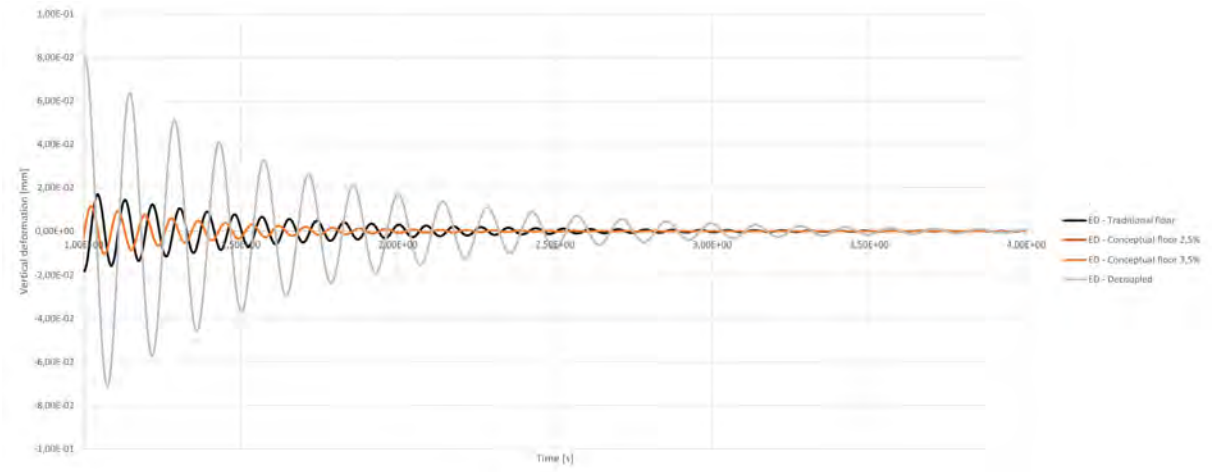

(a) Modified time frame

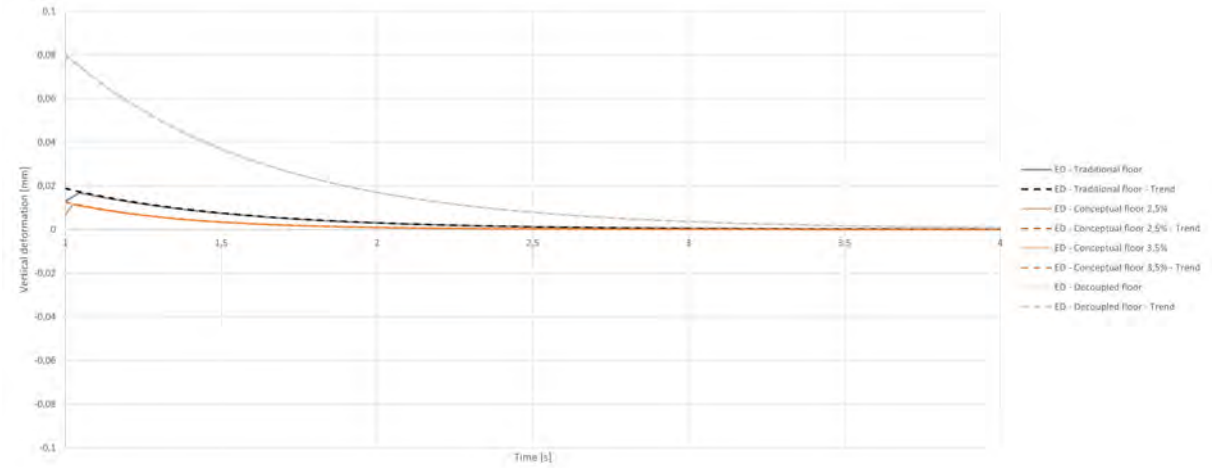

(b) Local maxima

Figure E.11: Deformation results for the top of the concrete of the Large Span Design+ (LSD+) floors.

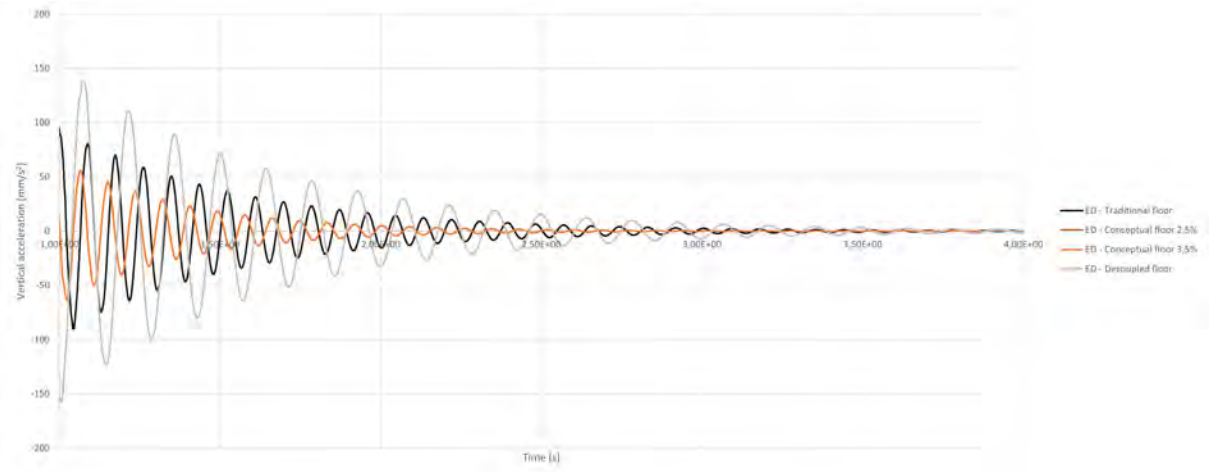

(a) Modified time frame

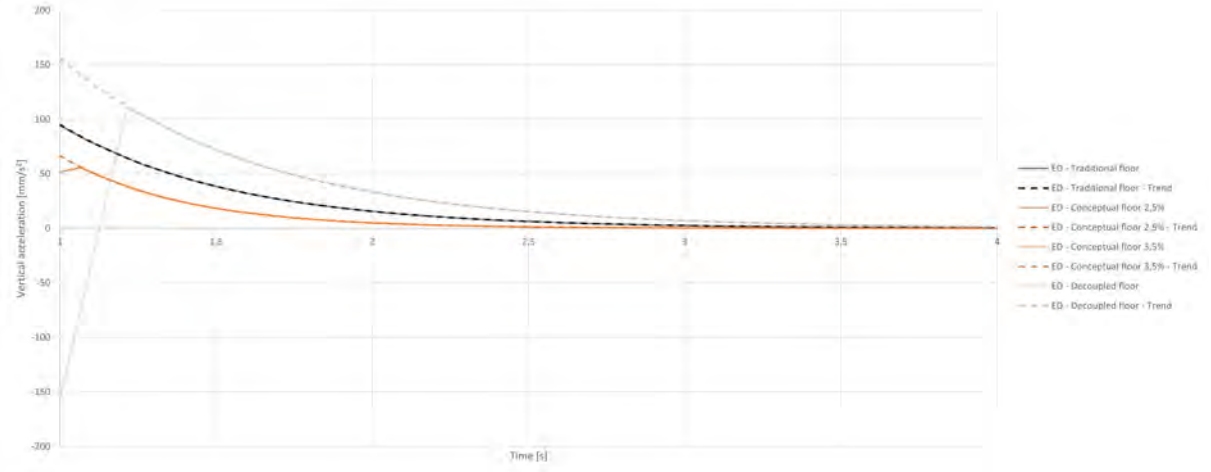

(b) Local maxima

Figure E.12: Acceleration results for the top of the concrete of the Large Span Design+ (LSD+) floors.

E.2 Harmonic response analysis for for vibration and acoustic performance

E.2.1 Top response

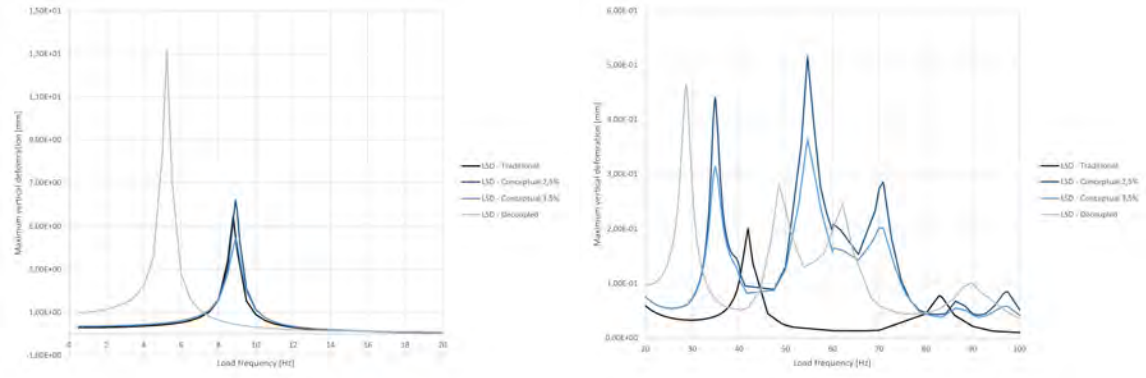

(a) 0-20 Hz (b) 20-100 Hz

Figure E.13: Results of Harmonic Response Analysis of the Large Span Design (LSD) floors for low frequencies, measured at the top of the concrete.

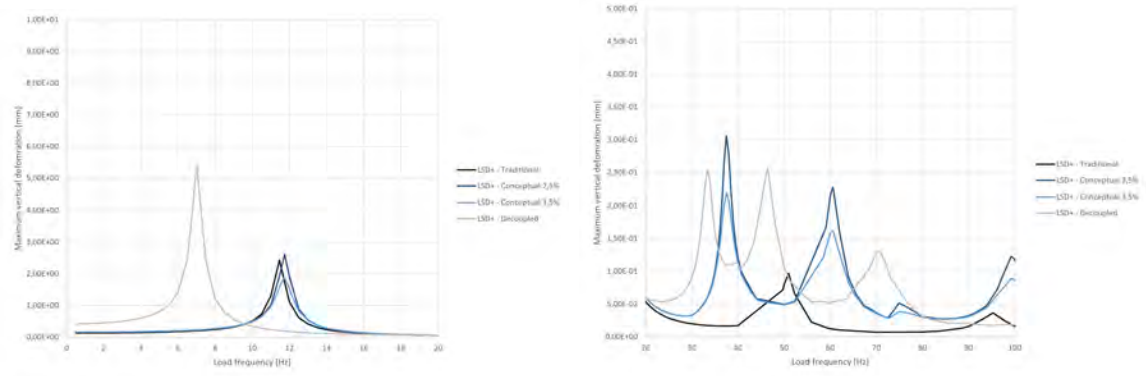

(a) 0-20 Hz (b) 20-100 Hz

Figure E.14: Results of Harmonic Response Analysis of the Large Span Design+ (LSD+) floors for low frequencies, measured at the top of the concrete.

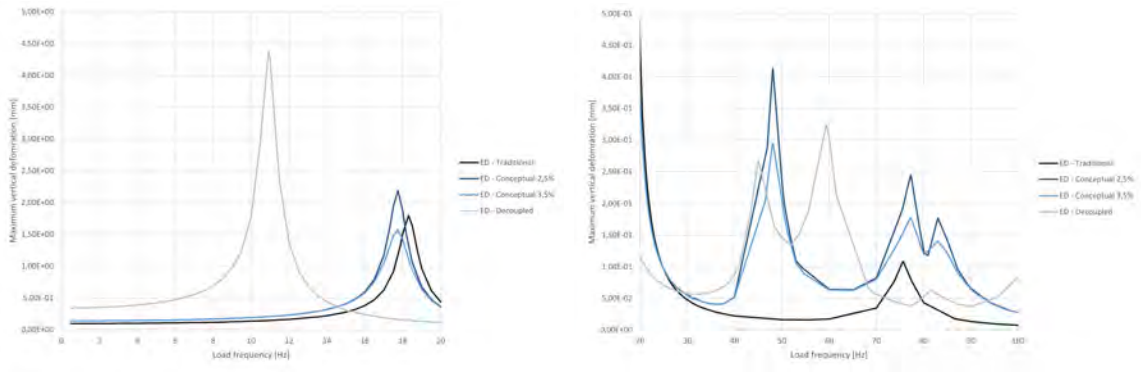

(a) 0-20 Hz (b) 20-100 Hz

Figure E.15: Results of Harmonic Response Analysis of the Experimental Design (ED) floors for low frequencies, measured at the top of the concrete.

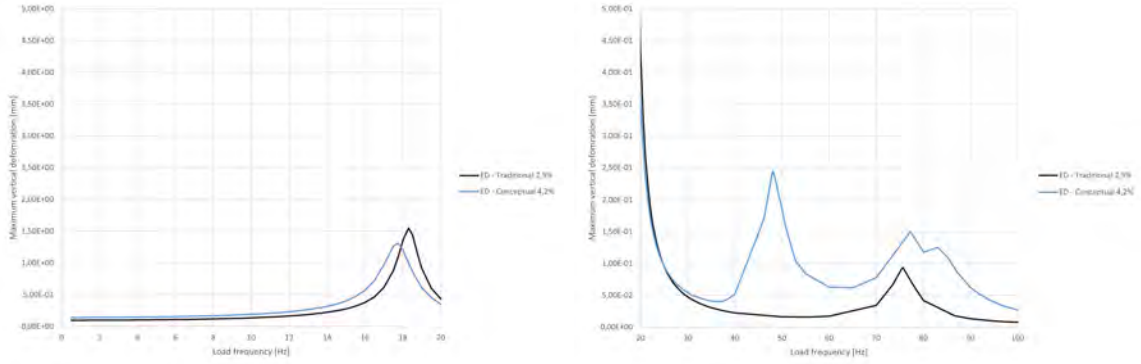

(a) 0-20 Hz (b) 20-100 Hz

Figure E.16: Results of Harmonic Response Analysis of the Experimental Design (ED) floors for low frequencies, measured at the top of the concrete, using the experimental damping ratio.

E.2.2 Bottom response and top-bottom transfer

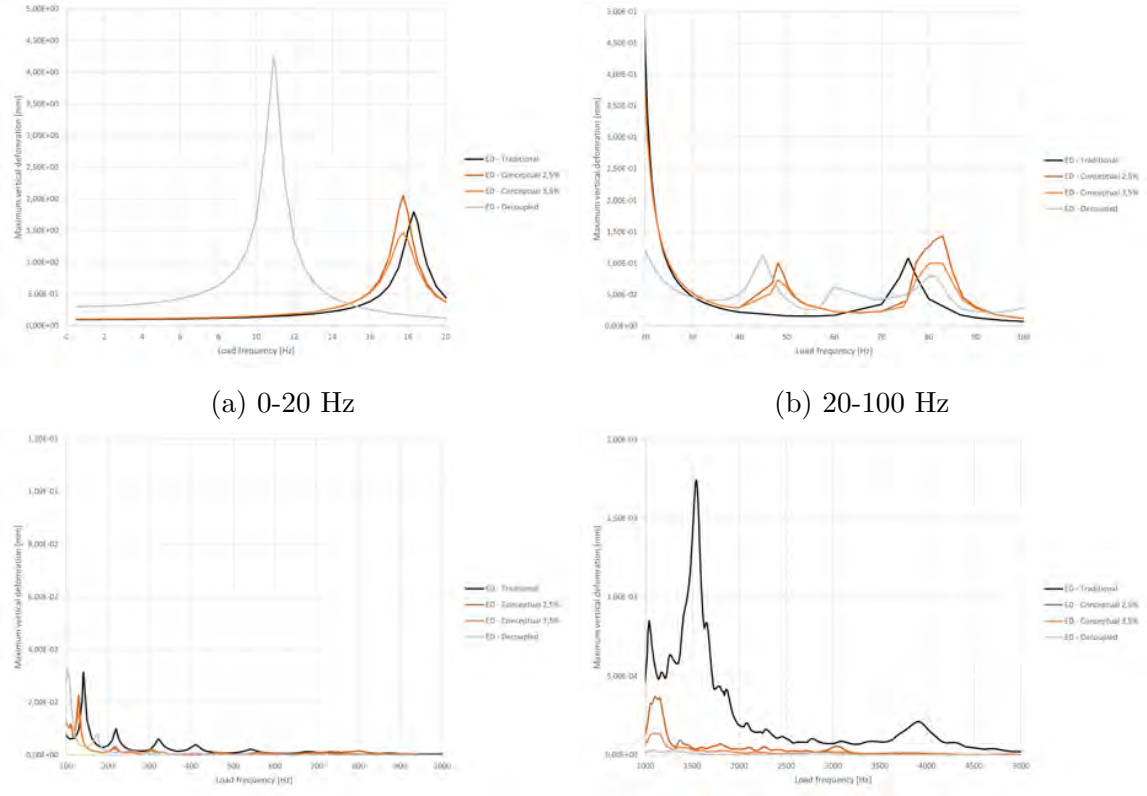

(a) 0-20 Hz

(b) 20-100 Hz

(c) 100-1000 Hz

(d) 1000-5000 Hz

Figure E.17: Results of Harmonic Response Analysis of the Experimental Design (ED) floors, measured at the bottom of the CLT.

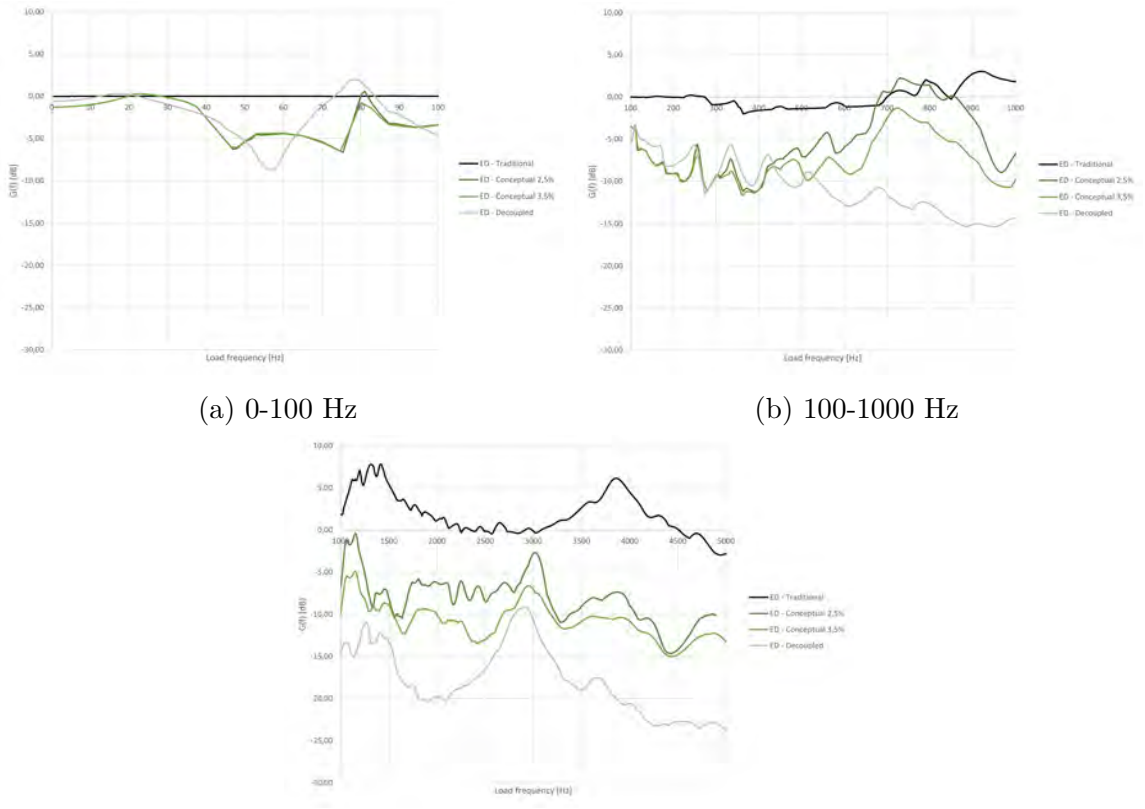

(a) 0-100 Hz

(b) 100-1000 Hz

(c) 1000-5000 Hz

Figure E.18: Top-Bottom transfer from the Harmonic Response Analysis of the Experimental Design (ED)

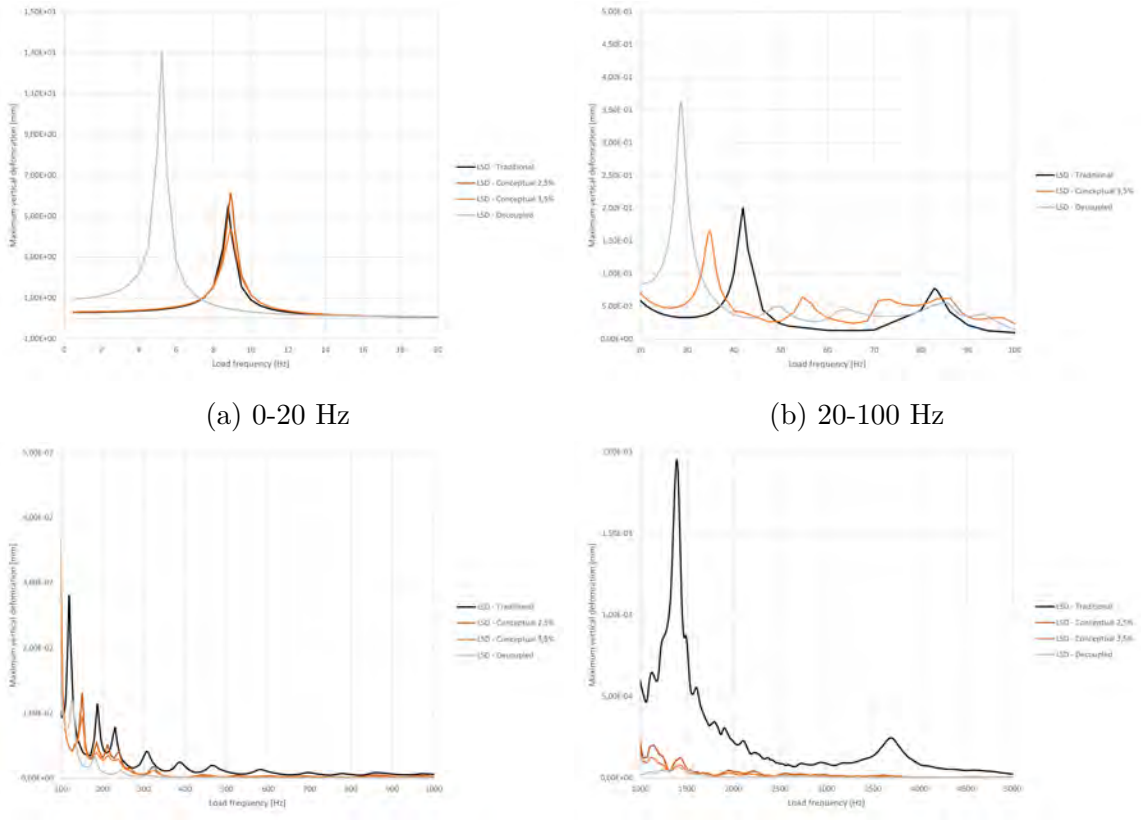

(a) 0-20 Hz

(b) 20-100 Hz

(c) 100-1000 Hz

(d) 1000-5000 Hz

Figure E.19: Results of Harmonic Response Analysis of the Large Span Design (LSD) floors, measured at the bottom of the CLT.

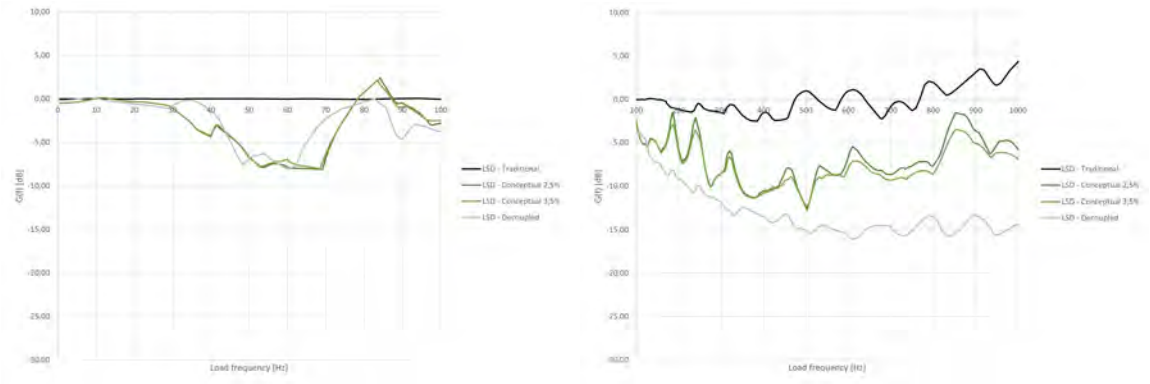

(a) 0-100 Hz

(b) 100-1000 Hz

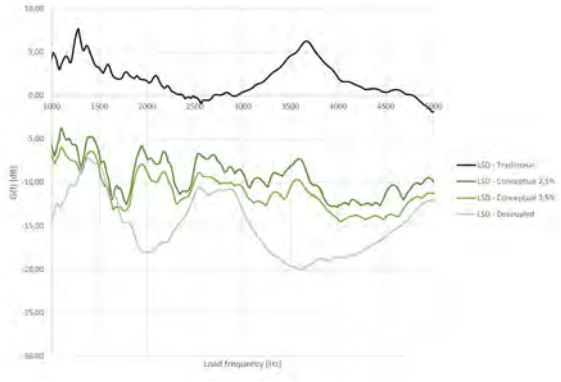

(c) 1000-5000 Hz

Figure E.20: Top-Bottom transfer from the Harmonic Response Analysis of the Large Span Design (LSD)

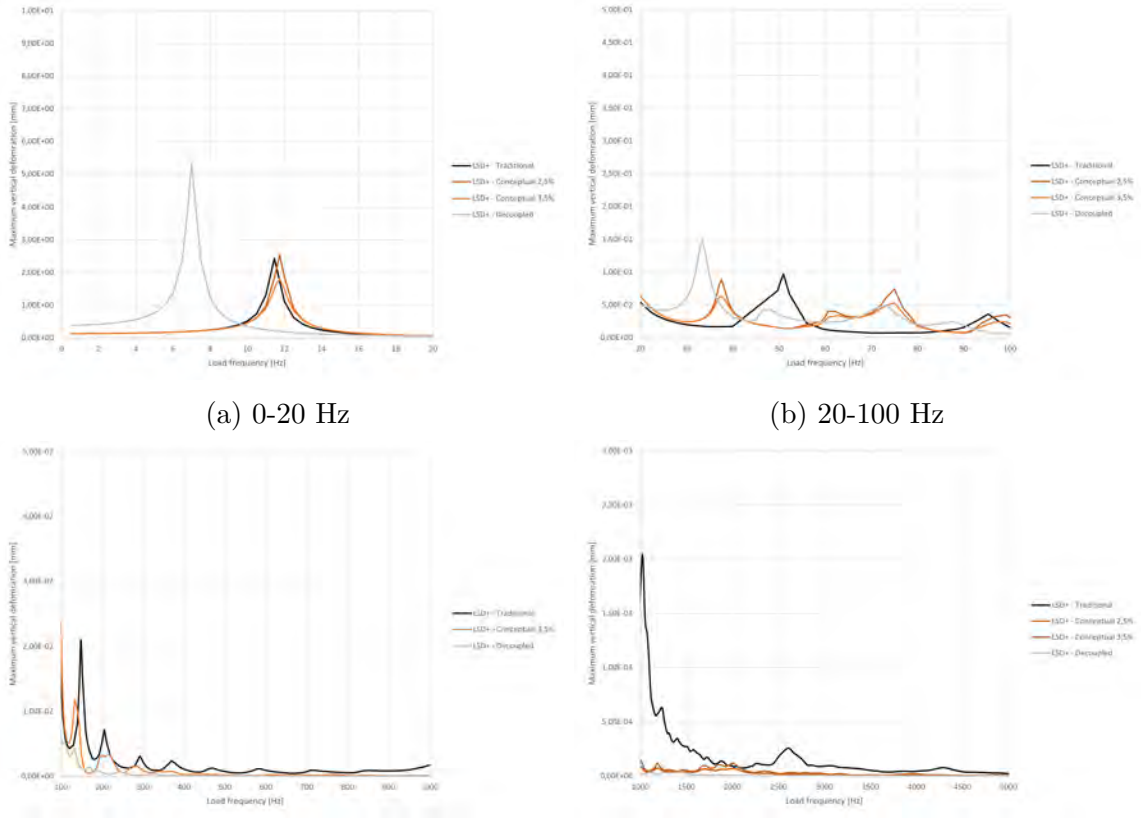

(a) 0-20 Hz

(b) 20-100 Hz

(c) 100-1000 Hz

(d) 1000-5000 Hz

Figure E.21: Results of Harmonic Response Analysis of the Large Span Design+ (LSD+) floors, measured at the bottom of the CLT.

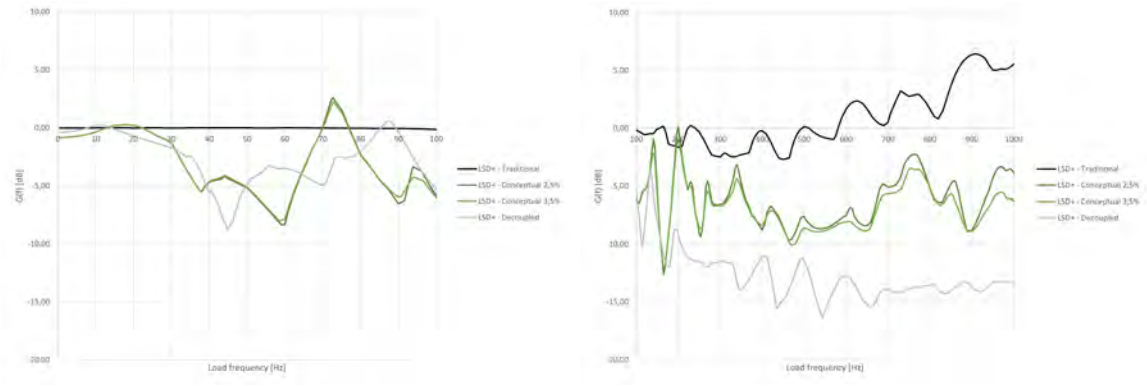

(a) 0-100 Hz

(b) 100-1000 Hz

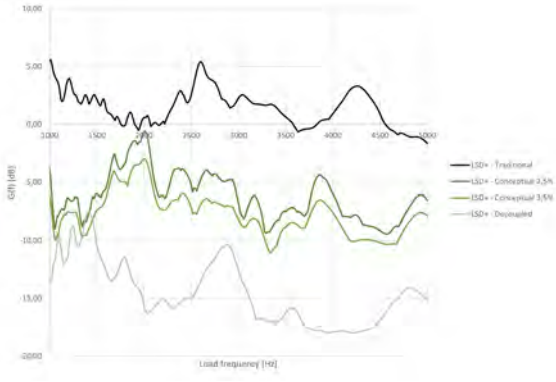

(c) 1000-5000 Hz

Figure E.22: Top-Bottom transfer from the Harmonic Response Analysis of the Large Span Design+ (LSD+)

F Bassist results

F.1 Results - ED

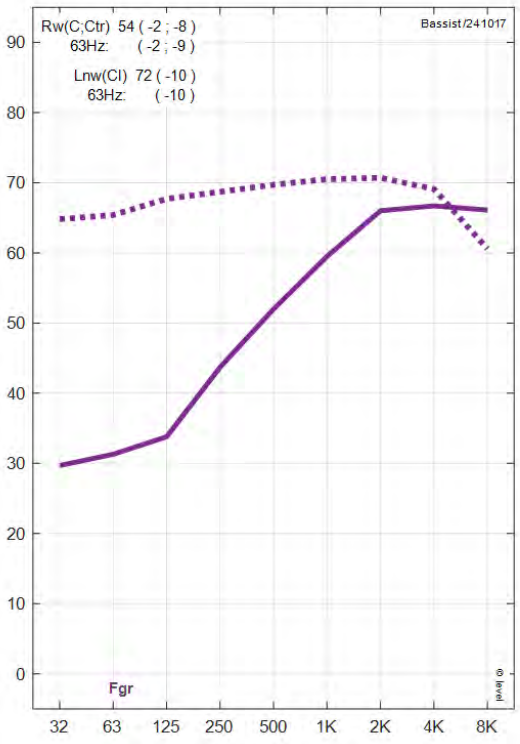

(a) Traditional

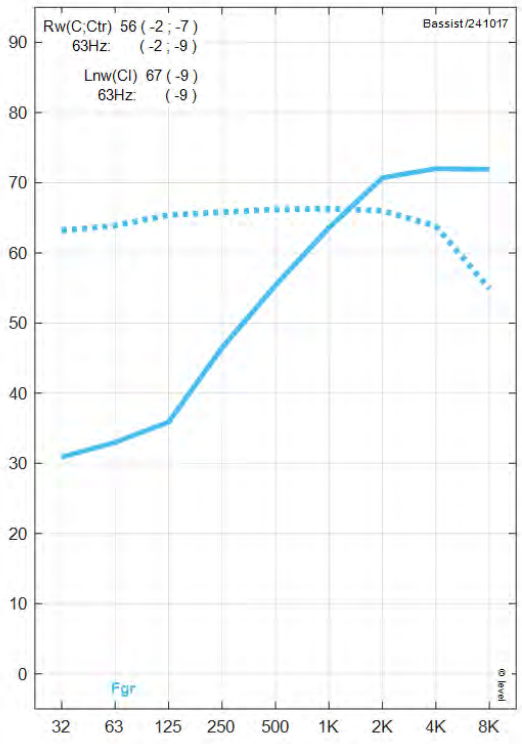

(b) Traditional with η_{exp}

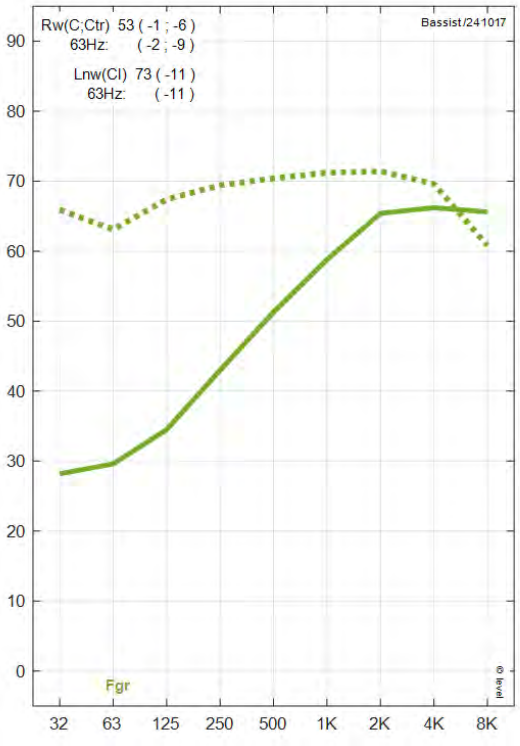

(c) Conceptual - lower bound

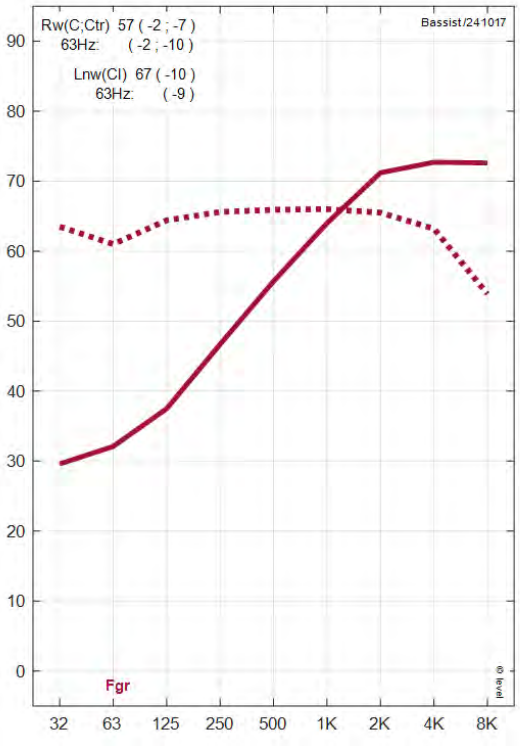

(d) Conceptual - lower bound with η_{exp}

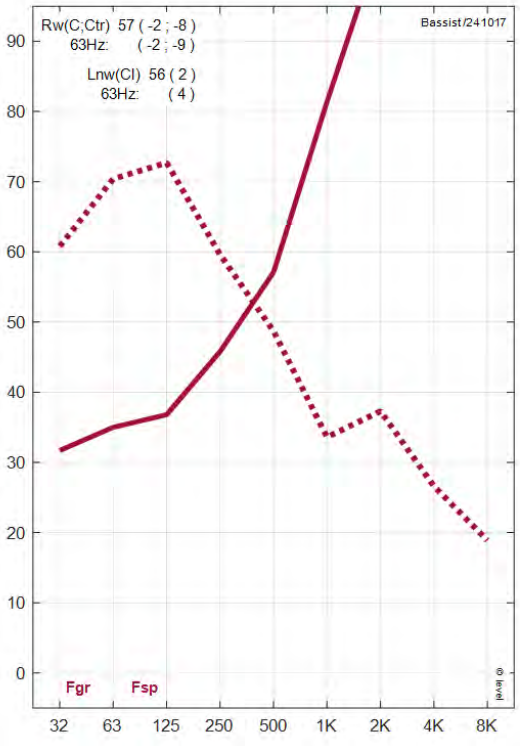

(e) Conceptual - upper bound

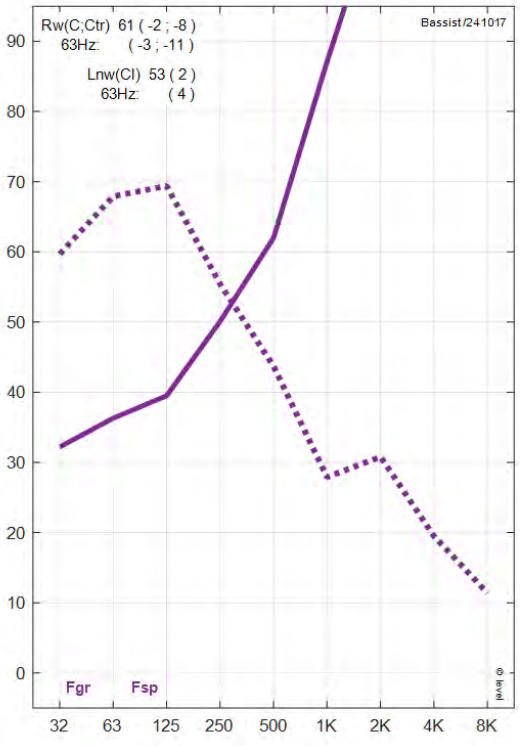

(f) Conceptual - upper bound with η_{exp}

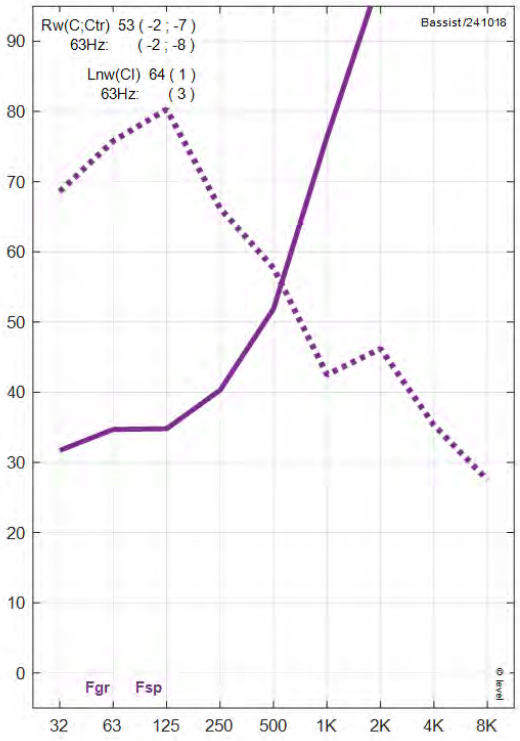

(g) Decoupled

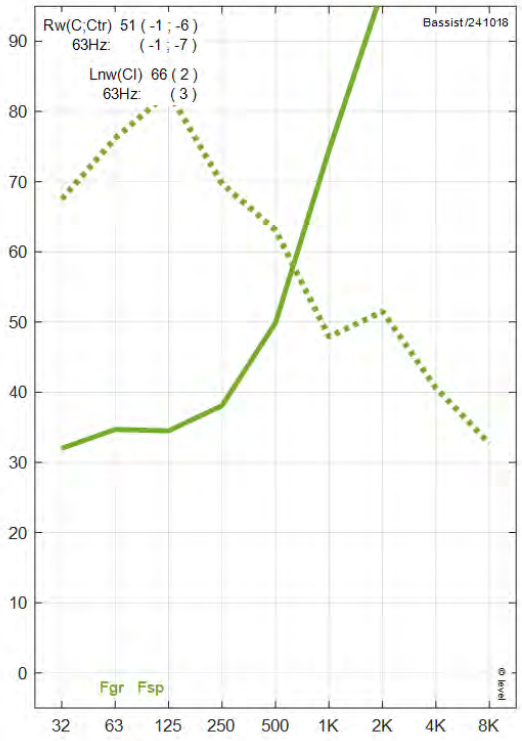

(h) Decoupled - reference

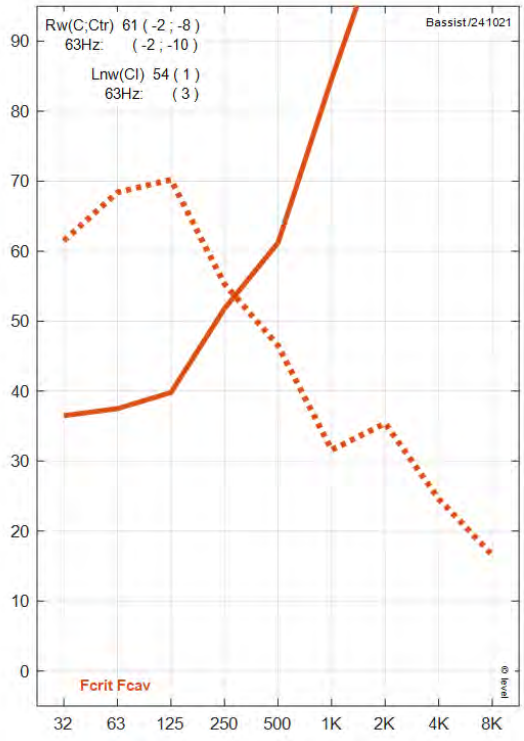

(i) Traditional with F.F.

Figure F.1: Airborne sound insulation and Impact sound pressure level per octave band of frequency calculated by Bassist for the floors in the ED category.

F.2 Results - LSD

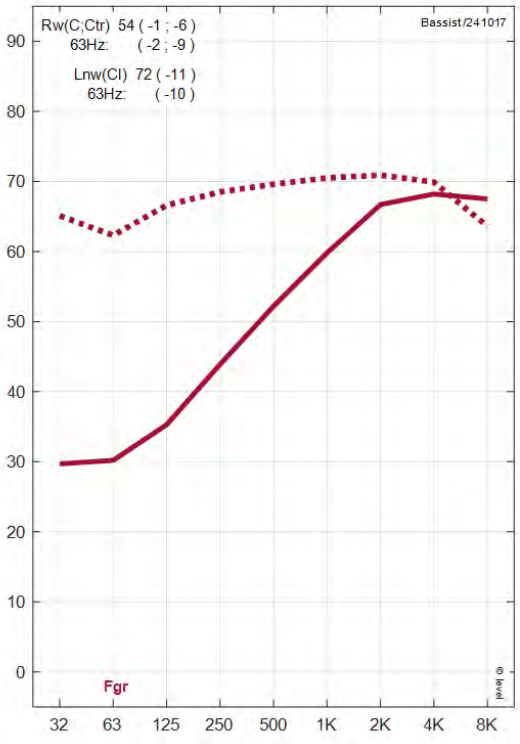

(a) Traditional

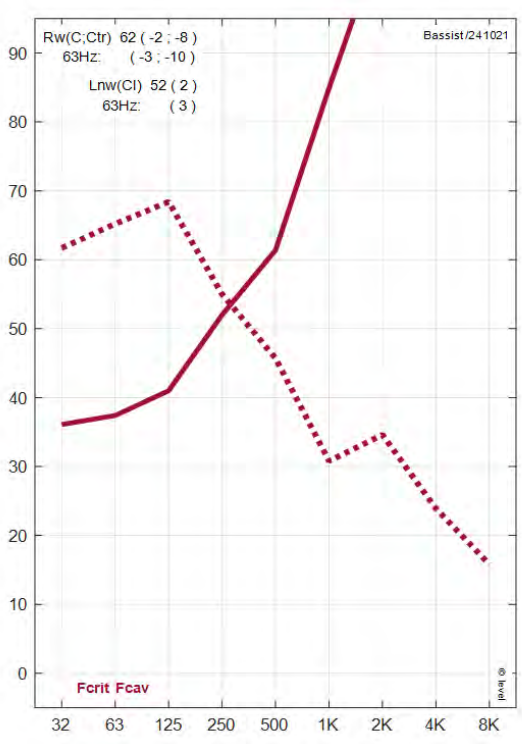

(b) Traditional with F.F.

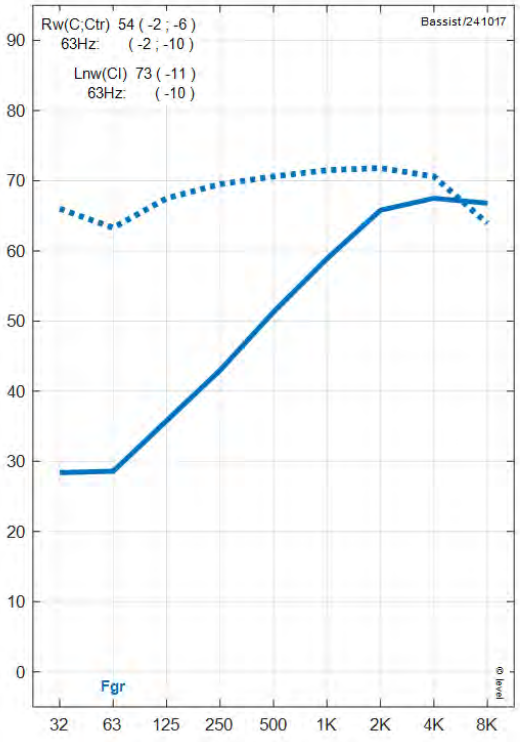

(c) Conceptual - lower bound

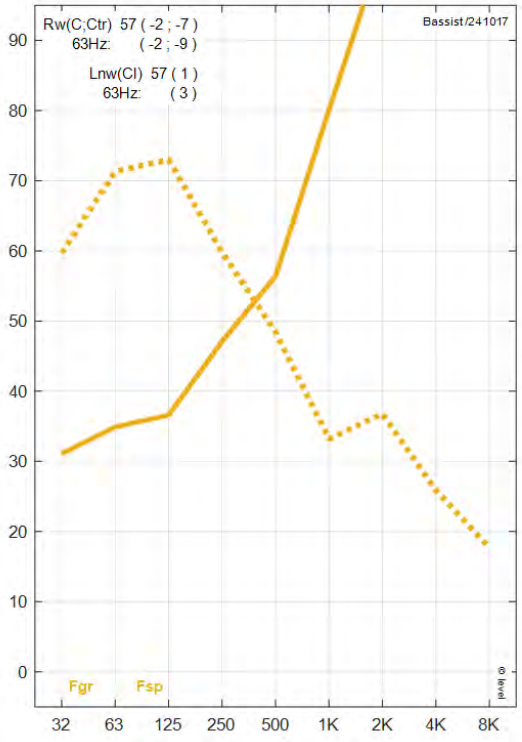

(d) Conceptual - upper bound

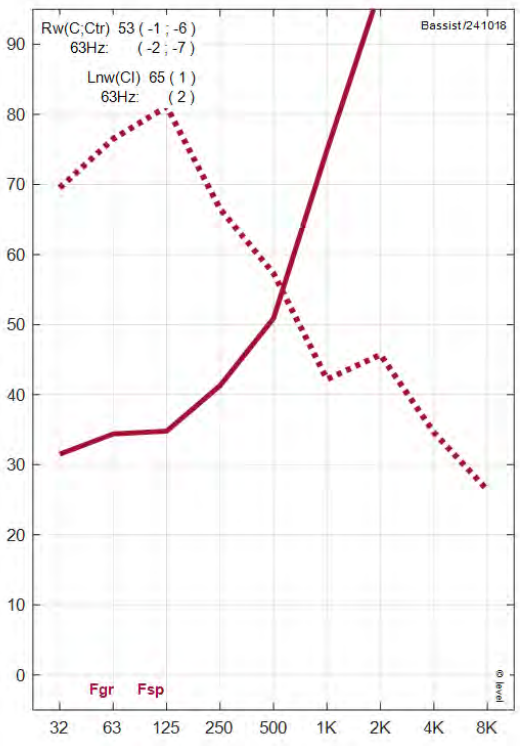

(e) Decoupled

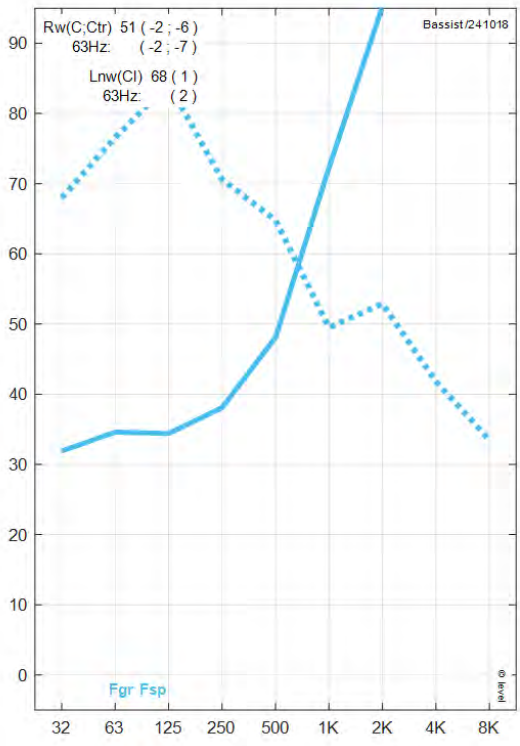

(f) Decoupled - reference

Figure F.2: Airborne sound insulation and Impact sound pressure level per octave band of frequency calculated by Bassist for the floors in the LSD category.

F.3 Results - LSD+

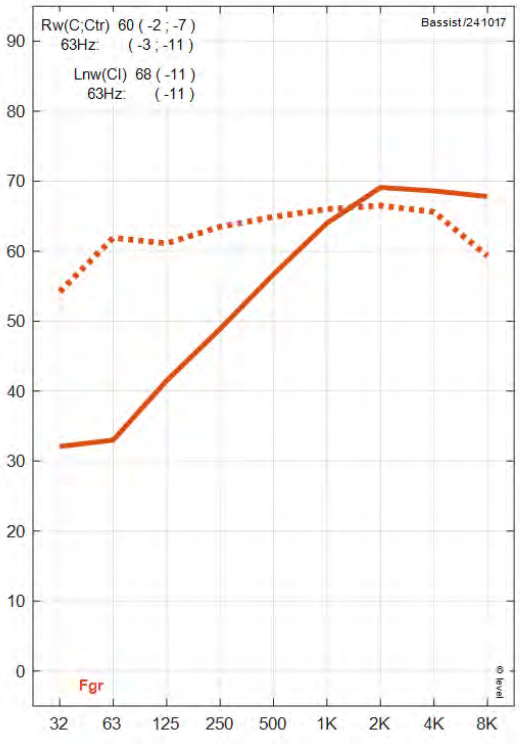

(a) Traditional

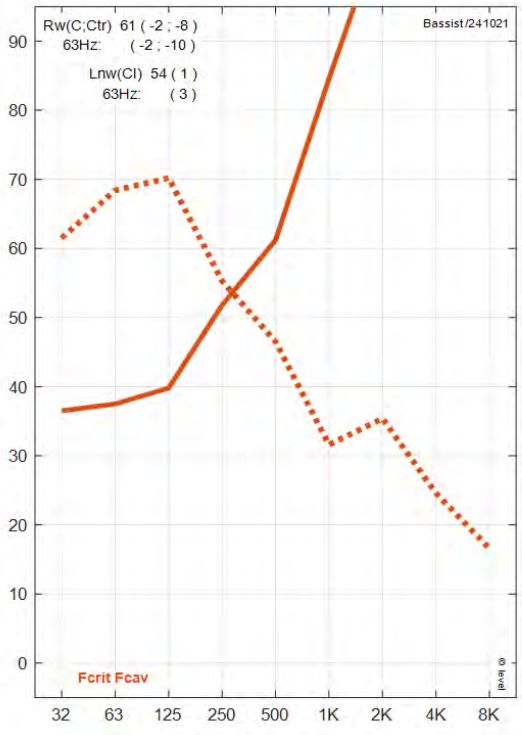

(b) Traditional with F.F.

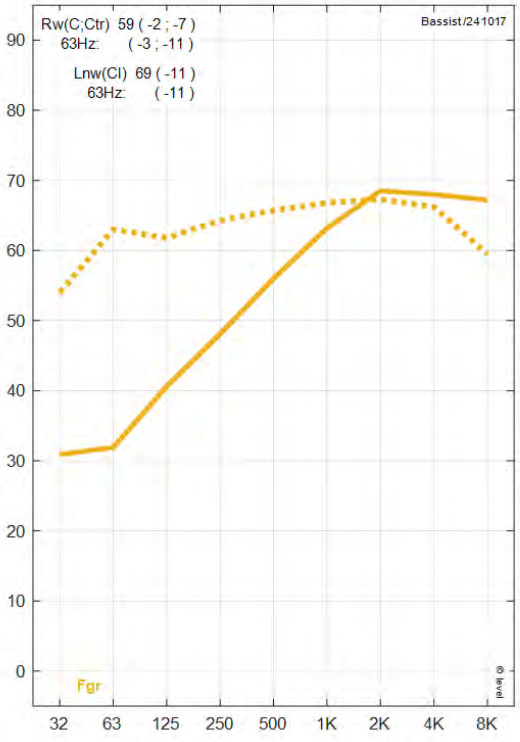

(c) Conceptual - lower bound

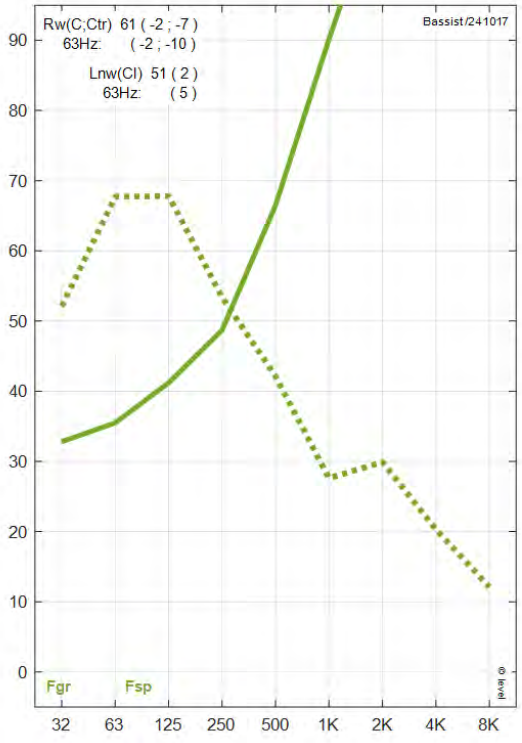

(d) Conceptual - upper bound

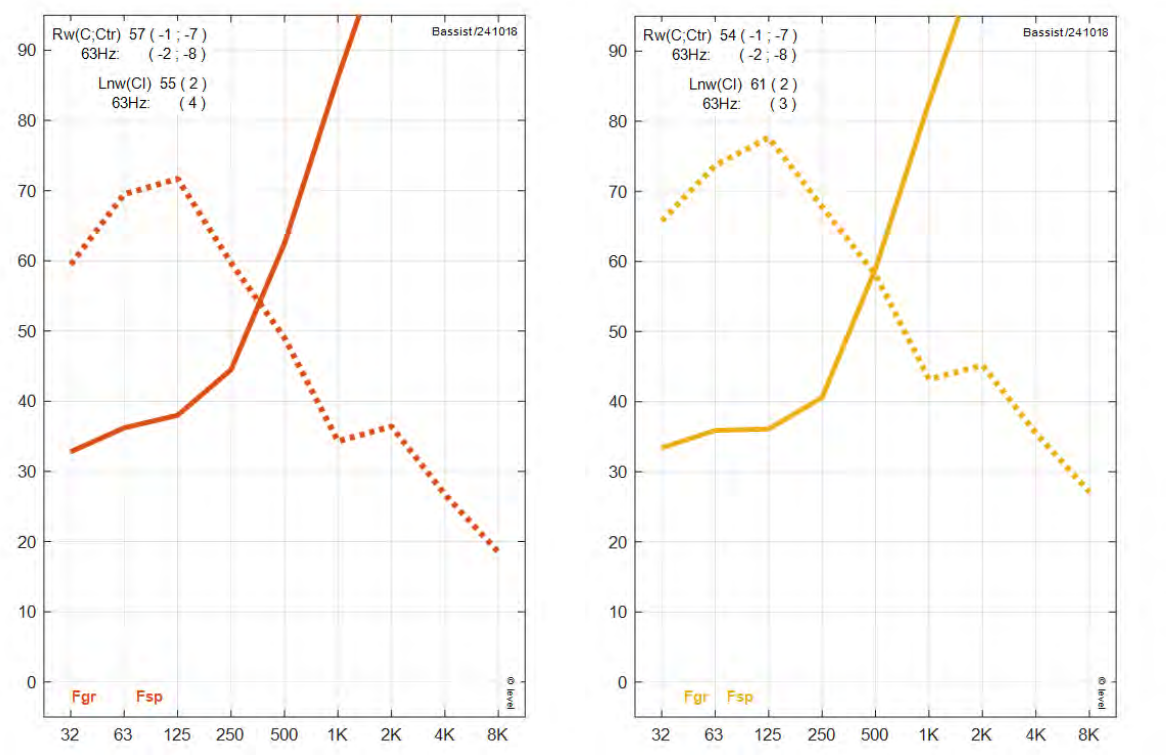

(e) Decoupled (f) Decoupled - reference

Figure F.3: Airborne sound insulation and Impact sound pressure level per octave band of frequency calculated by Bassist for the floors in the LSD+ category.

Eindhoven
University of
Technology

PO Box 513
5600 MB Eindhoven
The Netherlands

www.tue.nl